

WL-TR-96-2107



**THERMAL INSTRUMENTATION
A STATE-OF-THE-ART REVIEW**

**Richard D. Neumann
The University of Dayton Research Institute
Dayton, Ohio 45469-0111**

DECEMBER 1993

INTERIM REPORT FOR 3/92--12/93

Approved for public release; distribution unlimited

**AERO PROPULSION & POWER DIRECTORATE
WRIGHT LABORATORY
AIR FORCE MATERIEL COMMAND
WRIGHT-PATTERSON AIR FORCE BASE, OH 45433-7251**

19960925 111

DTIC QUALITY INSPECTED 1

NOTICE

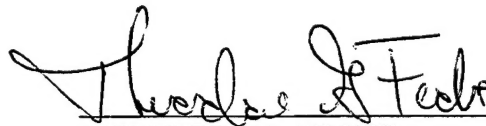
WHEN GOVERNMENT DRAWINGS, SPECIFICATIONS, OR OTHER DATA ARE USED FOR ANY PURPOSE OTHER THAN IN CONNECTION WITH A DEFINITELY GOVERNMENT-RELATED PROCUREMENT, THE UNITED STATES GOVERNMENT INCURS NO RESPONSIBILITY OR ANY OBLIGATION WHATSOEVER. THE FACT THAT THE GOVERNMENT MAY HAVE FORMULATED OR IN ANY WAY SUPPLIED THE SAID DRAWINGS, SPECIFICATIONS, OR OTHER DATA, IS NOT TO BE REGARDED BY IMPLICATION, OR OTHERWISE IN ANY MANNER CONSTRUED, AS LICENSING THE HOLDER, OR ANY OTHER PERSON OR CORPORATION; OR AS CONVEYING ANY RIGHTS OR PERMISSION TO MANUFACTURE, USE, OR SELL ANY PATENTED INVENTION THAT MAY IN ANY WAY BE RELATED THERETO.

THIS REPORT IS RELEASABLE TO THE NATIONAL TECHNICAL INFORMATION SERVICE (NTIS). AT NTIS, IT WILL BE AVAILABLE TO THE GENERAL PUBLIC, INCLUDING FOREIGN NATIONS.

THE TECHNICAL REPORT HAS BEEN REVIEWED AND IS APPROVED FOR PUBLICATION.


KATHLEEN A. SARGENT

Project Engineer, Components Branch
Turbine Engine Division
Aero Propulsion & Power Directorate


THEODORE G. FECKE

CHIEF, Components Branch
Turbine Engine Division
Aero Propulsion & Power Directorate


RICHARD J. HIEL

Chief of Technology
Turbine Engine Division
Aero Propulsion & Power Directorate

IF YOUR ADDRESS HAS CHANGED, IF YOU WISH TO BE REMOVED FROM OUR MAILING LIST, OR IF THE ADDRESSEE IS NO LONGER EMPLOYED BY YOUR ORGANIZATION PLEASE NOTIFY WL/POTC WPAFB OH 45433-7251 HELP MAINTAIN A CURRENT MAILING LIST.

COPIES OF THIS REPORT SHOULD NOT BE RETURNED UNLESS RETURN IS REQUIRED BY SECURITY CONSIDERATIONS, CONTRACTUAL OBLIGATIONS, OR NOTICE ON A SPECIFIC DOCUMENT.

REPORT DOCUMENTATION PAGE			Form Approved OMB No. 0704-0188	
Public reporting burden for this collection of information is estimated to average 1 hour per response, including the time for reviewing instructions, searching existing data sources, gathering and maintaining the data needed, and completing and reviewing the collection of information. Send comments regarding this burden estimate or any other aspect of this collection of information, including suggestions for reducing this burden, to Washington Headquarters Services, Directorate for Information Operations and Reports, 1215 Jefferson Davis Highway, Suite 1204, Arlington, VA 22202-4302, and to the Office of Management and Budget, Paperwork Reduction Project (0704-0188), Washington, DC 20503.				
1. AGENCY USE ONLY (Leave blank)	2. REPORT DATE December 1993	3. REPORT TYPE AND DATES COVERED Interim 3/92--12/93		
4. TITLE AND SUBTITLE TURBINE AERO THERMAL RESEARCH		5. FUNDING NUMBERS C: F33615-87-C-2770 PE: 62203F PR: 3066 WU: 03		
6. AUTHOR(S) Richard D. Neumann				
7. PERFORMING ORGANIZATION NAME(S) AND ADDRESS(ES) University of Dayton Research Institute 300 College Park Avenue Dayton, OH 45469-0110		8. PERFORMING ORGANIZATION REPORT NUMBER UDR-TR-93-132		
9. SPONSORING / MONITORING AGENCY NAME(S) AND ADDRESS(ES) Aero Propulsion & Power Directorate Wright Laboratory Air Force Materiel Command Wright-Patterson Air Force Base, OH 45433-7650 POC: Kathleen Sargent, WL/POTC, 513-255-2081		10. SPONSORING / MONITORING AGENCY REPORT NUMBER WL-TR-96-2107		
11. SUPPLEMENTARY NOTES				
12a. DISTRIBUTION / AVAILABILITY STATEMENT APPROVED FOR PUBLIC RELEASE; DISTRIBUTION IS UNLIMITED		12b. DISTRIBUTION CODE		
13. ABSTRACT (Maximum 200 words) The primary objective of this study was to collect, review, and organize the various methods for convective heat transfer measurement into a single, useful reference document. This report presents the state of that development from worldwide sources as of the date of publication.				
14. SUBJECT TERMS Measurement techniques, aerodynamic heating, instrumentation, thermal instrumentation			15. NUMBER OF PAGES 193	
			16. PRICE CODE	
17. SECURITY CLASSIFICATION OF REPORT UNCLASSIFIED	18. SECURITY CLASSIFICATION OF THIS PAGE UNCLASSIFIED	19. SECURITY CLASSIFICATION OF ABSTRACT UNCLASSIFIED	20. LIMITATION OF ABSTRACT SAR	

TABLE OF CONTENTS

<u>Section</u>	<u>Page</u>
I INSTRUMENTATION	I-1
II THERMAL MODELS	II-1
III SEMI-INFINITE SLAB THERMAL MODEL	III-1
APPENDIX III-1	
CALCULATION OF HEAT TRANSFER COEFFICIENT UNCERTAINTY FROM THE APPENDIX OF THE 1975 THESIS OF LARRY CARTER	AIII1-1
APPENDIX III-2	
THIN FILM THERMOCOUPLES - THE CONTRIBUTIONS OF TURBINE ENGINE RESEARCH	AIII2-1
APPENDIX III-3	
THE RELATIVE CALIBRATION TECHNIQUE AFTER EPSTEIN, 1986	AIII3-1
APPENDIX III-4	
EQUIVALENCE BETWEEN CONSTANT HEAT FLUX AND THE GENERAL 1D HEAT CONDUCTION MODELS	AIII4-1
IV THIN SKIN THERMAL MODEL	IV-1
V GRADIENT TYPE HEAT FLUX GAGES	V-1
VI STATIC VS DYNAMIC MEASUREMENTS	VI-1
VII ADIABATIC WALL TEMPERATURES	VII-1
VIII INSTRUMENTATION IN SHOCK INTERACTION REGIONS	VIII-1
IX THE EFFECT OF TEST VARIABLES ON SHOCK TUNNEL SURFACE TEMPERATURES	IX-1
X OPTICAL FIBRE-BASED HEAT FLUX SENSORS	X-1

TABLE OF CONTENTS (Continued)

<u>Section</u>	<u>Page</u>
APPENDIX A - REFERENCE HEAT-TRANSFER COEFFICIENTS	A.A-1
APPENDIX B - THERMAL SENSOR SENSITIVITY	A.B-1

LIST OF FIGURES

<u>Figure</u>	<u>Page</u>
1 Static Temperature Distribution Through a Boundary Layer Showing the Effects of Heat Transfer Near the Wall.	I-4
2 The Relationship Between Heating Rate, Heat Transfer Coefficient and Recovery Temperature in an Aero-dynamic Heating Problem.	I-7
3 Comparison of a Thin Film Resistance Calorimeter and an Isothermal Thermocouple Gage.	I-10
4 Comparison of a Bayonet Gage and an Isothermal Thermocouple Gage	I-10
5 Comparison of a Co-axial Thermocouple Gage Installed in an Insulative and a Conductive Model Surface	I-11
6 Comparison of a Conductive and Insulative Thermal Gage Installed in a Insulative Model	I-11
7 Conceptual Thermal Measurement Technique Using Physical Sensors	I-12
8 Examples of Models and Instrumentation Producing Non-Isothermal Wall Effects	I-17
9 Thermal Perturbation Caused by Non-Isothermal Surfaces after Consigny, 1992	I-18
10 The Physical Test Model Used by Collier, 1990, to Evaluate Shock Interaction with Coax Gages	I-19
11 The Surface Temperatures measured by the Coax Gages Located in the Collier Shock Interaction Model	I-19
12 Possible Modes of Heat Transfer on a Structure	II-2
13 Example of a Thermal Model of a Structural Element after Kidd, 19xx	II-4
14 Slender Cone/Cylinder/Flare Model Including the Internal Structure of the Model	II-4
15 Heat Flux Data From the Model Shown in Figure 14 Reduced Using 1D Methods	II-5
16 Simulated "Data" Using the Actual Model Structure and 2D Reduction Methods	II-5
17 The Lateral Heat Conduction	II-6

LIST OF FIGURES (Continued)

<u>Figure</u>	<u>Page</u>
18 Data Correction for Non-Classical Heating Using 2D Conduction Methods	II-6
19 The Effect of Thermal Coatings to Act as a Semi-infinite Surface for Very Short Test Periods (after Smith, 1989).	III-2
20 The Graphical Solution of a Semi-Infinite Slab Heating After Jones and Hunt, 1966	III-3
21 Heating Ahead of a Cylindrically Blunted Fin Attached to a Sharp Cone at Hypersonic Speeds. The Heat Transfer Coefficient Boundaries and the Centerline Distribution of Heat Transfer Coefficients	III-3
22 Experimental Data From Hung Superimposed on the Graphical Solution of Jones and Hunt	III-4
23 Example of Shock Interaction Results Generated Through the Use of Temperature Sensitive Coatings	III-5
24 Graphical Determination of the Effective Time Origin From Simeonides, 1991	III-7
25 The Change in the Parameter Beta as Model Materials Become More Conductive	III-8
26a Geometry of Maise and Rossi, 1974	III-9
26b Corrections Required to the 1D Analysis After Maise and Rossi, 1974	III-9
27 The One-Dimensional Heat Flow Model and Its Assumptions	III-11
28 Repeated Application of Temperature Sensitive Paint to a Thin-Winged Test Model	III-12
29 The Uncertainty Build-Up for Temperature Coatings from the Application of Uncertainty Analysis	III-13
30 The Relationship Between Phosphor Quenching and Indicated Temperature for Several Phosphor Types	III-14
31 Calibration of Phosphor Data (Through the AEDC Datacolor System) Against Gardon Gages and Surface Temperature Gages	III-15

LIST OF FIGURES (Continued)

<u>Figure</u>	<u>Page</u>
32 Schematic of an Advanced, Two-Color Thermographic Phosphor System Developed by and Located at Nasa Langley Research Center	III-15
33 Calibration of the Radelin Phosphor Mixture to Produce a Larger Temperature Range for Experimentation	III-16
34 The Phosphor Intensity at the Red and Green Wavelengths	III-17
35 Comparison of Advanced, High Temperature Thermographic Phosphor Data Against Thermocouple Measurements	III-16
36 Older Calibration Gages Producing Non-Isothermal Test Surfaces	III-17
37 Newer "Staple" Gages Yielding Isothermal Test Surfaces	III-17
38 The Relationship Between Non-Dimensional Heating and Non-Dimensional Temperature for Specific Ranges of Temperature	III-18
39 Gage Surface Showing the Matrix of Squares Each of Which Measures to Surface and Backface of the Gage	III-20
40 The Temperature Response of the Surface and Backface Sensors to a Thermal Pulse Defined in the Figure Inset	III-20
41 A Monochrome Presentation of a Line of Constant Heat Transfer Coefficient About a Cylinder/Flat Plate Model Using Liquid Crystal Coating after Moffat, 1988.	III-21
42 Physical Arrangement of French Stimulated Infrared Measurements in a Wind Tunnel	III-24
43 The Heat Pulse Due to Photon Stimulation and the Superposition of That Energy of Normal Convective Heating	III-24
44 An Uncertainty Analysis Plot for Infrared Sensors from Boylan, 1978	III-26
45 Uncertainty Increments for a Grey Body Approximation and for Data at Specific Wavelengths	III-29
46 Effect of Random Errors on the Model Surface Temperature Calculation	III-30
47 Error Sensitivity Functions Specific to a Given Camera and Model Installation	III-30

LIST OF FIGURES (Continued)

<u>Figure</u>	<u>Page</u>
48	Very Small Thin Film Resistance Thermometer Gages Applied to a Leading Edge Model . . . III-33
49	An All-Macor Model of the Space Shuttle Showing Dense Thin Film Instrumentation III-34
50	The Effect of Ionization on the Output of Uncoated Thin Film Gages III-34
51a	Temperature/Time Trace for a Thin Film Resistance Thermometer Gage III-35
51b	Temperature/Time Trace for a Chromel/Constantan Coaxial Thermocouple Gage III-35
52	Packing Density of Diamond Thin Film Gages III-36
53	The Resistance of Annealed Diamond Thin Film Sensors after Aslam, 1992 III-36
54	Temperature Coefficient of Resistance for the Annealed Diamond Thin Film Sensor as a Function of Surface Temperature after Aslam, 1992 III-36
55	Variation of Surface Heating Rate with Increasing Surface Temperature from Schultz et al, 1965 III-37
56	Heat Flux Corrections Due to Temperature-Dependant Substrate Thermal Properties III-40
57	Demonstration of the Analogy Between Heat Flow and Electrical Flow; the Basis of the Q-Meter Design III-41
58	Early Coax Gage Used in Germany, Giedt, 1955 III-44
59	Early Coax Gage Used in the US, Ferri 196x III-44
60	Modified Coax Gages after Mentre and Consigny, 1987 III-45
61	The Effects of Cable Treatment on the Quality of the Coax Heat Gage Signal III-46
62	Experience with Coax Heat Gages at Very Low Heating Rates after Scaggs, 1992 III-47
63	Surface and Backface Temperature Data From a Coax Gage Measurement III-50
64	Possible Errors in Coax Reduced Data Due to Inexact Time Intervals III-50
65	Demonstrating a Reduction of the Same Data Using a 1D Thermal Model of Finite Slab 20 Nodes Deep III-51

LIST OF FIGURES (Continued)

<u>Figure</u>	<u>Page</u>
66 Limits of Heat Transfer to be Measured by Thin Film Gages	III-52
67 Commercial 3-Wire Coax Gage Which Measures Both Surface and Backface Temperatures	III-53
68 One Dimensional Model of Heat Flow Down a Coax Gage	III-54
69 Classical, Semi-Infinite Slab Thermal Model. Doorly's Type I Gage	III-55
70 Doorly Type II Gage	III-55
71 Doorly Type III Gage	III-55
72 Plot of Thin Skin Data Using the Log-difference Method	IV-6
73 Interpolation of Thin Skin Data Back to Zero Time and Zero Conduction Losses	IV-6
74 Conduction Losses Down the Measurement Wire of Thin Skin Surfaces	IV-7
75 Sketch of the Attachment Technique for Thermocouple Wires Attached to a Thin Skin Measurement Surface	IV-7
76 Sensitivity of the Heat Transfer Coefficient to Errors in Specifying the Adiabatic Wall Temperature	IV-9
77a Heat Transfer Measurements in a Shock Tunnel. Figure 77a is Thin Film Data	IV-10
77b Heat Transfer Measurements in a Shock Tunnel. Figure 77B is Calorimeter Data	IV-10
78 Early Calorimeter Gage Used in the AEDB Hotshot Tunnel after Osgerby 1967	IV-10
79 Evolution of the Schmidt-Boelter Heat Gage	V-1
80 One Version of the Vattel Heat Flux Microsensor	V-3
81 Cross Section of the Microsensor	V-3
82 The Sensor Sensitivity of the Epstein Heat Gage After Epstein, 1985	V-5
83 Schematic View of the Gardon Gage after Hornbaker and Rall, 1968	V-6

LIST OF FIGURES (Continued)

<u>Figure</u>	<u>Page</u>
84 Response of a Gardon Gage to Aerodynamic Heating at Several, Typical Time Scales	V-7
85 Exploded View of the Multi-Layered Thin Film Gage after Hayashi et al, 198x	V-8
86 Use of a Single Multi-Layered Thin Film Gage to Evaluate Heat Transfer Distributions Within a Shock Interaction Region	V-9
87 Gradient Type Heat Sensors Attributed to Epstein (in the USA) and Doorly (in England). . .	V-10
88 View of an In-Depth, Thermocouple-Based Heat Gage	V-10
89 Plate/Cylinder Interaction Model Employing Dynamic Motion and Run in the Wright Laboratory Mach 6 Tunnel	VI-2
90 Space Shuttle Model Used in the NSWC Tunnel 9 with Coax Gages for Dynamic Testing . .	VI-3
91 Data Results Obtained from a Single, One-Second Sweeping Run in the NSWC Tunnel 9 . .	VI-3
92 Very Small Scale Space Shuttle Model Tested Dynamically	VI-4
93 Flap Instrumentation Detail for Small-Scale Space Shuttle Model	VI-4
94 Larger, Dynamically-Tested Space Shuttle Model with On-board Motor-Driven Control Flap	VI-4
95 Reduced Heating Rate Data for the Space Shuttle Model Tested at AEDC Showing Model Dynamic Motion	VI-5
96 The Flap Deflection Schedule Producing the Heat Transfer Data Shown i Figure 95	VI-5
97 Alternative Techniques for Accurate Data Acquisition	VI-8
98 Schematic of a Calibration Technique for Data Evaluation by Fourier Transforms	VI-9
99 The Calibration Process to Form Transformed Input and Output Data From Which a Transform Function is Created	VI-9
100 The Complex Transfer Function; Both Phase Angle and Magnitude	VI-10

LIST OF FIGURES (Continued)

<u>Figure</u>	<u>Page</u>
101 Reconstructed Test Data Using the Calibration-Developed Transfer Function, $H(I/O)$	VI-10
102 Results of the Paper of Gates and Allen, 1974, Demonstrating the Influence of Non-uniform Surface Temperature on the Level of Recovery Factor	VII-2
103 The Influence of Shock Interactions on the Distribution of the Recovery Factor	VII-3
104 Evaluation of Recovery Temperature Using an Infrared Camera Technique from Boscher, 1992	VII-3
105 Lateral Distribution of Local Recovery Temperature in the Reattachment Zone at x-48 mm	VII-4
106 Non-dimensional Heating of a Thin Skin Surface after Dorignac et al, 1991	VIII-2
107 Non-dimensional Heating of a Semi-Infinite Slab Surface after Dorignac	VIII-2
108 Pressure Rise Caused by an Experimental Interaction after Kussoy et al, 1975	VIII-4
109 Heat Transfer Rise Caused by a 5 Degree Wedge Leading to a Classically Defined Plateau	VIII-5
110 Demonstrating a Peaked Distribution for an 11 Degree Wedge	VIII-5
111 Angular Location Defined in Terms of the Fin Angle and Mach Number	VIII-6
112 Responses of a Coax Gage in a Uniform Heating Environment	VIII-7
113	VIII-8
114 Measured and Estimated Heat Flux Through the Interaction for Data of Callier, 1990	VIII-9
115 Measurements of Interference Heating with Poorly Selected Temperature Paint	VIII-10
116 The Accuracy of Coax Gages Used in a Dynamic Sweep Mode for Shock Interaction Heating Studies	VIII-10
117 Test Duration of Calspan Shock Tunnels as a Function of Shock Mach Number, MI, for Various Driven Tube Diameters	IX-1
118 Temperature Rise for Pyrex Material Subjected to Various Levels of Heating for Various Test Durations	IX-2

LIST OF FIGURES (Concluded)

<u>Figure</u>	<u>Page</u>
119 Temperature Rise for Stainless Steel Material Subjected to Various Heating Rates and Test Durations	IX-2
120 Temperature Difference Between Pyrex and Stainless Steel for Various Heating Rates and Imposed Test Durations	IX-3
121a The Large CALSPAN Sharp Cone Model Located Within the CALSPAN Shock Tunnel After Holden, 1984	IX-3
121b The Incremental Temperatures of Pyrex and Steel Materials for Test 6 of a Cone/Flare Heat Transfer Experiment after Holden 1984	IX-4
122 Surface Temperatures Measured About a Cylinder Sustaining a Severe Shock	IX-4
123 Measured Surface Temperature About the Interaction as Well as the Corresponding Temperature Rise for the (Assumed) Stainless Steel Model at Times Less than 3 ms From the Start of the Test IX-6	IX-6
124 Inferred Heat Transfer Rate as a Function of the Measured Surface Temperature on the Sidewall of a High Temperature Blowdown Test Cell	X-2
125 Inferred Recovery Temperature of the Test Cell Assuming that the Heat Transfer Coefficient Should be Constant with Surface Temperature	X-2
126 Schmidt-Boelter Gage Measurements Along a Surface as a Function of the Surface Temperature Level	X-3
127 Lumped Thermal Property Data for Pyrex 7740 from Miller, 19XX	X-3
128 Inverse Correlation of Coax Data Taken in a Shock Tunnel Demonstrating Constant Lumped Thermal Properties Up to 1000 Degrees R.	X-4
129 Material Properties for the Coax Gage System Together with the Ratio of Constantan to 17-4 Steel Properties (Which increases with Surface Temperature).	X-4
130 S.T. Kidd's Optical Fibre Heat Transfer Gage Embedded Within the Test	XI-1
131 Silicon Film sputtered Directly onto the Tip of the Optical Fiber	XI-2
132 Ratio of the Intensity at the Selected Frequencies is Directly Related to the Sensed Temperature of the Gage	XI-2

LIST OF TABLES

<u>Table</u>	<u>Page</u>
1.1 TESTING ISSUED FROM BOTH AN AERODYNAMIC AND STRUCTURAL PERSPECTIVE	I-13
3.1 TYPICAL DATA ACQUISITION PROCESSES FOR CONTEMPORARY THERMAL MAPPING TECHNIQUES	III-10
3.2 THERMOGRAPHIC PHOSPHOR TECHNIQUES	III-19
3.3 CHARACTERISTICS OF VARIOUS IR SYSTEMS EMPLOYED IN RECENT WIND TUNNEL TESTS	III-25
3.4 BOYLAN ERROR SENSITIVITIES	III-27
3.5 BOYLAN INDIVIDUAL UNCERTAINTIES	III-28
3.6 UNCERTAINTY ANALYSIS FROM VERMEULEN AND SIMEONIDES, 1992	III-30
3.7 MATRIX OF THERMAL GAGE DESIGNS BASED ON THE SEMI-INFINITE SLAB THERMAL MODEL	III-31
3.8 DIMENSIONS OF HEAT FLUX SENSORS	III-32
3.9 COMPARISON OF PLATINUM AND DIAMOND THIN FILM GAGES	III-36
3.10 COMPARISON OF THERMAL PROPERTIES OF CHROMEL/CONSTANTAN THERMOCOUPLE MATERIAL WITH STAINLESS STEEL MODEL SURFACE	III-45
3.11 DIFFERENCE IN THERMAL PROPERTIES BETWEEN THIN FILM SUBSTRATE AND COAX GAGE SUBSTRATE	III-45
4.1 PROPERTIES FOR A VARIETY OF POSSIBLE MODEL SURFACES	IV-2
4.2 GROUPING MATERIALS BY TERMS	IV-3
5.1 MATERIALS WHICH COULD FORM INSULATIVE LAYERS AND CONDUCTIVITY VALUES	V-4
5.2 GAGES AVAILABLE FROM THE AEDC HANDBOOK	V-6

LIST OF TABLES (Concluded)

<u>Table</u>		<u>Page</u>
8.1	FOURIER NUMBER FOR SEMI-INFINITE SLAB ANALYSIS, $E = 0.375$ INS	VIII-3
8.2	FOURIER NUMBER FOR THIN SKIN ANALYSIS, $E = 0.030$ INS	VIII-3
10.1	CURVE FITS TO THE THERMAL PROPERTIES FOR THE COAX GAGE SYSTEM	X-5
11.1	SPECIFICS OF TWO SENSORS, INCLUDING AREAS AS YET UNDOCUMENTED	XI-2

Preface:

This technical report is a state of the art review of thermal instrumentation applied to convective heating problems in high speed wind tunnel facilities. The current report updates, improves and extends the survey paper written by Neumann, 1989 which was prepared with the implicit limitations of a two-hour lecture. That previous report has been extensively modified and updated beyond being a catalog of conceptual heat transfer measurement devices.

In 1973 Schultz and Jones produced an AGARDograph entitled "Heat Transfer Measurements in Short Duration Hypersonic Facilities". which was and is an excellent review of instrumentation processes for short duration facilities that, in many respects, can only be referenced reverently in this report. There are, however, several areas where this work diverges from that previous effort. First, and most clearly, the present document is not focused entirely on short duration test facilities. There are sections in this report covering conventional blowdown and steady state test facilities. There are also a few pertinent comments in the area of aero-structural testing techniques. Second, this report presents a general updating and broadening of the database to include newer available international references. These references, it is felt, enrich the material and indicate the creativity of researchers worldwide. Finally, this report has more of a personal commentary to them than do the corresponding notes of Schultz and Jones.

Apart from the excellent review document by Schultz and Jones, two other reference documents are recommended. These are (1) Chapter 4 of Dr. Richards book, 1977, dealing with unsteady fluid dynamic phenomena; a book produced by the von Karman Institute. This chapter was prepared by T.V. Jones and is in some respects an update of the earlier work by Schultz and Jones and (2) a section of a more recent book entitled "Methods of Experimental Physics", 1981, which was prepared by Thompson. All three of these references present excellent material on the general subject of aerothermal instrumentation.

Substantial technical literature has been generated since 1988; particularly in the area of temperature measurement coatings and infrared measurement techniques. This new literature has been added to this report. Material has also been added on the quoted accuracy of basic measurements; such accuracy information is required as the basis of modern experiment uncertainty analysis which should accompany the use of modern thermal instrumentation in the future. Measurement accuracy information is extremely time-sensitive and the reader is urged to look both at the quoted accuracy of the measurement and the stated date of the report which was referenced.

This is a review paper on thermal instrumentation. While some of the material was developed by the author, most of the information contained herein is derived from a worldwide technical effort in thermal instrumentation. In all cases, special efforts were taken to credit the author of record. In most cases, only the highlights and conclusions of that author's work have been presented herein. The goal of this work is to develop, under one cover, a comprehensive body of information on the wide variety of thermal instruments available today and to give the reader ample references such that additional study can be conducted using the source papers of the developing author.

The subject of thermal instrumentation is currently a worldwide research activity spurred by a growing interest in hypersonics and fueled by scientific advances in such diverse subjects as micro-machining; chemistry and electronic chip production. No review of this type would be valid or comprehensive without a worldwide

perspective on ideas and advances. This report has endeavored to present that worldwide perspective based on the output of international symposia; international journals and personal contacts. It must be stated in all candor that U.S researchers are not generally aware of the bulk of international research because we don't subscribe to the international journals in which this material is reported or understand what has already been accomplished. That false economy on the part of our research organizations can lead us to expensive and incorrect conclusions and the expenditure of unnecessary test costs to either circumvent a problem already solved elsewhere or to re-invent instrumentation currently used elsewhere.

SECTION I INSTRUMENTATION

INTRODUCTION

Engineering involves understanding the response of a physical system to changes in imposed criteria or ground rules. Engineering solutions are, therefore, not static nor absolute but vary with the nature of the problem posed. Serious difficulties can be introduced by a routine or robotic engineering response to a newly posed question; the "force-fitting" of yesterday's technology to tomorrow's problems.

Instrumentation being a sub-set of engineering problems follows this trend. Instrumentation solutions are NEVER static nor absolute, they change with the nature of the problem that is posed. There are several reasons for investigating instrumentation. They are:

1. To be able to measure what has not been measured before; a reason driven, for example, by the very healthy contemporary tension between computational fluid dynamics (CFD) and experimentation.
2. To produce routine measurements with newer, state of the art instrumentation devices. An example of this is the supplanting of older mechanical scani-valve pressure measuring systems with newer electronic scanning valve pressure measurement systems produced by P.S.I., Inc..
3. To employ test facilities more effectively. This reason refers both to technical and economic responses to the escalating costs of experimental facilities.

The first reason is a response to new technology, Computational Fluid Dynamics (CFD), that burst on the engineering scene as a supposed threat to experimentation but which, in retrospect, depends upon experimentation for its formulation and in turn challenges experimentation and instrumentation. CFD is not a threat but a spur to experimentation which, in turn, challenges our ability to instrument those experiments. CFD must start with fundamental experiments to feed the many models which are internal to the program and rely on a variant of that same experimentation to "validate" the final product. Experimentation produces that data but in so doing must admit the difficulty in producing needed measurements as well as the inherent errors in all measurement technology; errors made more obvious by highly sophisticated numerical modeling of the flow field.

The second reason for investigating instrumentation is both a response to newer technology and a response to economics. Newer measurement technology continually causes a re-assessment of the cost of measurement and the efficiency with which it can be accomplished. Newer gages may well be faster as well as less prone to malfunction and thus must be considered.

The third reason for investigating instrumentation is a response primarily to economics. Chapman, 1975, highlighted a frustrating trend in experimentation; an ever increasing use of wind tunnels to develop new aircraft. The Rockwell Space Shuttle was a stellar data point in this respect; an enormous application of experimentation. Experimentalists were required to respond to the trend that Chapman outlined as well as to new economic realities caused by the cost of energy. A fascinating feature of such a response function is that it is rarely linear. Each level of challenge opens new options in addition to the obvious option of

improving past activities. The response to the challenge of higher energy costs has been to accomplish more with numerics as well as to compress testing times by orders of magnitude through the introduction of new test technologies. This area of compressed testing, which I term as "dynamic testing" will be discussed in greater detail later in this report.

So far, the terms "instrumentation" and "experimentation" have both been used and somewhat interchangeably. Experimentation, within the context of this report, is the use of wind tunnels to produce a flow field that can be observed and understood. Instrumentation involves the techniques used to achieve and quantify those observations. It must be stressed that viewed in this manner, instrumentation encompasses more than physical devices; it encompasses both the physical hardware and the mathematical computations with which to understand flow fields. In recent years, an increasing percentage of time and effort was associated with these experimental computations and the close relationship between computations and measurement will be discussed in this report.

The ability to measure some quantity of interest must be developed in relationship to the characteristics of the experiment undertaken. For a wind tunnel experiment, these characteristics are connected with the experimental facility and its limits; the model used in that wind tunnel facility and the required response characteristics of the signal being measured. Further, that which is being measured may well be an intermediate step between in the experiment and the ultimately desired knowledge. Not every quantity is directly measurable but every physical quantity is observable, either directly or indirectly, through experimental measurements. Heat transfer is not measured directly but inferred through an observation of temperature response in a calibrated structure.

This report will progress from a discussion of the features of thermal instrumentation to a discussion of the thermal model simplifications implicit in thermal instruments to a definition and discussion of thermal gages, the products of these simplifications.

How Temperature is Measured in Experimentation

There are two types of surface point sensors through which temperature can be measured in experimental test facilities. These are:

- * **THERMOCOUPLES:** A passive (unpowered) gage in which changes in the EMF at the juncture of two dissimilar materials are related, through calibration, to changes in temperature.
- * **RESISTANCE THERMOMETERS:** An active (electrically powered) gage in which changes in resistance through a thin film are related, through calibration, to changes in temperature.

The calibration required for thermocouples has already been accomplished for standard thermocouple material pairs. Thermocouple materials are highly standardized and rigidly controlled. Calibrations for those

materials are available and accurate. Additional accuracy may be achieved through a specific calibration of the installed thermocouple wires to remove any small batch-to-batch variations that may exist in the materials.

The calibration of resistance thermometers is sensitive to the specific gage fabrication techniques which vary from gage to gage and from one facility to another. This calibration is accomplished locally prior to use at the test facility. The primary calibration constant is the temperature coefficient of resistance which is either measured statically or dynamically depending on which calibration technique is applied.

Thermal sensors, both thermocouples and resistance thermometers have a limited operational temperature range. As the measured temperature increases, the available thermocouple types as well as their temperature sensitivity (mv/ deg R) reduces. There are several candidate thermocouples from which to choose at lower temperatures indicative of wind tunnel testing and each of the choices has an excellent sensitivity (mv of output vs temperature). As the application temperature increases, three trends change. First, the choice of thermocouple materials narrows. Second, self-protection of the thermocouple wires in an oxidizing environment becomes an important consideration decreasing the responsiveness of the thermocouple. Third, the basic sensitivity of the thermocouple (mv vs temperature) reduces decreasing the sensitivity of the measurement.

Practical thermal sensors used in wind tunnel models are metallic. Metallic thermocouples integrate best in metallic models. The material properties of Chromel - Alumel and Chromel - Constantan thermocouples are extremely close to the stainless steel materials used in conventional wind tunnel model construction. The same cannot be said for other combinations. Chromel-Constantan thermocouples attached to an iron model, for instance, create problems due to the substantial conductivity of iron relative to stainless steel. Resistance thermometers on the other hand, being active gages, require a current flow through the gage to activate and must be electrically insulated from the substrate material upon which they are placed. For this reason, resistance thermometers are normally attached to an insulative material and normally applied in impulse type facilities. Shock tunnels traditionally employ this instrumentation although they need not and resistance thermometers also need not be limited to shock tunnel applications.

For insulative, nonmetallic model materials, thermal gage installation creates three problems: knowing the properties of the actual substrate material accurately over the operating temperature of the application, minimizing the heat loss down the wires which form the gage and, possibly, thermal shock in the model material. Although resistance thermometers are normally used with insulative materials, both types of thermal sensors, thermocouples and resistance thermometers, have been applied successfully to insulative model materials. Examples of these installations are described by Miller, 1993, in the instrumentation of the AFE model for test in the NASA Langley 31 inch blowdown facility and by Neumann in the AEDC test facilities.

How Heat Flux is Derived in Experimentation (What Do We Sense and Why?)

Classically, aerodynamic heating is defined as proportional to the slope of the static temperature at the surface of the model as shown in Figure 1. The Fourier law of heat conduction equates the rate of heat transfer to the model surface to the slope of static temperature through the equation:

$$\dot{q}_{wall} = -k(dT/dZ)$$

The static temperature, in turn, deviates from its freestream level due to deceleration effects caused by the shock system about the body and the boundary layer within that shock layer. These decelerations trade flow kinetic energy for thermal energy raising the flow static temperature. In the absence of any transfer of this thermal energy into the surface, the conversion of energy would continue through the boundary layer until all the kinetic energy of the flow had been dissipated into thermal energy. This ideal situation is termed an adiabatic wall. Since no heat is transferred at the surface, the slope of the static temperature at the wall is zero.

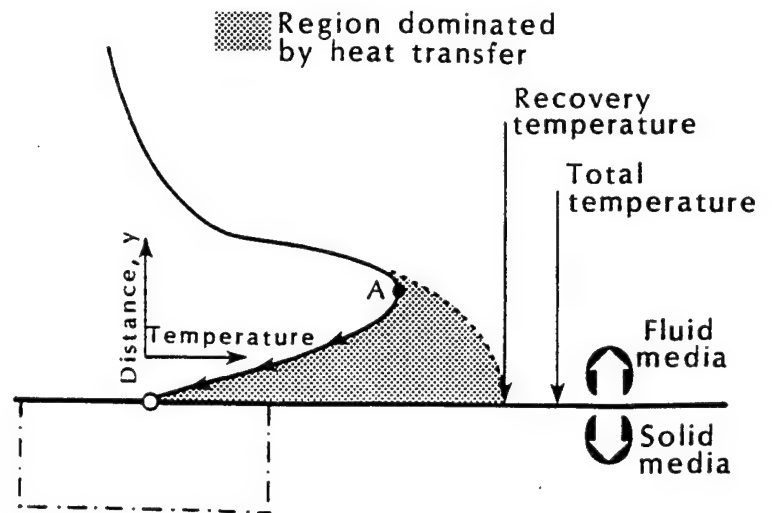


Figure 1 Static Temperature Distribution Through a Boundary Layer Showing the Effects of Heat Transfer Near the Wall.

Transfer of heat from the boundary layer to the surface modifies the distribution of the static temperature within the boundary layer near the surface. For the case of heat transfer a local maximum of the static temperature is noted within the boundary layer followed by a drop in the static temperature as heat is drained into the surface through heat transfer. The slope of the static temperature distribution at the surface is a direct measure of that heat transfer defined through the Fourier law of heat conduction listed above.

The magnitude and location of the local maximum in static temperature is not easily defined. It represents a balance between the two competing processes; the deceleration profile of velocity within the boundary layer which increases static temperature and the rate of heat transfer from the boundary layer to the surface which decreases the local static temperature.

Convective heat transfer is thus related to the presence and character of a physical surface which receives the heat from the enveloping fluid and is directly proportional to the slope of the static temperature at that surface.

The question is then ... how do we "measure" the rate of heat transfer at the surface? The most direct way would be to measure the static temperature gradient very near the surface. While this can, in principle, be done¹ for simple two dimensional surfaces, it is a difficult measurement to make because of the physical size of the high gradient region within the boundary layer near the surface. For three-dimensional surfaces, the corresponding measurement is not possible.

¹ Modern non-intrusive instrumentation could, in principle, evaluate heat transfer through measurement of the temperature distribution in the boundary layer for idealized, two-dimensional models. While this possibility exists in principle, practical tests of three-dimensional configurations use sensors embedded in the surface of the model.

The question remains then ...how do we "measure" the rate of heat transfer at the surface? Heat transfer measurements which are made in practice do not measure the flow in the boundary layer but rather measure the result of that boundary layer flow to the affected surface. This heat transfer to the surface must be reflected in the flow of heat into, through and away from the surface and that is what is measured. The measurement is made through the use of temperature sensors (typically thermocouples) which are carefully placed to define the entire heat flow pattern in, through and from the material and, through inverse heat transfer techniques, to define the heat flux that caused the heat flow within the surface.

Wind tunnel methods do not directly evaluate the heat transfer potential of the flowing gas (the slope of the static temperature in the gas with distance to the wall) but instead they measure the response of the model surface to that heating. As a result, this model measurement must "capture" the heat pulse in order to evaluate it. Capturing the imposed convective heat pulse requires understanding and accounting for all the modes of heat transfer within the model; convective, radiative and conductive for all the flow paths along which the heat transfer can go. The mechanism for modeling all the modes of heat transfer and all of the possible paths is termed a THERMAL MODEL and the design of a specific, localized thermal model which reduces the modes of heat transfer and the dimensionality of the problem is termed a HEAT GAGE.

The ideal heat gage reduces the many possibilities described above to a one dimensional flow of heat in the model by conduction alone. Such a heat gage can capture the heat pulse and define the heat flow to the model using a single, strategically placed thermocouple. The semi-infinite slab thermal model used in shock tunnel thin film gages and the coax gage instrumentation are examples of this simplified heat gage. Similarly, the heat flux can be "captured" by using the difference in measured temperatures between two points separated in depth. The Schmidt-Boelter gage and the Vatell gage are examples of this type of gradient gage.

How Wind Tunnel Heat Transfer Measurements Differ from Flight Measurements

Ground test heat flux measurements differ from flight measurements in that many of the variables discussed previously; the modes of heat transfer and the three-dimensionality of the heat flow, can be controlled on the ground and, possibly, eliminated through proper design of the ground test experiment but not as easily in flight.

The surface of the ground test model normally does not heat up sufficiently to radiate a measurable amount of heat from the model surface back to its surroundings, the tunnel walls. This amount of radiative heating is defined through the equation:

$$\dot{q}_{\text{RADIATION}} = \epsilon \sigma (T_w^4 - T_B^4)$$

where: ϵ is the surface emittance value (between 0 and 1), T_w is the model surface temperature and T_B is the background temperature of the receiver (tunnel walls in the wind tunnel case).

Bare stainless steel, a usual wind tunnel model material, has a low emittance and model surfaces are normally maintained at or near room temperature during heat transfer testing. Eliminating radiation as a heat transfer mode reduces a significant portion of the measurement problem. In flight, radiation from high temperature flight structures represents the largest heat transfer mechanism and the largest single source of measurement error in determining heat transfer. The amount of heat lost to the background by the surface is not measured by the thermal instrumentation and must therefore be estimated through pre-test calibrations using the equation given. Such an estimation contains several sources of error. First, surface temperatures are difficult to measure in flight and are usually inferred from sub-surface measurements of higher temperature (and thus lower sensitivity) thermocouples. Second, for sustained flight the surface temperature estimate enters into the equation as the fourth power magnifying both bias and random errors. Finally, the emittance values of materials used in flight must either be measured, estimated and/or extrapolated introducing yet another error. A more complete discussion of these factors can be found in "An Introduction to Flight Test Validation of Hypersonic Systems", Neumann, 1993.

Aerodynamic models, designed for measurement accuracy rather than system performance, tend to be uniformly thick, stainless steel structures which are machined from a single piece of material. Flight structures, in contrast, are built up structures of many elements, highly nonuniform in thickness and constructed of dissimilar materials. Stainless steel is a material of known and stable thermal properties. The thickness of the model supports the idealized heat flux instrumentation and the uniformity of the material reduces the possible errors due to three-dimensionality of the conduction which would negate a one-dimensional conduction solution. The complexity of flight structures, to the contrary, is dictated by flight performance objectives which tend to limit the quality of flight heat transfer measurements.

What Is The Purpose Of A Heat Transfer Test?

All of the problems and associated sources of error to be discussed in this report can be made apparent by careful consideration of the answer to this question. The final product of any heat transfer test is the determination of whether or not a particular structure will survive or fail at the thermal conditions to which it will be subjected. The goal then is the ability to duplicate or compute real structural temperatures at real environmental conditions to be found in flight. Present-day facilities limit our ability to duplicate structural temperatures for realistic structures and long periods of time. In order to compute these temperatures we must be able to predict the amount of heat transmitted to the structure from the environment in which it is to operate. This environment may be duplicated for a brief period of time in the test facility; perhaps in the order of milliseconds. If it cannot be duplicated, the experimenter must be able to extrapolate the data obtained to the actual (real) environmental conditions. If this cannot be accomplished, the data will have no engineering value. A case in point is transitional data which is all too easy to generate but difficult to impossible to extrapolate to flight conditions.

The question then is "in the absence of structural temperature duplication, how is the heat transfer rate measured in the test facility in such a way that it can be used to compute real structural temperatures at real operating environments?" Do we want to measure the HEAT TRANSFER RATE at the model wall or do we want to measure the HEAT TRANSFER COEFFICIENT of the flow field at a specific location? There is a significant difference. The HEAT TRANSFER RATE at the model wall is a dimensional quantity and a function not only of the flowfield character but also of the model temperature, thermal properties and the structural configuration. These data cannot be used to predict the heating rate that would occur under either

different flow conditions or on another model having a different internal structure and/or thermal properties. That is, the data so generated cannot be extrapolated to real flight hardware conditions. It is "tainted" by the incidental features of the experiment and thus valid only for the duplication of particular test hardware and at the conditions of the test. The HEAT TRANSFER COEFFICIENT on the other hand is primarily a property of the flowfield. Defining the heat transfer coefficient through test as opposed to defining the heat transfer rate through test produces the correct LOCAL boundary condition from which the surface heat transfer rate can be computed for any wall temperature. A finite element conduction code, which will be discussed later in this report and which models the response of any particular wall structure, can then use this general boundary condition to predict both surface and in-depth temperatures as a function of time. Figure 2 demonstrates the relationship among the heating rate, \dot{q}_{wall} , the surface temperature, T_{wall} , and the heat transfer coefficient,

$$h = \frac{\dot{q}_{wall}}{(T_r - T_{wall})}$$

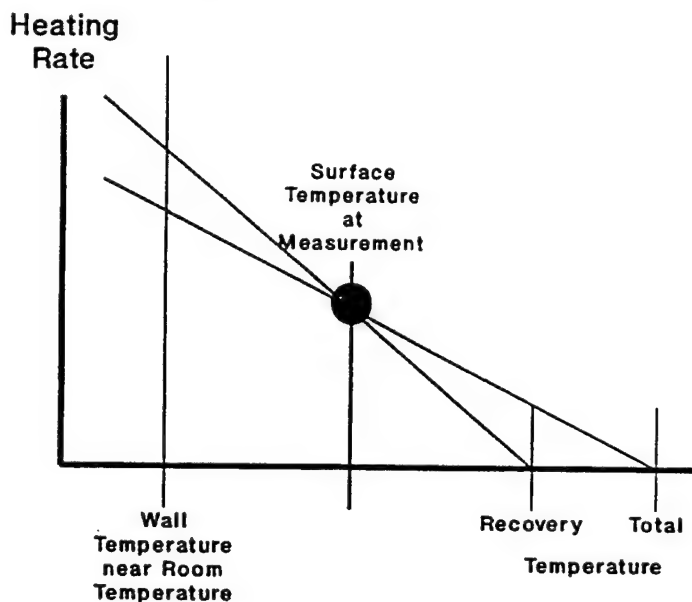


Figure 2 The Relationship Between Heating Rate, Heat Transfer Coefficient and Recovery Temperature in an Aerodynamic Heating Problem.

Obviously, the intent is to measure the heat transfer coefficient of the flow field. The only problem is that the heat transfer coefficient is not a directly measurable property. It is a definition of the local relationship between the surface heat transfer rate, the flowfield recovery temperature and the wall temperature of the model wall.

$$h = \frac{\dot{q}}{(T_R - T_w)}$$

Only the surface temperature can be measured and only the surface heating rate can be inferred from "PROPER" temperature measurements.

The question then distills down to "how do we evaluate the surface heat transfer rate in such a way that the definition of the heat transfer coefficient is valid and useful in extrapolations to flight conditions?" To answer this question we must understand that the test article and the flow field are one inter-related physical system; one affects the other. The flowfield produces aerodynamic heating at the model surface by converting the kinetic energy of the flow into thermal energy through the boundary layer deceleration. The level of this heating is dissipated both into and from the structure according to the thermal model and structural properties. This dissipation of energy determines the surface temperature history. The local surface temperature level and the surface temperature distribution, in turn, affects the boundary layer thickness which, in turn, can affect the inviscid flow field. A change in the flow field in turn changes the level of aerodynamic heating.

It would seem at first observation that no useful data can ever be obtained in a test facility which can be reliably extrapolated to conditions other than the test conditions. As in all engineering problems, there are

compromises and tradeoffs. In this case, the key is to minimize the effects of the model surface temperature on the flowfield by judicious design of the test model and its instrumentation and proper test techniques. In particular, the test article must be designed so that its surface temperature will remain as nearly isothermal as possible. The definition of the heat transfer coefficient will then be valid and useful for moderate variations in the global surface temperature.

This simple rule is difficult to implement and is the most often violated rule in the field of aerothermal instrumentation. If a gage is not thermally matched to the model wall then it not only disturbs the flowfield but also induces lateral conduction of heat between the gage and the surrounding model structure. In this case, the gage is now measuring the sum of the aerodynamic heating caused by the flowfield deceleration and that of conduction along the model surface. Unless the data reduction program can account for all modes of heat conduction (which is very difficult), the resultant data is in error.

Answering the original question then, we attempt to understand the heat transfer coefficient through the inference of the surface heating rate on an isothermal surface. No matter what type of gage is used to obtain the surface heating rate, it must be thermally matched to the model surface. If not perfectly matched then the reduction technique must at least accurately model all modes of heat transfer to and from the sensing element.

What Is A Heat Transfer Gage?

A heat transfer gage is the physical embodiment of a concept that reduces the general flow of heat into a structure to a more simplified and, hopefully, a uni-directional flow of heat and infers from that flow of heat the rate of heat transfer that caused it through strategic measurement(s) of temperature within the gage. The basic parts of such a gage are then:

1. A physical device that reduces the general flow of heat to a more simplified flow of heat hopefully, one dimensional flow.
2. A means of inferring the flow of heat through strategic measurements of temperature in the physical device.

These gages must then be both **LOCALLY WELL DESIGNED** to simplify internal heat paths and heat modes while minimizing losses (classically the heat transfer gage design problem) and **GLOBALLY WELL INTEGRATED** into the model since convective heat transfer is a function of the flow history over the model as it affects the streamline washing the gage as well as the general character of the streamline flow over the gage (converging or diverging). The instrument manufacturer is only responsible for local effects. The experimentalist is responsible for global effects.

It must be insisted that heat transfer gages be both locally well designed **AND** globally well integrated since, as it will be demonstrated, many of the "classical" errors in measuring heat flux violate one of these basic assumptions.

Why Is The Measurement Of Heat Transfer A Subject Which Changes With Time?

Why are we discussing heat transfer at all? Clearly, there are many handbooks and sales brochures which cover commercial hardware for the measurement of heat transfer. What can we learn about the measurement of heat transfer that is not in these handbooks and above all, why not just continue to measure heat transfer as it has been measured in my particular laboratory for the past decades?

Heat transfer, as with many subjects in engineering is part art and part science. The science part, the laws of heat flow and the modes of heat transfer, are well documented in textbooks and, if they develop, they develop slowly. The art part, the engineering application of this science to a particular situation or problem at hand, is not well documented. In fact, it may be totally overlooked in technical literature. Discussing the thermal measurement "art" is the purpose of this report.

There are two reasons for continually upgrading and improving the quality of measurements being taken. Those reasons are:

1. To improve the informational content of the measurement. Here we can consider improving the sensitivity of a steady state measurement to accurately evaluate lower strength signals or the development of more rapidly responding instruments to understand the higher frequency aspects of a measurement. There are two examples here. Of recent date, Bogdenoff, Dolling and others have investigated the high frequency aspects of pressure measurement - particularly for measurements in or near a separated flow region. Since most pressure transducers will not discriminate such a signal, newer instruments are required together with their associated data acquisition, conditioning, storage and analysis capabilities. As a second example, the shock tunnel experimenters have known for some time that very high frequency data from thin film transducers display the inherent characteristics of the boundary layer in which they are placed. In fact, much of the "noise" associated with such gages is, rather, the transitional behavior of the boundary layer over the gages. Conversely, there is growing understanding, to be demonstrated later, that an understanding of the boundary layer state is required. Such a merging of need and capability would require upgraded instrumentation.
2. To improve the economics of measurement. There are measurements that require substantial time to achieve. Reducing that time can reduce the cost of the measurement. Costs are reduced by either reducing "air on" test times in the acquisition of measurements or by reducing the amount of labor intensive work to reduce measurements to useful data. An example here is the use of temperature sensitive paint to "map" the heating to the surface. Such paints must be reapplied from run to run which is test-time intensive and paint data captured on photographic film are labor intensive to reduce and interpret. Similar data might be achieved using, instead, reversible coatings that require no run to run maintenance together with computer based, digital data acquisition and processing equipment that trades computer intensive efforts for labor intensive efforts. These newer mapping techniques, with the aid of VERY cost effective computers, can be handled much more effectively than reading photographs.

As a second example, thin skin heat transfer "gages" were used for decades to achieve point measurements of heating. These devices allowed the generation of a single test condition during a tunnel run. Newer gages of a different design allow the generation of an entire spectrum of data during the same tunnel run. Tunnel

operating costs are thus reduced and data quality is increased through the use of newer gages and their associated computer data manipulation techniques.

What's The Difference Between...

To further introduce the topic of aerothermal instrumentation, the following paragraphs describe several similar physical situations which will be used to introduce concepts which will be discussed later in this report.

Figure 3 indicates two gages in which metallic films are wrapped around the cylinder as shown. On the left, the film is Platinum, only one material. On the right, the film consists of two "dissimilar" materials, Platinum and a mixture of Platinum and Rhodium. What's the difference? These two figures demonstrate two completely different ways of inferring temperature. On the left is a resistance thermometer which measures the relationship between electrical resistance and temperature in the Platinum film. It employs a powered metallic film (platinum in our example) and a bridge circuit to measure the out of balance resistance of the Platinum with increasing temperature. Through pre-test calibration, the relationship between resistance and temperature is established. On the right is a standard thermocouple in which, at the junction of the two dissimilar materials, an EMF is set up which is proportional to temperature according to standards. A sensitive voltmeter is used to measure this induced EMF and from that measurement to infer temperature. Further, for the resistance calorimeter, the gage is powered by a regulated current to produce a resistance. The heat generated by this current flow must be far less than the aerodynamic heating to be measured. The thermocouple, on the other hand, is not powered but "transduces" temperature into EMF to be measured. Both measurements are the basis of instrumentation used in test facilities and will be discussed later in the report.

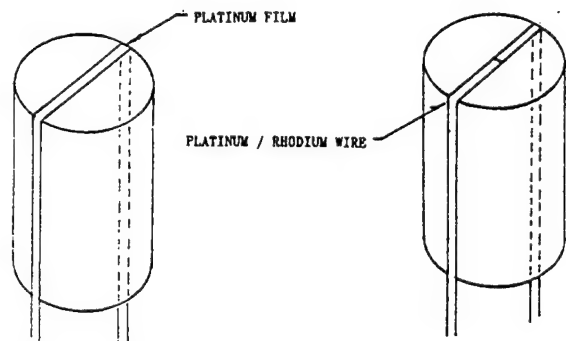


Figure 3 Comparison of a Thin Film Resistance Calorimeter and an Isothermal Thermocouple Gage.

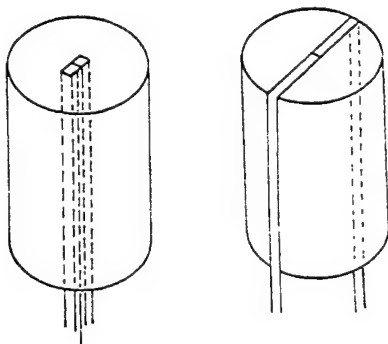


Figure 4 Comparison of a Bayonet Gage and an Isothermal Thermocouple Gage.

Figure 4 indicates two gages, each of which employs a type K thermocouple around a cylinder constructed of insulative material. Both junctions are on the surface. On the left, the wires are immediately drawn back from the surface. On the right, the wires draw away from the junction on the surface for a distance. What's the difference? Metallic wires have very different thermal response properties than insulators. These differences create heat flows along the wires that are unwanted and detrimental. The gage on the left will experience severe conduction losses away from the junction due to conductive heat removal down the wires. The gage on the right is an "isothermal staple gage" in which the heat

removal at the junction is minimized through holding the wires at an isothermal surface temperature (assumed constant in the vicinity of the gage juncture).

Figure 5 shows a coaxial thermocouple arrangement inset into a model material. Coaxial thermocouples are those created by a wire of one thermocouple material inside a cylinder of the second thermocouple material with a proper electrical insulation between the two along the axis of their juncture. What's the difference? The question posed by this figure refers to the difference brought about by the material in which the coaxial thermocouple is placed. On the left, the thermocouple is placed in an insulator while on the right it is placed in stainless steel which closely matches the characteristics of the Chromel/Constantan thermocouple.

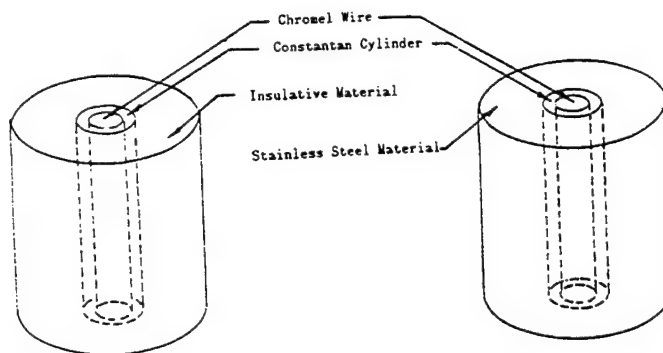


Figure 5 Comparison of a Co-axial Thermocouple Gage Installed in an Insulative and a Conductive Model Surface.

The difference is the installation. Instrumentation must be matched to the material on which it is measuring temperature. Installing the conductive coaxial gage within an insulator creates a heat sink and disturbs the thermal environment of the insulator. The gage, because of its higher heat conductivity and thus lower temperature, draws heat from the surrounding structure yielding an incorrect measurement. Further, the boundary layer is thermally disturbed by the non-isothermal wall created at the surface. The same gage installed in a material which matches the characteristics of the gage generates excellent data and is a contemporary high performance gage which we shall discuss later in these notes.

The point from this figure is that instrumentation must be matched to the materials in which it is introduced.

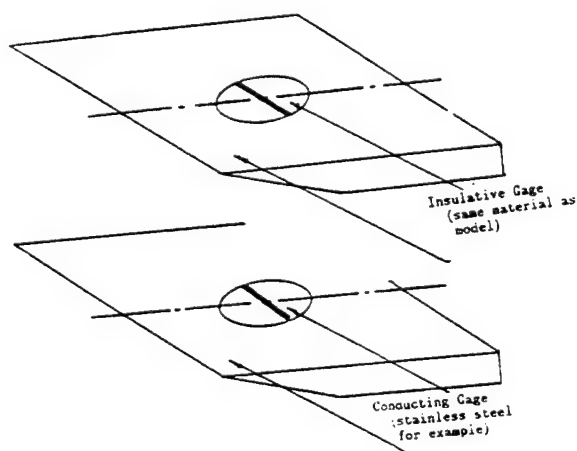


Figure 6 Comparison of a Conductive and Insulative Thermal Gage Installed in an Insulative Model.

Figure 6 indicates a flat plate model instrumented by a simple heat gage created by a thermocouple junction on the surface of a "plug". The plug material may be either insulative or conducting (steel or pyrex) but, in both cases, the model is an insulator. The difference in this set of figures is that, again, temperature changes are caused on the surface of the model when materials are changed. The model on top is well instrumented and boundary layer distortion is minimized. The model below that is an extreme example of the problems discussed in the previous set of figures. The heat sink gage will create a serious non-isothermal wall problem which will destroy the validity of the measurement. Non-isothermal wall effects are serious! Who would ever consider such an instrumentation arrangement as the one on the right? The Space Shuttle had this exact type of instrumentation on the Orbiter upper surfaces

and on the External Tank, ET of the system. Those data were invalid. We will discuss this phenomena of non-isothermal walls later in this report.

Conceptual Methods Of Measuring Heat Flux

Thompson, 1981 prepared an excellent and concise review of heat transfer gages. In that review, he listed three conceptual methods for "measuring" heat flux. They are:

1. Heat flux may be related to the temperature gradient set up in a thin material layer. These were termed "sandwich" or gradient-type heat flux gages.
2. Heat may be captured within a thermal mass which acts as a calorimeter or semi-infinite slab in which transient temperature change can be related to heat flux and in which boundaries do not respond to the imposed heating.
3. A heat balance in steady state may be established between incoming aerodynamic heating and a calibrated heat removal process.

These conceptual methods of inferring heat flux should be kept in mind as we look at the many ways in which heat flux is measured.

The reader is cautioned that, although these categories represent fundamentally different methods for "generating" aerodynamic heating information, there is not a unique relationship between the methods stated and their physical embodiment in a gage. The same physical gage, as for instance a wafer of material with a thermocouple attached to both the heated and backface surfaces, can be used to "measure" heat flux by any of the three stated methods. The method that should be used depends on the relationship between thermal diffusion time and test time. Test time is an important consideration in thermal flux measurement.

Clearly, the gage shown in Figure 7 is a "sandwich gage"; Thompson's category 1. However, if the material properties are such that the heat does not diffuse to the backface surface within the test duration, the backface thermal sensor is not responsive and the gage becomes one in which the thermal pulse is "captured" within the material mass. This is a Thompson category 2 gage and an example of it is a thin film gage. If the wafer of material is very thin and has high conductivity, the heated and backface temperatures will be the same (after a very short transition period due to thermal diffusion). The use of either thermocouple (the backface thermocouple is easier to use) will give rise to a calorimeter known as a thin skin gage. This is also a Thompson class 2 gage. Finally, if the backface of the wafer is heated or cooled with an active energy source (water or a Nichrome heater for instance), then this same device becomes a Thompson class 3 gage.

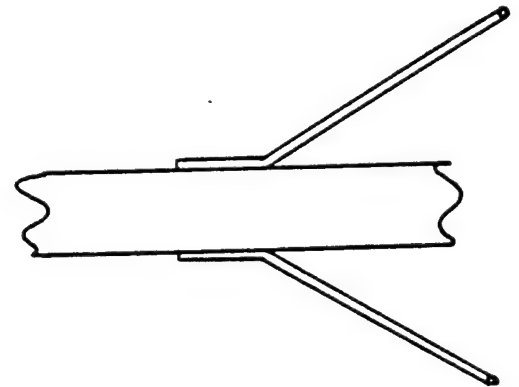


Figure 7 Conceptual Thermal Measurement Technique Using Physical Sensors.

Further examples of the non-uniqueness of instrumentation will be presented throughout the body of this report as the different gage concepts are introduced. The devices which will be discussed are designed

through BOTH various concepts of thermal models AND an appreciation of the limits of that thermal model with thermal diffusion time.

Test Duration And Model Construction Can Make Instrumentation Difficult If Not Impossible

Not every fabricated structure can be instrumented. Not every instrumented structure can be tested in an arbitrary manner and not every test is designed to generate the same quality data or even the same type of data. Understanding the true purposes of an experiment and matching the purposes of an experiment to the test facility and test instrumentation suited to that test facility is an important aspect of developing a heat transfer test program.

"Heat Transfer" is a study that integrates the fluid mechanics of heat production in the boundary layer with structural dissipation of that heat through a structure that may be actively cooled. As a result, at least two distinct groups of engineers, fluid mechanicians and structural engineers (with diverse backgrounds and differing goals and objectives) meet on this subject. Fluid mechanics has developed with a series of similarity parameters which allows experimental development to occur on small-scale geometric models in aerodynamic test facilities which need not duplicate (even if they could) all of the characteristics of the flight article. Structural verification focuses on the suitability of full scale and fully representative flight hardware to representative heat loads not necessarily in aerodynamic facilities. Both are valid reasons to test and each may be termed a heat transfer test but each represents a very different problem in test program development. Some of these issues are depicted in Table 1.

TABLE 1
TESTING ISSUES FROM BOTH AN AERODYNAMIC
AND STRUCTURAL PERSPECTIVE

Issue	Fluid Mechanics Perspective	Structural Perspective
Test Duration	Short durations are acceptable and preferred. 1-5 ms is an acceptable test duration.	Structural panel "soak" is required. Longer test durations are required. Minutes of test time are acceptable.
Thermal Instrumentation	Isothermal model structures allow instrument technology based on crystal deformation and heat transfer based on resistance thermometry. Temperature sensitive instruments can be used since the structure is isothermal.	High temperature structures with thermal gradients along and through the structure requires the use of specifically designed thermocouple based thermal instruments. Pressures measured with thermal compensation. Skin friction is tough. Strain measurements required.
Model Structure	Dictated by aerodynamic loads and constrained thermal dissipation. Test objectives dictate model materials not flight considerations.	Dictated by temperature and aerodynamic loads. Thermal dissipation characteristics must match intended flight application.
Instrumentation Issues	Enforcing a 1D thermal model for thermal instrumentation.	Measuring in-depth temperatures with high temperature dissipation modes.
Model Hardware Sophistication	Simple structures; near uniform material systems of known properties.	Complex structures; built-up multi-material systems.

The Influence Of Wind Tunnel Test Facilities On Instrumentation

The selection of aerothermal instrumentation is strongly influenced by the nature of the wind tunnel model, the type and quality of data required and the characteristics of the test facility employed. These factors require some attention before we can start to understand the types of instrumentation required.

The Nature Of The Wind Tunnel Model:

Historically, wind tunnel models were constructed of materials adequate to the test environment and simple enough not to be the focus of the experiment itself. The materials of aerothermal wind tunnel models were classically either metallic systems based on stainless steel or insulative systems. The principle characteristic of the models being that the materials and construction techniques were established as reliable. In particular, thermal properties of the selected material systems were to be well known and standardized so as not to vary from batch-to-batch.

Recently, the concept of "aero-structural" models was introduced. Models in this form of testing are actual structural elements of a proposed design with actual structural materials employed. The use of these actual aircraft elements complicates the instrumentation and test issues; not only are these material systems less well characterized but the type of testing conducted elevates the temperature to the point where radiation is an important heat flux mode and the built-up nature of the material systems creates very complex thermal dissipation paths that make instrumentation difficult. This type of testing will be discussed later in the report.

Type And Quality Of Data Required:

There are several reasons for conducting aerothermal experiments and each requires a level of instrumentation somewhat different from the others. The reasons for testing are:

1. The development and validation of unit physical "models" such as Reynolds analogy.
2. The understanding of the deviation of actual flow from established and normally closed form analytical models of flow such as how the actual Space Shuttle body deviates from ideal cone flow.
3. The "validation" of numerical computations such as the evaluation of many flow models working together within the framework of the Navier Stokes equation set.

Over the past 25 years most of the testing which has been conducted has been to understand the deviation of the actual flow over a complex, three dimensional body from simplified flow models which were amenable to closed form solution. This technique reached its ultimate application in the design of the Rockwell Space Shuttle where the most extensive wind tunnel data base of all time was established. The primary intent of this data base was to "correct" simplified analysis techniques based on closed form solutions about cones, cylinders and plates to account for three-dimensional effects that were not defined through the simplified solutions. This "effect" testing required substantial numbers of heat transfer measurements supported by far fewer measurements of other flow field quantities. It is termed "effect testing" because the intent is to observe the effect rather than to understand the cause of that effect.

In the same general time interval (although extending back to the late 1930's) there has also been a smaller and far more detailed effort to define and validate conceptual models of the flow. These models, such as turbulence models, reference temperature models, real gas flow models, definitions of Reynolds analogy factors and adiabatic wall temperatures to name a few were developed from empirical data of extremely high quality using far more detailed "cause and effect" instrumentation. Such instrumentation is necessarily of higher quality and more complete categorizing both the cause and its effect.

The "validation" of numerical codes is a newer and still a largely ill-defined use of experimentation. While such testing is discussed with increasing urgency of recent date, the design of such experiments, the necessary instrumentation and the underlying test philosophy are still less well defined features of such testing. In general, there will be a need for far more detailed data, higher volumes of high quality data and the acquisition of far more complex measurements which stress cause and effect relationships in any flowfield.

The Characteristics Of Aerothermodynamic Test Facilities

There is a strong and emotional interrelationship between instrumentation and the basic characteristics of aerothermodynamic test facilities. These facilities and their differentiating characteristics are a discussion in themselves. From an instrumentation standpoint, the differentiating characteristics of these facilities are (1) the duration of the test and (2) the level of heating rate achieved during the test.

Test Duration:

Current and anticipated wind tunnel facilities operate or will operate from hundreds of microseconds to many minutes per run. Aerothermal instrumentation problems with regard to this spectrum of facilities range from questions regarding the practicality of making ANY measurement in the very short run time test facilities to problems of making accurate measurements during very long duration tests of actual flight hardware. Both ends of the time spectrum represent challenging technological problems to the experimentalist. Both require an openness to new as well as recycled instrumentation hardware, acquisition techniques and analysis techniques.

Increased Test Duration Is Not Always Good

There are several reasons why increased test duration is not of value in a hypersonic test facility. Several of these reasons deal with the interaction between instrumentation and the test facility characteristics. Consider the following:

1. Model temperatures increase as the test duration increases. They create un-anticipated and unmeasured thermal paths in the instrumentation due to conduction along or normal to the measurement skin and they may either thermally deform or melt the model.

2. Model aerodynamic heating increases surface temperature non-uniformly producing surfaces which are no longer isothermal. Nonisothermal surfaces distort the boundary layer and distorted boundary layers change the heat transfer in several ways.
3. There are several instrumentation techniques which are as sensitive to the desired measurement of temperature as they are to other sensed quantities extraneous to the experiment. These techniques are based, for instance, on the piezo-electric effect. These techniques require that the gage temperature not vary substantially during test. Extended test durations violate that requirement. As an example of this, it is interesting to note that local skin friction can be routinely measured in a shock tunnel using a crystal deformation technique but it is far more difficult to measure in a continuous flow test facility where that same technique would fail due to the thermal sensitivity of the crystal.
4. Measurements are not made during consistent test times. Heat transfer measurements are made as fast as possible and normally within 2 seconds of injection. Pressure measurements may require somewhat longer time and force and moment measurements are normally made with the model held in the tunnel for extended periods of time. For a heated test facility, the surface temperature of the model can vary by hundreds of degrees between these complimentary measurements. The ratio of wall to total temperature, which is varied, is a sensitive indicator of phenomena like separation (and perhaps separated upper surface flows). It is possible that under this test scenario one set of measurements would be conducted with control surface-induced separation (the pressures and force and moment data) while another set of data would be conducted with no corresponding flow separation because of the gross differences in the ratio of the wall to total temperature between the two sets of data.

Test Economics

Perhaps a decade ago the entire subject of test economics would never have been considered. Certainly the question is a second generation question following ...can heat transfer be measured at all? The newer test facilities exemplified by the development of Tunnel 9 at the Naval Surface Weapons Center are very expensive in which to conduct experimentation; typically \$20,000 per one second run, and requires attention to efficient use of the test flow. How much can be accomplished in a one second run?

The continuous flow facilities at the Arnold Engineering Development Center, AEDC, represent another "opportunity" for creative instrumentation based upon the existing test economics. These facilities operate continuously for an entire test shift. Even a casual observer will be aware that more than 90% of the airflow time in these continuous flow facilities is not used during the aerothermodynamic tests because there is no model in the test section. At \$10,000 per hour, these testing inefficiencies must be addressed in the instrumentation. A study of testing trends at AEDC indicate that substantial contributors to wasted airflow time is the physical manipulation of the model during the test process and thermal cycling (cooling) of tested models. Gaining access to the model can cost 10 minutes of airflow time each time. During one typical test entry under the Space Shuttle program \$40,000 was consumed just changing the control deflections on the model manually. Newer instrumentation and model design concepts can dramatically reduce that cost. There are direct implications here for automated model changes; the use of motor driven control surfaces rather than manually changed control surfaces and alternative test techniques; the use of reversible temperature

indicating coatings rather than irreversible coatings. These newer techniques are driven by economic rather than technical considerations. These are replacement techniques which reduce the overall cost of test operations and increase test efficiency.

Non-Isothermal Wall Effects

The fundamental requirements for the successful measurement of aerodynamic heating in either a ground test facility or in flight are that the experimenter (1) properly locate thermal sensors in the structure of the model such that heat flux may be deduced through the application of thermal models and (2) that these measurements be made so that the material does not know there is a thermal sensor installed. The second criterion implies, in part, that the model under consideration have no local disruption of the thermal boundary layer due to the presence of a gage. The model must be isothermal in so far as possible and that is the discussion of this section of the report. Figure 8 from Schultz, 1965, indicates graphically the effects of placing poorly designed gages into wind tunnel models.

Many authors throughout the years have stressed the need for isothermal surfaces and yet again and again this criterion is violated and, as a result, poor data are generated. The non-isothermal effect itself when instrumentation is involved has several unrelated aspects that must be considered. Non-isothermal surfaces can be caused either by poorly integrated instrumentation (normally the use of off the shelf gages that are thermally far different from the model in which they are placed) or by models fabricated of dissimilar materials or having dissimilar physical characteristics in the same material. Examples include the fabrication of a model from insulative materials except in the nose where, for thermal reasons, the model has a steel nosecap or the model may be fabricated entirely of stainless steel wherein the nose is solid and aft of the nose it is of thin skin construction for heat transfer measurements.

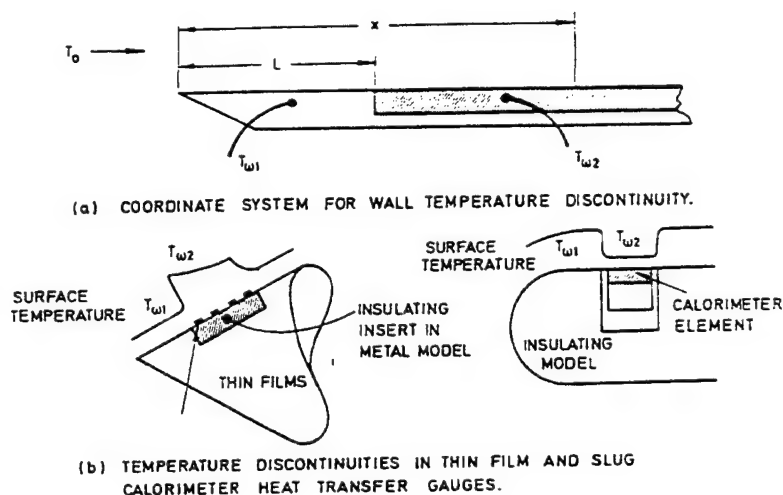


Figure 8 Examples of Models and Instrumentation Producing Non-Isothermal Wall Effects.

While we cannot and must not divorce the design of the model from its instrumentation, let us focus for a moment on the incorrect instrumentation of heat transfer models with gages which are poorly integrated into the structure. Such gages generate incorrect heat flux because of two aspects of the mismatch. First, the installed gage creates either a heat sink or hot spot on the surface of the model which distorts the boundary layer and generates a different heating rate over the gage and second, the installed gage exchanges heat with the surrounding model, either drawing in heat or giving it up in a manner not considered by the thermal model defined by the instrument.

The classic example of this is the installation of heat sink instrumentation in the insulative structure of the Space Shuttle external tank. The error in the measured heating rate caused by this mismatch in surface temperatures was a factor of 2! Similarly, poorly matched gages have been routinely installed in insulative wind tunnel models to aid in the calibration of some survey technique for measuring heat flux. These data were grossly in error as the temperature difference between the insulator and the gage increased.

There are numerical correction techniques available for the evaluation of measured heat flux under non-isothermal conditions. These techniques are referenced at the end of this section. All of these techniques require knowledge of the streamline history of the flow which, for a general body, may be difficult to accurately determine. Correspondingly, these effects increase in severity with test time and imposed heating rates in the vicinity of the gage. It is possible that rapid data acquisition may reduce these effects. The reader is encouraged to carefully design the model and integrate the instrumentation so that problems of this type do not occur in the first place.

The problem occurs because off the shelf instrumentation is applied without an understanding of integration problems. Instrument manufacturers are not concerned with the installed performance of their device; their concern is with the design of a self contained and properly sensed local thermal model that can be screwed or potted into whatever you choose. It is the experimenter who must be aware of the integration problem. A wide variety of instrumentation exists and has been validated for use which integrates well into the structure of the wind tunnel model contemplated. Proper selection of that instrumentation will reduce the difficulties of non-isothermal wall effects.

Isothermality of the test model is important from both the structural and fluid mechanic aspects: First, an isothermal surface assures that there is no unwanted conduction of heat to or from the heat gage that would confuse the evaluation of heat transfer. Second, an isothermal surface assures that the boundary layer over the surface is not distorted by surface temperature distributions along the surface. A corollary to the second point is that an isothermal wall produces a numerical boundary condition simple enough for the numeriscists to incorporate into their computations.

Figure 9 from a recent paper by Consigny, 1993 demonstrates the substantial perturbation of the heat transfer coefficient that occurs due to a change of material in a Mach 5 wind tunnel. The computation was produced using a nonsimilar boundary layer code.

The temperature perturbation, as in the case above, may be caused by a change of materials or it may be caused by a highly nonuniform heating rate over the surface of the model. Collier, 1990, evaluated the heat transfer ahead of a cylindrical protuberance attached to a blunted cone. The model is shown in Figure

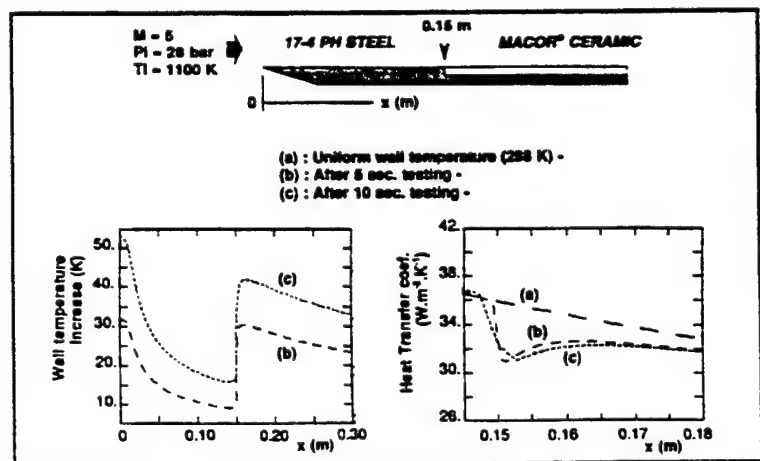


Figure 9 Thermal Perturbation Caused by Non-Isothermal Surfaces after Consigny, 1992

10. Within one second, the surface temperature of this model changed from isothermal to highly disturbed as shown in Figure 11.

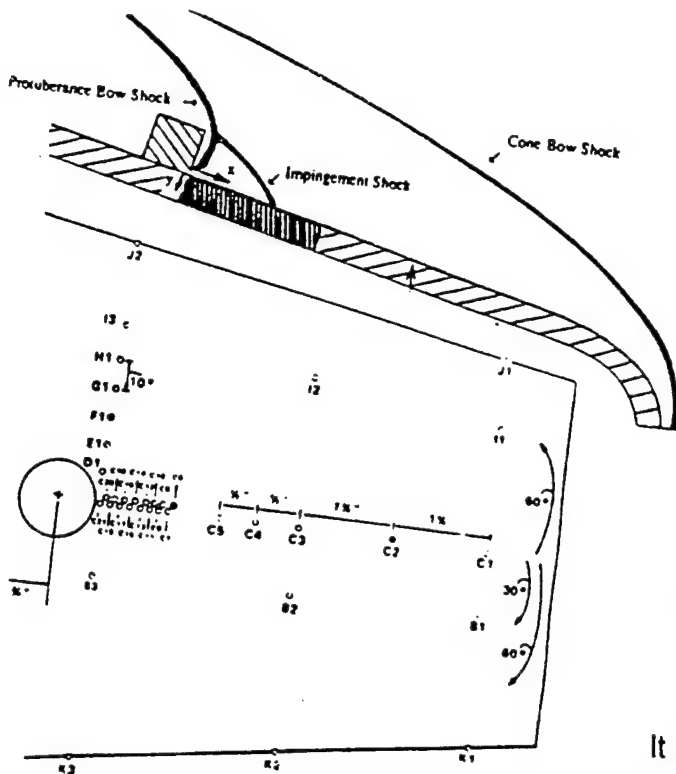


Figure 10 The Physical test Model Used by Collier, 1990, to Evaluate Shock Interaction with Coax Gages.

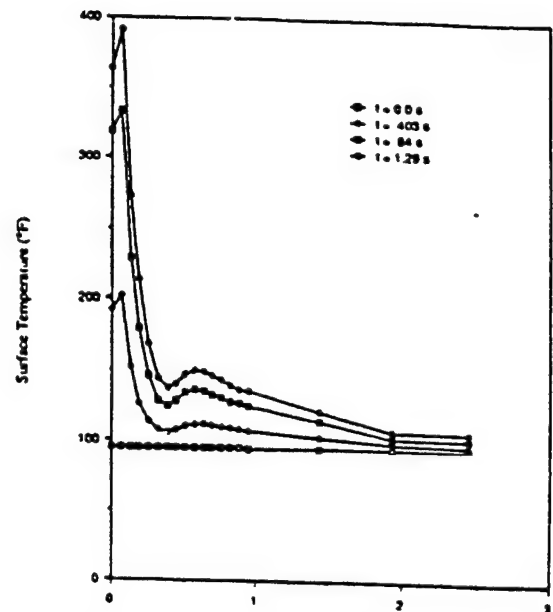


Figure 11 The Surface Temperatures measured by the Coax Gages Located In the Collier Shock Interaction Model.

It has been shown in Figure 11 that instrumentation can be quite sensitive to the effects of nonisothermality and there is a serious question whether any of these data are correct. The points to be made in this introduction is that (1) there are few surfaces that are isothermal. Material changes and nonuniform heating create substantial temperature differences across the surface of the model, (2) nonisothermality has two consequences; one within the material itself creating unwanted and unanticipated heat paths and the second within the boundary layer generating distorted boundary layer growth and temperature gradients within the boundary layer. and (3) that nonisothermality complicates the use of the heat flux data introducing several incidental features of the test that must be retained with the experiment and modelled in the comparison process.

Test Incidental Features

There are several incidental features to a heat transfer test that must either be reported and respected or designed out of the experiment. Among these are the materials of which the model is constructed; the properties of those materials, the design of the model in which the data is taken and the surface temperature distribution of the model at the time the data were generated. In many cases, these incidental features are designed out of the model. In others, little is said of the features which may have a first-order impact on the measured result.

There are no truly isothermal test surfaces once that surface is heated differentially. This statement is true for shock tube flows as for long duration heated flows. The key is to continue questioning the relative

SECTION II THERMAL MODELS

INTRODUCTION

Thermal models are mathematical representations of the flow of heat within media. In the present context, these thermal models are the response of the physical wind tunnel model to the imposed heat flow and the dissipation of that heat flow within the model and back into space. While in general these mechanisms can include the effects of thermal radiation, either externally from the model surface or internally within the model, in many wind tunnel applications, radiation may be ignored and we are left with a balance between the convective heat input and the conductive dissipation of that heat throughout the structure.

Thermal models may be either closed-form, analytical equations (for restrictive cases) or they may be numerical in nature where the structure is modelled by small elements of geometry that are free to communicate with each other according to the laws of heat flow. Models may also be direct in that the thermal dissipation of a known heat input is desired or they may be inverse in that, given a description of the temperature profile within a structure at a given time, the heating rate that caused that distribution is desired. Those interested in the structural dissipation of aerodynamic heating apply the direct method to problems and those interested in the design of aerodynamic heating instrumentation apply the inverse techniques.

The goal of aerothermal instrumentation is to reduce the general problem of three modes of heat transfer operative in the three principal coordinates to a far simpler system in which one dimensional flow of a single mode of heat transfer is allowed and that mode for our study will be conduction through the structure. Each and every successful heat gage is based on a model of heat flow that accomplishes that single task. Similarly, this document discusses simple thermal models and the gages that try to mimic them.

In the limit of tests for long time periods (including the process of flight testing) it is not always possible to create and install an aerothermal gage which mimics a simple thermal model. In these cases, the inference of heating rates from imbedded temperatures will require the application of a more complex numerical thermal model in which actual structure in all its complexities of three dimensional flow of all modes of heat transfer will be modelled. While flight test is not an issue in this report, the design of test articles for structural proof testing will be covered. This class of testing will exhibit the same problems and testing issues as those in flight.

It is shown in Figure 12 that several modes of heat transfer occur simultaneously on any surface exposed to aerodynamic heating. These general problems of heat dissipation can be solved by finite element numerical techniques. The method of solution begins by dividing the structure into a set of small elements among which heat can be exchange. It is assumed that the mass of each element is concentrated at a node in the center of that thermal properties of the conductor depend on the properties of the adjoining elements and its cross-sectional area is equal to the surface area between the elements.

The thermodynamics of each element can be written as:

where:

\dot{q}_{NET} is the heat absorbed by a node

\dot{q}_{INTO} is the heat conducted into a node from surrounding nodes

\dot{q}_{EXT} is the net heat transferred into a node from external sources

\dot{q}_{OUT} is the heat conducted into the surrounding nodes

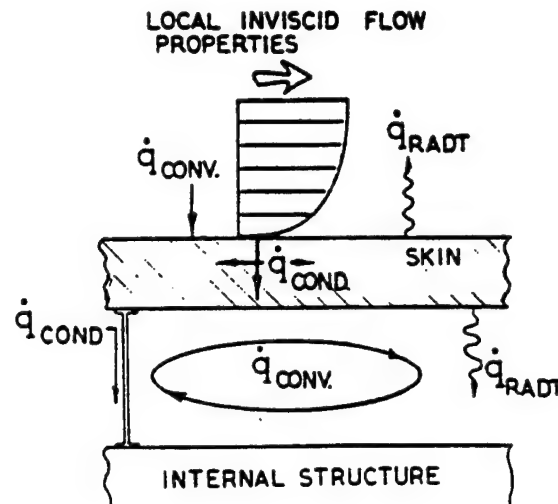


Figure 12 Possible Modes of Heat Transfer on a Structure.

In a typical case, \dot{q}_{EXT} is the net difference between the heat convected into and radiating away from a surface node. This value is usually zero for sub-surface elements.

Since \dot{q}_{NET} is absorbed by the node, the rate of heat transfer can be written:

$$\dot{q}_{NET} = mC_p(dT/dt)$$

If a forward difference method is applied to this equation and it is assumed that the heat transfer at the beginning of a time interval is constant during that interval of time, then the temperature change can be written as:

$$\Delta T = \left(\frac{\dot{q}_{NET}}{mC_p} \right) \Delta t$$

In calculating the terms in \dot{q}_{NET} the various paths joining the nodes are treated as thermal conductors. The quantity "thermal conductance" has been used to define the term which makes the following relation valid:

$$\dot{q} = -KA\left(\frac{\partial T}{\partial x_i}\right)$$

where T is the temperature difference between adjacent nodes and q is the heat transfer between them. The thermal conductance for conduction problems is defined as:

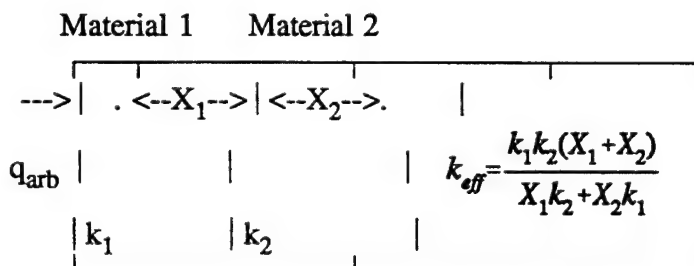
$$K = (k A/x)$$

where:

k is the effective thermal conductivity of the conductor
A is the cross-sectional area of the conductor
x is the length of the conductor

In most cases, the effective conductivity is that of the nodal material. However, in special cases of a conductor connecting nodes of different materials, the effective properties must be determined. The thermal conductance is the reciprocal of the thermal resistance which can be linearly summed across a series of resistors.

As an example, the effective thermal conductance for two dissimilar nodes shown below is found to be:



With these relations defined, the heat transmitted between each element and its neighbors is computed for small time increments. The resulting change in temperature of each node is then computed and the process is repeated. In this way the internal temperature history of a structure can be determined from a known and externally applied heat transfer distribution. The same method can be applied in reverse. If the temperature history of a set of internal nodes is known through measurements then the external heating rate causing these internal temperatures can be computed.

A contemporary example of thermal model analysis is found in Figure 13 where the influence of edge effects on a recessed thin skin surface is evaluated.

The importance of thermal modeling was also clearly stated by Hayes and Rougeux, 1991, where they demonstrated that sub-surface model structure can dominate the output of thermal sensors and the data reduction techniques to be used to infer heat flux data.

The model, shown in Figure 14 was an axisymmetric cone/flare configuration tested at low angles of attack in a Mach 12 flow. The reduced heat flux data, shown in Figure 15, was not constant with test time. It was observed that the internal structure of the heat transfer model was not symmetric (even though the external lines were symmetric). Figure 14 also shows the offset instrumentation access hole drilled along the axis of the model. Once the physical structure of the model was known and thermally modelled; the "simulated data", computed using the more complete 2D thermal analysis tools, demonstrated the same features as the actual wind tunnel data when reduced using standard, 1D techniques as shown in Figure 16.

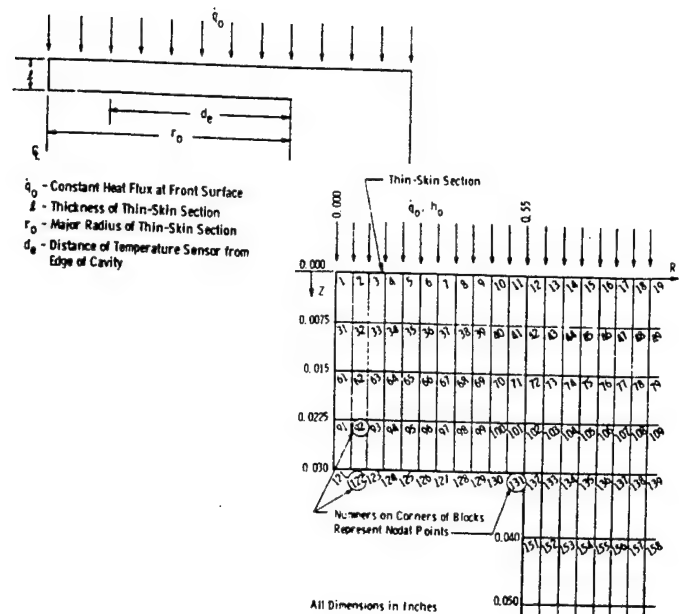


Figure 13 Example of a Thermal Model of a Structural Element after Kidd, 1989.

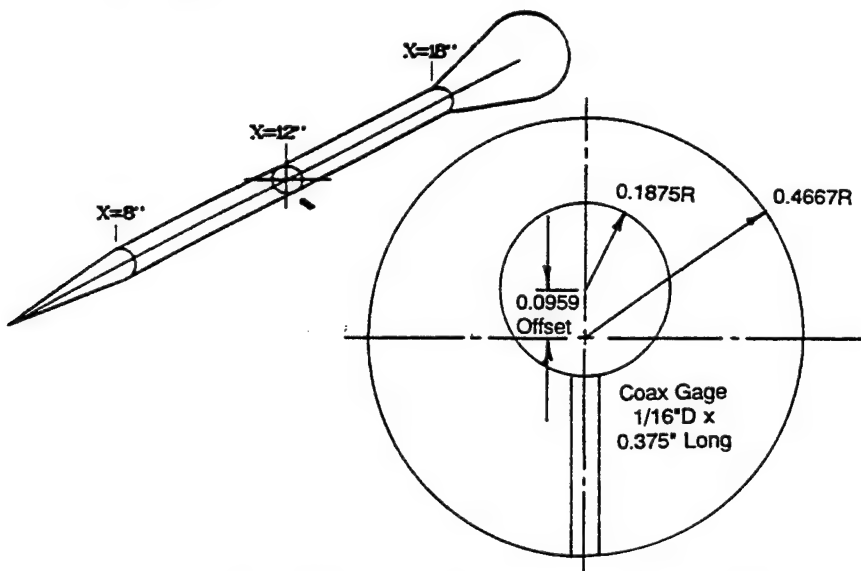


Figure 14 Slender Cone/Cylinder/Flare Model Including the Internal Structure of the Model.

The physical reason for the wind tunnel data changing with time was that lateral conduction was set up in the wind tunnel model due to the non-symmetrical, internal structure. That lateral conduction, plotted in Figure 17, was greatest on the lower surface of the model and increased in magnitude with test time as the differential temperature of the model increased. lateral conduction effects were present both at zero angle of attack and at angles of attack. For all angles of attack the non-uniform wall thickness created lateral conduction. With

increasing angle of attack the non-uniform heating about the body further increased that lateral conduction.

Early modeling of the test geometry would have demonstrated the problem and suggested alternative approaches to the physical model design and fabrication to foster designs capable of acquiring data that can be efficiently reduced. The modelling software for such a project is available from several sources.

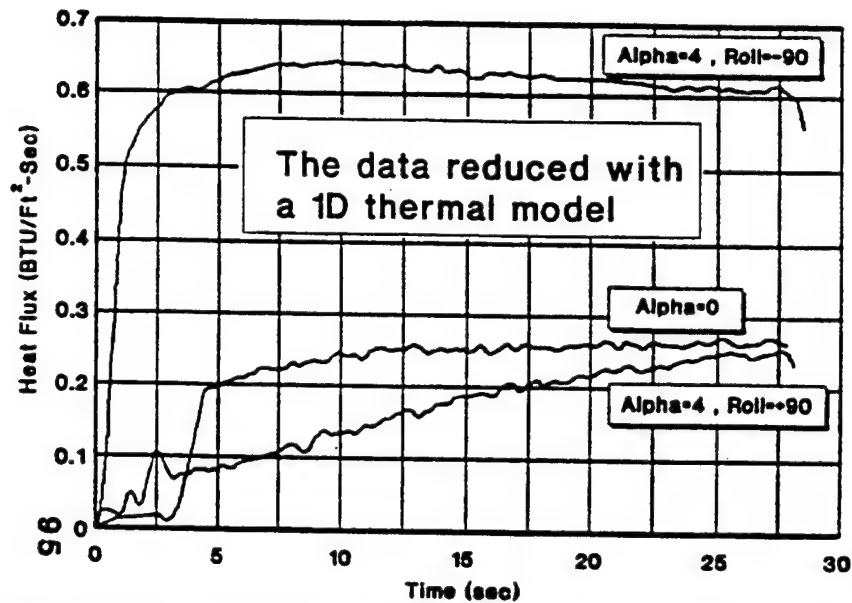


Figure 15 Heat Flux Data from the Model Shown in Figure 14 Reduced Using 1D Methods.

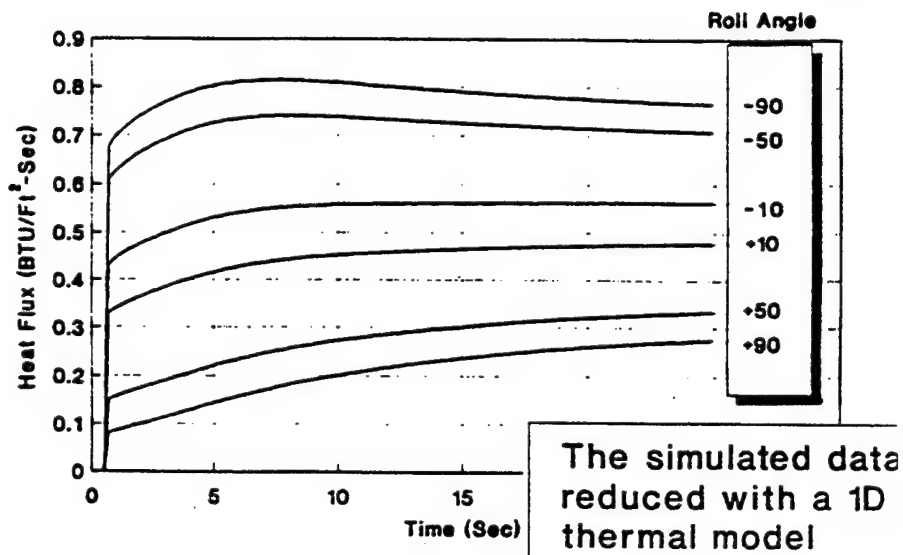


Figure 16 Simulated "Data" Using the Actual Model Structure and 2D Reduction Methods.

The TOPAZ and IHCP2D codes are available for direct and inverse modelling applications respectively. These codes will fit on a PC and can be run quite efficiently.

Thermal modeling can also be used after the test as an aid in data analysis and correlation. While multi-dimensional inverse modeling to deduce heat flux from sensed temperatures is computer-intensive, the use of direct modeling techniques to define the temperatures caused by a defined heating rate are not. Correction factors can be generated by developing a series of direct modeling solutions to define material temperature and then using simplified, 1D thermal model techniques to compare the reduced temperature data back to heating rates. This was accomplished, for example, in the correction of thin film data on small radius cylinders in long duration test facilities.

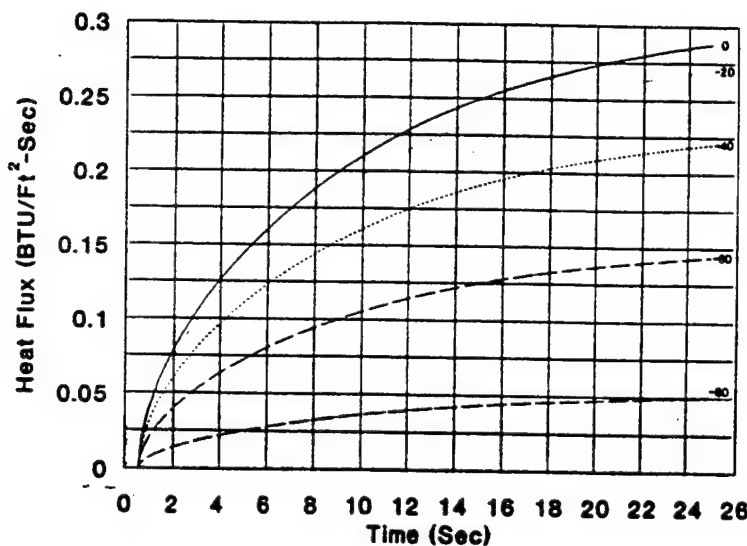


Figure 17 The Lateral Heat Conduction.

the structure. The difference between the input heating rate and the reduced heating rate creates a "correction factor" which can be applied to actual data. This is an efficient manner of correcting data using an interaction between experimentation and numerical thermal models.

Figure 18 graphically outlines the process of data correction using multi-dimensional thermal models. The physical model was a small leading edge to which were attached several thin film resistance thermometers. In normal, milli-second operation, the 1D, simplified analysis of the heating rate from measured temperatures would be satisfactory. This test, however, was in a blowdown facility operating for "seconds" rather than "milliseconds". The technique, as demonstrated, was to create a thermal model of the leading edge and compute what the thermal sensor would feel from the known, input heating rate distribution. Such a computation allows for the two-dimensional diffusion of heat through and along the model structure. These "synthesized data" would then be reduced to heating rate data ASSUMING that the flow of heat was one-dimensional into

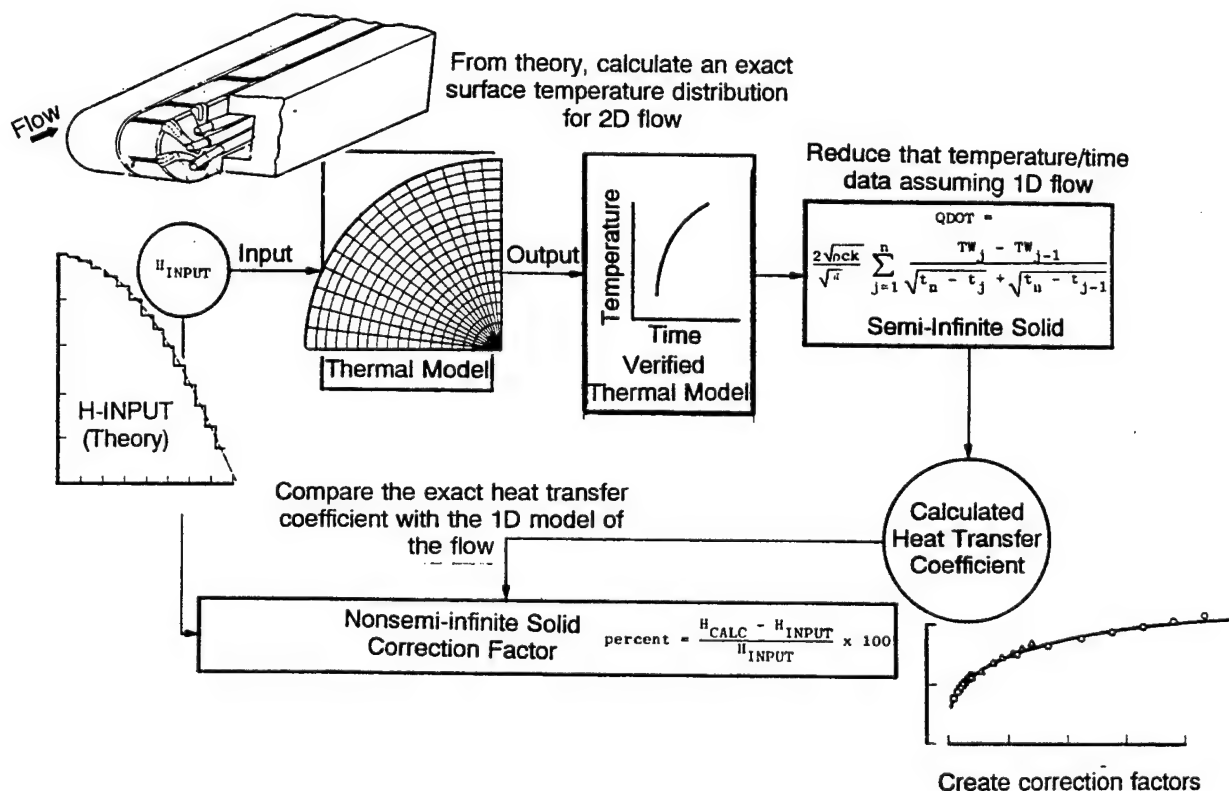


Figure 18 Data Correction for Non-Classical Heating Using 2D Conduction Methods.

Consigny, 1992 also demonstrated the importance of thermal modeling when evaluating the effects that a material change has in model surface temperatures. Figure 9 from his report, presented in Section I, indicates that the insulative qualities of a Macor (R) insert located in a stainless steel model can increase the surface temperature of that model substantially.

This example demonstrates that not only is the surface temperature perturbed but also the heat transfer into the structure of the model. The example reinforces the premise that a non-isothermal wall distorts the boundary layer over that wall. Boundary layer distortion and its affects on heat transfer must be addressed by modeling tools which treat the boundary layer flow in a non-similar manner. This can be achieved either through use of the Navier Stokes equation solvers directly or through the use of a non-similar boundary layer solver, such as the BLIMP code. The BLIMP code has a proven record of successful applications to instrumentation problems over the past 20 years and is recommended as an efficient computational tool for these problems.

SECTION III SEMI-INFINITE SLAB THERMAL MODEL

INTRODUCTION

The semi-infinite slab thermal model referred to by Thompson, 1981, as a gage which "captures" heat within the thermal mass is the most widely used thermal model for the inference of aerodynamic heating. Notwithstanding the continued use of the thin skin model in continuous and blowdown wind tunnels, the semi-infinite slab thermal model is the basis of many flight measurements, all of the survey techniques involving paint, reversible coatings and IR radiation as well as the thin film gages used in some shock tunnels. This same thermal model is adaptable to instrumentation requirements in millisecond shock tunnels, in continuous facilities operating for seconds and in flight with vehicles operating for a 1000 seconds such as in the flight of the Rockwell Space Shuttle.

That which distinguishes a thermal model as semi-infinite is that the thermal diffusion of heat through the material, as defined by the Fourier number, takes much longer than the test duration:

$$F_o = \frac{\alpha t}{L^2} > 1$$

α = Thermal Diffusivity
 t = Time
 L = Thickness

This can be accomplished by having a thick structure (increasing "L"); by having a highly insulative material (decreasing " α ") or testing very rapidly (decreasing "t"). Each of these approaches has been taken. In the limit of very short test durations, (milliseconds), the thermal characteristics of the coatings themselves may dominate the analysis. For shock tunnel flows, a few millimeters of coating is sufficient to define a semi-infinite slab thermal model and this can be applied over a highly conductive structure. Smith et al, 1989, experimented with this technique using liquid crystal coatings and showed that, in fact, there was sufficient thermal resistance in the coatings to use the paint substrate layer as a semi-infinite slab thermal model as shown in Figure 19. Even when the thermal pulse reaches the interface between the insulative paint and the metal structure, modifications to the semi-infinite slab thermal model may be used. These modifications, to be discussed later in this chapter, increase the complexity of the data reduction but they may present a viable instrumentation approach in certain situations.

This chapter of the report will discuss both the application of the semi-infinite slab thermal model analysis to survey techniques as well as point measurements in both impulse and continuous flow test facilities.

Survey techniques are defined as those in which an overall view of the model is generated in a continuous manner using some form of a temperature indicator attached to the surface. Point measurements are those with distinct instruments attached at point locations on a surface of a model.

There are three forms of temperature indicators employed in survey techniques. These are (1) irreversible temperature sensitive coatings such as Dectecto-temp (R) and Tempilaq (R) which can be sprayed on and are cleaned off after a single test injection. (2) reversible thermo-phosphors or liquid crystal techniques which

remain active on the model for extended cycles of test time and (3) stabilized emittance surfaces used with remotely located Infrared detectors to define a surface temperature field. In all of these various techniques as well as the point measurement techniques to follow the overriding feature is that the surface indicator be a virtually massless material whose presence does not affect the basic thermal performance of the thick substrate backing materials. In addition, the materials upon which the indicator is applied must not violate the basis of the semi-infinite slab model (that is, the thermal pulse must never reach and affect the backface of the material during the period of data acquisition). This feature may be relaxed somewhat through corrections to the thermal model which will be discussed later in this chapter of the report.

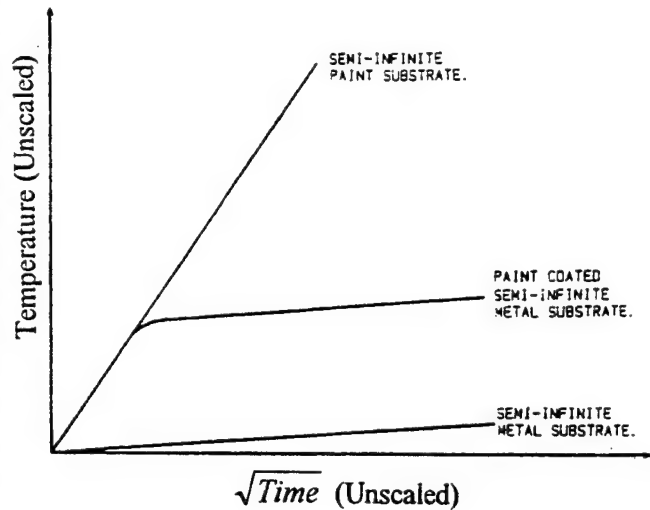


Figure 19 The Effect of Thermal Coatings to Act as a Semi-Infinite Surface for Very Short Test Periods (after Smith, 1989).

There are several forms of temperature indicators employed as point measurements within the context of the semi-infinite slab thermal model. These gages, using the material of the model as the semi-infinite slab material, are (1) thin wire "isothermal staple gages" either on the surface or imbedded in the surface and either singly or in groups. (2) thin film resistance thermometers constructed of single-type platable material and thin film thermocouples. Apart from these sensors which rely on the model material itself to form the gage, the coax gage can be considered as a semi-infinite slab type gage. The coax gage will be discussed in detail later in this chapter of the report.

Introduction to Survey Coating Techniques Based on the Semi-Infinite Slab Thermal Model

There are essentially four types of survey test techniques in use today. These are: (1) temperature sensitive coating techniques, (2) thermographic phosphor techniques, (3) liquid crystal techniques and (4) IR radiation techniques. Each of these will be discussed in turn following a more general discussion of survey test technology.

The Thermal Scope of Survey Test Techniques

There are significant limits to survey test techniques that must be understood and respected. No single technique during a single test entry will fully define the complete distribution of heating about complex shapes. This can be graphically illustrated by using the solution plot from Jones and Hunt, 1966 as shown in Figure 20. In this figure the "X" axis is test time in seconds. The "Y" axis defines a function of the heat transfer coefficient which includes the properties of the model material. The parameter plotted is a function of the temperature of the thermal coating, T_{pc} , the initial wall temperature, T_i , and the recovery temperature (related to the total temperature) of the facility. A single line in Figure 20, representing a single value of \bar{T} , indicates the application of a coating with a single, unique temperature change value. Coatings having a range of

temperature change values will be represented by an area on the curve bounded by \bar{T} lines specifying the limits of that range. The test duration for survey techniques is limited. At low times, the limited framing rate of discrete data; "snap-shots", initial time inaccuracies due to questions of what is initial time and how the non-uniformities of model injection through the tunnel shear/boundary layer are dissipated degrade the measurement. At high times, thermal diffusion destroys the 1D semi-infinite slab thermal model which is the basis of the technique. Between these nominal limits; from 1 second to 10 seconds, useful data is acquired. Note from Figure

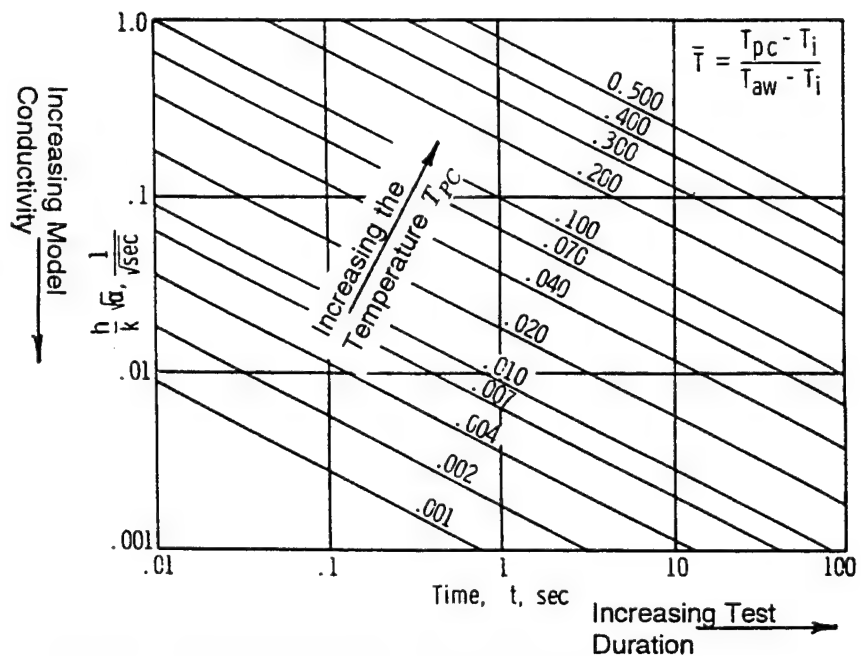


Figure 20 The Graphical Solution of a Semi-Infinite Slab Heating
After Jones and Hunt, 1966.

20 that within 10 seconds of useful test time a heat transfer rate range of $\sqrt{10 \text{ seconds}} = 3.16$ can be measured for a single temperature coating material. This range is insufficient to define interacting test flows and results in the peak heating levels being missed. Figure 21 from Gillerlain, 1979, shows that thermal paint

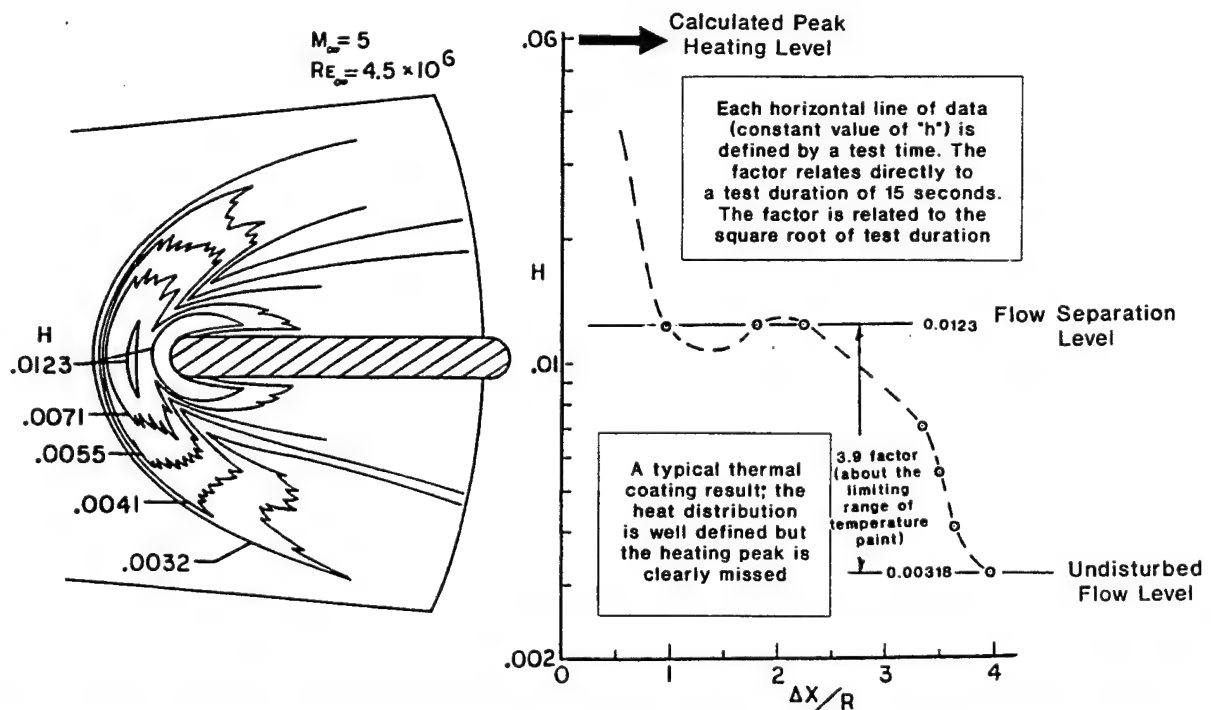


Figure 21 Heating Ahead of a Cylindrically Blunted Fin attached to a Sharp Cone at Hypersonic Speeds. The Heat Transfer Coefficient Boundaries and the Centerline Distribution of Heat Transfer Coefficients.

data up to (and including) flow separation was measured but that the peak heating (a level far above that of separation at a value $h=0.0123$) was completely missed. Note also that the span of measurements was a factor of 3.9 corresponding to a test duration of 15 seconds of data.

This same graphical solution figure can be applied to evaluate coating techniques which define continuous temperature measurements over a range of temperatures. Applying the temperature measurement capabilities of the Langley developed thermographic phosphor technique which is sensitive in the temperature range from 260 to 450 degrees K, Buck, 1991, to a similar shock interaction study from Hung, two areas can be identified; one, as before, due to the defined limits of measurement; typically 1 to 10 seconds and the second due to the range of heating rates measurable on the model bounded by the limits of available thermal coatings. The extremes of the actual heating rates encountered in the Hung data example were defined apriori through thermocouple data supplied by Hung and shown in Figure 22 as an inset sub-figure. The usefulness of the

survey technique is confined to the subset containing both areas. It can be seen from this example that even in this case the peak heating is totally missed and could only be captured by either a coating technique having a far higher activation temperature than possible with the phosphor mixture used by Buck or measurements at very short times after test initiation; less than 0.1 seconds.

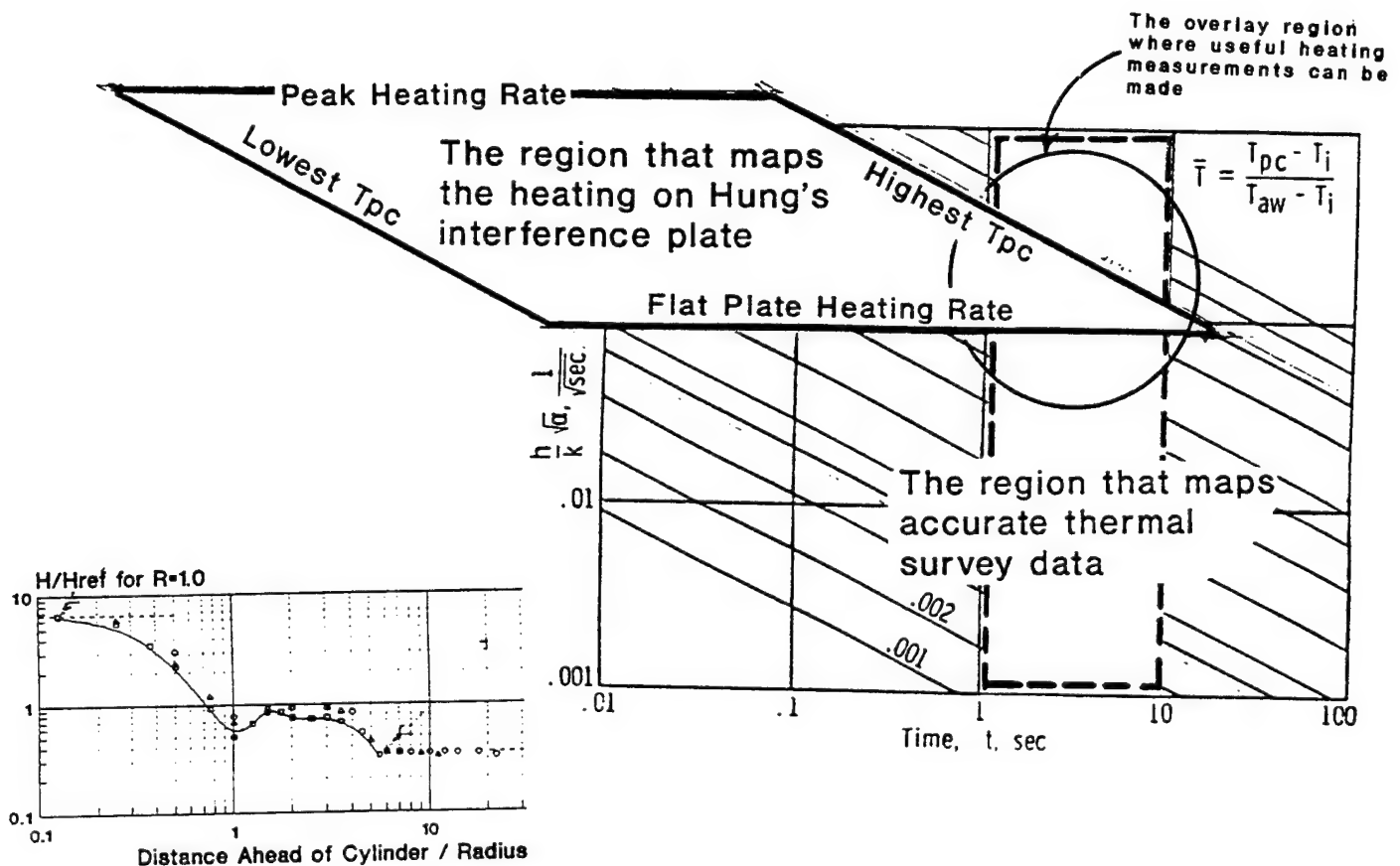


Figure 22 Experimental Data From Hung Superimposed on the Graphical Solution of Jones and Hunt.

These examples illustrate that surface coating techniques, in general, have limitations that must be respected and that these limitations reduce the peak heating that can be accurately measured. It is far too easy to incorrectly define the heating in a complex interaction region with the best of these techniques. A dead giveaway to problems with survey techniques is that large areas of the surface are defined by a single heating maximum as shown in Figure 23. Such regions probably bound but certainly do not define the true maximum.

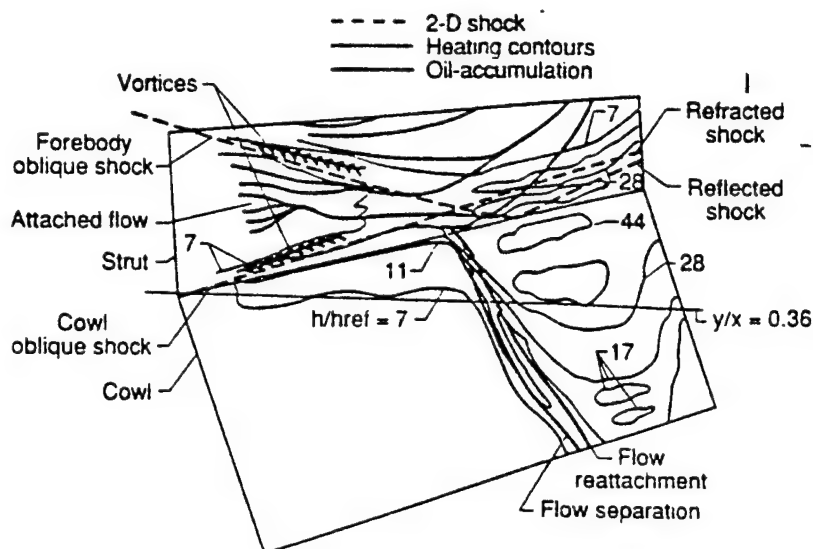


Figure 23 Example of Shock Interaction Results Generated Through the Use of Temperature Sensitive Coatings.

Physical Model Limitations

Model design also limits what can be observed with survey techniques and the accuracy of those measurements. For application of the semi-infinite slab thermal model technique, the model design must minimize the placement of load-distributing steel structure in regions near measurements. That alone is frustratingly difficult given that the model materials most useful with this technique are not structurally sound. Thick sections of insulative material are required to assure the semi-infinite slab thermal model is respected at long test times. In many cases that is not possible. Thin sections of the model will limit the application of the semi-infinite slab thermal model even further reducing the window of opportunity for testing. In some physically simple cases, corrections may be applied to the data reduction to account for the finite slab effects but these corrections are only valid for limited special cases.

The "Data Train" for Thermal Mapping Techniques- From the Surface to the Reduced Data

Survey test data, by one of the several techniques introduced, is acquired and evaluated by a "data train" that starts with the character of the sensor and ends with data manipulation and reduction. That data train has several components as follows:

(1) the surface-mounted sensor, (2) the recording medium and (3) the data reduction environment. The sensors are coatings of one form or the other from paints to activated phosphors to emittance-stabilized surfaces. The recording medium has undergone substantial changes in the past few years; from the use of motion picture film in the past to the use of digitally-stored video images at present. Finally, the data reduction environment follows from the choice of the recording medium; film creates an analog record that must be visually scanned and mapped while video records create a digital record that can be manipulated through computers. Modern survey data is most efficiently taken in a digital mode and manipulated digitally.

through the use of computers. Modern survey data is most efficiently taken in a digital mode and manipulated digitally.

Two techniques; Detecto-Temp paints and liquid crystals, produce color distributions on the test surface which are related to temperature. While these images of color gradation (opposed to computer-generated artificial color maps of grey scales) are pleasing to look at, they are difficult to use quantitatively and difficult to read reliably with an image processor ¹. In at least one case, narrow pass filters are used to produce a monochrome line from color scans of the model. One example of this is the work of Metzger et al, 1991. Metzger recorded the liquid crystal coating with a color CCD camera fitted with an analytic line filter peaked at 535nm with a 10nm bandwidth. This signal, focused on the green portion of the spectrum, was sent to a color monitor for which only the green color gun was used. Data frames of this information were acquired by a frame grabber and placed on file for further analysis. The temperature is directly related to color and the color is determined by the intensity level of the monochromatic data signal on the acquired frames. The preset intensity threshold level relating signal to temperature is determined by calibration of the surface indicator, in this case liquid crystals, against thermocouples.

Estimate of the Surface Temperature Rise for a Semi-Infinite Slab Surface

Semi-infinite slab surfaces normally have one-dimensional heating in the absence of conduction losses along the surface of the material. The one dimensional heat conduction is a problem with a classical solution. If it can also be assumed that the heating rate into the surface of the semi-infinite slab is constant with time, then the temperature rise in that solid is estimated by the equation:

$$\Delta T = \dot{q} \frac{2}{k} \sqrt{\frac{\alpha t}{\pi}} = \frac{2\dot{q}}{\sqrt{\pi}} \frac{\sqrt{t}}{\sqrt{\rho c k}} = \frac{2\dot{q}\sqrt{t}}{\sqrt{\pi}\beta}$$

where \dot{q} is the estimated heating rate to be encountered

k is the thermal conductivity of the material

α is the thermal diffusivity of the material

t is time.

$$\beta = \sqrt{\rho c_p k_w}$$

For the heating rate in $\frac{Btu}{Ft^2 Sec}$, time in seconds and the square root of the product of the thermal properties in $\frac{Btu}{Ft^2 Sec^{1/2} \circ R}$, the time rise is in seconds.

¹ pg 6b-8 of Consigny's paper "Heat Transfer Measurement techniques Used or in Development at ONERA/Chalais-Meudon

Thermal properties for typical substrate materials are presented in Appendix A at the end of this report. This technique has been noted to be useful on insulative materials (temperature mapping techniques as well as thin film resistance thermometer gages) and the for coax gages placed within stainless steel. Applying the technique to the heating rate data presented by Collier, 1990, the following comparison was achieved assuming the model and gages are defined by the properties for 17-4PH stainless steel:

Gage Number	Heating Rate	ΔT , DegsR (Collier data)	ΔT , DegsR (Eqn estimate)
C1	5.26	12.23	14.7
C20,21	113.3 (1D)	317.6	261.7

The results appear to be quite representative of the actual temperature rise. Recall from the paper by Collier that gages 20 and 21 were influenced by shock interaction heating and required a 2D thermal model to reduce the data. This simplification assumes constant heating into a 1D model and would be expected to produce a higher estimate of surface temperatures than the measurement which included conduction along the model surface.

Determination of the Exact Time of Model Exposure in the Facility:

All heating measurements based on the semi-infinite slab technique require, as initial data, the exact time at which the model felt the test flow.

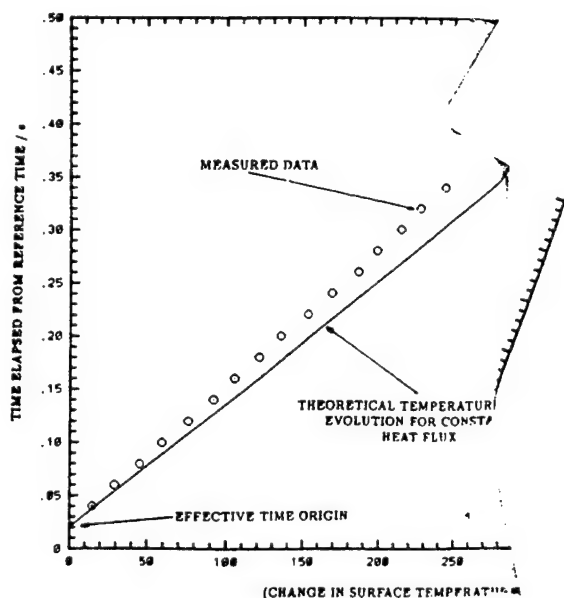


Figure 24 Graphical Determination of the Effective Time Origin From Simeonides, 1991.

If an injection mechanism is used with the model, that initial time may not be obvious. Simeonides, 1991, defines an effective time origin from the measured data itself. Using the change in surface temperature measured from an arbitrary time origin, the square of that temperature is plotted as a function of the elapsed time from that arbitrary reference. Since, for a constant imposed heating rate, the temperature/time variation is given as $\Delta T^2 \propto t$, a straight line correlation is formed as shown in Figure 24. Fitting that data with a linear curve, the effective time origin is defined.

Model Materials For Temperature Sensitive Coating Tests

Figure 25 demonstrates the range of commonly used model materials upon which temperature sensitive coatings are applied.

Plotted in this figure is the range of β values for these materials as well as the differences that occur due to the overlay of thermal coatings. In principle, the coatings are low conductivity materials that are closer in thermal properties to insulators than conductors. As the base material becomes more of a conductor (β increases) the effect of the coating to lower the effective value of β increases. Two points can be made from this figure: (1) there is a significant range in the parameter due to the individual characteristics of the materials; a change of the parameter β by a factor between 2 and 3 and (2) the insulative character of the coating, shown here, can be used to advantage in certain testing circumstances.

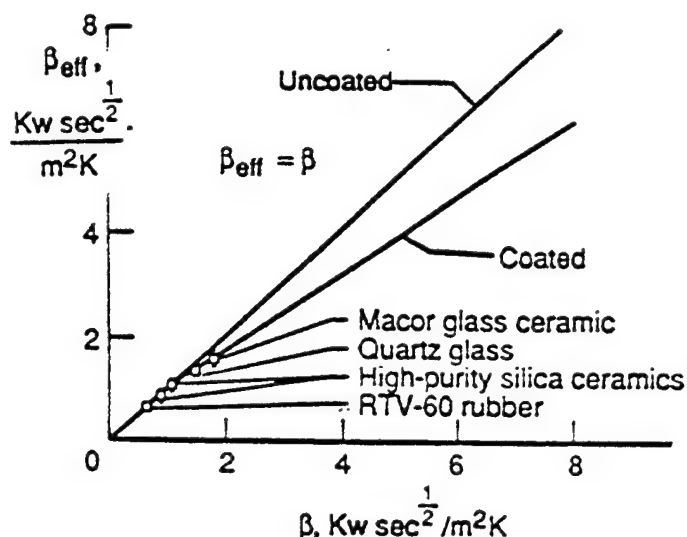


Figure 25 The Change in the Parameter Beta as Model Materials Become More Conductive.

Figure 22 demonstrated how difficult it was to capture heating peaks. The use of materials having different thermal properties can shift the time at which temperature indicators react. Higher conductivity materials increase the test time for a given temperature to be reached. It is possible that a series of models fabricated of different materials may broaden the range of measurements which are feasible during the acceptable test interval (from 1 to 10 seconds) however, these higher conductivity materials will also increase conduction from the heating peak making accurate measurements impossible. Note that the parameter

$$\frac{\sqrt{\alpha}}{k_w} = \frac{1}{\sqrt{\rho c_p k_w}} \text{ or the thermal diffusion, } \alpha, \text{ is related to material properties as } \alpha = \frac{k}{\rho c_p}.$$

It will be shown in discussing the various measurement techniques based on the semi-infinite slab thermal model that the uncertainty of the various techniques is critically dependant upon the accuracy with which the thermal properties of the materials employed are known. The error in the measurement of thermal properties involves both an error in those measurements at or near room temperature and the error in the variation of the properties with increasing surface temperature. With increases in material temperature, the thermal properties are, at first, a linear temperature function and then a quadratic increase with temperature. Based on the quality of these measurements and the extent of the calibrated thermal properties with respect to the measurements to be made, the uncertainty of that measurement may be many times greater than fundamental room temperature measurements. Note in Figure 25 that there is a divergence of thermal property data as wall temperatures increase.

The coating itself may well contain part of or the entire thermal pulse for tests in short duration shock tunnel facilities depending on the thermal diffusion of heat through the coating system. Smith and Baxter, 1989 have experimented with thermal coatings (in this case liquid crystal coatings) in short duration shock tunnel. Doorley and Oldfield, 1987 have developed the theory for heat transfer through these layers of dissimilar material. In short duration test facilities thermal survey coatings, in general, can be used over "thermally thick" models of higher conductivity materials to generate heat transfer data.

Survey techniques can also be applied to model materials which are not insulators for longer duration flows. These survey techniques measure surface temperature and may also be appropriate for other material systems. Application of specific techniques to other model material systems must begin with an understanding of the anticipated response; metallic systems conduct heat more readily and will therefore have a smaller temperature rise for a given heat flux. Heat conduction will occur both through the material and along the material leading to more complex data reduction and analysis. This more general application of survey test techniques is beyond the scope of this section and will be discussed more fully in Appendix B at the end of this report.

The effects of lateral conduction are always of concern in the selection of model materials and the need for numerical evaluation of conduction corrections. Maise and Rossi, 1974 created a chart for determining when corrections to 1D, semi-infinite slab reduction are required. The geometric variables referred to in the figure are shown in Figure 26 below.

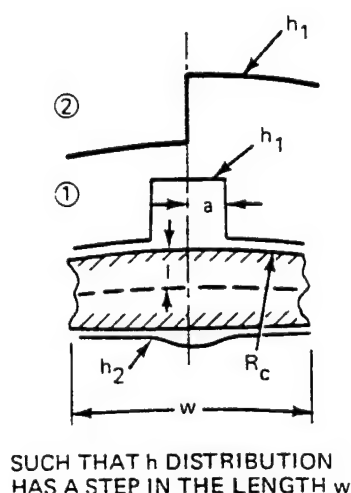


Figure 26a Geometry of Maise and Rossi, 1974.

A usual argument for the use of temperature survey techniques is that such techniques define the location of high heating regions that can then be properly instrumented to define the magnitude of the effect. This is clearly a legitimate need and survey techniques are clearly satisfactory to meet this need. In fact, the Space Shuttle development program used this technique effectively.

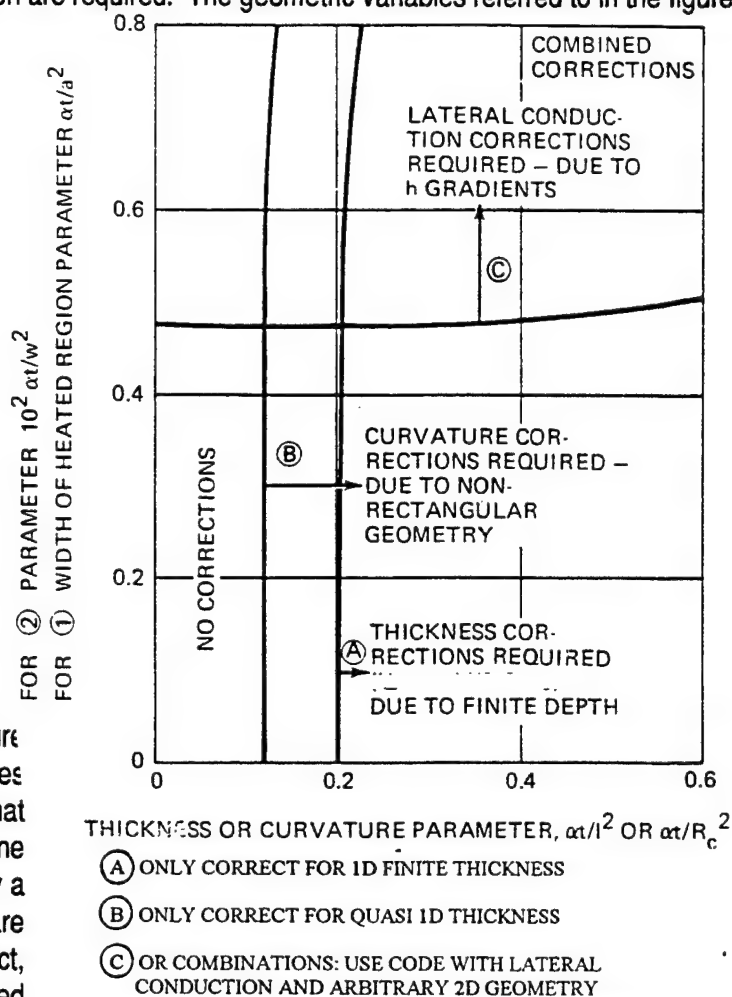


Figure 26b Corrections Required to the 1D Analysis After Maise and Rossi, 1974.

While this CAN be done, the best survey technique to achieve the goal must be carefully selected. The wrong choice of technique may simply not be cost effective. In development time alone, these techniques require an entry into the test facility, the generation, reduction and interpretation of data and the integration of that reduced information into the subsequent DESIGN of a point measurement model (since model structure cannot be defined until measurement regions are understood) and then the secondary test of the properly instrumented model must be accomplished. From the standpoint of cost, unique models must be

constructed, engineering time invested and wind tunnel time expended. It appears, all in all, that paint testing is 10 to 15 times slower than corresponding point measurement testing using thin skin techniques. But there is even a better method. The use of dynamic test techniques, which will be discussed later in this report, give us the option to use a FEW special sensors in such regions and observe the level of heating as the model orientation sweeps the region of high heating over the gage(s). This type of testing is an order of magnitude faster than traditional thin skin testing and 100 times faster than paint techniques.

The Video Data Acquisition Technique For Temperature Sensitive Coatings

A wide variety of the surface coating techniques (including IR measurements) use videography to acquire, store and manipulate the observed field of view. While it is not within the scope of this report to discuss the details of this acquisition process, the reader should be aware of this technology and the implications for efficient measurement. In general, color gradients are not useful in defining accurate temperature measurements. For this reason, many experimental set-ups convert the color video frames to high contrast, monochromatic frames and to quantify those frames of "data". Table 3-1 below shows typical systems from the literature.

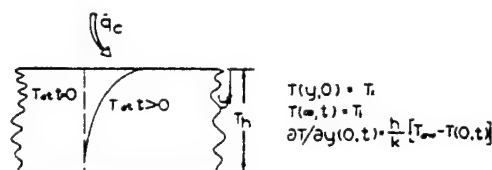
TABLE 3.1
TYPICAL DATA ACQUISITION PROCESSES
FOR CONTEMPORARY THERMAL MAPPING TECHNIQUES

Survey Sensor	Recorder	Acquisition System	<u>Reference</u>
Liquid Crystals	Color CCD Camera	Color Monitor, Frame Grabber, Computer	Metzger, 1991
Thermo Phosphor	3-Chip CCD Camera	Color Monitor, Image Processor, Computer	Buck, 1991 (NASA Langley)
Passive IR System	AGEMA Thermo-Vision Model 782LW	Image Digitized, 650Mb Worm Drive, Computer	Balageas, 1991 (ONERA, France)
Liquid Crystals	Film Camera	Digital Interactive Image Processing System	Scholer, 1980 (DLR, Germany)
Liquid Crystals	3-Chip CCD Camera	Color Monitor, Image Processor, Computer	Dabiri, 1991 (Univ. California San Diego)
Passive IR System	Infra-metrics 600 Camera	Video tape, Computer with a "Thermogram Card"	Henckels, 1991 (DLR, Germany)

TEMPERATURE SENSITIVE PAINT TECHNIQUES:

Two types of irreversible, temperature sensitive paints have been used in the United States over the past quarter of a century. These are a color-change paint known by the trade name of Detecto-Temp (R) and a phase-change coating known as Tempilaq (R). Although both techniques have been used, earlier studies were conducted with a Detecto-Temp paint. This technology was eliminated as a result of a landmark paper by Jones and Hunt, 1966, which cast doubt on the earlier technique and quantified the entire thermal paint data reduction procedure. The alternative, Tempilaq material is a fusible temperature indicator which undergoes an irreversible phase change from an opaque solid to a clear liquid at a single known and repeatable temperature. The coating is normally applied to models constructed of low conductivity material. The test sequence starts with a model injection and ends with either a complete phase change on the surface or with the imposed heat pulse soaking through the model materials and destroying the 1D thermal model which is the practical basis of the method. This available test duration depends upon materials and the thickness of those materials. It is roughly 10 seconds long.

Data reduction employs the standard, but limited one dimensional heat flow equation with surface and backface boundary conditions as well as an imposed heating rate at the surface of the model. This equation and its solution is shown in Figure 27.



ASSUMPTIONS:

- INITIALLY ISOTHERMAL MODEL
- HEAT PENETRATION SMALL COMPARED WITH WALL THICKNESS
- COATING (THERMAL SENSOR) IS MASSLESS
- HEATING STEP OF CONSTANT MAGNITUDE APPLIED
- MATERIAL PROPERTIES ARE KNOWN AND DO NOT VARY WITH TIME

Figure 27 The One-Dimensional Heat Flow Model and Its Assumptions.

Brazhko et al, 1990 investigated the errors implicit in the paint technique. Two significant errors were discussed. These were (1) the non-1D structural thermal flow due to shock impingements and (2) the problems of heating a surface from both sides. The reasons for scatter in shock impingement heating, according to Brazhko, should be investigated by testing the model over wide ranges of Reynolds

number and with both paint and thermocouple sensors. Thin section heating should be handled by uniformly pre-heating the model prior to convective heating in the test facility. Brazhko notes that the results obtained in experiments repeated many times did not differ by more than $\pm 10\%$ as shown in Figure 28.

In this figure the paint melt temperature is defined as $t_m, ^\circ C$ and the initial model temperature is defined as:

$t_{init}, ^\circ C$. T_∞ and P_∞ are the tunnel total conditions in degrees C and KPa/cm^2 and $\bar{T} = \frac{T_w}{T_\infty}$.

$$\Theta = \frac{T_\infty - t_{INIT}}{t_m - t_{INIT}}$$

There are several criticisms of the use of temperature sensitive paint techniques that should be carefully considered by the experimentalist.

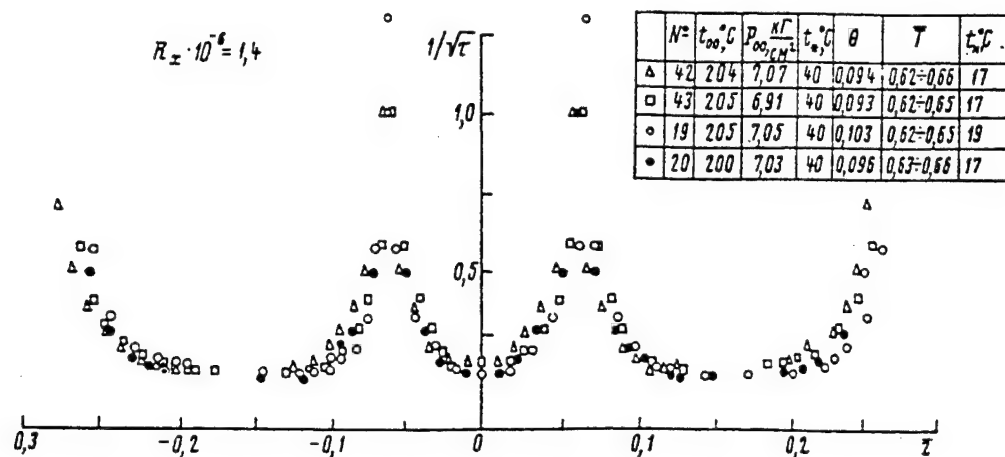


Figure 28 Repeated Application of Temperature Sensitive Paint to a Thin-Winged Test Model.

Economics

Temperature sensitive paint applications are labor intensive; for the most part slow and mechanical operations. For continuous flow test facilities, the amount of hand labor required to "turn the model around" is nearly prohibitive. Considering the test cycle times achieved at the AEDC, only one run every 15 minutes can be made with a single wind tunnel model. The use of multiple wind tunnel models, used in rotation, speeds up the test procedure somewhat but the limiting factor is still the time required to open the access door to the model and replace it; about 10 minutes. This criticism is specific to continuous flow facilities and does not apply to transient test facilities where large energy costs connected with an "on-line" test facility are not involved.

Temperature Peaks

Temperature sensitive paint applications are relatively poor in defining either the absolute level of heating in regions of high thermal gradient or, conversely, the level of heating in regions of very low thermal gradient. The heating rate is calculated from the observed melt time which is referenced to the beginning of the heat pulse. This definition of "zero time" can be somewhat vague for models which must be injected through the boundary layer of the tunnel. For regions of high heating, the melt time can be quite short leading to potentially severe errors in defining this incremental time from the start of heating to a clearly defined peak heating line. Regions of low thermal gradient are also difficult to observe as paint contour lines are not distinct. There is a relatively small window of opportunity defined previously through the error bucket in which to generate high quality temperature paint data. To operate within this window of opportunity, an approximation of the answer sought experimentally must be known already, namely some estimate of the actual heating rate in the interaction region. Paint techniques are excellent for defining the "region" where high and localized heating will occur. They are far less accurate in defining the actual peak within the region. If a clear estimate of the level of heating in the peak interaction region is required, paints with several activation temperatures are required to "shift the event" into or across the window of opportunity. It can be

done but it is quite expensive and time consuming. Shock interaction regions are known to be regions of severe thermal gradients. When paint data for such regions show large areas of a single heating level, it is important to critically question how the data were generated with an eye toward understanding the possible level of heating within the area shown. Figure 23 from a recent NASA test is an example of this. The designated areas are of questionable value.

Person-power Intensive

The generation and reduction of temperature paint data from photographs by hand is labor intensive and bad on the eyes. Many hours are required to trace off the contour lines from the film record. The automated generation of color or change lines is a difficult issue of contemporary interest.

It is the author's viewpoint that the use of temperature paint studies in present day environment is archaic, overly expensive and probably generates highly inaccurate data.

In the following sections of this report alternative techniques for survey testing will be discussed. These alternative techniques increase the productivity of survey testing and are more useful than paint techniques if survey testing is required.

The Uncertainty of the Temperature Paint Measurement in Wind Tunnels

Figure 29 demonstrates an uncertainty buildup for the temperature paint measurements from an AEDC report. The dashed lines in this figure indicate the contributions from individual uncertainty elements while the solid line reflects the aggregate effect of both random error and biases. Two temperature-sensitive issues are apparent: (1) understanding the effect of the initial temperature of the model, T_{wi} , on the temperature parameter and (2) understanding the effect of the recovery temperature, T_{aw} , on that parameter. While one may argue either the completeness or accuracy of the individual error elements, the buildup demonstrates a range of the temperature

parameter, $\frac{T_w - T_{wi}}{T_{aw} - T_{wi}}$ for which the least error in

data can be achieved and focuses attention on individual error sources which, if improved, would best improve the quality of the resultant measurement.

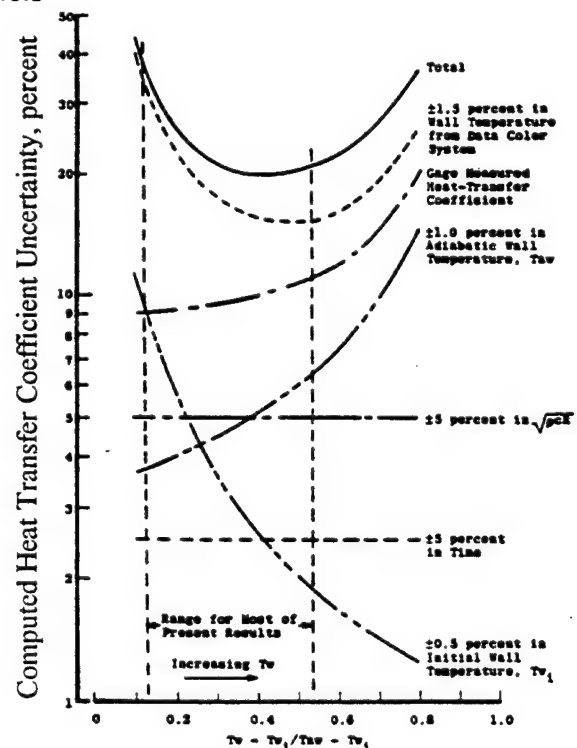


Figure 29 The Uncertainty Build-Up for Temperature Coatings from the Application of Uncertainty Analysis.

THERMOGRAPHIC PHOSPHOR TECHNIQUES

Thermographic phosphors are materials which radiate in the visible spectrum (fluoresce) when illuminated by a UV light source and diminish in emitted fluorescence, "quench", when exposed to increasing temperatures. These coatings have been used in wind tunnel testing for the past 20 years through one of several application techniques. These techniques either measure broad-band emissions, narrow-band emissions on specific lines or the decay time measurements of fluorescence at a specific, narrow-band line.

The broad band phosphor brightness varies according to an exponential relationship defined through the equation:

$$B_T = B_{T_c} e^{-K_1(T-T_c)}$$

where B_T is brightness T_c is the critical temperature; the minimum value of temperature for which the logarithmic relationship holds.

Thermographic phosphors were first applied to wind tunnel models in 1969. Cysz and Dixon, observed the level of broad-band radiation emitted from a UV activated thermographic phosphor surface with temperature as shown in Figure 30. For these earlier, broad band phosphor intensity measurements, the phosphor coating required calibration to create a response intensity vs the surface temperature as shown in Figure 30. The intensity, photographed as shades of grey, was then assigned a discrete "color" which defined regions of surface temperature at the time the photograph was taken. Tare photographs were also necessary in the facility without airflow to subtract the grey shadings attributed to lighting shadows. The calibrated surface temperature distribution (defined in terms of discrete colors) could then related to heating rate data through semi-infinite slab data reduction techniques or, more frequently, the relationship between the color assignments and surface heating rates were made using distributed heat flux gages as shown in Figure 31. Gardon gages were extensively used. These gages will be discussed in Section V of this report.

Unlike the temperature paint technique, the phosphors are reversible coatings and the phosphor data reduction can readily be automated through video imaging techniques with tare pictures subtracted from the actual data automatically as well as the resultant shades of grey assigned artificial colors to identify various heating regions. This technique was initially developed for the McDonnell, Hotshot wind tunnel which operated with test durations of the order of 100 ms. Later, the technique was adapted to the continuous test facilities at AEDC. It has also been applied in shock tunnel test facilities at Calspan Corporation with some difficulty; see Rogers, Bogdan and Kinzly, 1972.

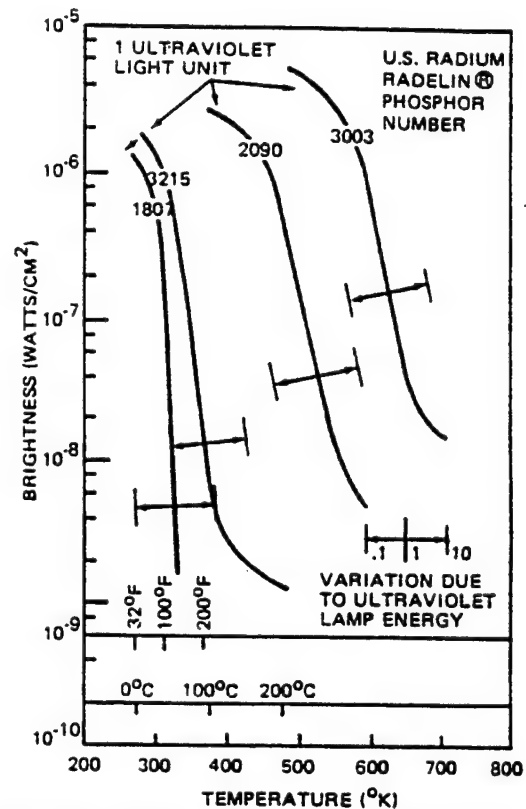


Figure 30 The Relationship Between Phosphor Quenching and Indicated Temperature for Several Phosphor Types.

Since the early experiments of Czysz and Dixon, 1969, substantial improvements have been made to the radiation emission mode of operation. The most significant improvement is the technique of Buck et al, 1991, which measures simultaneous relative-radiation at two wavelengths and uniquely relates temperature to these measurements of radiation. The data flow from this thermography system is shown in Figure 32. These measurements are taken using a special video camera with 3 detectors (known as Charged Coupled Devices or CCD's) illuminated by a single lens. These CCD's with their narrow-band filters record visible radiation at both the red and green frequencies independently. The phosphors which produce this radiation are mixtures of a commercial Radelin phosphor (1807) and a rare earth phosphor (lanthanum oxysulfide with 1% europium, $La_2O_2S:1\%Eu$). The temperature calibration of this mixture is shown in Figure 33. The distribution of frequency-dependant intensity with temperature for this mixture is shown in Figure 34.

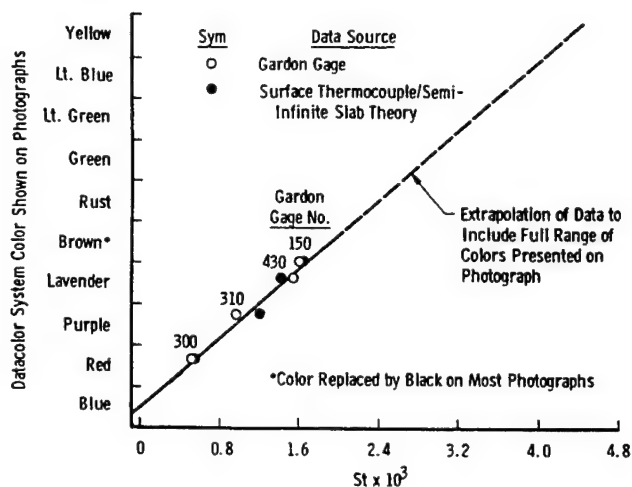


Figure 31 Calibration of Phosphor Data (Through the AEDC Datacolor System) Against Gardon Gages and Surface Temperature Gages.

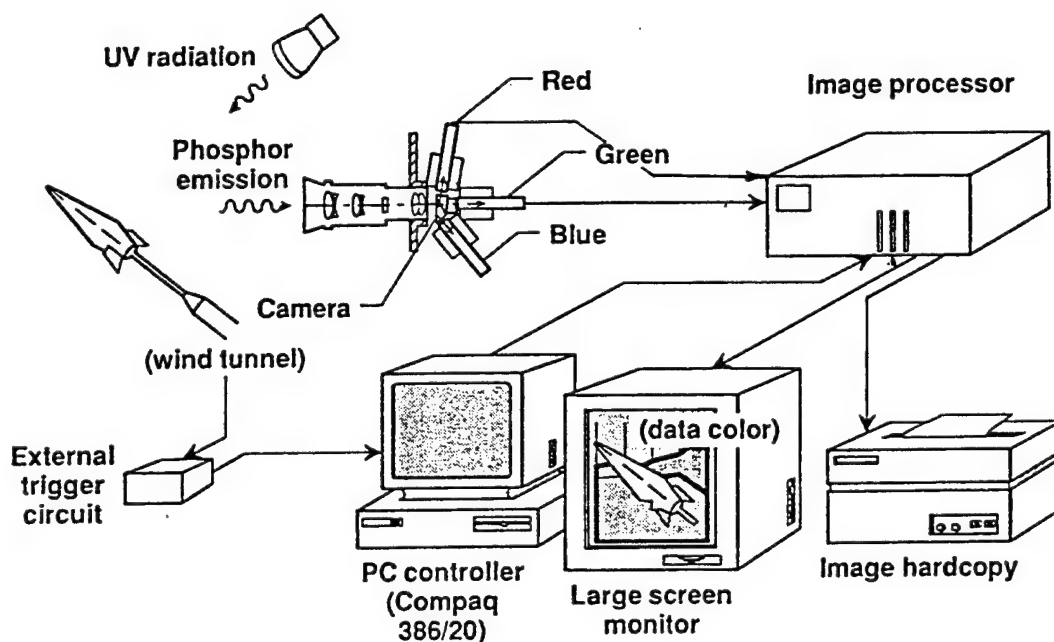


Figure 32 Schematic of an Advanced, Two-Color Thermographic Phosphor System Developed by and Located at NASA Langley Research Center.

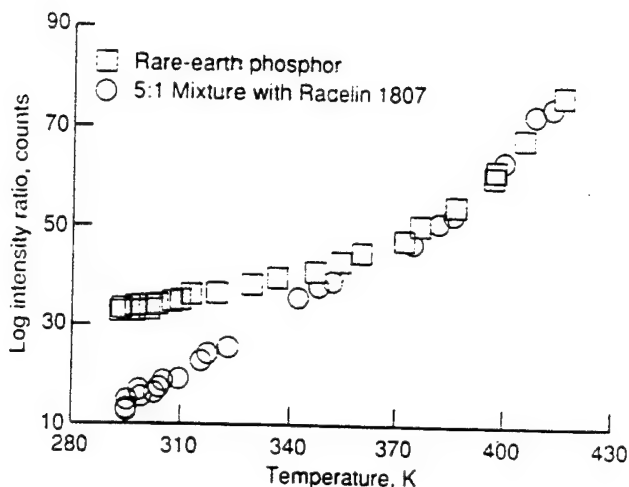


Figure 33 Calibration of the Radelin Phosphor Mixture to Produce a Larger Temperature Range for Experimentation.

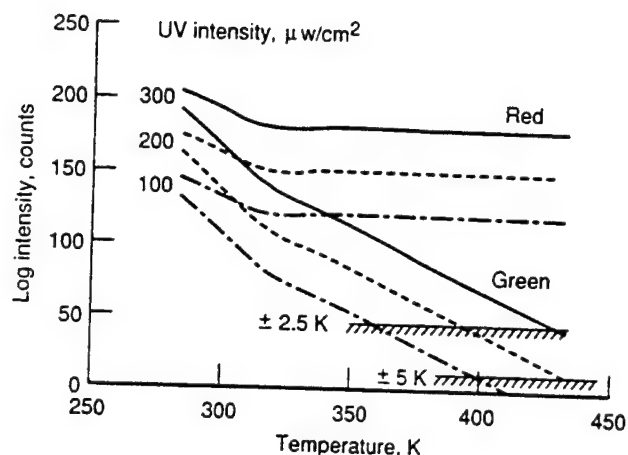


Figure 34 The Phosphor Intensity at the Red and Green Wavelengths.

This improvement in the thermographic phosphor technology by Buck et al produces more exact measurements of temperature without the need for tare photographs to evaluate the effects of grey shadings or uneven lighting. An accuracy of $\pm 5\%$ (relative to theory) is quoted for a simple sphere/cylinder calibration model and data comparable to thin film measurements has also been demonstrated.

Measurements based on the temperature-dependant decay time of the phosphor caused by stimulated radiation are relatively new. In this technique, pulsed UV laser radiation (typically a low power nitrogen laser) illuminates the phosphor surface at a low pulse rate. The stimulated surface emits radiation that decays from a given pulse with a decay rate that is directly related to temperature. Emission decay data is acquired at a specific emission line and over a very short time interval (300 ns to 1 ms). The acquired data is digitized and fit to a log least square curve. The only referencable engineering use of the technique to date is the paper of Noel et al, 1991 where measurements were made on the stator section of an operating turbine engine. These data matched comparable thermocouple data as shown in Figure 35. Substantial calibration data has been produced by Noel et al, 1987 up to 1650 degrees F and Lewis and Turley, up to 2600 degrees F. This approach holds the possibility of surface temperature measurement at flight-like surface temperature conditions in ground test or the measurement of boundary layer state on routine force and moment testing as well as survey measurements on hypersonic flight test systems.

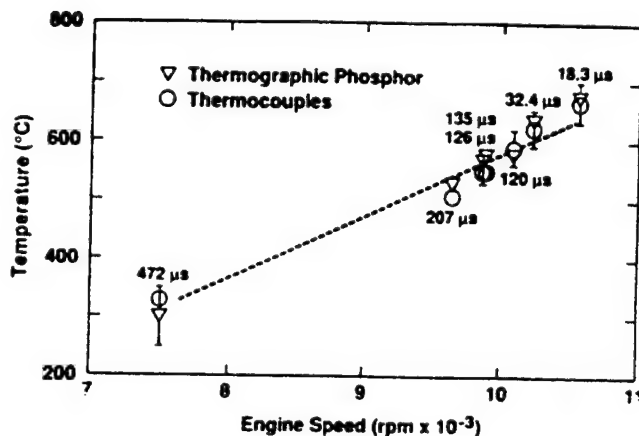


Figure 35 Comparison of Advanced, High Temperature Thermographic Phosphor Data Against Thermocouple Measurements.

Calibration:

Calibration of the phosphors during tunnel operation, when required in older broadband emission applications, is accomplished by placing thermal gages within the field of view of each picture. These gages must not affect the flow in which the data is being taken. Past instruments did not meet this goal. Figure 36 indicates the massive gages Gardon gages used in the past which yielded poor technical results. Figure 37 indicates the newer isothermal staple gage which has been quite successful in this capacity. The staple gages are simple an isothermal thermocouple placed on the surface with a sufficient land length that thermal conduction down the leads is not a problem. Newer two-color relative-intensity measurements do not require these on-board calibrating point measurements.

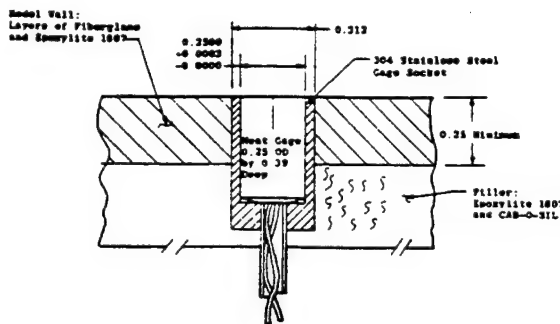


Figure 36 Older Calibration Gages Producing Non-Isothermal Test Surfaces.

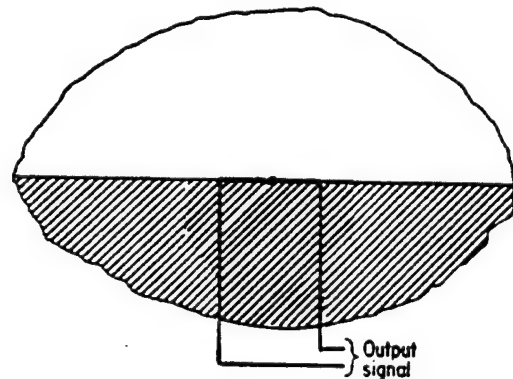


Figure 37 Newer "Staple" Gages Yielding Isothermal Test Surfaces.

The basic data reduction equation for either mode of application is dominated by the character of the substrate upon which the coating is applied and it is the same as previously described since, in all wind tunnel heat transfer applications to date the phosphor coating has been applied to a wind tunnel model constructed of insulative material within the semi-infinite slab thermal analysis model.

For a semi-infinite slab, the general 1D relationship between the non-dimensional temperature and the heating rate is given by the equation:

$$\bar{T} = \frac{T_w - T_i}{T_{aw} - T_i} = 1 - e^{\beta^2} [1 - \text{erf} \beta]$$

where $\beta = h \sqrt{\frac{\tau}{k \rho c}}$

h is Btu / ft²-sec-deg R
 $\rho \cdot c \cdot k$ is Btu / ft²- deg R - sec^{0.5}
 τ is in seconds

τ is the time to reach the specified wall temperature, T_w

k, ρ, c are material properties.

Simeonides, 1990 approximated the equation by curve fitting the error function according to:

$$\text{erf}(\beta) = 1 - (a_1 S + a_2 S^2 + a_3 S^3) e^{-\beta^2}$$

where $S = \frac{1}{1 + p\beta}$ and:

$$p = 0.47047$$

$$a_1 = 0.3480242$$

$$a_2 = -0.0958789$$

$$a_3 = 0.7478556$$

Vermeulen 1992 approximated the "general 1D model" shown above by a constant heat flux model for values of $\beta < 0.1$. The constant heat flux model is derived by Vermeulen in appendix III-4 and is the same equation presented earlier in this section as an estimate of the surface temperature for a semi-infinite slab surface. This equation and its linear approximation is plotted in Figure 38 shown below.

For coatings that react over a temperature range, T_w has a range of values from the lowest to the highest temperature at which measurements can be made.

For a constant initial temperature, assume room temperature, the non-dimensional temperature is a function of these coating limit temperatures as well as the adiabatic wall temperature of the facility which is closely related to the total temperature of the flow.

The limiting values of β which are related to the non-dimensional temperature are, in fact, the limiting values of heating rate assuming that the material properties and the test time, τ , remain constant. The ratio of heating rates possible are then the ratio of the β 's for the limiting temperatures of the coating.

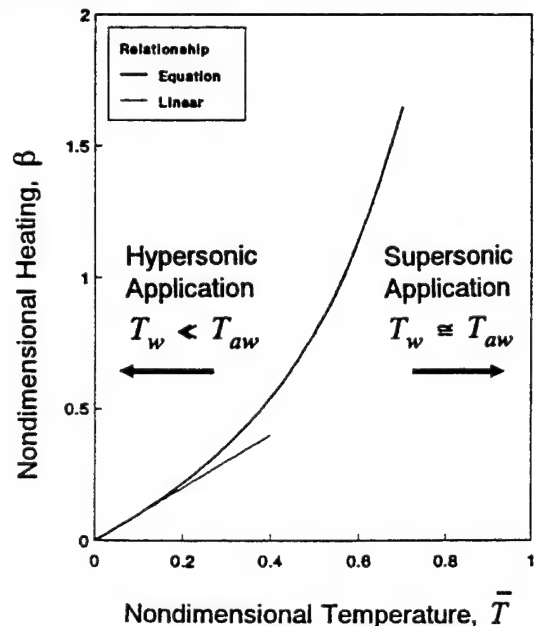


Figure 38 The Relationship Between Non-Dimensional Heating and Non-Dimensional Temperature for Specific Ranges of Temperature.

It can be shown that as the adiabatic wall temperature increases, the range of heating rates that can be covered by a coating having a given temperature span decreases. This is due to the shape of the function curve defined by the equation above and shown in Figure 38. The ratio of $\beta's$ is proportional to the shape of this curve. With increasing flow total temperature, the non-dimensional temperature, \bar{T} , becomes smaller, the slope of the curve also becomes smaller and so does the ratio of $\beta's$.

Thus, while the coatings might have a heating rate ratio (max/min heating rates measurable) of 10 at low tunnel total temperatures, that ratio might be close to 4 as the total temperature of the flow increases. Recall that such a ratio occurs at a constant test time. Test time with these, as any, coatings is dictated by the limits of the semi-infinite slab thermal model. As discussed previously, the semi-infinite slab thermal model is appropriate for test durations generally from 1 to 10 seconds. The total range possible with coatings having a multiple temperature measurement range is thus the product of the ratio at a single test time and the root of the possible test times, $\approx \sqrt{10} = 3.16$.

Table 3-2 summarizes the various ways in which thermal phosphors are used to measure surface temperature from which heat transfer is inferred.

TABLE 3.2
THERMOGRAPHIC PHOSPHOR TECHNIQUES

Technique	Characteristics
Broadband Emission	<ul style="list-style-type: none"> - Steady-state UV illumination of phosphors - Capture of broadband emissions from the irradiated phosphors - Simple photography or videography for emission observations
Narrowband Relative Emission	<ul style="list-style-type: none"> - Steady-state UV illumination of phosphors - Capture of narrowband emissions from the irradiated phosphors at specific lines - Videography for emission observations with 3 CCD video camera - Analysis required to digitize data and obtain relative intensities of signals
Emission Decay	<ul style="list-style-type: none"> - Pulsed UV laser illumination of phosphors - Capture of narrowband emissions from irradiated phosphor at specific line - Time-resolved decay data required from emissions in 1 ms or less

The 2-D Imaging Heat Flux Gage: New Technology in Development

A recent and innovative gage concept developed by Noel, 1991 for Dr. MacArthur at Wright Laboratory is a sandwiched gage with thermographic phosphors attached to both sides of an insulative material. The phosphors define temperature distributions over the gage, the insulative material separating them creates a temperature difference between the front and back surfaces and heat transfer is defined by that temperature drop through an insulator of known thickness, d , and known thermal conductivity, k , by the equation

$$\dot{q} = k\Delta T/d$$

The gage as shown in Figure 39 consists of a series of bisected squares each of which defines to a remotely located observer the temperature on the face and backface of the gage. Both temperatures are remotely measurable by standard narrow-band phosphor acquisition techniques since the insulative material selected; a polymethylpentene material, Polyceram 9606, is transparent to the emission wavelengths of the two thermographic phosphor materials used on the faces of the insulator.

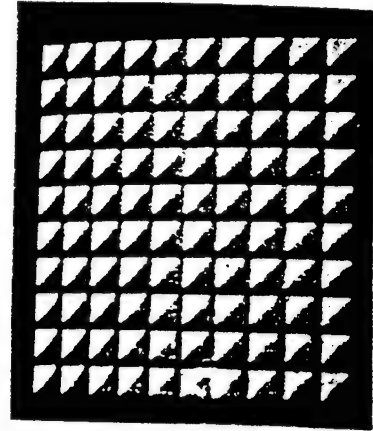


Figure 39 Gage Surface Showing the Matrix of Squares Each of Which Measures to Surface and Backface of the Gage.

The temperature is extracted from the thermographic phosphors by measuring the ratio of two spectrally filtered images at two discrete wavelengths. The surface and backface of the insulator were coated with different phosphors, each with different temperature sensitive lines. The materials and their temperature sensitive lines are as follows:

$Gd_2O_2S:Tb$ at 415nm and 490nm

$La_2O_2S:Eu$ at 511nm and 614nm

This application of thermographic phosphors defines a gradient type of heat transfer gage discussed in greater detail in Section V.

The calibration response of the gage to a pulsed heat flux is shown in Figure 40.

While this gage is very much a work-in-progress, the concepts which underlay the gage; the use of passive temperature measurement techniques which can be applied to surface areas as opposed to point measurements is very exciting.

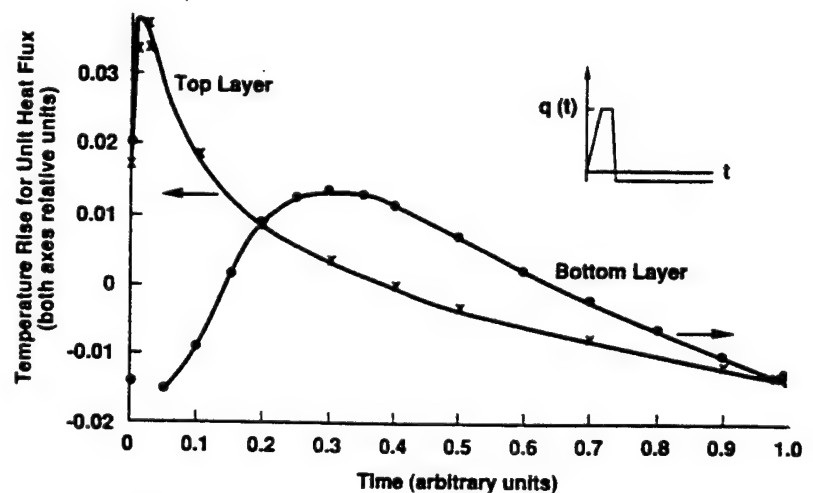


Figure 40 The Temperature Response of the Surface and Backface Sensors to a Thermal Pulse Defined in the Figure Inset.

LIQUID CRYSTAL COATINGS

There are a class of coating materials that selectively reflect light as they are heated and their temperature changes. These materials have an apparent color change as they change in temperature. The ranges of these materials are in both color play bandwidths and temperature ranges. Modern liquid crystals have color play bandwidths (temperature range in which all colors are observed) between 1 and 5 degrees C over an approximate temperature range from -10 to +50 degrees C. A detailed discussion of these materials can be found in a Hallcrest document entitled "Thermochromic Liquid Crystal Products" and in Moffat, 1988.

Moffat notes that there are two types of liquid crystal coatings which have applications in convective heat transfer experiments; Cholesteric liquid crystals which are noted to respond in 50 to 100 msec and chiral-nematic liquid crystals which are noted to respond in 5 to 10 msec or less. Other researchers; Zhang, 1989 and Ireland, 1987 note similarly short response times making these coatings suitable for shock tunnel applications.

Many commercial applications can be observed for these materials including that of a throw away thermometer. Liquid crystal formulations are also available which are sensitive to pressure, shear and temperature. Micro-encapsulation of liquid crystal materials has allowed the development of formulations which are sensitive only to temperature. These materials are available for lower temperature levels which relate to their use in either supersonic test facilities or low energy, short duration hypersonic facilities where the imposed heating is low. Like the thermographic phosphors, liquid crystal surfaces are reversible. With the exception of Prof. Moffat's work in subsonic flow channels at Stanford University, most of the recent work with thermal liquid crystal coatings has occurred in Europe. Prof. Moffat's powered, liquid crystal-based heat gage with which he can "dial in" a line of heat transfer coefficient, shown in Figure 41, is a fascinating application of this technology. Moffat, 1988, has described these coatings quite expertly and the reader is directed to this reference for additional information.

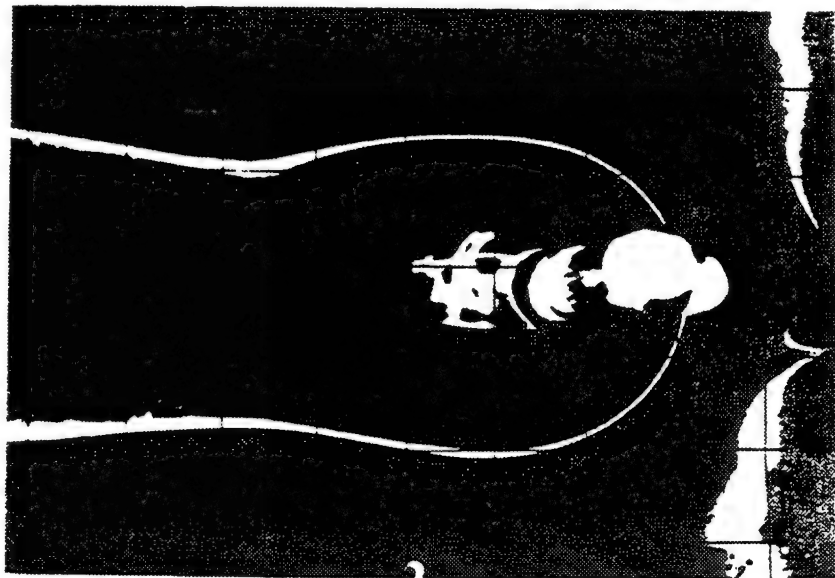


Figure 41 A Monochrome Presentation of a Line of Constant Heat Transfer Coefficient About a Cylinder/Flat Plate Model Using Liquid Crystal Coating after Moffat, 1988.

Liquid crystal coatings have been used to advantage in facilities of increasingly shorter test duration in Europe. Examples of application include the work of Butefisch and Schoeler, 1981, using the 350 millisecond duration Ludweig tube in Germany and the extensive work at Southampton University in a series of impulse test facilities including a shock tube operating for 5 milliseconds. Viewing angles at which the surfaces are observed can be critical with these materials and it is reported that they can be somewhat pressure as well as temperature sensitive.

The accuracy of temperature determination using liquid crystals is enhanced through filtering of the light source to provide a monochromatic source or filtering of the detector to define a monochromatic line. Simonich, 1982, quotes an accuracy of color calibration using a monochromatic light source to be $\pm 0.25^{\circ}\text{C}$. Other estimates of the accuracy of temperature measurement quote numbers as low as $\pm 0.1^{\circ}\text{C}$. Metzger, 1991 acquired the signal from the liquid crystal surface through a color CCD camera with a narrow bandwidth (10nm) filter centered at 535nm. This camera signal was sent to a color monitor in which only the green color gun signal at that frequency was used. The subject of monochromatic observation of color is a general topic which supports several temperature-measurement coating techniques.

INFRARED SCANNING

Conceptually the simplest survey technique is to "scan" a hot, uncoated surface with a remote sensor which has an output that is calibrated to read temperature. Commercial applications of this technology abound from the medical field to the remote sensing of the earth through satellites.

Temperatures can be measured on a model by remotely scanning the temperature of the model surface with a commercial IR scanning camera. The surface of the model is normally coated to stabilize the surface emittance at a high value. Fast scanning cameras are commercially available although equipment of this type is not inexpensive to purchase and develop. A series of experiments have recently been reported demonstrating that this technique is being used both in Europe and the United States.

The tutorial reference by Wendt ("Infrared Thermography") summarizes these recent experiments well outlining the technique of application of IR sensing as well as a review of recent experiments. Survey paper by Gartenberg, 1991, and Carlomagno, 1989 review the broader scope of IR imaging over the last quarter century.

In the 1970's several Space Shuttle tests were run with IR measurements acquired on wind tunnel models fabricated of insulative materials at Mach 8 in the AEDC Tunnel "B". These data were generally of high quality and compared well with the quality of standard thin skin thermocouple data with two exceptions:

- (1) The image produced by the scanning camera may observe both the hot surface of the model and the cool tunnel in background (near leading edges for instance) and integrate the temperature of interface between them. These data cannot be used.
- (2) The earlier data produced a large minimum spot size, 3/8 inch diameter in which accurate surface temperature data was measured. This limited the use of IR scanning in regions of high heat gradients and shock interaction regions. Later developments have reduced these problems.

The pictures developed are extremely visual and the data acquisition and analysis process can be automated through digitizing the video picture. This technique was developed in the 1970's at AEDC but is now phased out at that center for the two reasons listed above.

More recent applications of the IR technique have been reported at the NASA Langley Center by Venkateswaran et al in a convention tunnel, and at von Karman by Wendt and Simeonides in conventional and impulse facilities, by Henckels and Maurer in a conventional hypersonic facility; by Henckels, Maurer, Olivier and Gronig in the Aachen shock tunnel within the 5 ms test duration of that facility and by Allegre et al in a low density hypersonic test facility. The work of Simeonides is particularly important as it demonstrates a level of spatial resolution which is far superior to the earlier AEDC experiments. The work of Henckels and Maurer as well as that of Allegre et al demonstrate that the IR technique can be combined with differing thermal models to derive heat transfer data. Henckels and Maurer measured the temperature of a solid, low conductivity material and evaluated aerodynamic heating through the 1D semi-infinite slab technique. Allegre, on the other hand, measured the surface of a thin skin model and evaluated heat flux through the thin skin technique.

In addition to the use of a wide variety of test facilities, IR techniques have recently been applied to a series of investigations of small-scale phenomena. In particular, several authors have investigated heating caused by Goertler vortices using highly focused IR cameras. These measurement densities (6 pixels/mm over a 20 mm x 20 mm field) are generating important information on complex phenomena that require both high point accuracy and field comprehension. Obtaining high quality data requires both improving the spatial resolution of the electro-optic signal as well as corrections to the lateral thermal conduction which occurs within measurement materials. See, for instance, the work of de Luca, 1991.

The paper by Balageas et al, 1991, is noteworthy because of the fundamental nature of the work and the breadth of the inquiry. Details are presented regarding the measured directional emittance of Macor (R) and painted Macor models as well as detailed discussions of problems related to this technique. These problems are related to the heating of the tunnel walls and, possibly, radiation from the throat of the wind tunnel nozzle.

More recent work by Balageas et al, 1991 at Onera has discussed the use of an active IR mode wherein the model surface is stimulated by an incident "photon source" and the IR camera records the decay of that imposed, superimposed radiation. Figure 42 shows the test arrangement schematically. The photon sources are each twelve 2-kw infrared tubes. Figure 43 demonstrates the radiant energy from these sources which are superimposed on the normal convective heating from the facility.

Balageas has also noted and documented problems associated with radiation from the nozzle throat and walls of the tunnel. He has recommended painting the nozzle walls black to diminish this reflection. Radiation from the hot, stagnation region beyond the nozzle throat has long been a matter of concern. This is some of the first data published bearing on this question. Those who would measure real gas effects in shock tunnels would do well to be concerned about this effect. Since radiation measurements from the throat will be recorded immediately on the model while convective measurements will require of the order of 1 ms to arrive at the model, the effect can easily be discerned through appropriate stagnation point measurements in the test section.

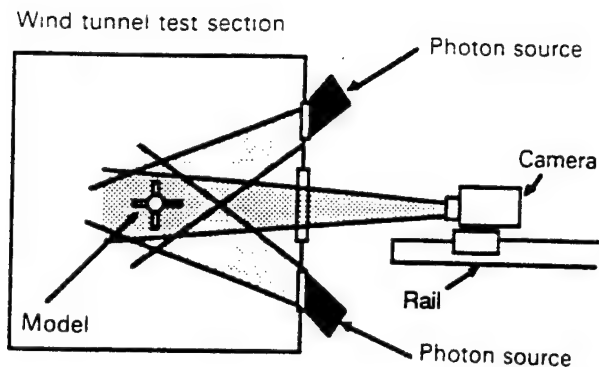


Figure 42 Physical Arrangement of French Stimulated Infrared Measurements in a Wind Tunnel.

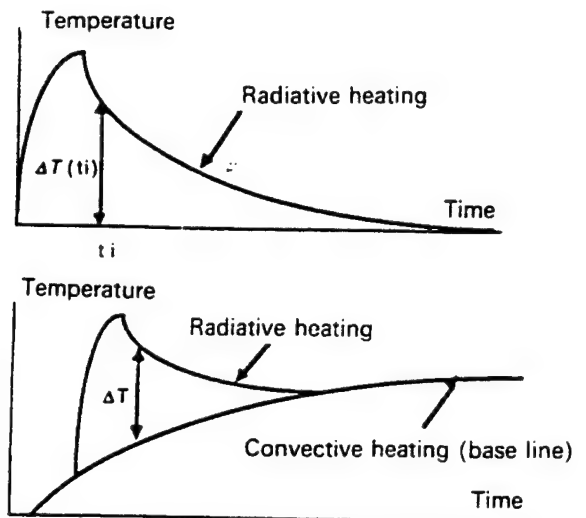


Figure 43 The Heat Pulse Due to Photon Stimulation and the Superposition of That Energy on Normal Convective Heating.

Test Models For Use With IR Detectors

Measurements Made on Metallic Models

Although most IR studies fabricate the test model from insulative materials, an effort by Collier, 1990 concentrated on the use of uncoated stainless steel models constructed of 17-4 PH material with a material thickness of 0.187 ins.. The test configuration consisted of a cylindrical protuberance located within the nose region of a spherically-blunted cone as shown in Figure 10 of Section I. The study compared measurements of surface temperature obtained with an IR camera with surface mounted coax gages. The uncoated stainless steel model had an experimentally-determined surface emittance value of 0.32. It was determined that within the localized shock interaction region (within a distance of 0.25 of the diameter of the protuberance) sizable temperature gradients existed on the model surface that required a two-dimensional (rather than the standard 1D inverse analysis) reduction technique. The difficulty of measuring heat transfer within shock interaction regions will be discussed later in Section VIII of this report. The location of the high surface gradients is consistent with design experience on the location of shock interaction effects. A compendium of these rules of thumb will be presented in Appendix C at the end of this report.

In a subsequent paper, Collier, 1991, noted that the inherently low emissivity of stainless steel precluded the generation of useful quantitative results from the earlier experiment and that a coating to increase the surface emissivity of model surfaces to a value of 0.8 or greater without changing the thermal properties of the model is required.

The results of this experimentation can be generalized to state that while measurements (IR measurements in this case) will generate surface temperature data on models of either metallic or insulative materials, the

inference of aerodynamic heating from those temperature measurements requires the use of an appropriate thermal model that accounts fully for the structural flow of heat. In general, that flow of heat is more complicated in regions where the heat transfer is highly variable, during longer test durations and with model materials which have a higher thermal diffusivity. Accurate measurements in such regions are not precluded but reduction of the data is more difficult and time consuming.

TABLE 3.3
CHARACTERISTICS OF VARIOUS IR SYSTEMS
EMPLOYED IN RECENT WIND TUNNEL TESTS

Camera Type, Researcher and (Test Location)	Detector Type	Sensitivity Range μm / Window Material	Source of Reference and Date of Publication
Inframetrics Model 525 (VKI/Brussels)	Mercury Cadmium Telluride sensor (HgC- dTe)	8-12 / Germanium Window	AIAA Jour. of Thermophysics Vol 4, Nr. 2, April 1990, pp 143-148
AGA Thermo- vision 782 SWB (ONERA/Meudon)		2-5.6 (fig 2 and fig 3)/ not defined window materials	Volume 116 of Progress Series pp 157-16?
Inframetrics Model 600 (DLR/Aachen)	Mercury Cadmium Telluride detector	8-14 / coated Germanium window	ICIASF '89 Record, pp 516-524 also 18th ISSW Conf.
AGA Thermo-vision 680 Scanning Camera (AEDC)	Indium Antimonide Detector	3-5.8 / IRTRAN 2 Window	61st STA Mtg. K.W. Nutt et al, AEDC and 45th STA by K. Hube and AIAA 78-799
		8-12 / Zinc Selenide window	AIAA Paper 89-2205
Inframetrics Model 600 System (NSWC)		8-12 / ZeSe window	ICIASF '91 Record, p169
AGEMA Thermo-vision 782 LW		ZnSe window	La Recherche Aerospatiale #1991-4, p51, Balageas etal
AGEMA Thermo-vision 880 System (NASA/LRC)		8-12 / Open jet, no window	AIAA Paper 90-2341; Burt Northam paper

The Uncertainty of Infrared Detector Measurements in Wind Tunnels:

Boylan, 1978 completed a study of measurement uncertainty for the semi-infinite slab measured by an arbitrary surface temperature sensor. This methodology was applied specifically to IR detectors in the test facilities they were using. The result of that investigation resulted in a plot of total uncertainty for their several test facilities shown in Figure 44.

While details of the topic of uncertainty analysis are beyond the scope of this report, it is instructive to note that very valuable insight into the measurement quality was achieved through this technique and to caution the reader that the result shown should be considered only as indicative of what such an analysis could develop; the absolute results are obviously dated and specific to their particular application.

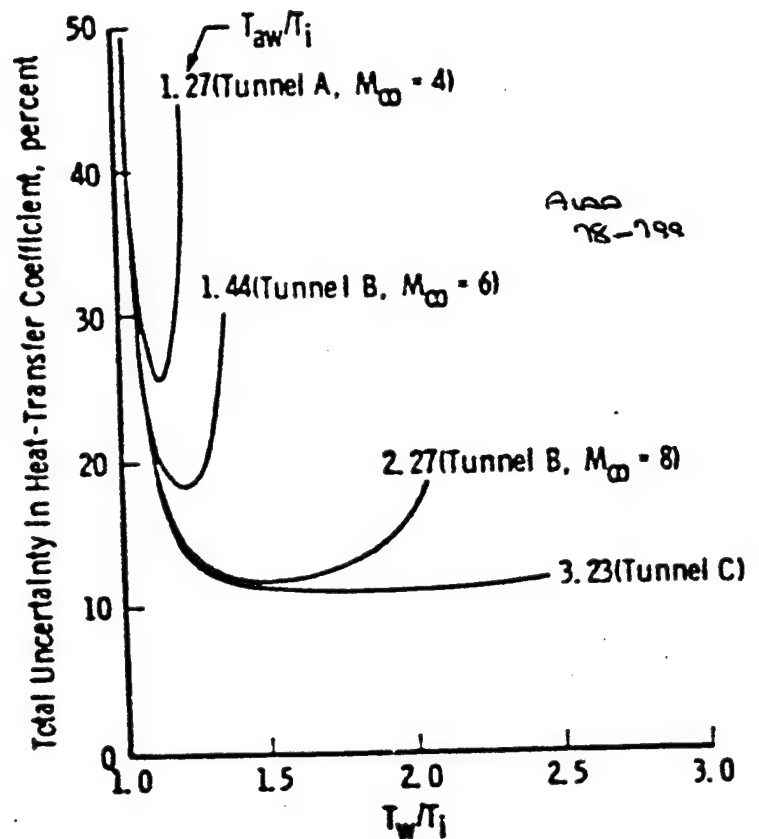


Figure 44 An Uncertainty Analysis Plot for Infrared Sensors from Boylan, 1978.

The parameters which they considered and the uncertainty they assumed are shown in the table below.

The development of IR detectors is progressing at such a rate that estimates of measurement uncertainty are frequently out of date. Values quoted in this report may not be up to date and the reader is urged to review current literature for current numbers.

Purnam et al, 1991, discussed recent experimentation dealing with the accuracy of IR detectors. While pointing out that earlier research by Compton, 1972, quoted a best accuracy for IR detectors to measure heating rates at 10%, numerous improvements have been made in detectors. Purnam thus quotes, as of 1991, the accuracy of IR detectors to measure temperature to be $\pm 5\%$ in the range from -20 to 1500°C . In subsonic calibration experiments on a heated plate with type "T" thermocouples, Purnam noted that the thermocouple data had a maximum uncertainty of 1.6°C at 20:1 odds; somewhat higher than the value of 0.2°C at 20:1 odds quoted by Moffat, 1988 due to temperature fluctuations in the rig. The IR camera tracked those temperatures with a difference mean of 1.44°C and a standard deviation of 2.65°C . Note that these accuracies are for temperature only; heat flux accuracy requires an understanding of the level of heat flux to be measured and the rate of temperature measurements with the IR sensor system.

Boylan's model for the uncertainty analysis for the semi-infinite slab thermal model uses the solution to the one dimensional heat transfer rate equation:

$$\bar{T} = 1 - \exp(\beta^2) [1 - \operatorname{erfc}(\beta)]$$

From this equation using the Taylor series method, the uncertainty in the heat transfer coefficient, $\frac{\omega h}{h}$, is determined by the individual uncertainties in the parameters defined in the semi-infinite slab solution given above. For those 5 parameters, the error sensitivities are given by Boylan in the Table 3.4 as follows.

TABLE 3.4
BOYLAN ERROR SENSITIVITIES

Item, j	Parameter, P _j	Error Sensitivity, (ES) _j
1 Time	t, time	0.5
2 Material Properties	$\sqrt{\rho c_p k}$	1.0
3 Wall Temperature	T_w	$\frac{QT_w}{2(T_{aw} - T_w)}$
4 Adiabatic Temperature	T_{aw}	$\frac{Q(1-Z)T_{aw}}{2(T_{aw} - T_w)}$
5 Initial Wall Temperature	T_i	$\frac{QZT_i}{2(T_{aw} - T_w)}$

The uncertainty in h is thus given as:

$$\frac{\omega h}{h} = \pm \left[(ES_1 \frac{\omega t}{t})^2 + (ES_2 \frac{\omega \sqrt{\rho c_p k_w}}{\sqrt{\rho c_p k_w}})^2 + (ES_3 \frac{\omega T_w}{T_w})^2 + (ES_4 \frac{\omega T_{aw}}{T_{aw}})^2 + (ES_5 \frac{\omega T_i}{T_i})^2 \right]^{1/2}$$

Where $Q = \frac{\sqrt{\pi} Z}{\beta(\beta\sqrt{\pi}Z - 1)}$ and $Z = \frac{T_{aw} - T_w}{T_{aw} - T_i} = e^{\beta^2} \operatorname{erfc}\beta$.

Details of the method are presented in Appendix III-1 at the end of this chapter.

The individual uncertainties used by Boylan were given in Table 3.5 for the various facilities as:

TABLE 3.5
BOYLAN INDIVIDUAL UNCERTAINTIES

Parameter	Uncertainty, ±%, Tunnel "A"	Uncertainty, ±%, Tunnels "B" and "C"
time, t	2	1
$\sqrt{\rho c_p k_w}$	10	10
Initial Temperature, T_i	0.75	0.75 (±4°) at 530°R
Wall Temperature, T_w	1.5	1.5 (±8°) at 530°R
Adiabatic Wall Temperature, T_{aw}	0.5	0.4 (± 6°) ΔT 1350 = T_o ; M = 8

This model may be applied to any surface temperature measurement technique which relies on a semi-infinite slab thermal model. What will change is the level of uncertainty assigned to each elemental factor.

Note from Figure 44 that the aggregate uncertainty is, in most cases, a function of measurement temperature. By manipulating the elemental uncertainties it is possible to define the experimental technique(s) that will give an acceptable level of uncertainty at certain values of the surface temperature.

Carlomagno, 1989, evaluates the accuracy of the temperature measurement starting with the integration of Planck's law over the entire spectrum which gives:

$$E = \epsilon \sigma T^4$$

where E is the total radiation heating

ϵ is the emittance (total hemispherical emittance)

σ is the Stefan Boltzmann constant

$$\frac{\Delta T}{T} = -\frac{1}{4} \frac{\Delta \epsilon}{\epsilon} \left[1 - \left(\frac{T_a}{T} \right)^4 \right]$$

where T is the temperature of the target

T_a is the ambient temperature of the background

Considering only a small window in the IR band, the monochromatic spectral response is written as:

$$\frac{\Delta T}{T} = 1 - \frac{\lambda T}{C_2} \ln \left(1 + \frac{1 + \Delta \epsilon / \epsilon}{A} \right)$$

where A is defined by the equation: $A = \frac{\lambda^5}{C_1} [E_{\lambda 0}(T) + \frac{\Delta \epsilon}{\epsilon} E_{\lambda 0}(T_a)]$

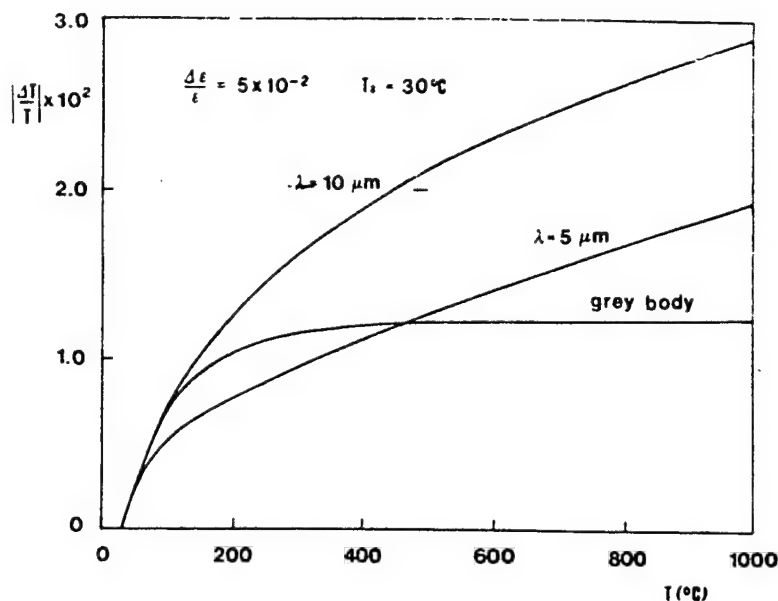


Figure 45 Uncertainty Increments for a Grey Body Approximation and for Data at Specific Wavelengths.

Figure 45 from Carlomagno, 1989, plots the equations developed. The grey body case is from the first equation for $\frac{\Delta T}{T}$

while the other two wavelength-specific lines are from the second equation presented. Note that when specific wavelength peaks are determined, the error increases as the wavelength peak increases.

The wall temperature uncertainty was shown in Table 3.5 to be a constant, $\pm 1.5\%$. These overall estimates depend, in turn, on how the temperature was measured. Stallings et al, 1982 and Boylan et al, 1978, developed the uncertainty analysis with which to evaluate the effect of random errors on the temperature uncertainty of an IR

measurement. The analysis started from the relationship between wall temperature and the detector output as given by the equation:

$$T_w = \frac{K_2}{\ln\left[\frac{\gamma \epsilon_m K_1}{c_2 + \frac{\gamma \epsilon_R K_1}{(e^{K_2/T_R} - 1)}} + 1\right]}$$

Where the seven parameters are:

- K_1 and K_2 are calibration constants
- γ is the window transmittance factor
- ϵ_m is the model emissivity
- ϵ_R is the reference target emissivity
- C_2 is the difference in camera counts between a point on the model and the reference target
- T_R is the reference target temperature

Figure 46 shows each of those sensitivities individually and Figure 47 shows the aggregated effect of all sources on the uncertainty in the model temperature. The aggregated uncertainty in the surface temperature measurement is given by the relationship:

$$\frac{\omega T_w}{T_w} = \pm \left\{ \sum_{j=1}^7 ((ES)_j \frac{\omega P_j}{P_j})^2 \right\}^{1/2}$$

where the ES's are error sensitivities for the parameters P_j .

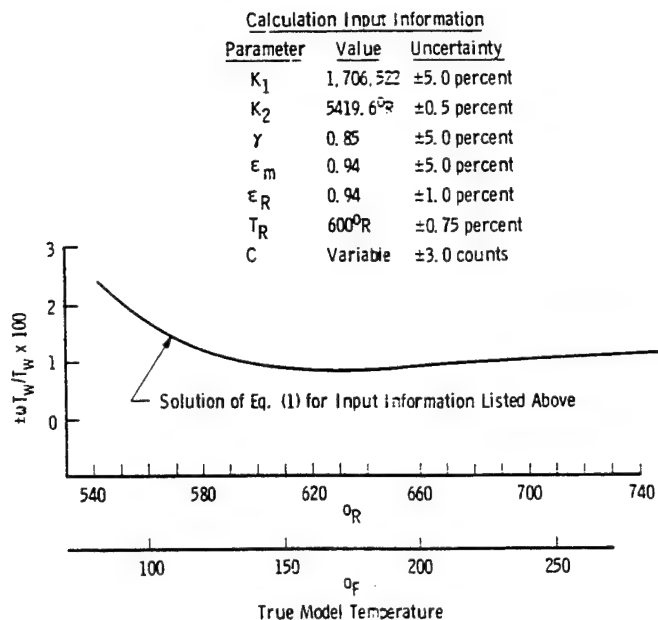


Figure 46 Effect of Random Errors on the Model Surface Temperature Calculation.

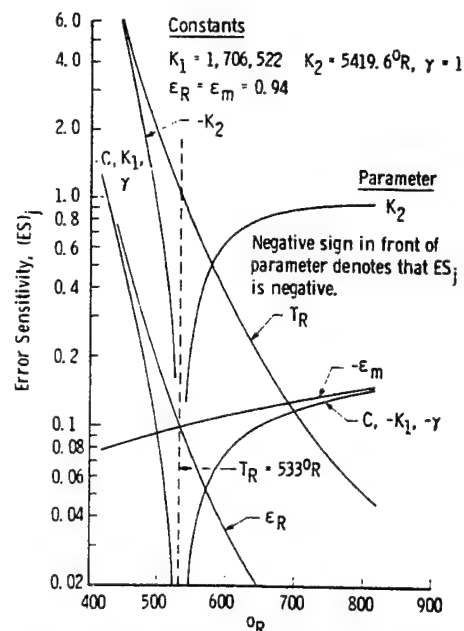


Figure 47 Error Sensitivity Functions Specific to a Given Camera and Model Installation.

Finally, a recent IR model evaluation was reported by Vermeulen and Simeonides, 1992. Appendix B of that report shows the various quantified error sources which are reproduced here as Table 3.6. The unique error sources noted by Vermeulen et al are (1) the uncertainty in the slope of the calibration curve, $\pm 4\%$; (2) the uncertainty in the IR measurement intensity due to noise, $\Delta I_{noise} = \pm 2 \text{ pixels}$ and (3) geometric scaling between the physical plane and the stored image, $\pm 6 \text{ pixels}$. The framing rate of the camera introduces an uncertainty of $\pm 20 \text{ ms}$, which is reflected in a time uncertainty of 4%. The several error models to which the reader has been exposed will allow for an efficient development of an error model for new efforts. Please note that the quantified errors are specific to a certain experiment and may be substantially different for any other experiment considered.

TABLE 3.6
UNCERTAINTY ANALYSIS FROM VERMEULEN AND SIMEONIDES, 1992

Variable	Value & Error	Total Uncertainty	Unit
P_o	10 ± 0.1	$\pm 1\%$	bar
T_o	530 ± 5	$\pm 1\%$	K
Δ	0.155 ± 0.006	$\pm 4\%$	K/Int
\sqrt{pck}	576.5 ± 10	$\pm 1.7\%$	$W_s^{1/2}/m^2 K$
\sqrt{t}	0.25 ± 0.02	$\pm 4\%$	s
ΔI	150 ± 2	$\pm 1.3\%$	Int
T_w	295 ± 0.5	$\pm 0.17\%$	K
χ	350 ± 6	$\pm 1.7\%$	pix

INTRODUCTION TO POINT GAGE DESIGNS: BASED ON THE SEMI-INFINITE SLAB THERMAL MODEL

There are several possible gage configurations for point measurement of heat transfer using the semi-infinite slab thermal model. These various gages are distinguished by the type of surface sensor employed and the type of backing material upon which the surface sensor is applied. Table 3.7 indicates the matrix of such gages as well as combinations of parameters for which no gages are known to exist. Each of these gages will be discussed in the paragraphs that follow.

TABLE 3.7
MATRIX OF THERMAL GAGE DESIGNS BASED ON THE
SEMI-INFINITE SLAB THERMAL MODEL

Substrate Material	Surface Sensor Type			
	Thin Film Resistance Thermometer	Thermo-couple	Semi-Conductor	Surface Coating
Insulator	Thin film gage	Isothermal staple gage or thin film thermocouple	McDonnell gage	Thermal paint, IR scan or Thermal phosphors
Conductor	Ainsworth, Oxford University, 19xx	Coax gage	Not used	Not used; requires a difficult data evaluation

Of the gage types shown in the above table, the "thin film resistance thermometer" and "coax" designs are actively used. An earlier design of Covert and Gollnick, 1968 used an isothermal thermocouple on the model surface which has a modern analog in the thin film thermocouple gages. The "McDonnell Gage" was also an earlier design based on the interesting properties of semiconductors as temperature sensors, see Dixon, 1968. The semi-conductor temperature sensor was later used by Jenke, 1978 and termed the "Temp Sensor Gage". The instrument is commercially available from Kulite Corporation.

Even this matrix does not strictly confine the spectrum of gages which could be produced. The blank square do not all represent gage impossibilities but rather a lack of current gage applications. In some cases, the gages which would be represented in these blocks offer no unique advantage to the experimenter. In other cases, as for example the thin film resistance thermometer attached to a conductor, the combination requires

an insulative layer between the sensor and the surface. Recall that the thin film gage is electrically powered so that this possible gage would be required to be electrically insulated from the substrate.²

The Size of Various Point Thermal Measurements

Table 3.8 shows the relative dimensions of thermal sensors. Many of these are point measurements based on the 1D semi-infinite slab thermal model. Note from this table that current gages are roughly 0.063 inches in diameter and that the demonstrated technology will allow the development of gages as small as 0.008 of an inch square. Knowledge of the sensor dimensions is important for regions having high thermal gradients; shock interaction regions which will be discussed in Section VIII of this report.

TABLE 3.8
DIMENSIONS OF HEAT FLUX SENSORS

Heat Flux Sensor Type	Typical Diameter (Ins.)
Thin Film resistance Thermometer *	0.0030 x 0.200 or 0.004 x 0.005
Schmidt-Boelter Gage	0.250
Coax Gage *	0.0150
Plated Thermocouple Gage *	0.008 x 0.008

* Requires proper materials to form a valid thermal model

Thin Film Gages

A few years ago the term "thin films" specifically denoted thin film resistance thermometers; a class of surface temperature gages that infer temperature from the change of resistance of a metallic film placed on the surface. The thin film resistance thermometer is highly sensitive and that, in conjunction with a semi-infinite slab thermal model, allowed the inference of heat transfer data. In current instrument discussions the term "thin film" is somewhat ambiguous. Thin film gages can, indeed, refer to thin film resistance thermometers which is the subject of this section of the report or they can refer to thermocouples deposited as films on insulative substrate which provide the same type of thermal gage as the thin film resistance thermometer gage. The Vattel heat flux gage, which will be discussed in section 5, is also a thin film gage; a thin film thermocouple gage that by virtue of its gradient design generates a measurement proportional to heat flux. Appendix III-2 at the end of this section briefly reviews the literature of thin film thermocouples for readers who are interested.

² It should be noted that some insulator materials used to back thin film resistance thermometers are relatively higher conductors and can be used for that purpose as for instance the use of sapphire which has a $\sqrt{\rho ck}$ product 42 times that of pyrex but still only 3% that of stainless steel.

The thin film resistance thermometer is simply a very thin film of metallic material applied over an insulator on the surface of the model. The resistance measured is proportional to the temperature sensed by the film. The resistance is measured by supplying a constant current to the film and measuring the change of voltage caused by the film response to temperature through a bridge circuit. The basic sensitivity of this type of gage is typically 3 mv / deg K; 50 times that of a low temperature thermocouple. The response time of the thin film resistance thermometer is of the order of micro-seconds.

Physical Sizes and Characteristics

Thin film resistance thermometers are applied to insulative substrates by one of several processes; painting, vapor depositing or sputtering. The film thickness deposited is typically 0.1 micron giving the film a response time of 10^{-7} seconds. The films can be made very small and many gages can be placed in close proximity. Table 3.8 shows only typical dimensions of such gages. Far smaller gages are possible if carefully crafted and fabricated of the right materials. Figure 48 from Holden³ shows very small thin film resistance thermometer gages applied to a 0.75 inch diameter cylinder.

Thin film resistance thermometers are highly sensitive instruments which can be used to measure very low rates of heat transfer (below 0.1 *Btu/Ft²Sec*). The substrate of these gages electrically insulates this powered gage from the model and minimizes lateral conduction away from the gage (important in shock interaction processes) at the expense of creating a non-isothermal surface about the gage. Some effort has been made to fabricate models made entirely of the insulator that backs the thin film gage. Macor (R) is frequently used in this capacity. Miller et al, 1981, has created outstanding benchmark experiments using

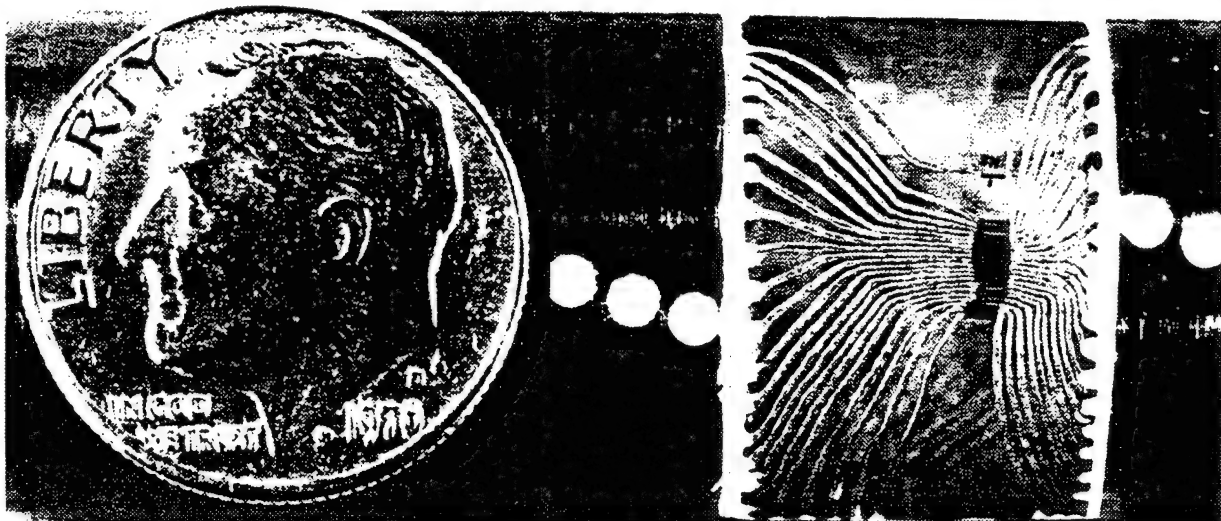


Figure 48 Very Small Thin Film Resistance Thermometer Gages Applied to a Leading Edge Model.
Photo from Dr. M.S. Holden of the Calspan Corporation.

³ Photograph from Dr. Holden's instrumentation of small leading edges with thin film gages. Craftsmanship completed at the Calspan Corporation, Buffalo N.Y.

models fabricated entirely of Macor insulator and heavily instrumented with thin film gages. The space shuttle model shown in Figure 49 is an example of this approach. Alternatively, models may be fabricated of steel with the thin film resistance thermometer attached through the use of an intermediate, insulative layer. This technique, used in turbine measurements at Oxford University by Ainsworth, 1989, an co-workers retains the structural integrity of the model while reducing the temperature rise due to the higher thermal properties of the substrate materials.

The Need for Gage Topcoats:

In high enthalpy flows, the test flow is electrically conductive and the films must be protected from electrical shorting by an insulative topcoat. Several materials are used including mother of pearl, silicon monoxide, Germanium and Magnesium fluoride. These materials are, in addition to being electrically insulating, chemically non-catalytic and do not cause chemical recombination of the gases or measure heating caused by chemical recombination. Jessen, 1991, suggests the use of a Germanium topcoat layer since this material has a relatively higher thermal diffusivity than other materials and does not increase the response time of the sensor significantly.

Marrone, 1959, discussed the output of thin film gages with shock Mach number and the development of overcoating techniques. Figure 50 from his reference shows the output of coated and uncoated gages as the shock Mach number increases. There are cases where a second topcoat material is added to cause the gage to become chemically catalytic once more. These materials, such as Gold, further increase the response duration of the sensor in a high enthalpy test flow where test duration is already low.

Cassady, 1991, discussed comparable measurements with coated thin film resistance thermometers and chemically cleaned and catalytic coax gages. Figures 51a and 51b from that reference demonstrates a measurable difference in output between the two classes of gages. These two figures demonstrate

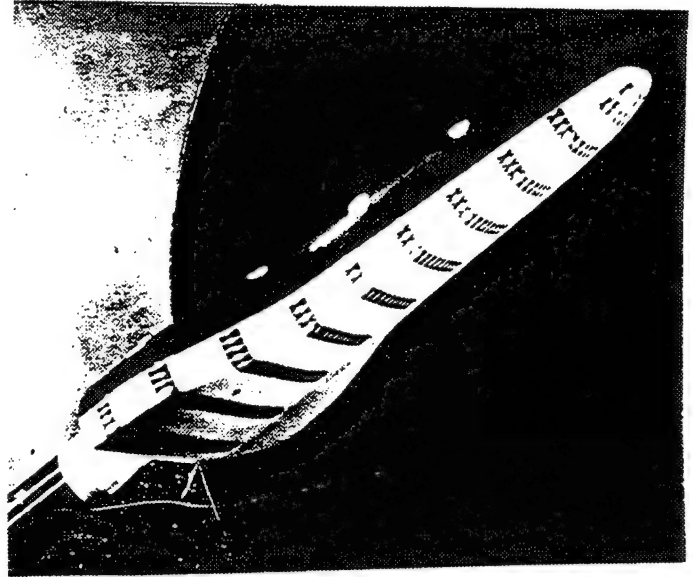


Figure 49 An All-Macor Model of the Space Shuttle Showing Dense Thin Film Instrumentation.

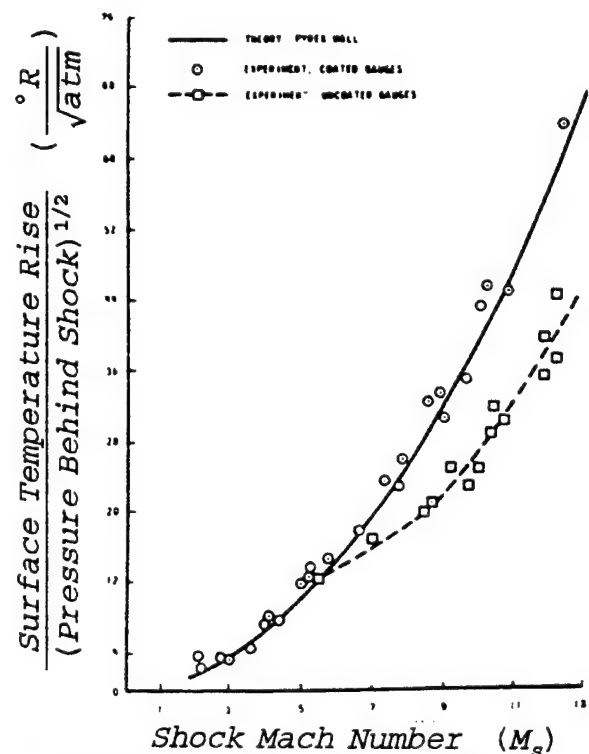


Figure 50 The Effect of Ionization on the Output of Uncoated Thin Film Gages.

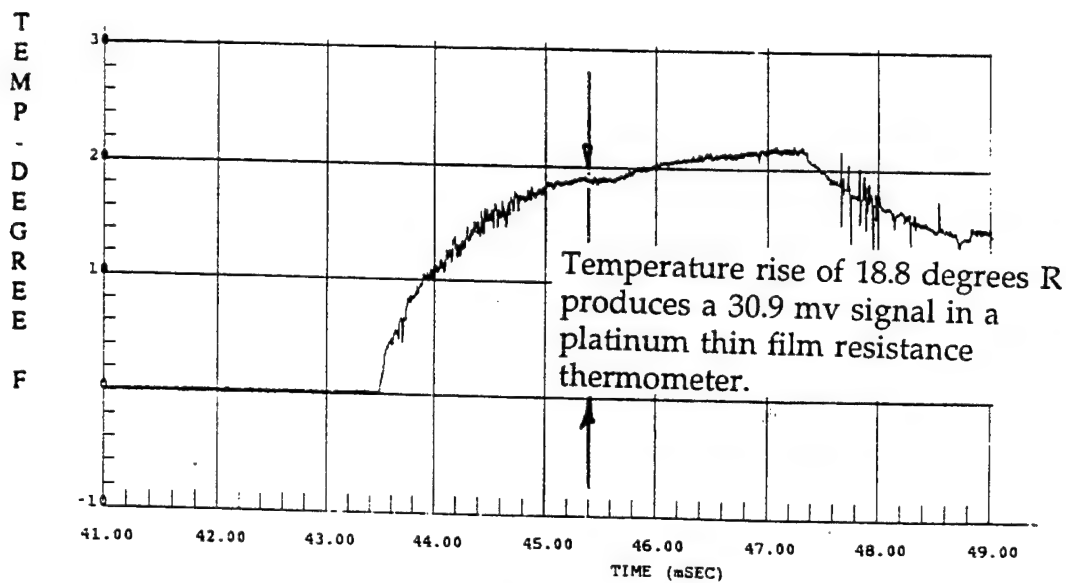


Figure 51a Temperature/Time Trace for a Thin Film Resistance Thermometer Gage.

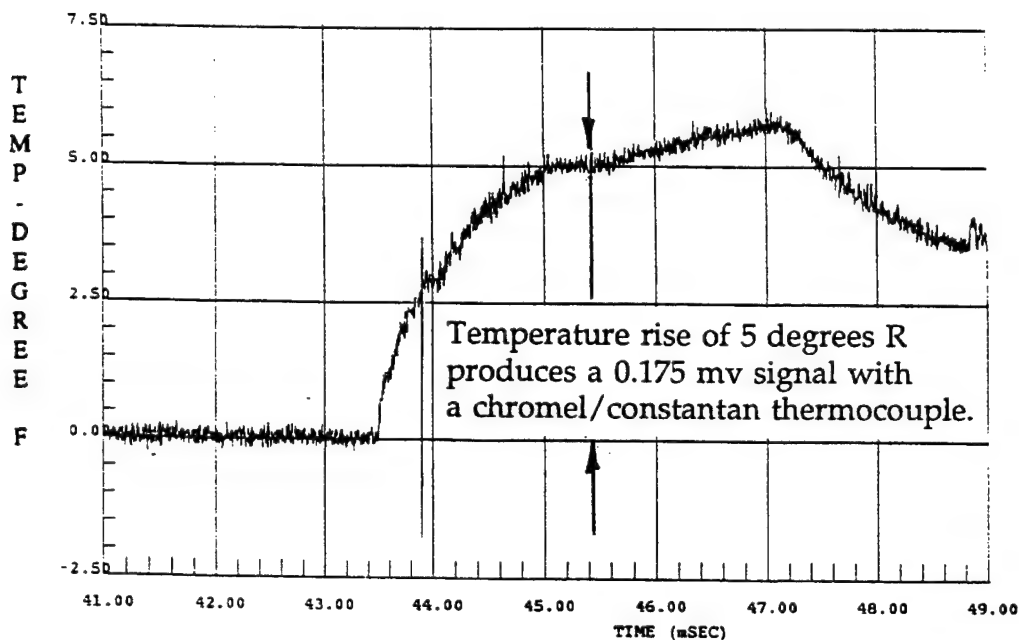


Figure 51b Temperature/Time Trace for a Chromel/Constantan Coaxial Thermocouple Gage.

identical measurements on a simple sphere-cylinder-flare test configuration. The measurements shown were made at the same model station but 180 degrees apart. Figure 51a is the thin film measurement and shows a 19 degree temperature rise together with a 31 mv signal. Figure 51b is a coax measurement and shows a 5 degree temperature rise together with a 0.175 mv signal for the same imposed heating. The ratio of the two signals is 177. This ratio is caused by the increased sensitivity of the resistance thermometer relative to that of a thermocouple and the increased temperature rise of the insulating substrate relative to that of the conducting thermocouple.

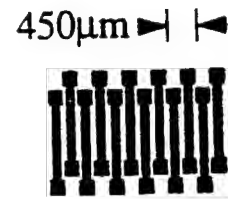
Very recently research has been conducted on the use of polycrystalline CVD diamond films as resistance thermometers. These sensors have extremely useful thermal properties as gage material as well as the ability to be densely packed on a practical substrate material. Table 3.9 contrasts the diamond materials against the more standard platinum thin films.

TABLE 3.9
COMPARISON OF PLATINUM AND DIAMOND THIN FILM GAGES

Property	Platinum Thin Film	Diamond Thin Film
Resistance, Ohms	60	10^5 to 10^3
Temperature Coefficient, α	0.0039	0.017 at 500 R to 0.003 at 1800 R
Substrate	Various Materials; adhesion no problem	Oxidized Silicon; single substrate found now.
dR/dT , Ohms/ $^{\circ}$ R		1000 at 500 R to 1 at 1800 R

Figure 52 from Aslam, 1992, demonstrates the packing density of these new thin film sensors. Each sensor strip is 0.15 mm wide (0.0059 ins) by 1.5 mm long (0.059 ins).

The resistance of the diamond thin film sensor is noted in the table to be highly temperature-dependent. This can be observed in detail in Figure 53 where the resistance drops by two orders of magnitude as the temperature increases. Similarly, the temperature coefficient of resistance, α , is observed to drop as temperature increases as shown in Figure 54. These effects are more complex than for metallic thin film gages and will require more complex functional relationships in the data reduction process.



Layout of
diamond sensor array, each
element is 150 μ m wide
and 1.5 mm long.

Figure 52 Packing Density of Diamond Thin Film Gages.

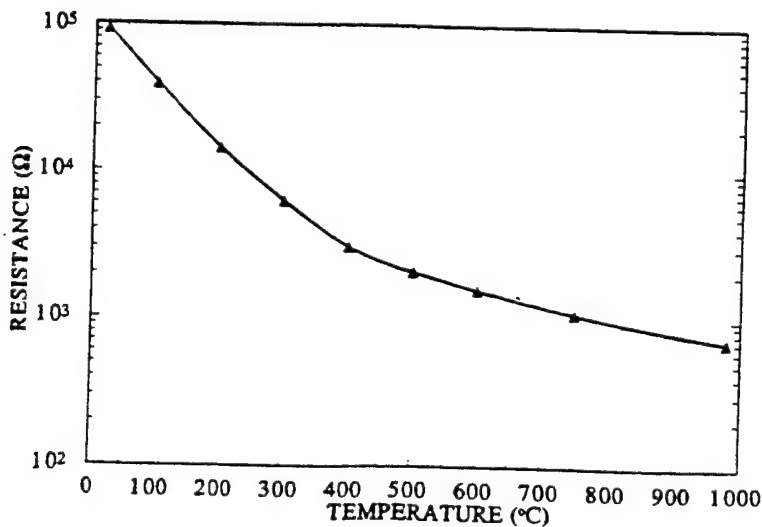


Figure 53 The Resistance of Annealed Diamond Thin Film Sensors after Aslam, 1992.

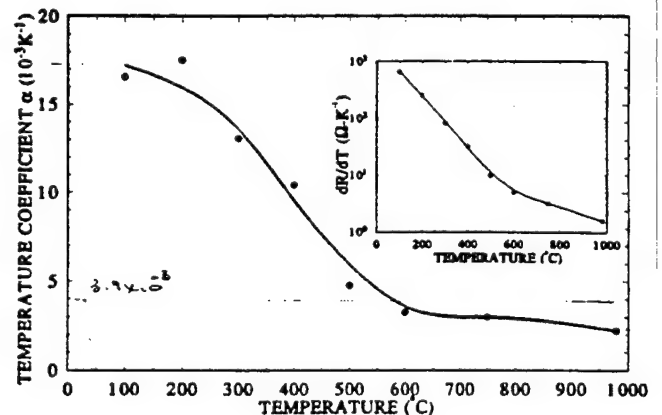


Figure 54 Temperature Coefficient of Resistance for the Annealed Diamond Thin Film Sensor as a Function of Surface Temperature after Aslam, 1992.

Long Duration Use of Thin Film Resistance Thermometers

Schultz et al from Oxford have used thin film resistance thermometers in turbine testing for long periods of test time (up to 1 second). These long test durations increase the potential difficulties of generating heat flux data and, as well, present new opportunities for data analysis and understanding. If an electrical analogue technique is used to reduce the data then the repetition rate for the R-C circuit must increase to correctly define the heating rate profile. Schultz states the repetition rate to be given by the equation $t = 0.2n^2$ where "n" is the number of repetitions and "t" is the test duration in milliseconds. More details on these R-C circuits is given by Schultz, 1973. Long test durations, for a given level of heating rate, increase the surface temperature approximately as the square root of test time. For a given test condition, the measured heat transfer rate will decrease as test duration increases. The measured increase in gage temperature, a function of test time, and the corresponding decrease in the heating rate (due to the difference $(T_{aw} - T_w)$ decreasing) is shown in Figure 55 from Schultz, 1965.

That data can also be displayed as shown in Figure 2 demonstrating the slope of the heating rate with wall temperature which is, in the absence of other factors, the heat transfer coefficient. It must be noted that the variation of heat flux with time may in fact be due to temperature rise but it may also be due to (1) a variation in surface heating rate with time, (2) an inexact model of the thermal properties of the substrate material with temperature (3) the conduction of heat along the surface of the model with time (temperature difference between the gage temperature and the blade temperature) and/or (4) non-isothermal wall temperatures developing as a function of test duration. The experimentalist must carefully understand which of these phenomena are present and whether the extrapolation of heating rates to isothermal temperature is proper.

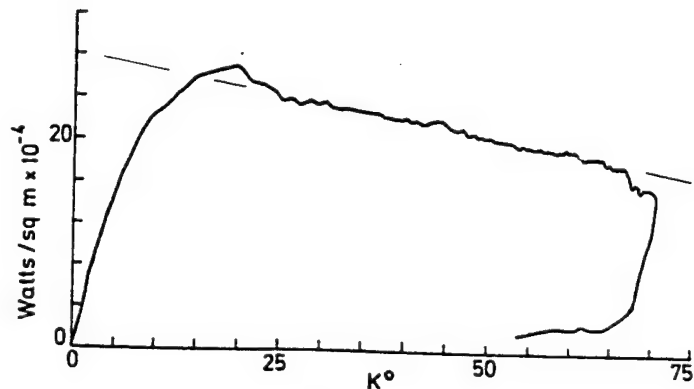


Figure 55 Variation of Surface Heating Rate with Increasing Surface Temperature from Schultz et al, 1965.

The isothermal heating rate can then be evaluated by reconstructing the original temperature history from the heating rates derived from analogue networks. A least squares line fit of the linear section of the $\dot{q} \approx t$ curve is used to extrapolate the heating rate back to the isothermal wall temperature.

CALIBRATIONS REQUIRED OF THIN FILM RESISTANCE THERMOMETER GAGES PRIOR TO USE

There are two basic calibrations required for thin film resistance thermometer gages prior to their use. These are:

1. The calibration of the temperature coefficient of resistance, α , of the applied film which defines the characteristics of the resistance thermometer composed of a plated film such as platinum.
2. The calibration of the thermal properties of the combined substrate and sensor materials, β .

Calibration of the Temperature Coefficient of Resistance

The resistance of the installed platinum film, from which temperature is deduced during the test as an out-of-balance resistance in a bridge circuit, requires developing the required temperature/resistance relationship through pre and post test calibrations. A thermally controlled oil bath can conveniently be used to produce this calibration. Miller quotes a maximum uncertainty in this parameter to be less than 3%.

Calibration of Thin Film Substrate Materials

The thermal properties of any substrate are not known to sufficient detail for calibration purposes. Further, the physical properties of the substrate immediately behind the thin film are affected by the film which is fused to the substrate surface (see for instance Reddy, 1980). There are several techniques available to experimentally determine the parameter beta as shown below.

Measurement of Stagnation Point Heating Use of a Pulsed External Heat Source Dissipation of Heat Generated By a Pulsed Current Through the Gage Application of the "Relative Calibration Technique"

One straightforward technique is to use the fabricated gage at the stagnation region of a sphere in a calibration shock tube. Knowing the stagnation point heating from the Fay and Riddell theory (model), the substrate characteristics of the material can be deduced from the experiment.

The thin film gage itself may be used in the calibration process by pulsing a current through the film and observing the dissipation of heat through the substrate material. This technique requires an accurate measurement of the surface area covered by the film; a difficult measurement for a gage of irregular shape with inexact surface boundaries.

The relative calibration technique has been used in several forms in order to eliminate the need to precisely define the surface area covered by the film. In this technique either an external energy source (see Epstein, 1986) or an internal energy source such as a current pulse is used. The heat is dissipated through the substrate material with the gage placed in air and through both the substrate material AND a fluid of known thermal properties when the gage is placed in that fluid. The assumption is made that the heated gage in the designated fluid will loose heat evenly to both gage substrate and fluid. Knowledge of the surface area of the gage is not required because the air calibration is related to the fluid calibration. Appendix III-3 at the end of this section outlines the technique from a paper by Epstein, 1986.

Several fluids have been used in the relative calibration technique. Distilled water was suggested as its lumped thermal properties approximate those for Pyrex (R). For uncoated gages, distilled water has been replaced by a Dow Corning Silicon fluid. More recently, Epstein, 1986, used Dibutyl Phthalate as a calibration fluid.

The calibration techniques reviewed have in common the observation that uncommon substrate materials (other than Pyrex (R)) present calibration data quite different than handbook published values. Further, these calibration data contain the largest potential source of error - both in the substrate being calibrated and in the reference calibration fluid.

In general, the variation of substrate resistance with temperature is a quadratic function written as:

$$\frac{\Delta R}{K_{70}} = (T-70) - K_2(T-70)^2 = T_m$$

where ΔR is the change of resistance with temperature

K_{70} is the temperature coefficient of resistance

T is the actual temperature of the gage

T_m is the temperature of the gage from linear relationships

This nonlinearity is particularly apparent at the higher surface temperatures; a linear relationship being appropriate for small levels of temperature rise.

Figure 56 presents the temperature sensitivity of the substrate thermal properties for several materials. Note that pyrex 7740 has the highest temperature sensitivity while Macor (R) has a far smaller sensitivity. Data in this figure are only presented for smaller temperature rises, up to 325 degrees R. Far larger temperature rises have been experienced in recent applications of these gages and in these extreme cases, the linear extrapolation of these data must be questioned.

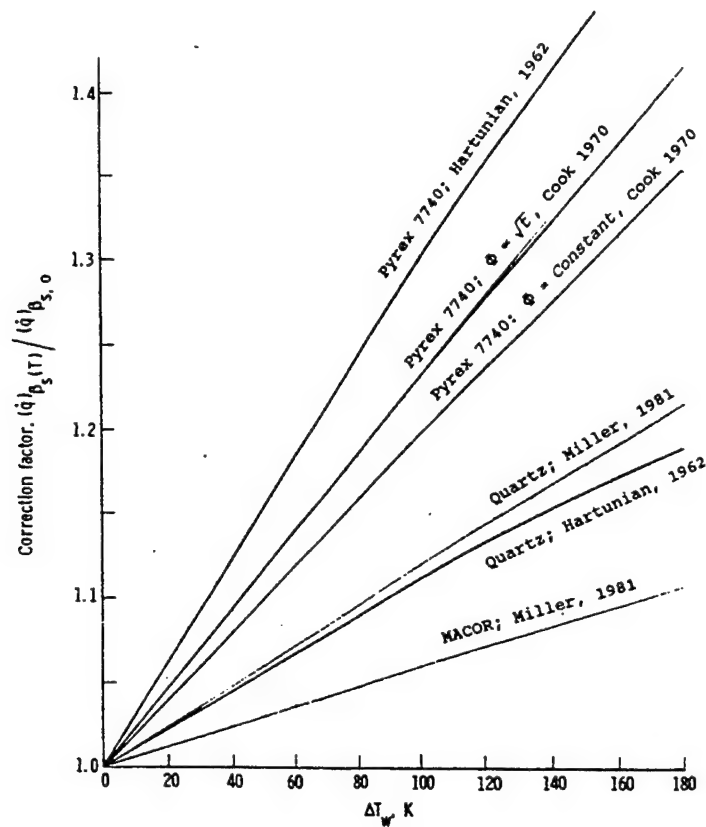


Figure 56 Heat Flux Corrections Due to Temperature-Dependant Substrate Thermal Properties.

Reduction of Temperature Data to Heat Flux

Classical Techniques:

Cook and Felderman

From the basic equation defining the relationship between the measured temperature distribution and the causal heat flux, Cook and Felderman, 1966, use a piecewise linear approximation to the digitally acquired temperature measurements. This piecewise analytical expression can be locally integrated to define the heat flux. The technique of Cook and Felderman is limited to constant thermal properties although corrections can be applied to the data reduction results to approximately account for variable thermal properties.

Q-meter technique

There exists an analogy between the heat flow through the substrate material and the current flow through an R-C circuit. This analogy results from the fact that both the heat flow and current flow present the same form of differential equations as outlined in Figure 57 and discussed by Skinner, 1960, Schmitz, 1963 and Walenta, 1964 among others. Early data reduction techniques made use of this analogy and constructed repeated R-C circuits to define the thin film heat transfer over an interval of test time. The number of R-C circuit elements is proportional to the duration of the test flow.

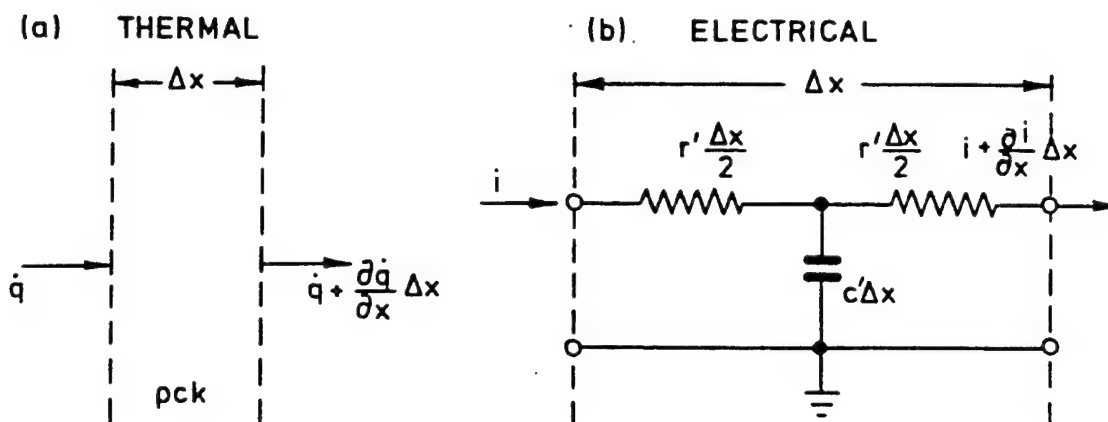


Figure 57 Demonstration of the Analogy Between Heat Flow and Electrical Flow; the Basis of the Q-Meter Design.

Digital sampling technique

The availability of A/D convertors made the Q meter unnecessary and relatively unresponsive to highly variable signals. PC based A/D boards allow the conversion and numerical reduction of thin film data to be accomplished quite conveniently. A recent paper by George, 1991, outlines the difficulties implicit in numerically sampling thin film data, particularly when unsteady heat transfer is anticipated.

Both of the classical techniques, the Q-Meter analogue technique and the Cook-Felderman technique, assume that the material properties are invariant with surface temperature. This can lead to a substantial error at high levels of imposed heating rate. Miller, 1981, has shown correction factors which are substrate-material dependant as a function of surface temperature. These data were previously shown in Figure 60. Physically, constant properties underestimate the temperature-dependant level of the thermal conductivity. As a result, heat flux is larger when time dependant thermal properties are accounted for. The figure from Miller ends with a temperature rise, ΔT_w of 180 degrees K, however temperature rises of up to 300 degrees K are possible as the pressure and enthalpy of the flows increase and as the duration of the test increases $\Delta T \approx t^{1/2}$. Holden, 1988 cites temperature increases of over 278 degrees K for interactions made at Calspan.

Numerical Techniques

The Rae-Taulbee Algorithm:

Holden, 1988, has employed a "Rae-Taulbee algorithm" to reduce shock tunnel heat flux data associated with shock/shock interaction processes. This algorithm solves the 1D heat conduction equation numerically and introduces temperature-dependent thermal properties as well as a Crank-Nicholson finite-difference solution to the basic, one-dimensional heat transfer equation which introduces the temperature dependant thermal properties into the solution.

The Dunn-George-Rae-Woodward-Moller-Seymour Technique:

Dunn et al, 1986, have addressed the problem of high frequency temperature perturbations superpositioned on the longer time-scale shock tunnel temperature-time signal. The classical techniques previously discussed were deemed to be inaccurate under these circumstances. Under this technique, both the surface temperature and its first derivative are digitized on separate data channels and a composite signal is reconstructed from these data through an FFT algorithm which minimizes quantization errors on the fluctuating temperature signals. Variable thermal properties are introduced into a Crank-Nicholson finite-difference solution to the basic, one-dimensional heat transfer equation. Although developed for rotating turbine blades, the technique has application in shock interaction regions where high frequency instabilities are noted in the data.

Seymour, 1987, discussed the several techniques to manage the situation where a high frequency temperature perturbation was superpositioned on the longer time-scale shock tunnel temperature-time signal comparing the finite difference techniques with the exact solution of Cooke and Felderman. He demonstrated, through simulations that the numerical techniques were in agreement with the exact analysis only for the low frequency portion of the temperature signal where sufficient temperature data points were available per cycle. Seymour concluded that at least 30 points were required per cycle to assure that the reduced heat flux data were not distorted. Lesser data points introduced both an attenuation in the heat flux level as well as a time delay in the signal. A more recent discussion of the problem is attributed to George, 1991.

The Design and Sensitivity of Thin Film Gages (From Epstein and Guenette, 1986)

Thin film gages are heated with a constant current and produce a voltage change as the resistance of the film changes with temperature. Epstein, 1986 developed a sensitivity equation for the thin film gage written as:

$$\frac{\delta V}{\delta T} = (It)^{1/2} \propto I Q^{1/2}$$

where α is the temperature coefficient of resistance (previously discussed under calibration)

δV is the change in voltage with a change in temperature δT .

Q is the ohmic heat dissipated in the gage

l is the film length

r is the volume resistivity of the film

t is the film thickness

From this equation Epstein has shown that long, thin films (large " l ") with high volume resistivity (high " r ") and a high temperature coefficient (α) are best for high temperature measurement sensitivity. It is for this reason that thin film gages are long, thin strips of metallic film that are sometimes formed into serpentine patterns and it is for this reason that advanced film materials with high resistivity such as diamond are being investigated for thin film gages.

COAX HEAT GAGES

The coax gage is a thermal instrument based on a one dimensional thermal model with heat flow into a metallic structure. The coax gage is a thick wall gage based upon the capture of heat within a thermal mass of the instrument. In its most simple form, the coax gage is a semi-infinite slab gage; thermally, the same type of gage as the thin film gage. It is a Thompson class 2 gage. Modified versions of this gage eliminate the requirement that the gage have an isothermal back face temperature and, in so doing, change the character of the gage making it closer to a Thompson class 1 gage; a sandwich gage.

The coax gage, has been used to measure heat transfer for nearly a half century. Figure 58 from Giedt, 1955 indicates experiments using such a gage on gun barrels. This work had its genesis in Germany during World War II. Ferri used such a gage in the 1950's as shown in Figure 59. The gages shown in this figure indicate an improved fabrication technology over the past 30 years but hardly an improvement in concept. Coax gages are matched to the thermal properties of the model to which they are attached. Chromel-constantan coax gages installed in 17-4 ph stainless steel models are nearly thermally-transparent having close to the same properties as the model material. Table 3.10 from Mentre and Cosigny, 1987, demonstrates how close these properties are. Data for this combination of gage and model characteristics is responsive enough to measure flows in a shock tunnel and can be error-free for up to 30 seconds before the slight differences in thermal properties are apparent in the data.

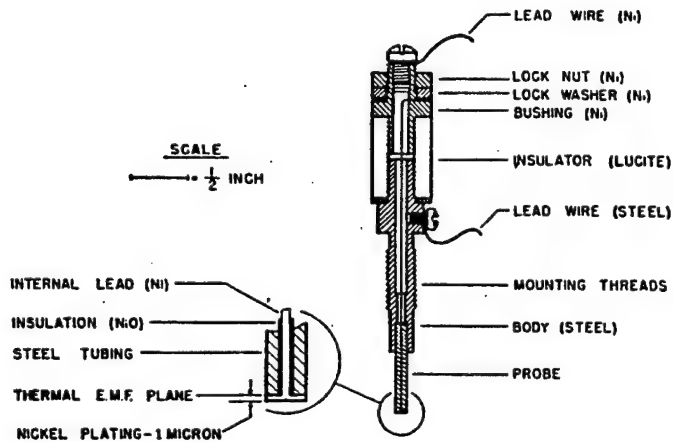


Figure 58 Early Coax Gage Used in Germany, Giedt, 1955.

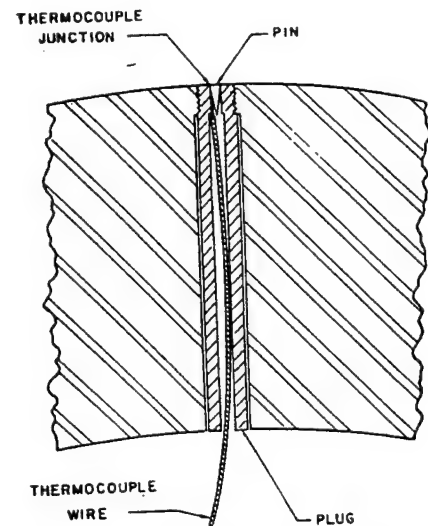


Figure 59 Early Coax Gage Used in the US, Ferri 1957.

Mentre and Cosigny at Onera, 1987 have extended the useful duration of these gages even further by replacing the coaxial constantan jacket by a larger constantan block into which chromel wires are installed as shown in Figure 60. Clearly this would reduce the problem of the commercial coaxial gage being heated by a stainless steel model of slightly different thermal properties.

Semi-infinite slab gages (coax gages and thin film gages for example) respond to imposed heating according to the substrate thermal properties. If the substrate is an insulator (as in the case of a thin film resistance gage), the response is strong because the surface temperature increases rapidly. If the substrate is a conductor (as in the case of the coax gage), the response is moderated by the faster dissipation of the heat

TABLE 3.10
COMPARISON OF THERMAL PROPERTIES OF CHROMEL/CONSTANTAN THERMOCOUPLE
MATERIAL WITH STAINLESS STEEL MODEL SURFACE

	17-4 ph Stainless Steel	Constantan	Chromel
thermal conductivity, k	17.81	22.57	18.81
thermal diffusivity, a	4.55x10-06	6.21x10-06	4.88x10-06
$\sqrt{\rho c k}$	8,350	9,060	8,510

where:

k has dimensions of W/m-deg K

a has dimensions of m²/s

rho has dimensions of kg/m³

c has dimensions of J/kg-deg K

through the conductive medium and the surface temperature rise is lower. Table 3.11, taken from a calibration report by Lyons and Gai, 1988, demonstrates the difference in thermal properties between a thin film substrate and a coax gage substrate.

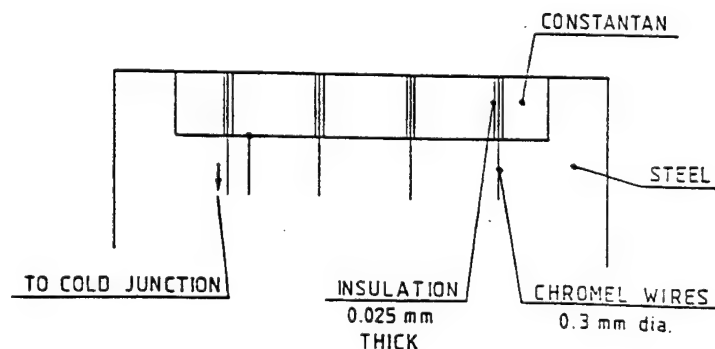


Figure 60 Modified Coax Gages after Mentre and Consigny, 1987.

TABLE 3.11
DIFFERENCE IN THERMAL PROPERTIES
BETWEEN THIN FILM SUBSTRATE AND COAX GAGE SUBSTRATE

Gage Type	$(\rho_w c_p k_w)^{1/2}, J m^{-2} K^{-1} S^{1/2}$
Thin film resistance thermometer, palladium on Macor (R) in this example	2070
Miniature coaxial thermocouple sensor	9997

The temperature rise, ΔT , on the surface of the semi-infinite slab is written (after Schultz and Jones) as:

$$\Delta T(t) = 2 \frac{\dot{q}}{\sqrt{\pi}} \left(\frac{t}{\rho c k} \right)^{1/2}$$

From Table 3.11, the relative temperature rise for these two gage types in the same heating environment is given by:

$$\frac{(\rho c k)^{1/2}_{film}}{(\rho c k)^{1/2}_{coax}} = \frac{2070}{9997} = \frac{\Delta T_{coax}}{\Delta T_{film}} = 0.208$$

The temperature rise with heating for the coax gage can be relatively low and thus the measurement of temperature can be difficult and can produce error. To a large extent, the amount of this error depends upon the level of the imposed heating rate.

Error can also be induced in these gages by external sources. Figures 61 a and b demonstrate noise in the gage output as a result of stepping motor operation within the model as well as the effects of cable shielding with these low-output gages. Because of the low output characteristics of coax gages, careful attention must be paid to proper cable shielding and shielded connectors, minimizing lead wire lengths and the possibility of ground loops in the signal.

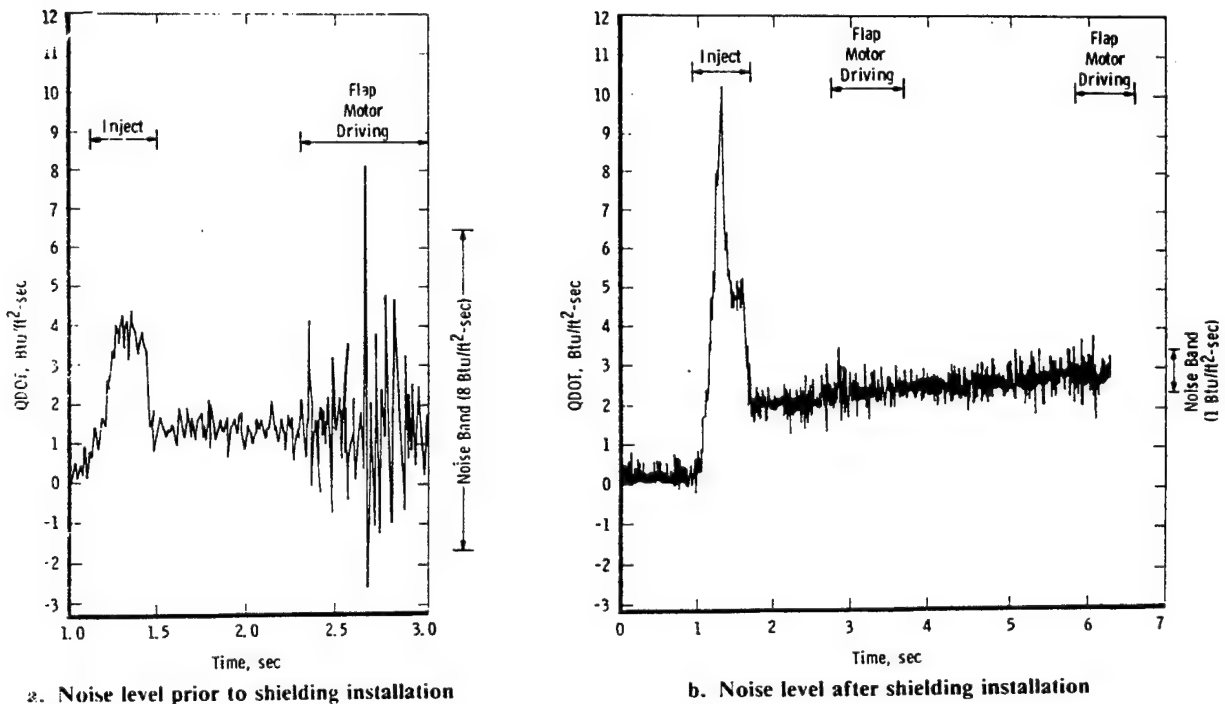


Figure 61 The Effects of Cable Treatment on the Quality of the coax Heat Gage Signal.

Flanagan, 1992, described in detail his efforts to eliminate RF noise from coax gages. He noted that the most serious problem was the long lead wires used during testing. This noise, for his low heating applications was of the same order as the signal output at 60 and 120 Hz. Signal to noise was increased for his work by locating external amplifiers and signal conditions next to the test section and using shielded cable for data lead wires.

Another problem often raised is the effective thermocouple junction developed with a metal-to-metal contact of the gage and structure. Flanagan, 1992a, measured the effect of this junction and noted that it caused a temperature difference of about 1.5 degrees at 300 degrees F. This was considered a definite second order effect on the data.

The major contributors to measurement uncertainty for coax gages are the inaccuracy introduced by the lower sensitivity of coax gages to temperature variation and the lower temperature rise of coax gages relative to thin film resistance thermometers for the same imposed heating rate. Over the temperature spectrum, the thermal properties of highly standardized thermocouple materials are well known and defined. Experience with these gages at extremely low levels of heating rate (down to

0.1 Btu/Ft²Sec) has demonstrated that the gages, while self consistent, deviate from one another. Figure 62 from Scaggs et al, 1992, shows the accuracy of coax gages applied to a hypersonic nozzle wall. Shown in this figure is the coax data in terms of the turbulent heating parameter,

$St Re^{0.2}$ as well as the range of absolute levels of the heating rate measured (as a function of the flow Reynolds number). Those using such gages are urged to assure the flushness of the gages in the test structure and to complete pre-test calibration of the individual instruments rather than accepting the standard thermocouple calibration data.

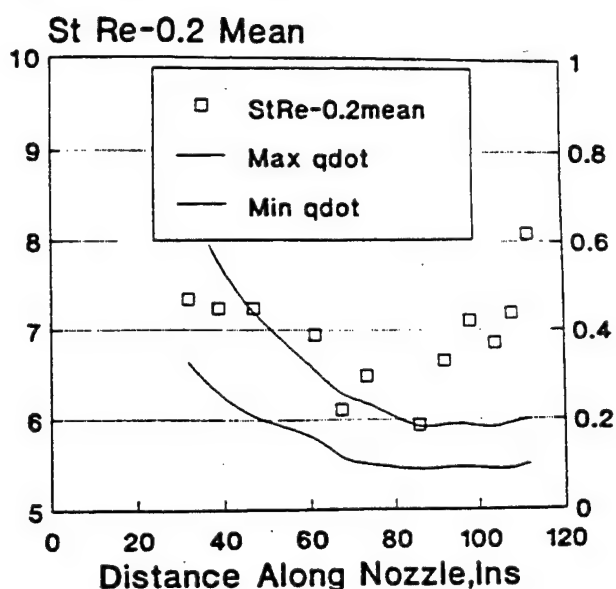


Figure 62 Experience with Coax Heat Gages at Very Low Heating Rates after Scaggs, 1992.

The Dracula Gage

A new variant of the coax gage is being developed by Simon at the California Institute of Technology. This gage consists of a "pin" of one material, in this case aluminum, driven into the model consisting of a second material, in this case a chromium-copper. The junction between the two materials is held at the test surface by anodizing the surface of the pin. In Simon's application, the pin is slightly tapered for a solid fit. The external diameter of the pin is about 0.050 ins and the model thickness is determined by the duration of test flow. Since the thermocouple produced is non-standard in materials, a calibration of each thermocouple is required as a prerequisite of accurate measurement. Simon notes that the 0.050 diameter dimension is not as small as the gage can be made. The junction is formed at the test surface about the perimeter of the contact surface between the two materials. Wires of the same material are placed on the back surface of the plate attached to the aluminum pin and the copper test surface.

This gage concept, apart from Simon's particular application, demonstrates how gages can be fabricated for particular applications. All models and gages are best compromises. In the case of Simon's shock interaction application, the copper model was required to avoid localized melting that would occur with a model of lesser conductivity. While the higher conductivity of copper maintains the thermal integrity of the model in this test situation, the errors due to radial conduction away from the highly-spiked heating (temperature) distribution must be analyzed and codes, such as TOPAZ, discussed in section II of this report and indispensable in this respect.

Data Reduction of Coax Gages

There are two techniques for the reduction of coax gage data which begin from an exact formulation of the semi-infinite slab thermal model; the direct and the indirect methods. Both techniques have been reduced to a finite difference representation with the resulting equations listed below.

The DIRECT METHOD computes the rate of heat transfer directly from temperature data on the surface, $T(t)$, and the INDIRECT METHOD computes first the integral of the heating rate with time, $Q(t)$, and then differentiates this quantity to generate the rate of heat transfer. Neither technique has an obvious advantage over the other. The indirect method results in smoother data without the need to smooth the data because of the intermediate step of computing the integral of heating rate. Both techniques are slow because of the need to integrate from initial time to generate each computational step.

A. Data Reduction Technique:

$$\dot{q}(t) = \left[\frac{\rho c k}{\pi} \right]^{0.5} \int_0^t \frac{dT(\tau)}{d\tau} \frac{d\tau}{\sqrt{t-\tau}}$$

where t is the time from start of heating

$T(t)$ is the surface temperature rise during heating

ρ is the density of the gage material

c is the specific heat of the gage material

k is the thermal conductivity of the gage material

Note that typical values of the thermal properties can be found in Appendix A at the end of this report.

The finite difference representation of the above equation is:

$$\dot{q}(t) = 2 \left[\frac{\rho c k}{\pi} \right] \sum_{j=1}^n \frac{T_j - T_{j-1}}{\sqrt{t_n - t_j} + \sqrt{t_n - t_{j-1}}}$$

This finite difference technique is known as the "direct method". With it, the rate of heat transfer is directly obtained. A second technique known as the "indirect method" obtains first the integral of the heating rate and then differentiates that value to obtain the heating rate. The corresponding equations for the indirect method are given as:

$$Q(t) = \left[\frac{\rho c k}{\pi} \right]^{0.5} \int_0^t \frac{T(\tau)}{\sqrt{t-\tau}} d\tau$$

and the corresponding finite-difference representation of this equation is:

$$Q_n = \left[\frac{\rho c k}{\pi} \right]^{0.5} \sum_{j=1}^n \frac{T_j + T_{j-1}}{\sqrt{t_n - t_j} + \sqrt{t_n - t_{j-1}}} (t_n - t_{n-1})$$

An expression for differentiating the discrete function $Q(t)$ is given as:

$$\dot{q}_n = \frac{dQ_n}{dt} = \frac{1}{40(t_n - t_{n-1})} [-2Q_{n-8} - Q_{n-4} + Q_{n+4} + 2Q_{n+8}]$$

1D Coax Data Reduction Technique For A Finite Slab:

$$\frac{\partial T}{\partial t} = \frac{k}{\rho c} \frac{\partial^2 T}{\partial x^2}$$

Applying a forward time and central-spaced explicit difference method to this equation produces:

$$\frac{T_{n+1,i} - T_{n,i}}{\Delta t} = \frac{k}{\rho c} \frac{T_{n,i+1} - 2T_{n,i} + T_{n,i-1}}{\Delta x^2}$$

where i is the number of nodes in the 1D model and n are the time steps in the computation.

solving this equation for $T_{n+1,i}$ results in:

$$T_{n+1,i} = \Theta [T_{n,i+1} + T_{n,i-1} + (1/\Theta - 2) T_{n,i}]$$

where Θ is defined as:

$$\Theta = \frac{k \Delta t}{\rho c (\Delta x)^2}$$

which, for stability must be less than 0.5.

At each time step, the temperature of all nodes are computed $T_{n,i-1,max}$

The heating rate is then obtained as:

$$\dot{q}_n = \frac{-k}{\Delta x} [4T_{n,2} - 3T_{n,1} - T_{n,3}]$$

Note that temperature data at the $i+1$ node is required to advance the computation of temperature at node (i). This means that the temperature of the backface node ($i=imax$) must be measured. It has been observed that assuming the temperature at the ($imax$) and ($imax-1$) nodes are the same can be used without noticeable error. That is, $T_{n+1,imax} = T_{n,imax-1}$.

Data Character and Problems in Reduction:

Figure 63 indicates both the surface and backface temperatures calculated by a heat conduction code for a sample case simulating the convective heating to a model in a wind tunnel. Note the classic parabolic nature of the surface temperature; a characteristic of this class of gages. The parabolic surface temperature trace has two features which indicate tunnel induced phenomena. At times less than one second there is a "blip" in the surface temperature caused by the model traversing the tunnel shear layer during injection. At times greater than 8 seconds, the model is withdrawn and the surface temperature decreases. The backface trace shows no temperature increase until the model has been in the tunnel for 2 seconds. This

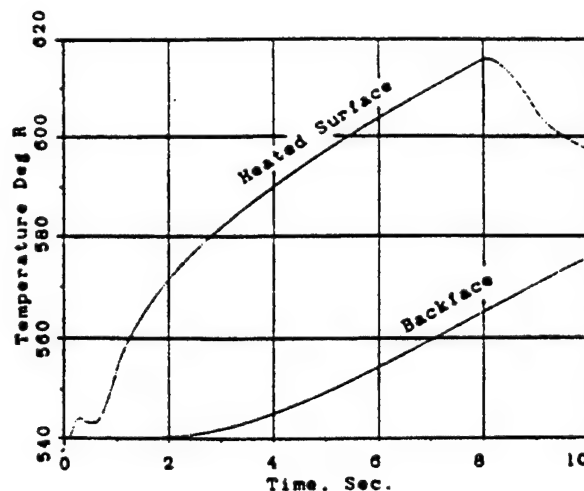


Figure 63 Surface and Backface Temperature Data From a Coax Gage Measurement.

thermal diffusion lag is also demonstrated by the lack of influence of surface temperature cooling on backface temperature levels up to 2 seconds after turned off.

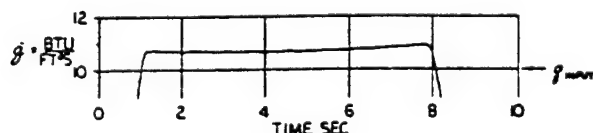


Figure 64 Possible Errors In Coax Reduced Data Due to Inexact Time Intervals.

Figure 64 indicates the reduced data from this example using the indirect method. The input heating rate of

$$10 \frac{\text{Btu}}{\text{Ft}^2 \text{Sec}}$$

produced the temperature profiles previously discussed. Note that the output heating rate is not equal to that input. This error was induced by statistically "perturbing" the input data so that the data in the sample case were not defined exactly at constant

time intervals. The result, as noted, is a serious error. Input temperature data must be taken at exactly constant time interval or interpolated to a uniform, constant time interval. The reduced data appears smooth because the indirect method, which implicitly smooths the data, was used.

Figure 65 demonstrates a reduction of the same data using a 1D thermal model of a finite slab 20 nodes deep. This reduction technique produced data 20 times faster than in the previous figure because the finite slab model, unlike the previous semi-infinite slab example, did not require a summation of each test time for all previous times.

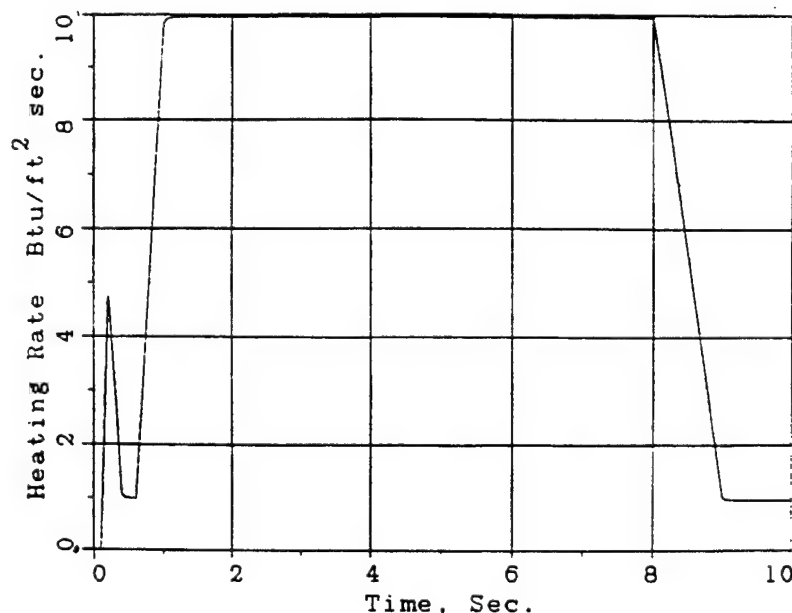


Figure 65 Demonstrating a Reduction of the Same Data Using a 1D Thermal Model of Finite Slab 20 Nodes Deep.

While the application of coaxial thermocouple gages to interference heating tests will be discussed in depth in section VI of this report, an introduction to the subject is in order here. Coaxial thermocouple gages can be used in place of thin film resistance thermometers for shock tunnel measurements. These gages use the same semi-infinite slab thermal model as their base but (1) replace the resistance thermometer with a thermocouple junction (normally a chromel/constantan thermocouple) and (2) use the thermocouple material as the semi-infinite slab material. These gages were directly compared with thin film resistance thermometer gages by Cassady et al, 1991 during a shock tunnel test. Figure 51 demonstrated the temperature rise characteristics of these two gages. On the positive side, both gages respond to the impulsive heating created in a shock tunnel equally well but the coax gage has a lesser temperature rise because the backing material is a conductor rather than an insulator upon which the thin film is placed. In addition, since the thin film gage has a higher sensitivity (3mv/deg K) than the chromel/constantan thermocouple (0.063 mv/deg K), the total signal during the shock tunnel run for the thin film gage was 177 times that of the coax gage output. In spite of this sensitivity issue, there are valid reasons to use coax gages in place of thin film resistance thermometers for shock tunnel measurements. Some of these include:

- Longer test durations and/or higher heating rates can vaporize the thin film gages.

- The thin film gage requires a non-catalytic overcoat for high enthalpy operation. This overcoat measures heating with finite catalyticity rather than fully catalytic heating for the metallic coax gages.
- The coax gages are tougher gages which better resist the higher heating levels to be found at the stagnation point and measurements in flows where particles are likely present.
- For higher levels of imposed heating rate, the temperature rise induced in the insulative gage substrate can be quite different than that of the structure of the model.

This differential surface temperature can create non-isothermal "hot spots" on the model that impede the correlation of the results with computational techniques. The estimating equation for temperature rise discussed on Page III-6 of this report can be used to estimate these temperatures. Using that equation and the thermal properties for stainless steel and pyrex glass, Figure 66 plots limiting levels of surface heat flux that are recommended for the use of thin film gages in shock tunnels. These are "rule of thumb" estimates which are mitigated by the specifics of any proposed test.

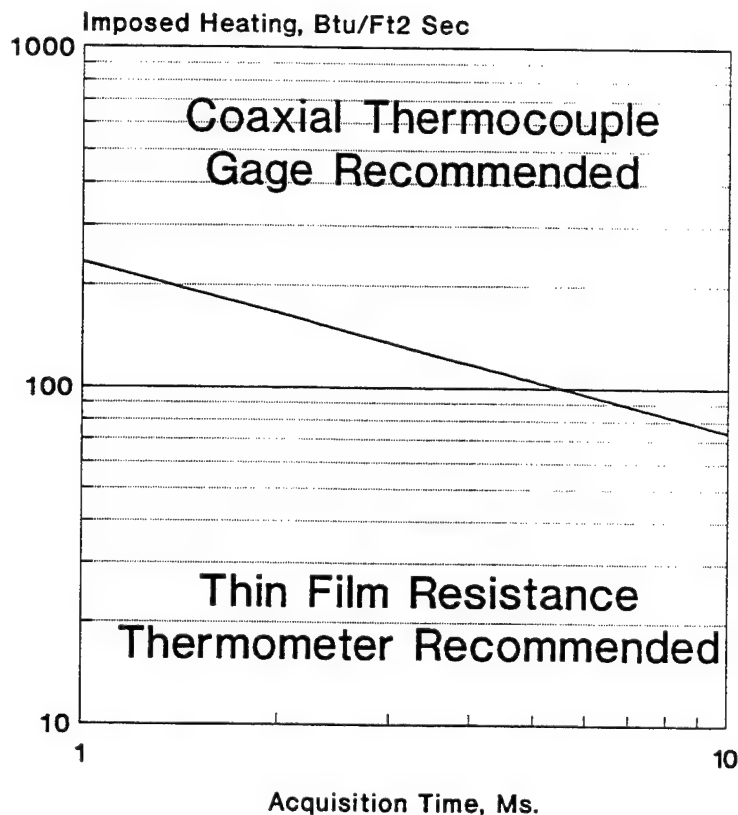


Figure 66 Limits of Heat Transfer to be Measured by Thin Film Gages.

THE EXTENDED DURATION COAX GAGE

Gages modeled about coaxial thermocouples are limited in test duration not by the diffusion time of materials but by the limitations of the thermal model and its bounding conditions.

Certainly, within a short time, the heat pulse from the front (heated) face of the gage will travel to the rear surface of the gage. This thermal diffusion time can be adjusted somewhat by changing the thickness of the gage.

When the diffusion time is exceeded, the backface temperature of the gage will increase and the thermal model is no longer definable as a semi-infinite slab. Use of the coax gage for times exceeding the diffusion time however requires more sophistication in formulating the thermal model, additional experimental measurements and, perhaps, another example of the integration of numerics and experimentation.

There are commercially available "three wire Coax gages" shown schematically in Figure 67. These gages measure temperatures on both the heated surface and backface temperature. This additional sensor together with a finite slab thermal model for data reduction eliminates, for a time, the limitations imposed by the semi-infinite slab thermal model. Three wire gages have been used in wind tunnel tests to generate valid test data for up to 30 seconds. This upper time limit is caused by minor differences in the thermal properties between the gage and the model and results in extraneous heating of the gage through the sides of the gage leading to inaccuracies in the measurement. Of course, three-wire Coax gages require additional data acquisition capacity such that fewer gages can be sensed during any one entry into the tunnel. In addition, the larger wire bundle from three-wire gages may not fit through model stings.

Another solution to this problem is to use classical two-wire gages together with computations from a finite slab numerical thermal model to numerically define the backface temperature. The numerical computation of the backface temperature replace its measurement in the three wire gage; a linear extrapolation of the numerical computation of inner node temperatures to the backface node is used as shown in Figure 68. Since the backface temperature is not extremely sensitive to surface heat flux variations in the wind tunnel, the computational estimate of the backface temperature will generate data of acceptable quality. This technique again suggests some philosophical questions about "pure experiments" that, in the last analysis, must be answered by the experimenter.

What Happens As The Thickness of the Coax Gage is Reduced?

The nominal thickness of the coax gage is about 0.4 ins. This thickness of material allows a semi-infinite slab model to be used for a number of seconds in the test section; perhaps 5 seconds. There is however no fixed requirement that the gage be held at this thickness and there is no optimum gage thickness dimension; it

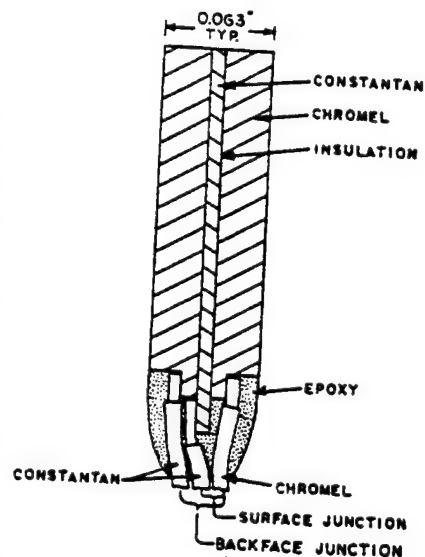


Figure 67 Commercial 3-Wire Coax Gage Which Measures Both Surface and Backface Temperatures.

could be made shorter. The requirement, if any, might be that the thermal model used in data reduction be a semi-infinite slab thermal model. For blowdown tunnels and normal usage in transient heat transfer testing, 0.4 ins is reasonable.

The required thickness of the gage to allow reduction by the semi-infinite slab thermal model is defined by the thermal diffusion time through the gage in relationship to the test duration. Shorter tests allow shorter gages. The use of the coax gage in an impulse tunnel, as for instance T5 at the California Institute of Technology would, in theory, permit the use of a very short gage while retaining the validity of the semi-infinite slab thermal model which defines a surface thickness of

Thickness = $\sqrt{\frac{\alpha t}{5}}$. Semi-infinite slab thermal models can be maintained in impulse facilities with very thin insulative coatings painted over structural materials of the order of several mils in thickness.

There are cases where the longer gage thickness cannot be tolerated within the lines of the configuration or where The test time is far longer than the thermal diffusion time through the coax material. These cases do not necessarily invalidate the use of the coax type gage but they introduce modifications into that use. Several cases will be discussed:

For The Case of Long Test Times With No Heating Into The Gage From The Rear Surface:

Long test times relative to the thermal diffusion time of the gage materials produce a temperature rise on the backface of the gage. Two techniques for dealing with this have been discussed: the addition of another thermocouple at the gage backface (known as a 3-wire coax gage) or the use of an approximate analysis to approximate the backface temperature (a 1-D analysis is discussed later in this report). Both of these techniques extend the usefulness of the coax gage to longer test durations.

Use of the 3-wire coax gage can perturb the coax gage into an altogether different type of thermal sensor and demonstrates the flexibility and non-uniqueness of thermal sensors in general. If the 3-wire gage were used with the gage thickness substantially reduced, the coax gage would be perturbed into a Schmidt-Boelter type gage in which the surface a backface temperatures are a direct reflection of the heat transfer across the thickness of the coax material. If the thinner coax gage were installed in a model cooled on the backface, a steady state heat transfer gage is created. This gage was used to generate heat transfer data in a "cold" wind tunnel (one with no ability to aerodynamically heat the model) by heating the gage backface with hot water.

For The Case Of Long Test Times With Heating Into The Gage From the Rear Surface:

Coax gages placed within thin model hardware such that the gage is inadvertently heated from both the intended measurement surface as well as the backface create more complex situations that require situation-

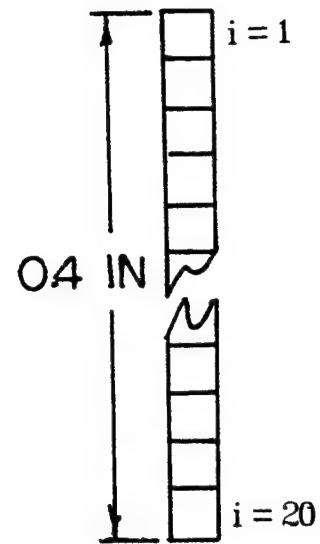


Figure 68 One Dimensional Model of Heat Flow Down a Coax Gage.

specific solutions. Heating into the gage from the backface requires that the backface heating rate be known exactly and should, in general, be avoided. The time at which this is a problem is defined by the thermal diffusion of heat into the structural materials as well as the gage itself. Backface heating can be forestalled by placing a slab of insulating material behind the gage(s) to extend the thermal diffusion time of the undesirable heating. When thermal diffusion reaches the gage backface from an undefined heating rate, the test is concluded. This type of situation is yet another complexity of long duration ground testing or flight test measurements. For the engine flowpath application, backface heating can easily occur on the cowl surface which is both thin and heated from both external aerodynamic heating about the engine as well as the internal heating caused by both aerodynamic flow fields and combustion.

There is no inherent requirement to define any specific thickness of coax gages. Flexibility exists in this dimension at the possible expense of more complex data reduction due to more representative thermal models.

Extensions To the Semi-Infinite Thermal Model According To Doorly:

Doorly et al, 1988, developed the theory for three types of substrate surfaces from the semi-infinite substrate to finite, multi-material substrates. While the presentation of their solutions is beyond the scope of this review report, the characteristics of these three surfaces are shown in Figures 69 through 71. Doorly calls the classic, semi-infinite slab gage a "type 1 gage" shown in Figure 69.

A variant of that gage is a two layer gage with a semi-infinite but conducting substrate upon which is placed a finite, insulative layer. This model is used with the gradient type gages which will be discussed in section V of this report and, as well, can be applied to the case of an insulative surface applied to a conductive model in a short duration test facility (such as a shock tunnel). This thermal model is shown in Figure 70 below and is termed a "type 2 gage".

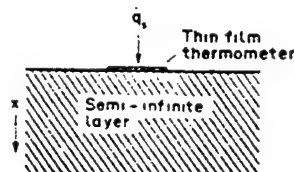


Figure 69 Classical, Semi-Infinite Slab Thermal Model. Doorly's Type I Gage.

The final variant evaluated is an extension of the type 2 gage considering the finite thermal thickness of the metallic sublayer. This gage, termed a "type 3 gage" is shown below in Figure 71.

The reader is reminded that even though these models were developed for thin film thermometer gages, temperature can be measured by any other means discussed in this section as long as the temperature is measured on a modification of the semi-infinite slab thermal model.

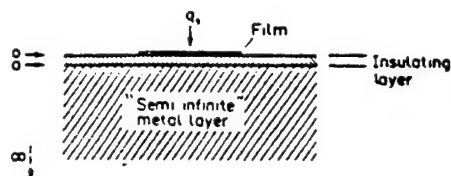


Figure 70 Doorly Type II Gage.

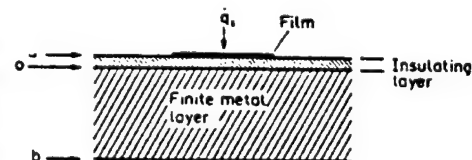


Figure 71 Doorly Type III Gage.

The various substrates defined by Doorly were those of direct interest for turbine blade measurements although they also have direct relevance to a broader range of measurements. As an example, Ainsworth, 1989 discussed the placement of a thin film resistance thermometer on a semi-infinite metal layer, the Doorly

type II gage. The intermediate insulating layer was a vitreous enamel layer. Ainsworth performed a number of sensitivity studies wherein the thickness of the enamel layer and its thermal properties were varied. Conclusions reached were that for an enamel thickness greater than $100\mu m$, the response of the gage to high frequency information (greater than 100Hz) is invariant to the enamel thickness; the enamel material acts as a semi-infinite surface to the high frequency information and the enamel material conductivity changes have an effect on the heat flux only above 10Hz measurement frequency.

Ainsworth noted that the vitreous enamel layer must have a coefficient of linear expansion matched to that of the metal substrate to which it is applied for the firing temperatures (so it doesn't flake off). The vitreous enamel layer selected was WB 5847 from Ferro G.B. Ltd and Ainsworth discusses, in some detail, the blade instrumentation process and the restoration of blade strength after instrumentation.

APPENDIX III-1 **CALCULATION OF HEAT TRANSFER COEFFICIENT UNCERTAINTY** **FROM THE APPENDIX OF THE 1975 THESIS OF LARRY CARTER**

In 1975 Larry Carter developed expressions for the uncertainty in heat transfer coefficient that are represented by the curves shown in Figure 29 of this report. While his work was specifically aimed at thermographic phosphor coatings, the developed expressions are generally applicable to any sensor applied to a semi-infinite slab thermal model. The mathematical development of these equations was worked out by Carter in an appendix to his thesis. It is presented in this report as shown in that appendix because of its generality to the heat transfer problem.

The basis of this development is the Taylor series method of error propagation applied to the simplified expression developed by Carslaw and Jaeger for the temperature rise in a semi-infinite slab thermal model:

$$\frac{T_w - T_{wi}}{T_{aw} - T_{wi}} = 1 - e^{\beta^2} \operatorname{erfc} \beta = f(\operatorname{erf} \beta) = 1 - Z(\beta)$$

where β is defined as: $\beta = \frac{h\sqrt{\Delta t}}{\sqrt{\rho c_p k_w}}$

or $h = f(\beta, \sqrt{\rho c_p k_w}, \sqrt{\Delta t})$

Recall that $\operatorname{erfc} \beta = (1 - \operatorname{erf} \beta)$.

Note also from this figure that the relationship between the heating rate parameter, β , and the temperature parameter is shown in the Figure III-1A. Note that the greatest sensitivity in this relationship requires that the heating parameter be less than or equal to 0.5. Within the range $0.5 > \beta > .01$ the levels of heating can be accommodated by modifying the time of data acquisition and/or the thermal properties of the model material and β can be obtained from the $f(\operatorname{erf} \beta)$ through the curvefit:

$$\beta = A + B * f(\operatorname{erf} \beta) + \frac{C * f(\operatorname{erf} \beta)}{\ln(f(\operatorname{erf} \beta))}$$

where $A = 0.004176804$
 $B = 0.66077948$
 $C = -0.60211991$

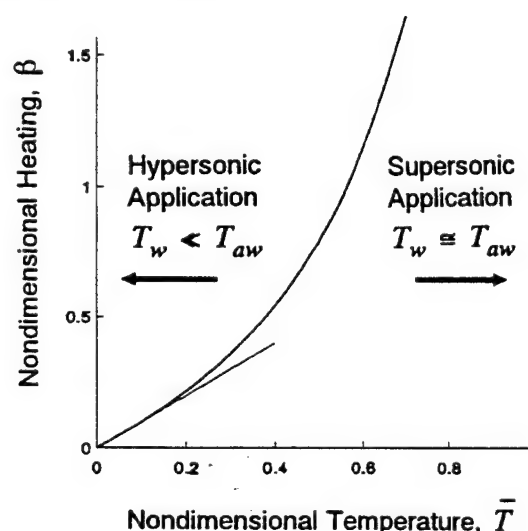


Figure III-1 The Relationship Between the Heating Rate Parameter and the Wall Temperature Parameter.

$$\omega h = \frac{\partial h}{\partial X_i} \omega X_i$$

The uncertainty in the heat transfer coefficient, written as ωh , is defined in terms of beta as:

$$(\omega h)^2 = \left[\frac{\partial h}{\partial \beta} \right]^2 (\omega \beta)^2 + \left[\frac{\partial h}{\partial \sqrt{\rho c_p k_w}} \right]^2 (\omega \sqrt{\rho c_p k_w})^2 + \left[\frac{\partial h}{\partial \Delta t} \right]^2 (\omega \Delta t)^2$$

where the partial derivatives are evaluated in the equation for β given above.

The uncertainty using the heat transfer coefficient is then divided by the heat transfer coefficient resulting in the equation for uncertainty given as:

$$\left(\frac{\omega h}{h} \right)^2 = \left(\frac{\omega \beta}{\beta} \right)^2 + \left(\frac{\omega \sqrt{\rho c_p k_w}}{\sqrt{\rho c_p k_w}} \right)^2 + \frac{1}{4} \left(\frac{\omega \Delta t}{\Delta t} \right)^2$$

The second and third terms in this equation relate the uncertainties in material properties and the time of heating to the uncertainty in the heat transfer coefficient, h . These relationships are shown in Figure 29 as independent of the temperature function plotted on the "X" axis. The first term contains the uncertainties associated with the various temperatures, T_w , T_{wi} , T_{aw} . This uncertainty gives rise to the nonlinear character of the curves in Figure 29 and will be discussed now.

From the equation relating z and beta, $z = e^{\beta^2} \operatorname{erfc} \beta$, the equation:

$$\left(\frac{\omega \beta}{\beta} \right)^2 = \frac{1}{4} \left[\frac{\sqrt{\pi} z}{\beta(\beta \sqrt{\pi} z - 1)} \right]^2 \left(\frac{\omega z}{z} \right)^2 = \frac{1}{4} Q \left(\frac{\omega z}{z} \right)^2$$

can be derived which contains the uncertainty in z . The coefficient ahead of the uncertainty of "z" presents asymptotic behavior as the temperature function, $\frac{T_w - T_{wi}}{T_{aw} - T_{wi}}$, approaches zero.

This uncertainty can be obtained through the second equation for z , $z = \frac{T_{aw} - T_w}{T_{aw} - T_{wi}}$

This development gives rise to three terms relating the uncertainty in the various temperatures to the uncertainty in z as:

$$\left(\frac{\omega z}{z}\right)^2 = \left[\frac{(1-z)T_{aw}}{T_{aw}-T_w}\right]^2 \left(\frac{\omega T_{aw}}{T_{aw}}\right)^2 + \left[\frac{T_w}{T_{aw}-T_w}\right]^2 \left(\frac{\omega T_w}{T_w}\right)^2 + \left(\frac{T_{wi}z}{T_{aw}-T_w}\right)^2 \left(\frac{\omega T_{wi}}{T_{wi}}\right)^2$$

The above equation IS equation A-18 in Carter's thesis.

The coefficients for the uncertainty of adiabatic wall temperature and the uncertainty of wall temperature both present a function that increases strongly as the temperature function, $\frac{T_w - T_{wi}}{T_{aw} - T_{wi}}$, approaches unity. The third coefficient, associated with the initial temperature, is independent of the level of temperature.

So that the functions assigned to the uncertainties of adiabatic wall temperature (term 1), wall temperature (term 2), and initial wall temperature (term 3) are the nonlinear curves seen in Figure 29.

With that preamble, pages 48 through 52 of Carter's appendix follow.

The modelling equation relating causal heat transfer to the surface temperature rise of a semi-infinite slab surface is written as:

$$h = \frac{\beta \sqrt{wc_p k_w}}{\sqrt{t}} \quad (A-1)$$

The uncertainty of the heat transfer coefficient, h , was computed from the Taylor series method of error propagation as:

$$(\omega h)^2 = \left[\frac{\partial h}{\partial \beta} \omega \beta \right]^2 + \left[\frac{\partial h}{\partial \sqrt{wc_p k_w}} \omega \sqrt{wc_p k_w} \right]^2 + \left[\frac{\partial h}{\partial \Delta t} \omega \Delta t \right]^2 \quad (A-2)$$

where ωh refers to the absolute uncertainty in h , $\omega \beta$ is the absolute uncertainty in β , etc... By taking the partial derivatives of the modelling equation, we obtain:

$$(\omega h)^2 = \left(\frac{\sqrt{wc_p k}}{\sqrt{\Delta t}} \right)^2 (\omega \beta)^2 + \left(\frac{\beta}{\sqrt{\Delta t}} \right)^2 (\omega \sqrt{wc_p k})^2 + \left(\frac{\beta \sqrt{wc_p k}}{2 \Delta t \sqrt{\Delta t}} \right)^2 (\omega \Delta t)^2 \quad (A-3)$$

and

$$\frac{\partial h}{\partial \Delta t} \omega \Delta t = \left[-\frac{\beta \sqrt{w c_p k_w}}{2 \Delta t \sqrt{\Delta t}} \right] \omega \Delta t$$

which becomes:

$$\left[\frac{\omega h}{h} \right]^2 = \left[\frac{\omega \beta}{\beta} \right]^2 + \left[\frac{\omega \sqrt{w c_p k_w}}{\sqrt{w c_p k_w}} \right]^2 + \frac{1}{4} \left[\frac{\omega \Delta t}{\Delta t} \right]^2 \quad (\text{A-4})$$

The three terms in the above equation represent the uncertainty of the heating rate to the non-dimensional heat transfer coefficient, to the thermal properties of which the model is constructed and to the time at which the data is taken. The non-dimensional heat transfer coefficient, in turn, is defined as:

$$z = \frac{T_{aw} - T_w}{T_{aw} - T_{wi}} = e^{\beta^2} \operatorname{erfc} \beta \quad (\text{A-5})$$

and is related to the wall temperature, the initial wall temperature and the adiabatic wall temperature.

Obtaining a relationship for the uncertainty of β , we relate it to z through the Taylor series expansion which, formally, is written as:

$$[\omega z]^2 = \left[\frac{\partial z}{\partial \beta} \right]^2 [\omega \beta]^2 \quad (\text{A-6})$$

and which, upon the indicated operations, becomes:

$$(\omega z)^2 = \left[\frac{\partial (e^{\beta^2} \operatorname{erfc} \beta)}{\partial \beta} \right]^2 (\omega \beta)^2 \quad (\text{A-7})$$

By performing the indicated differentiation, one obtains the following Equation:

$$(\omega z)^2 = \left[2\beta e^{\beta^2} + e^{\beta^2} + e^{\beta^2} \frac{d(\operatorname{erfc} \beta)}{d\beta} \right]^2 (\omega \beta)^2 \quad (\text{A-8})$$

By definition

$$\operatorname{erfc} \beta = 1 - \operatorname{erf} \beta. \quad (\text{A-9})$$

Hence

$$\frac{d(\operatorname{erfc} \beta)}{d \beta} = - \frac{d(\operatorname{erf} \beta)}{d \beta}. \quad (\text{A-10})$$

$$\frac{d(\operatorname{erf} \beta)}{d \beta} = \frac{2}{\sqrt{\pi}} e^{-\beta^2} \quad (\text{A-11})$$

$$\frac{d(\operatorname{erfc} \beta)}{d \beta} = \frac{-2}{\sqrt{\pi}} e^{-\beta^2} \quad (\text{A-12})$$

Substitution Equation (A-12) into Equation (A-8) yields:

$$(\omega z)^2 = \left[2\beta e^{\beta^2} \operatorname{erfc} \beta - \frac{2}{\sqrt{\pi}} \right]^2 (\omega \beta)^2. \quad (\text{A-13})$$

Dividing Equation (A-13) by Equation (A-5) squared yields:

$$\left(\frac{\omega z}{z} \right)^2 = 4 \left[\frac{\beta (\beta \sqrt{\pi} z - 1)}{\sqrt{\pi} z} \right]^2 \left(\frac{\omega \beta}{\beta} \right)^2 \quad (\text{A-14})$$

Rearranging, Equation (A-14) becomes:

$$\left(\frac{\omega \beta}{\beta} \right)^2 = \frac{1}{4} \left[\frac{\sqrt{\pi} z}{\beta (\beta \sqrt{\pi} z - 1)} \right]^2 \left(\frac{\omega z}{z} \right)^2. \quad (\text{A-15})$$

The following equation was obtained by applying the Taylor series method to the definition of z , Equation (A-5).

$$(\omega z)^2 = \left(\frac{z}{T_{aw}} \omega T_{aw} \right)^2 + \left(\frac{z}{T_w} \omega T_w \right)^2 + \left(\frac{z}{T_{wi}} \omega T_{wi} \right)^2 \quad (\text{A-16})$$

Hence

$$(\omega z)^2 = \left[\frac{(T_{aw} - T_{wi}) - (T_{aw} - T_w)}{(T_{aw} - T_{wi})^2} \right]^2 (\omega T_{aw})^2 + \left(\frac{1}{T_{aw} - T_{wi}} \right)^2 (\omega T_w)^2 + \left[\frac{T_{aw} - T_w}{(T_{aw} - T_{wi})^2} \right]^2 (\omega T_{wi})^2. \quad (\text{A-17})$$

Dividing Equation (A-17) by Equation (A-5) squared yields:

$$\left(\frac{\omega z}{z} \right)^2 = \left[\frac{(1-z)T_{aw}}{T_{aw} - T_w} \right]^2 \left(\frac{\omega T_{aw}}{T_{aw}} \right)^2 + \left(\frac{T_w}{T_{aw} - T_w} \right)^2 \left(\frac{\omega T_w}{T_w} \right)^2 + \left(\frac{T_{wi} z}{T_{aw} - T_w} \right)^2 \left(\frac{\omega T_{wi}}{T_{wi}} \right)^2 \quad (\text{A-18})$$

Substituting Equations (A-18) and (A-15) into Equation (A-4) yields:

$$\left(\frac{\omega h}{h} \right)^2 = \left(\frac{\omega \sqrt{w c_p k}}{\sqrt{w c_p k}} \right)^2 + \frac{1}{4} \left(\frac{\omega \Delta t}{\Delta t} \right)$$

$$\begin{aligned}
& + \frac{1}{4} \left[\frac{\sqrt{\pi} z}{\beta (\beta \sqrt{\pi} z - 1)} \right]^2 \left[\frac{1}{T_{aw} - T_w} \right]^2 \\
& \left\{ \left[(1-z)T_{aw} \right]^2 \left(\frac{\omega T_{aw}}{T_{aw}} \right)^2 + (T_w)^2 \left(\frac{\omega T_w}{T_w} \right)^2 + (z T_{wi})^2 \left(\frac{\omega T_{wi}}{T_{wi}} \right)^2 \right\}
\end{aligned} \tag{A-19}$$

Equation (A-19) is plotted in Figure 6, page 27.

Carter estimated the precision with which he could measure basic quantities in the test facility. Among these were the temperatures and more precisely the wall temperature. It was assumed that the wall temperature could be measured to a constant $\pm 1\%$. This measurement alone was the subject of a more in-depth analysis by Wannenwetsch, 1983. Wannenwetsch correctly points out that the measurement of temperature (as with other quantities) is a function of the sensitivity of the transducer which relates the quantity of interest to millivolts and the sensitivity of the amplification system which includes the overall digital counts of the system; the gain of the amplifier (the percentage of counts available that are used in the specific measurement) and the basic uncertainty in the counts of the system for a known measurement (the noise).

In practice, this can be observed by understanding that for a given thermocouple type applied to measure the temperature rise in a semi-infinite slab, the magnitude of the temperature rise is controlled by the material properties of the slab. If two identical slabs are constructed of different materials, the temperature rise for a given heating rate will be different. The basic thermocouple sensitivity ($^{\circ}R/mv$) will be the same but the overall measurement precision will differ because the measured temperature interval changes. For a fixed gain, the number of counts between the initial wall temperature and the wall temperature at any time also changes as does the relationship between the basic uncertainty of the system in counts and the level of the measured signal. In the limit of a very small temperature rise, the signal (in counts) could be equal to or less than the uncertainty of the signal: the signal to noise ratio is thus equal to or less than 1. The amplifier gain can be changed in such a situation but the basic uncertainty of the measurement in counts will also increase as the gain of the amplifier is changed.

Wannenwetsch estimated the basic uncertainty of the signal in counts, ω COUNTS, by considering the statistics of a thermocouple signal measured during the injection process and before any aerodynamic heating is sensed. This will be discussed in greater detail in Section VI of this report.

The uncertainty of heat flux measurements using a semi-infinite slab thermal model is related to the data reduction equation used for the semi-infinite solid. The overall uncertainty can be broken down into components due to (1) the temperature related terms, (2) the time related terms and (3) the terms due to thermal properties. Wannenwetsch et al, 1983, developed an expression for the temperature related terms which can be written as:

$$\omega \dot{q} = \pm \frac{2\sqrt{\rho c_p k_w}}{\sqrt{\pi}} \left[\frac{10^4 (SENS)(\omega COUNTS)}{(GAIN)(SFC)} \right] f(t)$$

where $f(t)$ is a complex series of terms containing only time.

Concentrating on the terms which reflect the facility data stream and its amplification, the term "SENS" is the thermoelectric sensitivity of the gage in $^{\circ}R/mv$. The term "GAIN" is the amplifier gain used with the instrument. The term " $\omega COUNTS$ " is the random error level in the raw gage output signal in counts and the term "SFC" is the number of counts to full scale.

For the experiment that Wannenwetsch et al discussed, these uncertainty values were as follows:

SENS= 29.41 $^{\circ}R/mv$ the sensitivity of chromel/constantan which is also given in Appendix B as 63 $\mu V/^{\circ}K$.

GAIN= 1000; the Amplifier Gain

SFC= 16,384 counts, a 14 bit system. ($2^{14} = 16,384$). The uncertainty in the facility data stream was then:

$$\omega \dot{q} = \pm(0.0175) \frac{2\sqrt{\rho c_p k_w}}{\sqrt{\pi}} f(t) (\omega COUNTS)$$

Combining the acquisition terms with the thermal properties gives us:

$$\omega \dot{q} = \pm 0.008102 f(t) \omega COUNTS$$

For this particular experiment, the term $\omega COUNTS = 6$. The uncertainty in the heat flux with respect to measurement counts was then:

$$\frac{\omega \dot{q}}{\omega COUNTS} = \pm 0.008102 f(t)$$

This compares with the values given by Buck, 1991, of 0.7% to 1.25% for a completely different facility, data acquisition system and measurement technique.

TABLE AIII.1
ESTIMATED DATA PRECISION

Quantity	Estimate of Precision %	Comments Regarding the "Measurement" Note: All measured Quantities are subject to data acquisition system quality.
$C_{p_{\infty}}$	1.0	Specific Heat at Constant Pressure
h	18-38	Heat transfer coefficient: inferred through a fusion of measurements and a guess $h = \frac{\dot{q}}{T_{aw} - T_w}$ where \dot{q} is further a fusion of measurements and calibrations based on the specifics of the instrument used as described by the data reduction equations defined in this report
M_{∞}	0.5	Inferred through nozzle calibration and isentropic flow relations
P_0	0.5	Transducer measurement backed by calibration of transducer.
T_{aw}	0.375	Mythology: assumed to be a percentage of the total temperature. Accuracy, in fact, totally uncertain.
T_0	0.375	Thermocouple measurement backed by the calibration of the transducer
T_w	1.0	Measurement of Surface Temperature with Time
T_{wi}	0.5	Initial wall temperature: Same measurements as above for the wall temperature
Δt	5.0	Time Interval From Start of Heating to Time of Surface Temperature Measurement: May include the error due to discretation of the data if taken in "frames".
S_t	18-38	Stanton number: Inferred through fusion of several measurements and/or calibration. $S_t = \frac{\dot{q}}{\rho_{\infty} U_{\infty} C_p (T_{aw} - T_w)}$
V_{∞}	0.2	Inferred through calibration data and isentropic flow relations for the nozzle expansion process
$\beta = \sqrt{\rho C_p k_w}$	6.0	Inferred through offline calibration of material properties and/or handbook values.
ρ_{∞}	2.0	Inferred through calibration data and isentropic flow relations for the nozzle expansion process

There are two issues to be raised with respect to this table: (1) few of the stated quantities are directly measured, most are inferred. This requires, in turn, that the functional relationship implicit in the inference technique be considered and (2) the estimated precision can be highly variable and driven by the specifics of the technique used. The table above is a statement of the estimate of precision from the technology available to Carter in 1975 for the specifics of the test technique he was evaluating. The comments are from the author of the present report and not those of Carter. They are appended to his table to suggest to the reader the greater depth of analysis possible. Newer applications and different applications will generate different quantity precision that must be considered.

APPENDIX III-2

THIN FILM THERMOCOUPLES

- THE CONTRIBUTIONS OF TURBINE ENGINE RESEARCH

While in external aerodynamics little attention has been paid to thermocouples sputtered onto metal substrates, the turbine engine community has been working with these gages for some time. The NASA/Lewis Research Center has a substantial volume of reference material on the subject with the work of Liebert, 1984 an excellent example.

The history of thermal measurements on turbine blades demonstrates intensive work aimed at accurate measurements in a difficult situation. Thin film resistance calorimeters have been used for some short duration measurement applications (as, for instance, the work of Schultz et al at Oxford) and the thin film thermocouple was applied to measurements at higher surface temperatures (like 1000 degrees K). The work of Liebert, 1984 has, in recent years, been joined by that of Epstein, 1986, and Kreider, 19xx in this country and that of Portat et al, 19xx at ONERA in France.

The measurement techniques for either thin film thermocouples or thin film resistance thermocouples are the same. In most applications to date the resistance thermometer measurements are made on an insulative substrate placed within a steel blade whereas the thin film thermocouple is sputtered onto a thin insulator which, in turn, is sputtered onto a steel blade. This need not be so. Thin film resistance thermometers, like thin film thermocouples, may be layered onto a steel blade subject only to the limitation that the sensor be electrically insulated from the metal model. The true differentiators are (1) that resistance thermometers are powered and thermocouples are passive and (2) that resistance thermometers are more sensitive than thermocouples for measurement.

While these applications for thermal measurements are beyond the scope of the current report, the technology underlying them may well be of value for future applications. Specifically, this technology is the basis of some of the Gradient heat flux measurements discussed in Section VI of this report and this technology has application to high temperature heat flux gages discussed in Section X of this report.

APPENDIX III-3 THE RELATIVE CALIBRATION TECHNIQUE AFTER EPSTEIN, 1986

Epstein has presented a calibration technique which replaces an exact knowledge of the calibrating heating rate and the film thermometer scale factor with the requirement that these properties remain stable over the calibration period. He has applied this technique to a dual-film heat gage although the method for determining the bulk thermal properties is general for all thin film resistance thermometer gages.

The relative calibration technique described by Epstein, 1986, measures the step response of the gage to be calibrated both directly radiated by a radiant heating source in a vacuum or still air and radiated by the radiant heating source after being covered by a reference fluid of known thermal properties. The ratio of heat entering each substance, the gage and the known fluid, is equals the ratio of their respective bulk properties, $\sqrt{\rho ck}$. Since the method involves the comparison of methods, the absolute value of the incident heating rate is not required nor is the film thermometer scale factor.

Epstein thus develops a relationship between the known bulk properties of the reference fluid and the gage through the equation:

$$\sqrt{(\rho ck)_{\text{sensor}}} = \left[\left(\frac{m_I}{m_{II}} \right) - 1 \right]^{-1} \sqrt{(\rho ck)_{\text{ref. fluid}}}$$

where m_I and m_{II} are the two measurement outputs of the sensor to be calibrated as a function of time. These outputs for the constant heating rate calibration signal are linear with the square root of time as shown in Figure III3-1.

Calibration of Dual Film Sensor:

If the calibration heating rate is applied for times far greater than the characteristic time of the sensor (the time required for the heating pulse to reach the backface of the gage), the steady state heating parameter, k/d , is obtained from the equation:

$$\frac{k}{d} = \frac{Q}{(T_u - T_l)}$$

where k is the thermal conductivity of the insulative interface layer and d is the thickness of that layer. Q is the calibration heating rate applied and the two temperatures T_u and T_l are the upper and lower temperatures measured by the thin film resistance thermometers.

APPENDIX III-4 **EQUIVALENCE BETWEEN CONSTANT HEAT FLUX** **AND THE GENERAL 1D HEAT CONDUCTION MODELS**

The equation for the general 1D heat conduction model is:

$$\frac{\Delta T_w(t)}{T_r - T_i} = 1 - e^{\beta^2} (1 - \text{erf}(\beta))$$

The limit of this equation as $\beta \rightarrow 0$ is:

$$\lim_{\beta \rightarrow 0} \text{ of } e^{\beta^2} = 1 + \beta^2 + \frac{\beta^4}{2}$$

and

$$\lim_{\beta \rightarrow 0} \text{ of } \text{erf}(\beta) = \frac{2}{\sqrt{\pi}} \beta$$

which reduces the general 1D model to:

$$\frac{\Delta T_w(t)}{T_r - T_i} = 1 - (1 + \beta^2) \left(1 - \frac{2}{\sqrt{\pi}} \beta\right)$$

Neglecting higher order terms, this reduces to:

$$\frac{\Delta T_w(t)}{T_r - T_i} = \frac{2}{\sqrt{\pi}} \beta$$

Using the definition of β this develops to:

$$\dot{q} = \sqrt{\frac{\pi \rho c_p k_w}{4}} \frac{\Delta T_w(t)}{\sqrt{t}}$$

from Vermeulen and Simeonides
 von Karman Institute TN 181, 1992

SECTION IV THIN SKIN THERMAL MODEL

Historical Note:

In 1959 Durand and Rhudy documented the techniques of the day for the generation of heat transfer data from thin skin models. Discussing the generation of heat flux data on the X-15 aircraft in the AEDC Tunnel "B", the model was exposed to the flow for about five minutes and then cooled for about five minutes. The technique was to generate high speed temperature-time data using recorders for 30 seconds and then to continue to heat the model in the tunnel for an additional four minutes to generate "equilibrium temperature data". This excessively long test duration was followed by a cooling period of five minutes in which the temperature of the model was reduced to 100 degrees F prior to the second injection in the series.

Thin skin heat transfer testing has changed little from these early experiments of 35 years ago. Overall, the intent is to expose the model to the flow as a step function; generate a stream of temperature vs time data on recorders and then cool the model back to a reference temperature. The difference is that whereas the technique took 10 minutes to cycle in 1959, today it can be cycled in few minutes. No longer is equilibrium temperature data generated because such data was found to be of no value in the analysis of the overall heating rate data. Current day intent is to generate temperature-time data in as short a period of time as possible (about 5 seconds) and then retract and cool the model to ambient temperature conditions, about 540 degrees Rankine (80 degrees F). Most of the cycle time is model cooling and that cooling time varies with the imposed aerodynamic heating rates and cooling effectiveness of the tunnel-supplied model cooling equipment.

The thin skin technique has been successfully applied to the generation of heat transfer data for the past 30 years. The technique, while having limited applicability, is straightforward in application and accurate in results. The limited applicability refers to the problems introduced by non-uniform surface temperatures which are introduced by extremes in curvature or regions of highly localized interference heating.

Basis of the Technique

Heat transfer is inferred through temperature measurements using the thin skin thermal model according to the equation:

$$\dot{q} = \rho_w C_p b \frac{\partial T}{\partial t} - kb \left[\frac{\partial^2 T}{\partial s^2} + \frac{1}{r} \frac{dr}{ds} \frac{\partial T}{\partial s} \right]$$

where ρ and C_p refer to material properties, b refers to the material thickness and $\frac{\partial T}{\partial t}$ refers to the slope

of surface temperature with test time.¹

The first term assumes that the rate of heat transfer and hence the surface temperature on the measured surface is constant. The second term presents a correction for the more general case where the temperature over the surface is not constant. Material properties enter into both terms. In the first term, the product of the density and specific heat occurs while in the second (correction) term the thermal conductivity appears. Tables 4.1 and 4.2 list the material properties for a variety of possible model surfaces. Stainless steel is the preferred surface material. These properties are:

TABLE 4.1
PROPERTIES FOR A VARIETY OF POSSIBLE MODEL SURFACES

	Density, ρ	Specific Heat, C_p	Thermal Conductivity, $k \times 10^{**3}$
Stainless Steel	0.291	0.120	0.217
Nickel	0.320	0.107	1.200
Iron	0.284	0.107	0.854
Copper	0.320	0.092	4.930

The dimensions of density are: Lbm/in**3
specific heat are Btu/lbm-deg F
thermal conductivity are Btu/ in-sec-deg F

¹ There is an initial delay in the backface sensor response which is related to the material properties of the thermal sensor, the level of heat transfer measured and the surface area of sensor contact. This initial thermal

diffusion time, $t_D \approx \frac{\delta^2}{\alpha}$, is normally during the short model injection phase of the test and of no practical concern however; George and Reinecke, 1963 discussed this and estimates can be formed to determine the significance of the finite response time for the temperature sensors.

Grouping these materials by terms, Table 4.2 is arrived at:

TABLE 4.2
GROUPING MATERIALS BY TERMS

	Density x Specific Heat (Term 1)	Thermal Conductivity x 10**3 (Term 2)
Stainless Steel	0.0349	0.217
Nickel	0.0341	1.200
Iron	0.0304	0.854
Copper	0.0293	4.930

The thermal properties of these materials indicate that if there is uniform heating of the surface, the response of these materials to the imposed heating is quite similar but if there is non-uniform surface heating, the corrections involved to account for that non-uniformity are substantially greater with any of the cited materials relative to stainless steel, the preferred baseline.

Nickel is highlighted because this material is commonly used in the electro-plating of models having complex, three-dimensional geometries. These same complex geometries create highly non-uniform surface temperatures which, in turn, create higher conduction corrections. The induced corrections are 5 times the magnitude of corresponding corrections in stainless steel.

Iron is shown because some tunnel hardware is constructed of iron rather than stainless steel. One notable example is the nozzle component of many test facilities. Note that the conductivity of iron is many times that of stainless steel and must be considered in instrumentation selections for these components. The induced corrections are 4 times the magnitude of corresponding corrections in stainless steel.

Copper is highlighted because copper is the material of choice for conceptual engine test rigs. Such devices create highly non-uniform surface temperatures by virtue of their design. The induced corrections for thin skin copper are 23 times the magnitude of corresponding corrections in stainless steel.

The test interval during which valid thin skin heat transfer data can be taken was defined by Chpoun, 1989 as:

1. The minimum time is defined by a Fourier number larger than 0.3 generating an equation:

$$t_{MIN} = 0.3 \frac{C_p b^2 \rho}{k_w}$$

2. The maximum time is defined by conductive heat transfer along the skin being a significant part of the convective heating. The equation formed by Chpoun was:

$$t_{MAX} = \left| \frac{\dot{q}_{CONV}}{d\dot{q}_{CONV}/dx} \right| \left(\frac{\rho c_p b}{k_w} \right)$$

Because heat flux data is nominally taken near room temperature, the heat transfer due to radiation can be ASSUMED to be negligible.

Conduction losses, while conveniently ASSUMED to be negligible may have an important effect on the measurement and must be considered in some detail. Conduction losses or gains may occur in three areas: (1) conduction through the skin wherein heat is lost to backing material behind the thin skin, (2) conduction along the skin caused by surface temperature distributions along the surface of the model and (3) conduction losses associated with the temperature sensor; temperature gradients down the thermocouple wires. These losses will now be discussed in greater detail.

CONDUCTION EFFECTS IN THIN SKIN MODELS

Normal Conduction to the Backing Material:

For reasons of structural strength, a thin skin panel may be backed by some insulative material. Heat transfer can occur between the thin skin and the backing material. The rate of loss is far greater if the backing material is conductive. Even the use of air as a backing material can cause some heat loss. Certainly, stagnant air at ambient tunnel conditions causes small losses which can be neglected. However, improper model design can cause forced convection within the model and losses which are measurable. While no one would knowingly vent the internal cavity of a model, lack of attention to detail can produce this effect. As an example, a Space Shuttle model in Tunnel "9" (test duration of less than 2 seconds) had its thermocouple wires "scoured" by an inadvertent sub mold line flow. This scouring destroyed the wire insulation.

Conduction Along the Surface of the Model:

Dramatic effects can be observed through the conduction of heat along the skin. These errors are induced by non-uniform heating of the surface creating, with time, non-isothermal wall temperatures. Shock interaction regions create losses which easily overpower the measurement to be made. Corrections can be made to these measurements ... but with great difficulty. At a given time, the magnitude of conduction losses along the skin are proportional to the second derivative of the surface temperature with distance along the surface. Classically simple to make through curve fitting techniques, this correction technique requires substantial numbers of surface measurements not always present and high accuracy of measurement in order to generate numerically the second derivative function. This technique is rarely used in practice.

With time, each measurement location is subjected to increased conduction losses as the surface temperature gradients increase. Thus, it is also possible to extrapolate data from a given gage back to low

time where conduction effects are less important. Such a strategy requires a clear understanding that the measured heat flux at a given station is affected only by conduction as the test time is reduced. Other effects can occur at short test times. Starting effects in wind tunnels, for example, must be considered as a potential "other effect".

Kidd, 1987, presented a significant review of lateral conduction effects which are present on thin skin models with several recommendations with regard to the design of thin skin models having nominal model thicknesses of 0.030 inches. These recommendations, reproduced from his paper, are as follows:

1. If the model is to be designed with locally thin skin cavities which are machined into a relatively thick material, these should be at least 1.1 inches in diameter.
2. Similarly, if two dimensional slots are machined into the model, the width of these slots should be at least 1.0 inch.
3. The loads are distributed in thin skin models through the use of a hardback system consisting of bulkheads. Thermocouples should be located at least 0.45 inches from these structural members.
4. The local radius of curvature at the point of measurement for bodies of revolution should be at least 1.5 inches.

The reader should note that these recommendations are for stainless steel models with a skin thickness of 0.030 inches to be used in facilities like those at AEDC.

The recommendation for having the local radius of curvature greater than 1.5 inches is somewhat in deference with AFWAL experience in testing slender delta wings. Whereas substantial losses were observed in such data for leading edges of 0.25 inches, data of acceptable quality was generated using leading edges of 0.50 inches. Irrespective of such differences in detail, the basic fact is that there are limitations in the use of thin skin models that must be understood. There are also analysis techniques available to accomplish that job.

An indication of conduction along the surface of the model can be achieved by plotting the data as shown in Figure 72 (derived at the end of this section of the report). A linear curve in these parameters indicates measurements which are free of conduction losses along the model surface. Two data-correction techniques can be used to correct data corrupted by surface-wise conduction. These are (1) the interpolation of data back to zero time where the surface temperatures are nearly isothermal as shown in Figure 73 and (2) determination of second derivatives of temperature with spatial distance. The first is do-able but because of individual temperature errors, the second technique is "challenging".

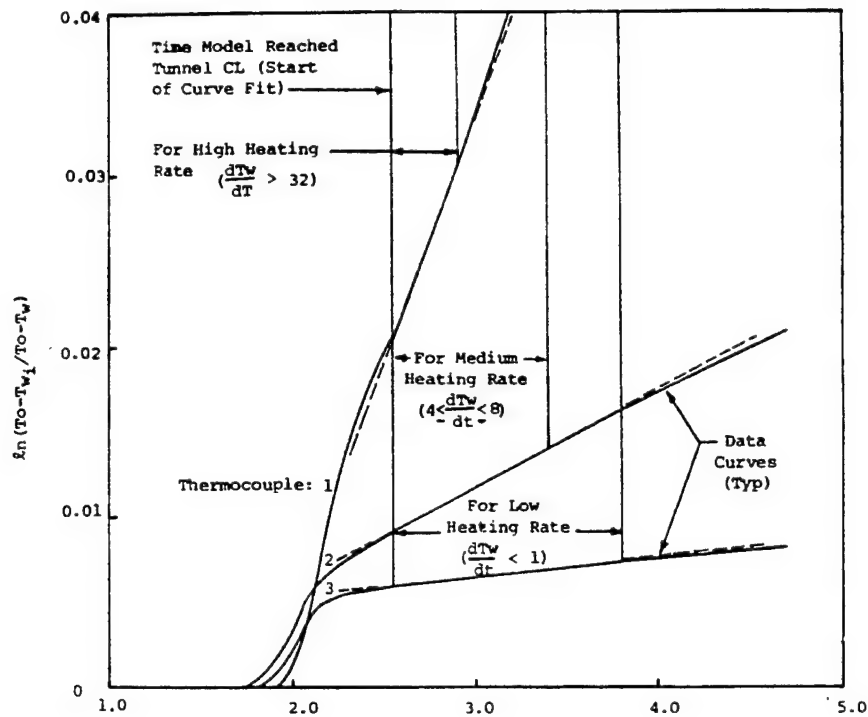


Figure 72 Plot of Thin Skin Data Using the Log-Difference Method.

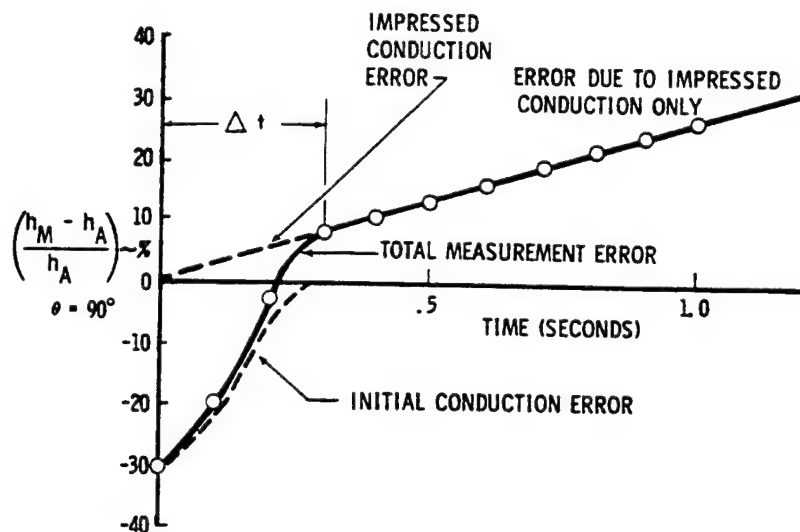


Figure 73 Interpolation of Thin Skin Data Back to Zero Time and Zero Conduction Losses.

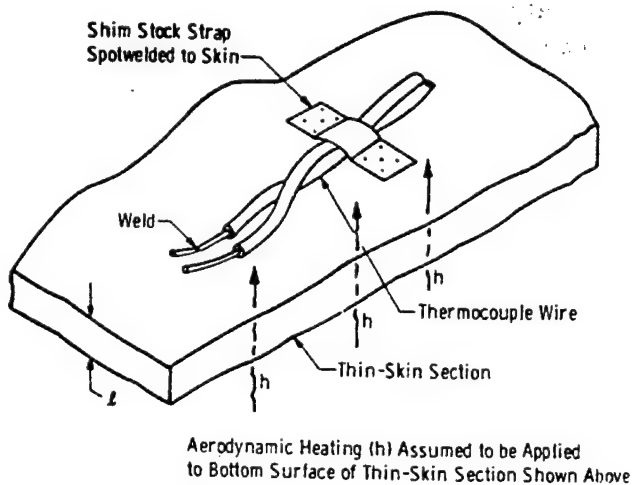
CONDUCTION OF HEAT DOWN THE THERMAL SENSOR WIRES

Kidd, 1985, has discussed the loss of heat down thermocouple wires attached to a thin skin surface. Using the "TRAX" thermal model, Kidd has developed a series of ground rules relative to this phenomena. The experimenter is caught between two effects in the selection of thermocouple wire diameter. On the one hand, small diameter wire may fail more easily during test and is certainly harder and more tedious to install. On the other hand, large diameter wire drains away heat due to conduction effects.

A conclusion figure from Kidd's paper is shown as Figure 74 of this report. Based upon his analysis, wire diameters of 0.005 inch or less are recommended with the material of those thermocouples as low in conductivity as possible. Chromel/Constantan thermocouples are noted as the best from a conduction loss standpoint. Copper with its high conductivity is not recommended.

ATTACHMENT OF THIN SKIN THERMOCOUPLE WIRES

Several studies have been conducted concerning the best technique for attaching thermocouple wire to wind tunnel models. In general, thermocouple wire can be attached either normal to or tangential to the surface of the model. Clearly, from previous discussions, the application of wire normal to the surface maximizes the loss of heat down the wires. Tangential attachment, on the other hand, creates less conduction loss by having more of the thermocouple length at the same temperature as the model surface. Figure 75 is a sketch from Kidd's paper indicating the preferred attachment technique.



Thin-skin thermocouple installation

Figure 75 Sketch of the Attachment Technique for Thermocouple Wires Attached to a Thin Skin Measurement Surface.

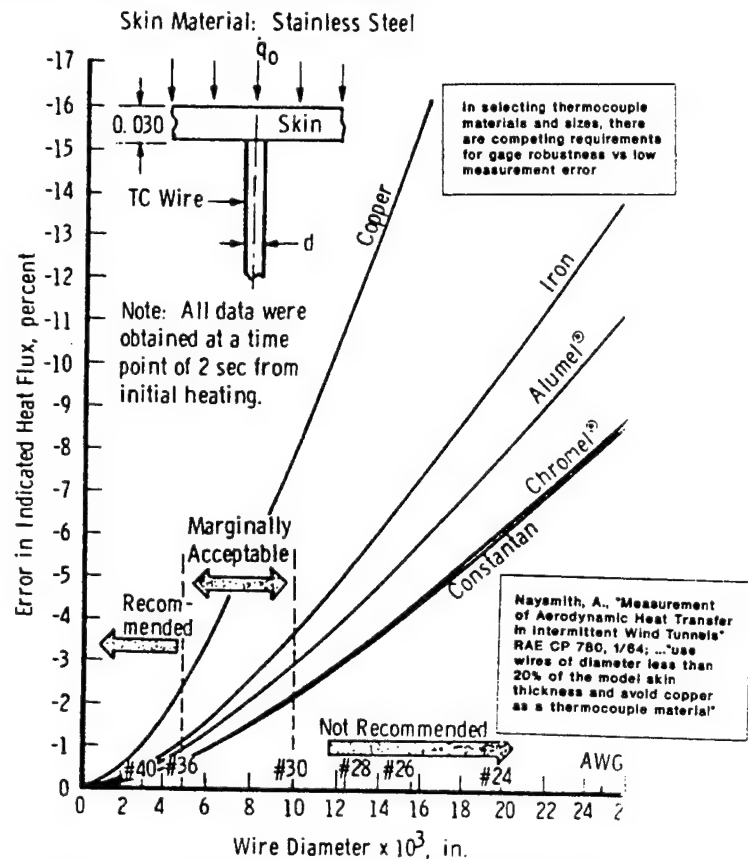


Figure 74 Conduction Losses Down the Measurement Wires of Thin Skin Surfaces.

Apart from the question of conduction losses down the wire, there are several other criteria implicit in the location and attachment of thermocouple wires. First, the thermocouple junction formed by the wires must occur at the surface of the model. Care must therefore be taken not to create a junction below the surface of the model. Twisting the wires together... and it has been done ... is unacceptable. Second, the location of the surface thermocouple junction must be known exactly in model coordinates.

The tangential attachment of thermocouples introduces some difficulties in this respect and makes dense instrumentation more difficult.

ERRORS IMPLICIT IN THE THIN SKIN MEASUREMENT TECHNIQUE

The several errors implied in the evaluation of heat through the thin skin technique are (1) an error in the measurement of skin thickness at the instrument locations, (2) an error in the material properties of the instrumented surface and (3) conduction errors previously discussed.

Skin Thickness Measurement:

Careful measurement of the skin thickness at each gage location is required. The heating rate is directly related to the accuracy of these measurements. An accuracy of measurement of $\pm 3\%$ is required to match the overall accuracy of the instrumentation system. Measurements are particularly important when electroformed models are employed since these models have, traditionally, poor fabrication quality control in regions where they are employed; complex curvature regions.

Material Properties:

Over the years it has become clear that the material properties quoted for a particular class of stainless steel are approximate and must be verified through a batch analysis of the material to be used for the model in question. The evaluation of material properties, particularly the property of specific heat is required.

Specifying the Adiabatic Wall Condition:

Figure 76, Nutt, 1986, indicates the sensitivity of the deduced heat transfer coefficient to errors in specifying the adiabatic wall temperature. The recovery temperature will be discussed in Section VII. It is sufficient to note here that errors in the resulting heat transfer coefficient grow substantially as the wall temperature of the test model approaches the total temperature of the facility. This normally occurs in heat transfer tests which are conducted at low Mach numbers in test facilities designed to produce only enough heat to avoid liquefaction effects.

APPLICATION OF THE THIN SKIN TECHNIQUE TO IMPULSE TUNNELS

Experiments in a Hotshot Wind Tunnel:

In 1965 Harvey discussed the application of thin skin techniques to facilities operating nominally for 100 msec. The measurement surface was "clad" to the load carrying model by double backed tape. The cladding was very thin, 0.002 inch stainless steel stock to which Chromel/Alumel thermocouples 0.001 inch in diameter were spot welded. The stress carrying model was locally cut away at the measurement stations by a hole 0.25 inch in diameter about the thermocouple.

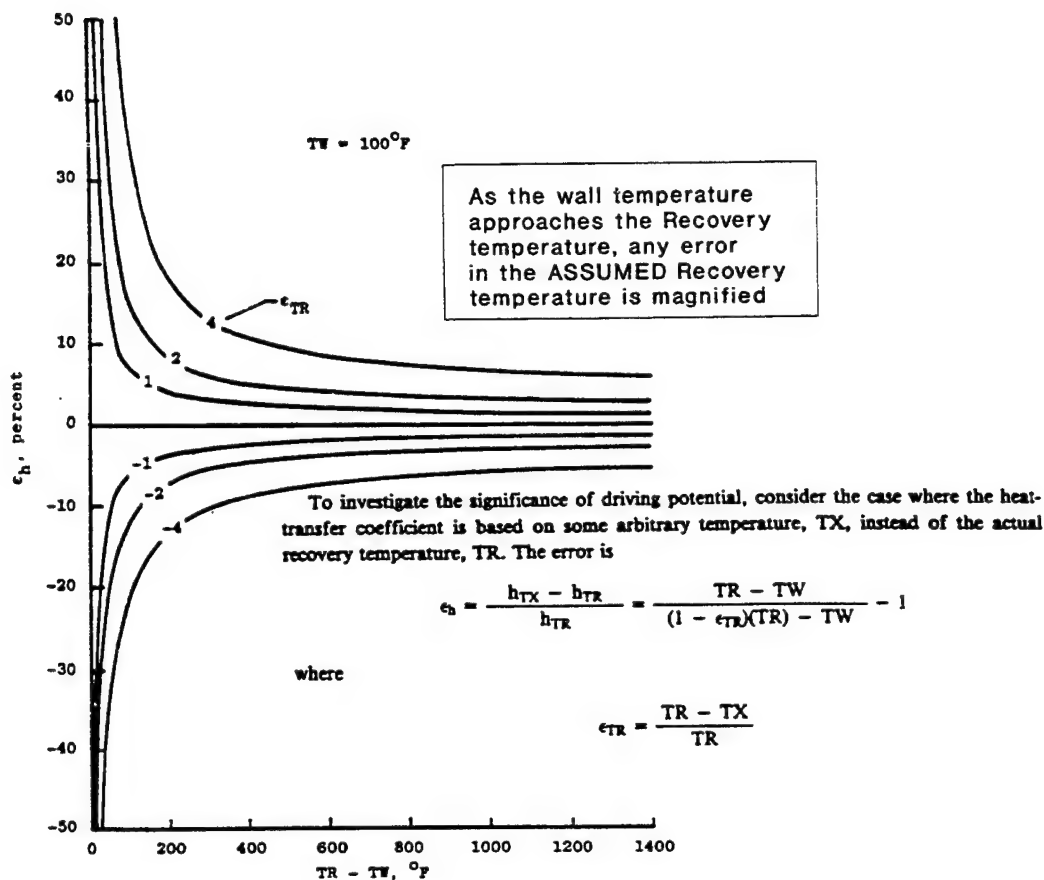


Figure 76 Sensitivity of the Heat Transfer Coefficient to Errors In Specifying the Adiabatic Wall Temperature.

Experiments in a Conventional Shock Tunnel:

Borovoi et al, 1991, describe experiments in a shock tunnel to measure the shock impingement on a cylinder. The experiments were performed in a tunnel operating at low Reynolds numbers ($R_{\rho} = 1.7 \times 10^5 / \text{ft.}$) at Mach 15.5 and a total temperature of 3000 degrees R. Data were generated within 7 msec and the random scatter of the data was estimated at 12%. Apart from the completeness of the data generated, the unique aspect of this experiment is that heat transfer data were taken, not with thin film resistance thermometers, but with the thin skin technique. The thin skin was stated to be 0.0067 ins thick; a "stainless steel foil" and the single wire thermocouples of Copel were 0.004 ins in diameter and flattened at the surface to a thickness of 0.0012 ins.. At close spacing, the thermocouples were placed about one thin skin thickness apart; 0.004 to 0.008 ins..

Holden et al, 1990 discusses the use of both thin film resistance thermometers discussed in Section III and calorimeter gages in conventional shock tunnels. Figures 77a and 77b show the heat transfer time history from these two types of gages. Calorimeter gages were used to obtain an integrated heating value for a complex, roughened surface whereas the thin film gages were used to obtain distributions within that integrated value. The calorimeter gage was fashioned of silver (rather than stainless steel), sensed with a nickel resistance thermometer (rather than a thermocouple) and placed on a Macor substrate with an ultra-low conductivity polyurethane adhesive. The silver material was suited for the millisecond operation of the facility and the resistance thermometer, being more sensitive than a thermocouple, was better suited for low

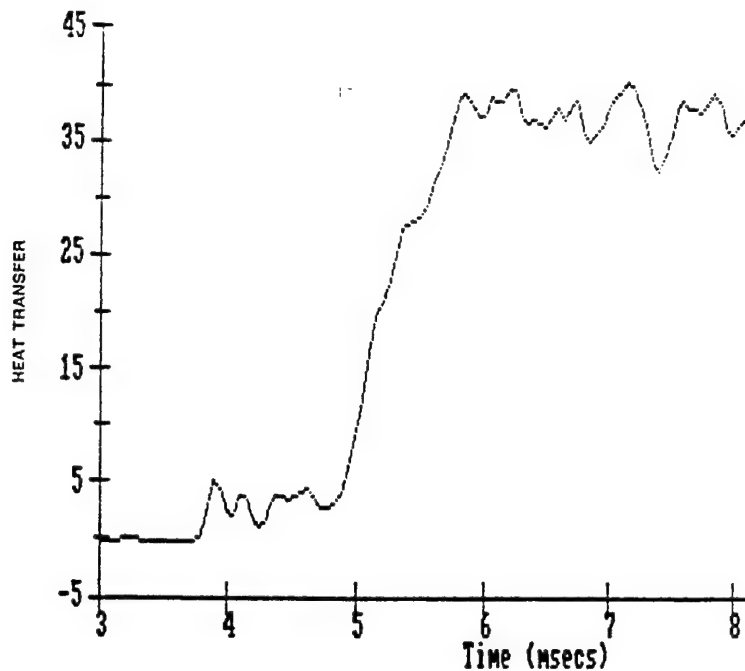


Figure 77 a Heat Transfer Measurements in a Shock Tunnel.
Figure 77a is Thin Film Data.

temperature increases measured in milliseconds. Finally, the thickness dimension of a plated gage was better suited to the very thin silver material than wires which would be welded to the surface material.

Gronig, 1992, has experimented with calorimeter gages in shock tunnel flow. His gages are either silver or copper slugs 0.006 to 0.008 inches thick and 0.08 to 0.12 inches in diameter with temperature measured by a thermocouple. Example data shown indicates measurements at levels of heating rate near 700 Btu/Ft² sec.

This type of gage has been used in short duration facilities for many years. Figure 78 from Osgerby, 1967 shows a gage much like that used by Holden which was placed in the AEDC Hotshot test facilities.

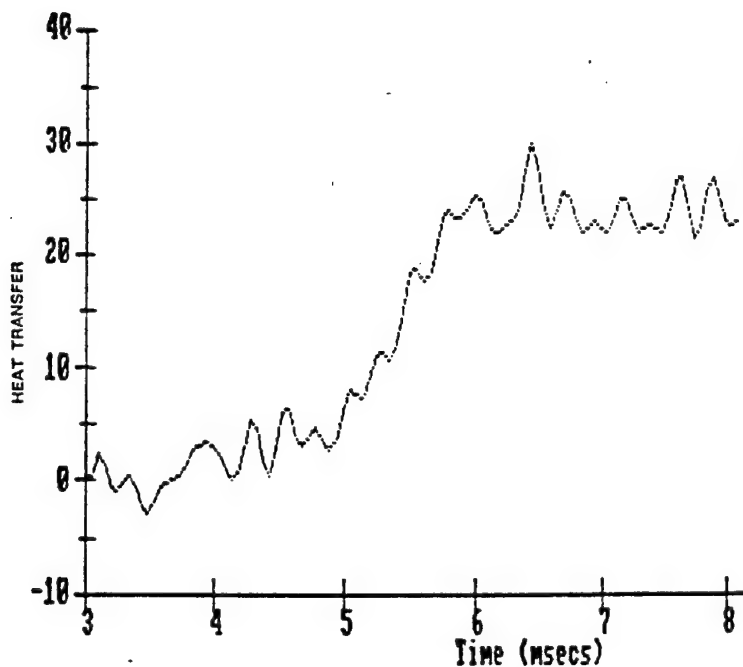


Figure 77b Heat Transfer Measurements in a Shock Tunnel.
Figure 77b is Calorimeter Data.

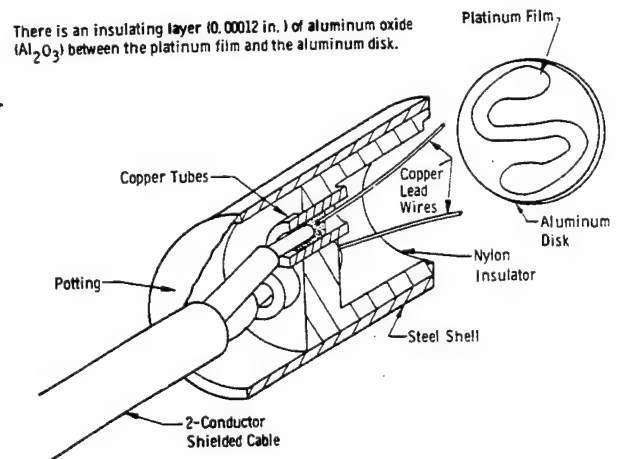


Figure 78 Early Calorimeter Gage
Used in the AEDC
Hotshot Tunnel after
Osgerby, 1967.

Unusual "Thin Skin" Applications

Kussoy, 1975, generated shock interaction data on an ogive/cylinder centerbody using an annular, shock-generating ring. The documentation of that experiment; verified through correspondence, stated that the "thin skin" was 0.497 ins thick with thermocouples attached to the backface. Kussoy noted that this thickness, while requiring a longer time to establish that the backface of the material tracks the surface of the material, allows for measurements in a shock interference region with no temperature discontinuities (no localized hotspots relative to the model) and with very small conduction along the surface (less than 5 percent). The experiment was run within a test duration of 3 minutes. The temperature rise due to aerodynamic heating was between 20 and 90 degrees R. This modeling was established by calculation procedures and the heat flux deduced using the best linear least squares fit to the log difference equation (developed in Appendix IV-1 to this report. Further, Kussoy reports that one instrumentation port was modified to create a thin skin of 0.246 ins and these data agreed with the data taken with the thicker surface.

This application of the "thin skin" is substantially different than classical thin skin surfaces. The comments by Kussoy, 1975, however terse, address many of the questions that could be raised. Clearly, very thin surfaces (like 0.030 ins thick) create high surface gradients in shock interaction regions. The reader is left to ponder the very interesting data of Kussoy and to apply analysis methods discussed in Section II to proposed modeling situations to demonstrate for ones self the claims made by Kussoy in this interesting application of "thin skin" techniques. It should be observed that in later references, Kussoy, 1991, the skin thickness was reduced to about 0.1 ins. which still is thicker than conventional "thin skin" models.

It must be noted, however, that the temperature rise in the thin skin material is inversely proportional to the thickness of that material. A surface 0.497 ins thick will have a temperature/time slope only 5% that of a very thin surface, 0.030 ins thick. For the Kussoy 1975 experiment, the undisturbed heating rate of 6240 watts/m² (0.549 Btu/Ft² Sec) will have a backface temperature increase of only 7.4 degrees in 40 seconds of test time. This temperature rise is extremely small and can result in high measurement error when thermocouples are used.

APPENDIX IV-1
DERIVATION OF THE "LINEAR LOG DIFFERENCE RELATIONSHIP"
FROM NUTT AND MATTHEWS, AIAA PAPER 86-0774-CP, 1986

From the definition for heating rate:
$$h_{TR} = \frac{\dot{q}}{T_R - T_W} = \rho bc \frac{dT_W/dt}{T_R - T_W}$$

which is true assuming that (1) radiation is negligible and (2) heat conduction is negligible. This equation was integrated assuming that (1) the material properties are invariant with time and (2) recovery temperature was invariant with time. The integrated equation is:

$$\frac{h_{TR}}{\rho bc} (t - t_i) = \ln \left[\frac{T_R - T_{W_i}}{T_R - T_W} \right]$$

differentiating this equation with respect to time yields:

$$\frac{h_{TR}}{\rho bc} = \frac{d}{dt} \ln \left[\frac{T_R - T_{W_i}}{T_R - T_W} \right]$$

Since, by assumption, the left side of the equation is constant with time, the slope of the log difference function on the right side must also be constant if the assumptions listed are satisfied.

APPENDIX IV-2 THIN SKIN THERMAL MODEL UNCERTAINTY ANALYSIS

From the thin skin thermal model, the heating rate is defined as:

$$\dot{q} = \rho c_p b \frac{dT}{dt}$$

The heat transfer coefficient, h , is defined as:

$$h = \frac{\dot{q}}{T_r - T_w}$$

It has been shown that the under restrictive conditions (see Appendix IV-1) the following relationship exists between the heat transfer coefficient and the measured temperatures:

$$\frac{h_{TR}}{\rho c_p b} (\Delta t_2 - t_1) = \ln \left[\frac{T_R - T_{wi}}{T_R - T_w} \right]$$

$$h = f(T_R, T_{wi}, T_w, \rho c_p b, \Delta t)$$

The restrictive conditions are :

- (1) no conduction along the skin
- (2) no radiation away from model
- (3) constant material properties
- (4) constant recovery temperature

Determining the uncertainty in the heat transfer coefficient, h , as Carter had done in Appendix, III-1, the following expression obtains:

$$(\omega h)^2 = \left(\frac{\partial h}{\partial T_R} \omega T_R \right)^2 + \left(\frac{\partial h}{\partial T_w} \omega T_w \right)^2 + \left(\frac{\partial h}{\partial T_{wi}} \omega T_{wi} \right)^2 + \left(\frac{\partial h}{\partial \Delta t} \omega \Delta t \right)^2 +$$

$$\left(\frac{\partial h}{\partial (\rho c_p b)} \omega (\rho c_p b) \right)^2$$

where:

$$\frac{\partial h}{\partial T_R} = \frac{1}{[]} \frac{(T_R - T_w) - (T_R - T_{wt})}{(T_R - T_w)^2}$$

$$\frac{\partial h}{\partial T_w} = \frac{1}{[]} \frac{(T_R - T_{wt})}{(T_R - T_w)^2}$$

$$\frac{\partial h}{\partial T_{wt}} = \frac{1}{[]} \frac{(-1)(T_R - T_w)}{(T_R - T_w)^2}$$

$$\frac{\partial h}{\partial p} = \frac{\ln[]cb}{(t - t_i)}$$

$$\frac{\partial h}{\partial t} = \ln[]pcb(-1)(t - t_i)^{-2}$$

$$\frac{\partial h}{\partial t_i} = \ln[]pcb(t - t_i)$$

SECTION V GRADIENT TYPE HEAT FLUX GAGES

Several "heat flux gages" exist that produce a signal directly proportional to the rate of heat transfer through the structure. These gages measure the temperature difference across a known thickness of material and have implicit in their development some assumptions concerning how heat flows within a structure and within the gage as a part of that structure. This chapter of the report will discuss several of these gages including the following:

- The Schmidt-Boelter gage
- The Vattel heat gage and Epstein gage
- The Gardon gage
- The in-depth thermocouple gage

THE SCHMIDT-BOELTER GAGE

Historical Note:

Heat flux can be deduced under steady state conditions by measuring the temperature drop across a surface of known material properties and known thickness. This is a Thompson Type 1 Gage E. Schmidt designed the first instrument making use of this observation. His instrument consisted of a rubber strip around which was wound a "pile" of 100 thermocouples wound in such a way that the junctions are alternately in the middle of one surface and then the other surface of the rubber strip as shown in Figure 79.

Boelter (L.M.K. Boelter) introduced an ingenious modification to this gage by wrapping the surface (plastic in the case of Boelter) with Constantan wire and then silver plating half of the wires to form a silver-constantan thermopile. Hence, the Schmidt-Boelter gage is intrinsically a thermopile gage using the temperature drop across a material of known thermal and physical properties.

Because of the thermopile design, the output signal from the gage is magnified and that feature may well be important in its practical application in wind tunnel testing.

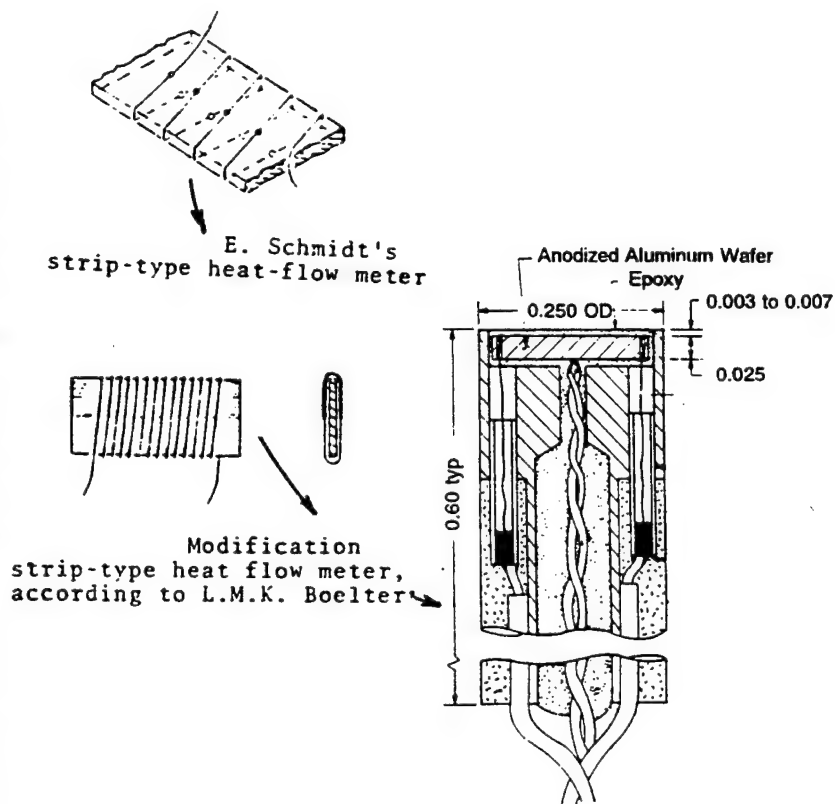


Figure 79 Evolution of the Schmidt-Boelter Heat Gage.

The drawing on the right side of Figure 79 indicates the current gage design based on the Schmidt-Boelter principle. This gage is a direct reading, "semi-contourable" design that can be contoured in the plane of the strip of anodized Aluminum.

Current Use:

The Arnold Engineering Development Center is a large and enthusiastic user of the Schmidt-Boelter gage. Matthews, 1987, lists several advantages of the gage including durability, sensitivity (by virtue of the thermopile feature), semicontourability and a self-generating output signal proportional to the incident heat flux imposed upon it. Disadvantages noted are "...some concern about hot-spot effect..."; in effect, non-isothermal wall effect and their applicability as wall temperature increases. This may limit its long duration applicability in tests. From personal experience, high temperature gage operation is another concern.

The equation for the heat flux sensitivity of the Schmidt-Boelter gage is given by Kidd, 1981, to be:

$$\frac{\Delta E_0}{\dot{q}_0} = (\Delta T) (N) (\delta/\dot{q})$$

where ΔE_0 is the gage output signal in mv.

ΔT is the temperature difference across the measurement wafer considering the conductivity of the potting material

N is the effective number of thermocouples around the wafer of material

δ is the thermoelectric sensitivity of the thermocouple material in $\mu V/^\circ F$
and \dot{q} is the imposed heating rate in $Btu/ft^2\text{-sec}$.

From Kidd, 1981, the overall measurement sensitivity of this gage, $\frac{\Delta E_0}{\dot{q}_0} \approx 3 \frac{mv}{Btu/ft^2\text{sec}}$ and this depends upon the temperature difference set up across the measurement wafer. This temperature difference is directly related to the thermal conductivity of the potting materials.

For an AEDC application, the values of the various terms defining the measurement sensitivity are:

$$\Delta T = 3.9^\circ R$$

$$N=35$$

$$\delta = 22.7 \times 10^{-3} mv/^\circ R; \text{ Sensitivity of chromel/alumel thermocouples}$$

so that the equation for sensitivity becomes:

$$\frac{\Delta E_0}{\dot{q}_0} = \frac{(3.9^\circ R)(35)(22.7 \times 10^{-3})}{1.0 Btu/ft^2\text{-sec}^\circ R} = 3.099 \frac{mv}{Btu/ft^2\text{sec}^\circ R}$$

In Figure 79 the "potting material" was Epoxy. It was located both on top of and below the wafer. The wafer was made of anodized aluminum.

The uncertainty of the Schmidt Boelter calibrations conducted in January 1981 and reported by Kidd, 1981, was 4.28% at room temperature conditions. Data were taken up to 500 degrees F ambient with gage to gage variations increasing with the ambient temperature. Operation at other than nominally ambient temperatures requires a specific calibration of the instrument at those conditions.

THE GRADIENT HEAT FLUXMETERS

Technically similar to the Schmidt/Boelter gage but fabricated with more advanced micro-fabrication techniques are a class of heat flux gages known collectively as gradient heat fluxmeters. These gages are composed of thin films attached to either side of a thermally-resistive layer. The films can be either thin film resistance thermometers or thin film thermocouples and the resistive layer is a very thin layer of insulator, such as Kapton, to which the thin film gages adhere.

The impetus for this development has come from the turbine engine community and examples of this form of gage can be found in France, Japan, Great Britain and the United States. Current research activities are centered on producing gages capable of proper operation at elevated surface temperatures. This topic will be discussed in greater detail later in this report.

THE VATELL HEAT GAGE

The VateLL heat gage is a commercial product of the VateLL Corporation having augmented sensitivity (by virtue of "n" thermopile, thin film thermocouples applied on both sides of the thermally-resistive layer), fast response (by virtue of the small mass of the thermal sensors attached), relatively small size (about 0.1 in x 0.1 in by 0.0002 ins thick) and increasingly high temperature application. Figure 80 shows one version of the gage under development and Figure 81 shows a cross-section of the gage. High temperature heat gages will be further discussed in Section 10 of this report.

The response time, from Hager, 1989, is given by the equation:

$$\tau = 1.5 \frac{\delta^2}{\alpha}$$

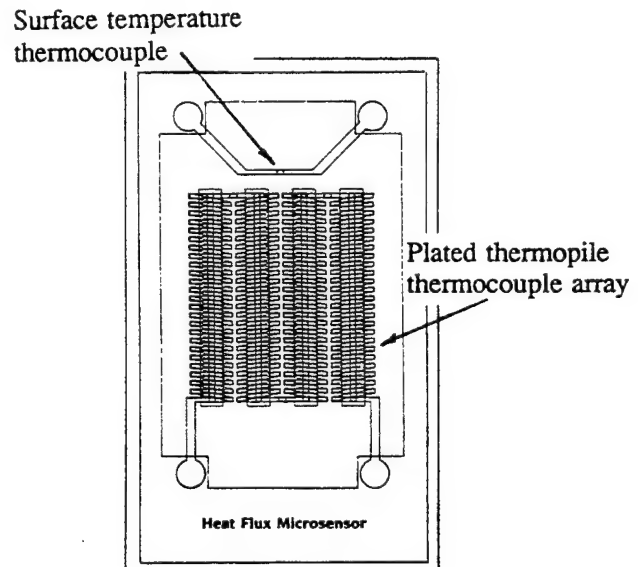


Figure 80 One Version of the VateLL Heat Flux Microsensor.

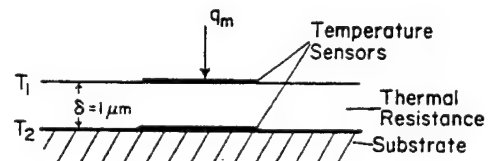


Figure 81 Cross Section of the Microsensor.

where δ is the thickness of the gage typically $1\mu m$.

and α is the thermal diffusivity of the thermal resistance layer typically $5 \times 10^{-7} m^2/sec$.

The steady state temperature drop across the insulative layer is given by:

$$\Delta T = \left(\frac{\delta}{k}\right)\dot{q}$$

Thus, the gage sensitivity is related to the temperature drop across the insulative layer which, in turn, is related to the material of which the layer is constructed (through the thermal conductivity, k) and the thickness, δ , of that layer.

Table 5.1 shows several materials which could form such an insulative layer and their conductivity values.

TABLE 5.1
MATERIALS WHICH COULD FORM INSULATIVE LAYERS
AND THEIR CONDUCTIVITY VALUES

Material	Thermal Conductivity,
	$\frac{Btu}{Ins.-Sec.-^{\circ}F}$
Macor	2.25×10^{-5}
Kapton	2.074×10^{-6}
Silicon Dioxide	1.739×10^{-5}
Ultem 1000	3.241×10^{-6}

The Epstein Gage

Alan Epstein of M.I.T., 1985, developed the theory and practice for a gradient heat flux meter which placed a single thin film resistance thermometer on either side of a Kapton resistance layer similar to the Vattel gage arrangement. The resistance calorimeter has roughly 100 times higher sensitivity than a wire thermocouple which, in turn, has up to twice the sensitivity of a plated thermocouple. Kapton was selected as the insulative material because it has a thermal conductivity about 10% that of silicon dioxide. Because of these design features, the Epstein gage should have response performance roughly equivalent to that of the Vattel gage.

Gage factors for the Epstein gage are shown in Figure 82 as a function of the desired frequency response of the gage. The numbers shown in the body of the figure represent the thickness of the thermal insulative layer in micro-meters.

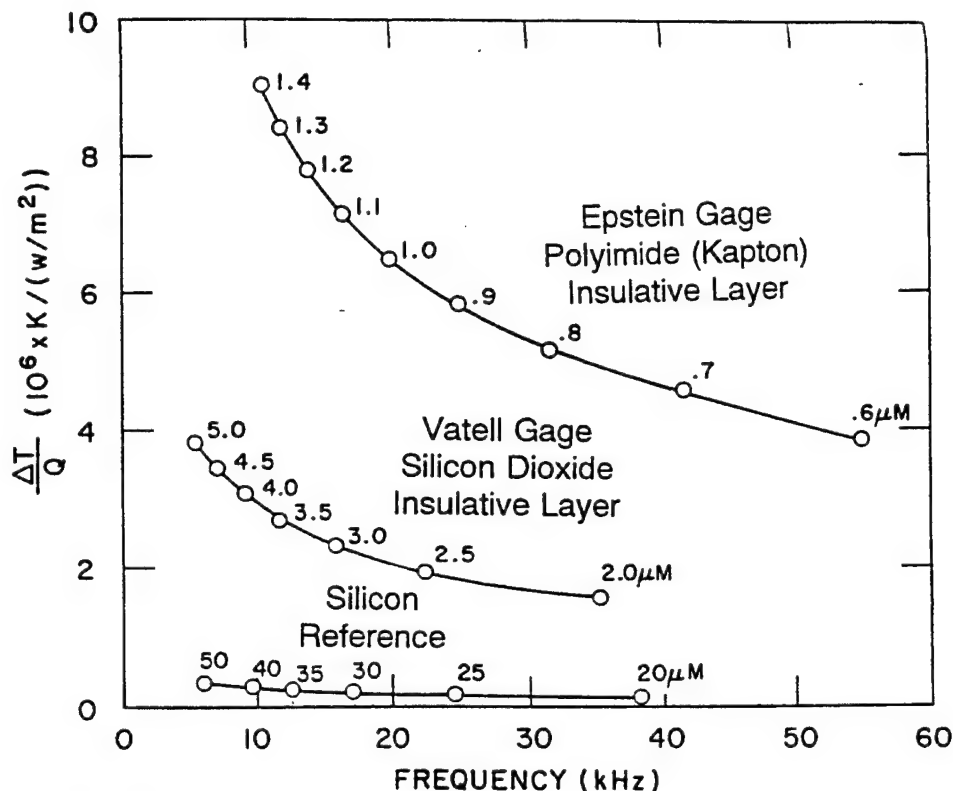


Figure 82 The Sensor Sensitivity of the Epstein Heat Gage After Epstein, 1985.

The French Heat Fluxmeter at ONERA

Kayser et al, 1992 demonstrate a flux gage quite similar to the Vateil gage which is being developed at ONERA in France. The gage is designed to be usable at temperatures up to 1000 degrees C and to be directly deposited on aerodynamic profiles or turbine blades. The thermal elements discussed are Copper/Nickel thermocouples applied to a Kapton substrate. The French gage, at this writing, was substantially thicker than the Vateil gage (62 μm as opposed to several μm for the Vateil gage but thickness is a function of development. The sensitivity of the Copper/Nickel thin-film thermocouple is quoted as $17.6 \mu VK^{-1}$. Corresponding wire thermocouples have twice that sensitivity.

Gardon Gages

Figure 83 from an excellent basic reference by Hornbaker and Rall, 1968, indicates the physical design of the heat transfer gage known as a Gardon gage. The Gardon gage was developed by Robert Gardon, 1956 as a radiation gage. The gage concept and the design was transferred into the measurement of convective heat transfer and is used in both wind tunnels and flight research.

As with many of these gages, the data output is proportional to the imposed heating rate. and the gage can be configured as a thermopile gage (with multiple thermocouple junctions) to produce higher gage sensitivity. Table 5.2 from the AEDC Handbook demonstrates the gages available as well as the order-of-magnitude increase in sensitivity due to the thermopile design.

The gage design sets up a radial temperature gradient between the thin constantan foil and the copper heat sink surrounding it. The hot center junction is measured with a copper wire attached to the center of the

constantan disk. The cold edge temperature is often measured with a separate constantan wire attached to the copper heat sink. One dimensional heat flow in a radial direction is the basis of the thermal model. The heating rate is proportional to the temperature difference between the hot center region of the thin foil and the cold edge junction of the heat sink. In Thompson's view, this would be considered as either a Type 1 or Type 3 gage depending upon the time scale of the application. This is graphically demonstrated in Figure 84 where the data traces change character with test time. At large test times, trace #1; the output signal demonstrates a steady-state signal that is proportional to imposed heating rate. At short test times, trace #3; the output signal demonstrates heat flow into a slug calorimeter having a thickness equal to the foil thickness.

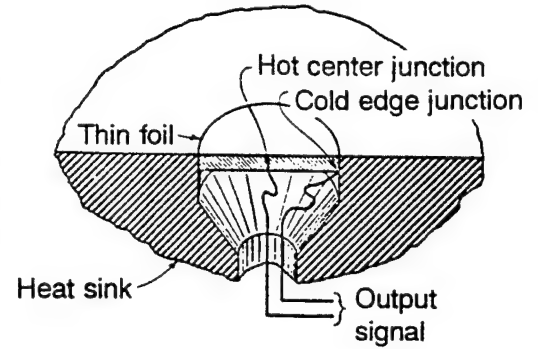


Figure 83 Schematic View of the Gardon Gage after Hornbaker and Rall, 1968.

TABLE 5.2
GAGES AVAILABLE FROM THE AEDC HANDBOOK

Sensor	Size	Heat Flux Sensitivity <i>MV/(Btu/ft²-Sec)</i>	Maximum Continuous Service Temperature °F	Heat Flux Measurement Range <i>Btu/ft²-sec</i>
Conv. Gardon	0.25D x 0.35	0.12	1000	0.2 to 20
Thermopile	0.25D x 0.35	1.4	300	0.02 to 20
Schmidt Boelter	0.187D x 0.30	1.5	600	0.015 to 20

In this, as in all gradient gages, the imposed heating rate is defined in terms of the measured temperature through the relationship:

$$\dot{q} = CE$$

where the calibration factor, C, is empirically determined through calibration and E is the gage output in mv. It can be shown in the more general case that "C" is not truly a constant but a non-linear function of the edge temperature of the instrument.

* ...during the initial period of heating, the center of the foil behaves basically as a single capacity element (a slug) since the incident heat flux at the surface is considerably greater than the heat being conducted out from the edge of the foil to the heat sink" ... "The method of data reduction, of course, would be different for the two time regions"

ONE GAGE, TWO THERMAL MODELS,
THE GAGE IS NOT UNIQUE.

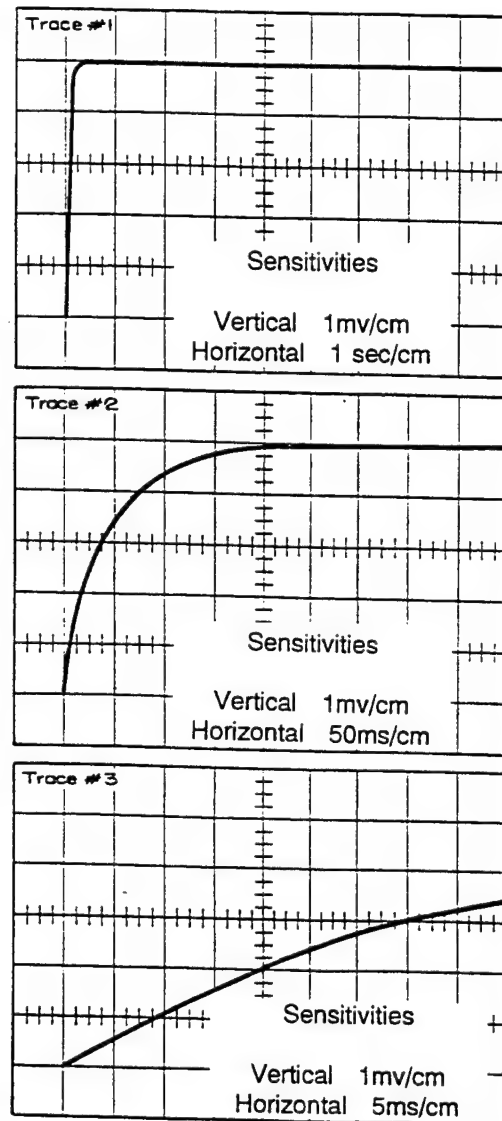


Figure 84 Response of a Gardon Gage to Aerodynamic Heating at Several, Typical Time Scales.

Since "wall temperature" is not measured, calibration has been employed to define an effective "wall temperature" for the gage based on the edge temperature and the temperature difference between the center of the foil and the edge of the instrument:

$$T_w = T_{EDGE} + 0.75(\Delta T)$$

where ΔT is the difference between the foil center and the heat sink gage edge represented by an expression $\Delta T = KE$ where "K" is a calibration factor and E is the gage output in millivolts.

The problem with this gage is that it can never be well integrated into a model since it presents two fundamentally different structures to the flow; a thin foil that heats quickly and a heat sink that, ideally, does not change in temperature during the run. These different structural elements heat at different rates and cause a non-isothermal surface temperature which perturbs the boundary layer flow and causes errors in surface heating rate measurements. The temperature difference between the center of the foil and the heat sink around the perimeter of the foil is a linear function of the foil diameter; small foil dimensions minimize the temperature difference and the boundary layer perturbation caused.

The equation that relates the temperature difference across the Gardon gage is:

$$\Delta T = \frac{1}{4} \frac{R^2}{kt} \dot{q}$$

$$C \equiv \frac{4kt}{R^2}$$

See Pg V-6

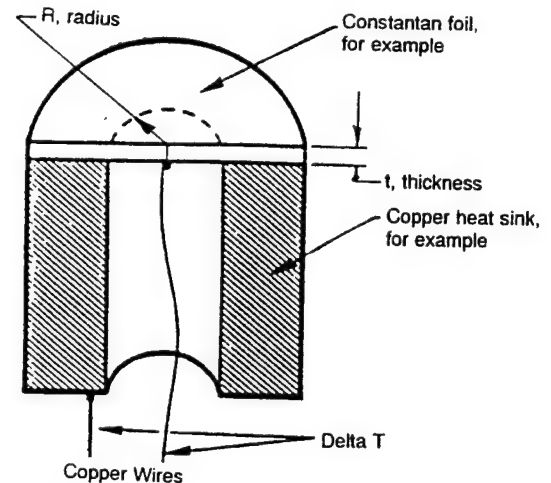
$$E \propto \Delta T$$

where R is the radius of the thin, disk-shaped, foil
k is the thermal conductivity of the foil material
t is the thickness of the foil material

The time response of the Gardon gage is given by the equation:

$$\tau = \frac{3}{4} \frac{R^2}{\alpha}$$

to reach 95% of the steady state value of the signal.



Advanced Multi-Layered Thin Film Gages

These gages proceed from international studies of the heat transfer to turbojet engines and references from the Oxford University group under the late Don Schultz, the Massachusetts Institute of Technology group under Epstein and the Japanese group under Hayashi.

In the last several years the Hayashi and coworkers, 1984 have developed a gradient type heat flux gage and published details on its construction and application.

Figure 85 indicates the structure of the gage which Hayashi et al have termed a "multi-layered thin film gage". This gage combines rapid response characteristics of thin film instruments with the long term application of a sandwich gage. This is a Thompson Type 1 gage. In its intended application, the gage measures the temperature difference between the heated face and the backface. The heat resistant layer creates a thermal choke and the gage is placed on a heat conductor so that the thermal reservoir of constant temperature is, for all practical purposes, infinite. In this respect, the operation of the Hayashi gage acts as a Thompson Type 3 gage where the heat conductor plays the part of the active source.

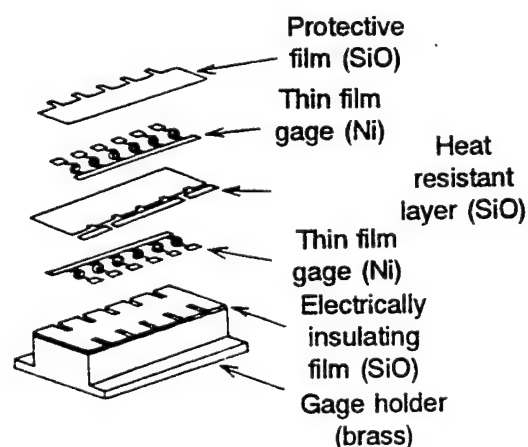


Figure 85 Exploded View of the Multi-Layered Thin Film Gage after Hayashi et al, 1989.

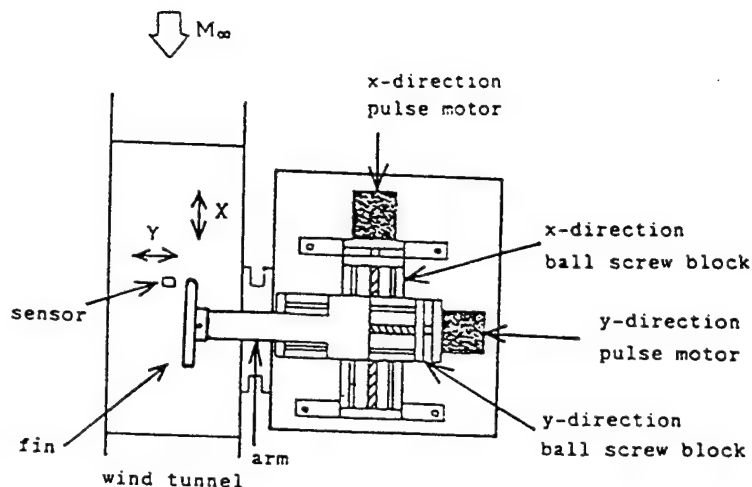


Figure 86 Use of a Single Multi-Layered Thin Film Gage to Evaluate Heat Transfer Distributions Within a Shock Interaction Region.

The gage has been employed by Hayashi to generate dynamic test data. The model including the single gage was placed in the flow and the shock generator (fin) is drawn across the gage as shown in Figure 86. Continuous data are then taken through the interaction as shown in this figure. Comparison pressure data are also taken as shown in that figure.

The only criticism of this application may be in the development of a non-isothermal boundary layer perturbation caused by the "heat resistant layer" in a conducting steel model although the assumption made by the authors was that this is not the case. This may be particularly difficult where shock interaction regions are present since (1) it may be impossible to separate one affect from the other and (2) temperature perturbations may cause different phenomena in a flow situation near separation.

In spite of these difficulties, the gage is an interesting application of instrumentation technology and the dynamic test capability, which will be

discussed in more detail later in this report, is an important aid to productivity in the development of large amounts of data and understanding in the development of continuous data traces.

More recently, Epstein of M.I.T., 1986, and Doorly of Oxford University, 1987, have documented very interesting gages based upon dual thin films deposited on a thin, insulative sheet. This technology, in both cases, is motivated by gas turbine research.

Characteristics of this type of gage are shown in Figure 87. Epstein states that this gage is useful to 400 degrees C with high frequency response to 100 kHz. The gage operates either as a sandwich gage for low frequency operations or as a semi-infinite slab gage for very high frequency operations. Intermediate frequency data are obtained through numerical signal processing reconstruction.

The Epstein and Doorly papers present an outstanding and comprehensive review of this type of gage and its application.

For his gage Epstein cites the following sources of error and their magnitude:

scale factor error on calibrations <1%

knowledge of p_{ck} of the calibration fluid 3-5%

the change in p_{ck} of the polyimide insulator 2.5% over 50 deg C

In-Depth Thermocouple Gage

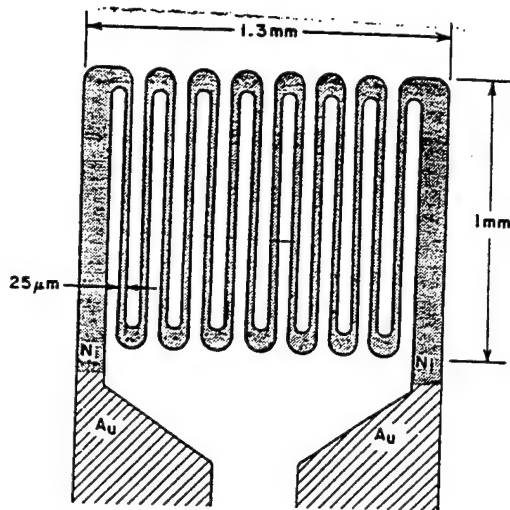


Figure 87 Gradient Type Heat Sensors Attributed to Epstein (in the USA) and Doorly (in England).

Figure 88 presents a schematic view of an in-depth thermocouple gage; a gage using the materials of the wind tunnel model together with one or a series of thin wire thermocouples placed at different depths in the material to generate an in-depth temperature difference.

In depth thermocouple gages are used extensively in flight test applications. These gages are also known as "Isothermal Thermocouple Gages" because there is a substantial length of wire on either side of the thermocouple bead which is at the same temperature as the bead thus reducing the conduction losses which can be severe since the wire and insulator are such dissimilar materials.

These gages have also been used to advantage in wind tunnel testing. They have been used in continuous high speed tunnels which had no injection capability. By using the indepth feature of the gage; long term, steady state heating rates could be measured without the need for rapid injection.

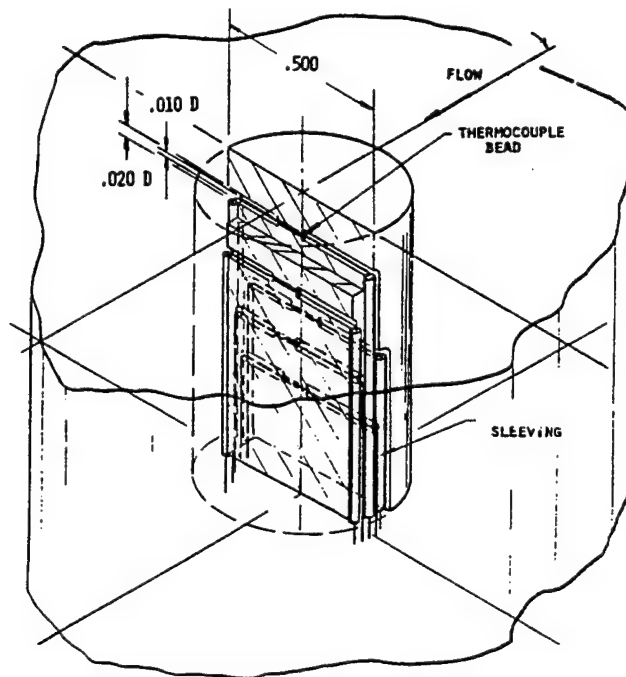


Figure 88 View of an In-Depth, Thermocouple-Based Heat Gage.

SECTION VI

STATIC VS DYNAMIC MEASUREMENTS

Historically, some 30 years ago when heat transfer measurements were first made at the Arnold Engineering Development Center; back when the X-15 was being tested, a single test point of heat transfer data required 60 seconds of time during which the model was in the tunnel. 20 years later during the Space Shuttle development program, that same test point required 5 seconds in the tunnel. Of course, in addition to the actual test time, there was a substantial time required in both cases to cool the model and return it to a cooled, test ready state. This time is a multiple of the test time and related to the amount of heat that the model receives as well as the quality of the cooling system for the test under consideration. During the Space Shuttle development, the time between test points was of the order of 5 minutes but more recently, the time interval between successive injections has reduced to as low as 1 minute. At this point, the thin skin technique appeared to have reached a plateau of capability in which it could not easily be further improved. Newer instrumentation techniques that allows for "dynamic testing" have reduced the test intervals even further. Today, a series of 10 data points that at one time required 600 seconds can now be accomplished in less than 200 seconds - including cooling time.

Dynamic testing as a heat transfer test technique refers to the ability to generate multiple points of test data during a single injection as the model configuration is maneuvered through the test section or changed in configuration as a function of time. Several examples of dynamic testing have been demonstrated to date. This technique requires the use of an integrating heat gage which measures the variation of temperature or heating during rapid model movement as a function of time and hence configuration orientation.

The several examples of "dynamic testing" explored to date are as follows:

1. Space Shuttle with Rapid Pitch Sweep
2. Dynamic Shock Impingement Studies
3. Space Shuttle Remotely Driven Flap
4. Fully Integrated Lifting Body Model
5. Slender Rotating Cone with Pitch Oscillating

The particular characteristics of these model applications will be discussed in somewhat greater detail later in this section of the report. For now, it is important to understand why dynamic testing would be useful in a wind tunnel model and under what circumstances it could be used.

There are two basic reasons for the development of dynamic measurement techniques. They are (1) the generation of higher quality data and (2) the generation of higher quantity data at lesser cost and in shorter periods of time. Two examples are worth discussing here.

Shock interaction phenomena create highly localized regions of aerodynamic heating with large thermal gradients about the peak. Since the location of the peak is not clearly known, some initial and exploratory measurements are required to locate the peak. Once located, instrumentation can be strategically placed to measure peak values. The process is costly in both development time and wind tunnel time. Dynamic testing allows the placement of lesser numbers of gages within the general region of the heating peak. The peak is then defined by observing the relative output of this gage array as a function of the local motion of the

configuration (such as the angle of attack of the model). This technique was used to advantage in an experiment at the AFWAL which is shown in Figure 89.

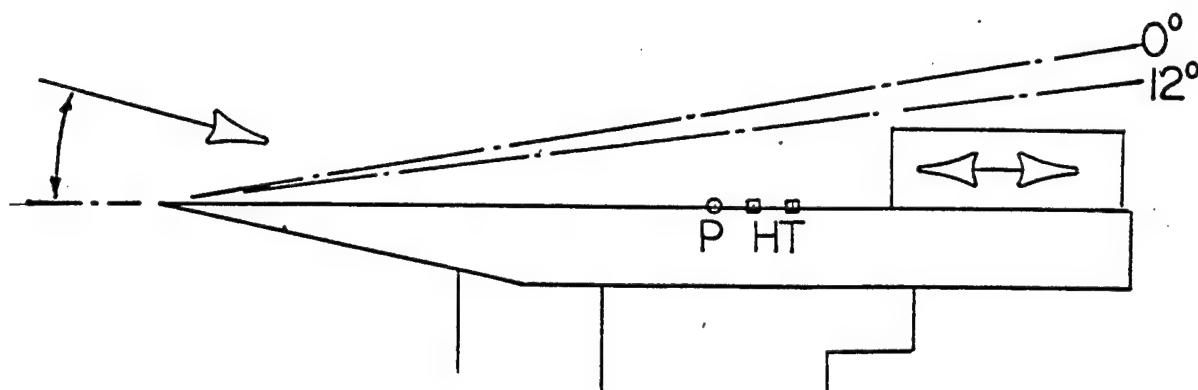


Figure 89 Plate/Cylinder Interaction Model Employing Dynamic Motion and Run in the Wright Laboratory Mach 6 Tunnel.

In present day engineering, cost is an integral factor in all engineering decisions. Dynamic test techniques minimize the cost of test facilities by maximizing the productive work that can be accomplished during each hour of testing. In most cases, this process requires an entire systems evaluation of cost factors in which the model cost and the data reduction and manipulation costs are important parts.

Dynamic test techniques require technological developments both in the area of advanced sensors, which I have termed "integrating sensors" as well as in test techniques which optimize the dynamic movement of the model within the test section environment.

Integrating sensors are those which respond rapidly to changes in the test environment, which absorb and retain the character of the heat pulse obtained in the tunnel and which can be decoded to yield data from continuously changing test maneuvers. Four such gage designs are (1) coax gages, (2) Schmidt-Boelter gages, (3) isothermal staple gages and (4) thin film gages. Only the first two have been used in a dynamic mode. All such gages are based upon the semi-infinite slab analysis and modifications which account for a finite backface temperature rise.

Dynamic testing involves a continuous movement of the model within the test section. Such movement can be classed as either slow or fast with respect to the response characteristics of the gage. In the former case, the data reduction may be considered as quasi-steady state. In the latter case, the data reduction requires a more complex reconstruction of the imposed signal through fast Fourier transforms.

Techniques for Quasi-Steady State Data Acquisition

This application of instrumentation began in the early 1980's when AFWAL tested a Space Shuttle model in the NSWC Tunnel 9. The facility is a fast blowdown tunnel operating at a high Mach and Reynolds number condition for less than a second at substantial cost. Our goal was to make maximum use of the test environment by driving the test model through a complete pitch cycle in one second.

The model shown in Figure 90 was pitched at rates from 40 to 85 degrees per second during which time valid heating data were acquired. Figure 91 shows the quality and completeness of the data as a function of the vehicle angle of attack for a single run. Note that both the trend of peak heating on the side of the Space Shuttle fuselage and its location as a function of the model angle of attack is defined during a single, one second entry using an array of coax gages on the model.

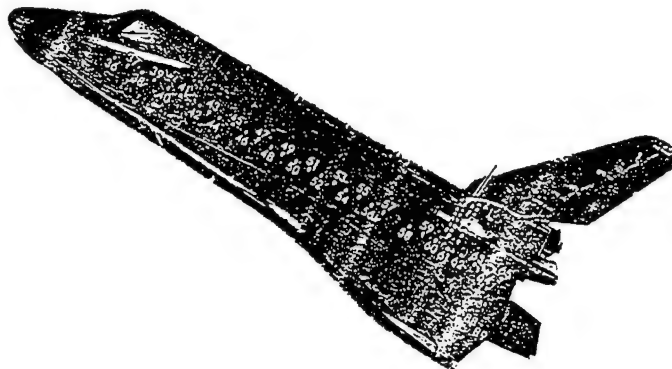


Figure 90 Space Shuttle Model Used In the NSWC Tunnel 9 with Coax Gages for Dynamic Testing.

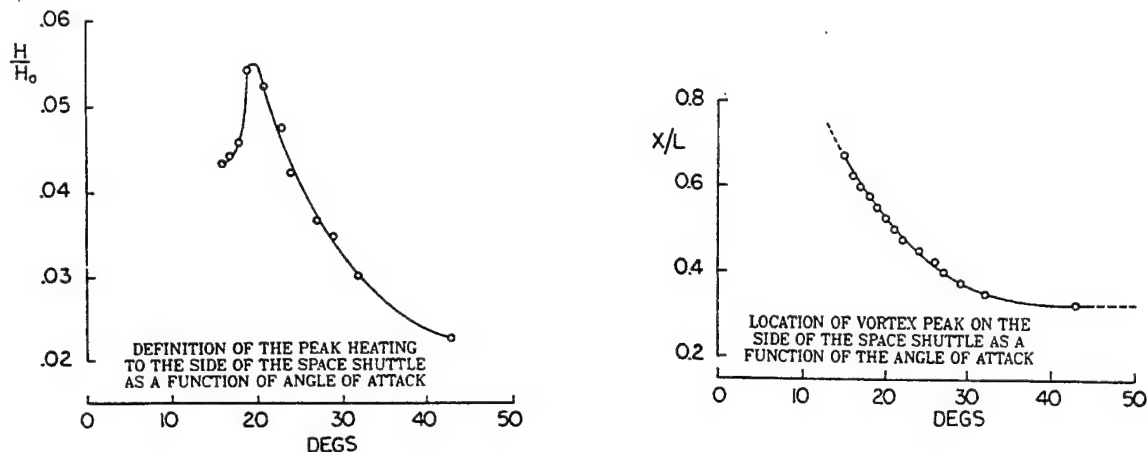


Figure 91 Data Results Obtained from a Single, One-Second Sweeping Run in the NSWC Tunnel 9.

Building on this success, experiments were formulated for continuous wind tunnel facilities both at AFWAL and at AEDC. Two experiments were run at AFWAL, both stressing complex shock interactions in a Mach 6 facility. In the first experiment, the interaction region ahead of a cylinder attached to a flat plate was instrumented with a single gage. The model was pitched during a single test injection and interaction data were generated. The interaction data were unique in that through pitching the model, the interaction process "swept" across the limited instrumentation defining the true peak heating. The second experiment, also run at Mach 6, evaluated heating to deflected control surfaces in the same manner using miniature coax gages. That model is shown in Figure 92 with the flap and instrumentation detail shown in Figure 93.

A larger Space Shuttle model was tested hypersonically at AEDC. This model, shown in Figure 94, was modified to incorporate, on board, the mechanism required to power the body flap during test. Data during a single run were taken as the flap moved. Phenomena, such as flap induced separation, was observed in a continuous manner rather than at discreet flap angles. The onboard motor eliminated the manual flap

adjustments required during previous tests. This saving was estimated at \$30,000. More data on flap-induced phenomena were taken during a single shift of dynamic testing than during the entire, prior, Space Shuttle development program.

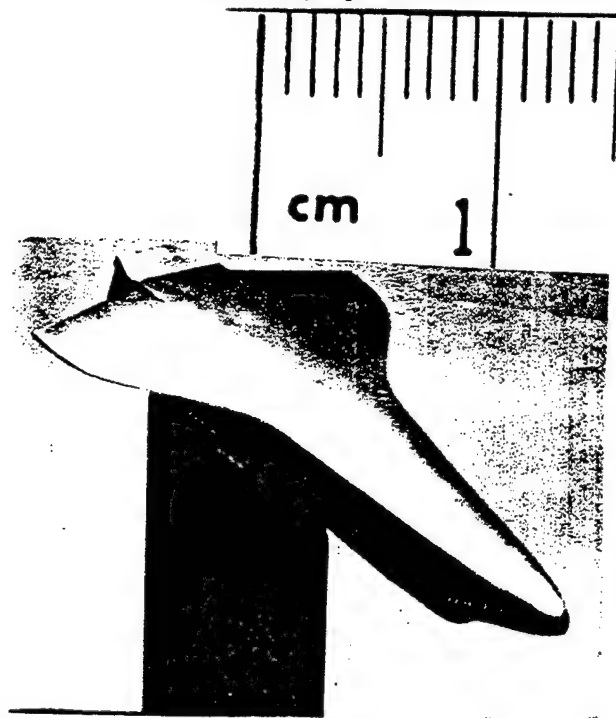


Figure 92 Very Small Scale Space Shuttle Model Tested Dynamically.

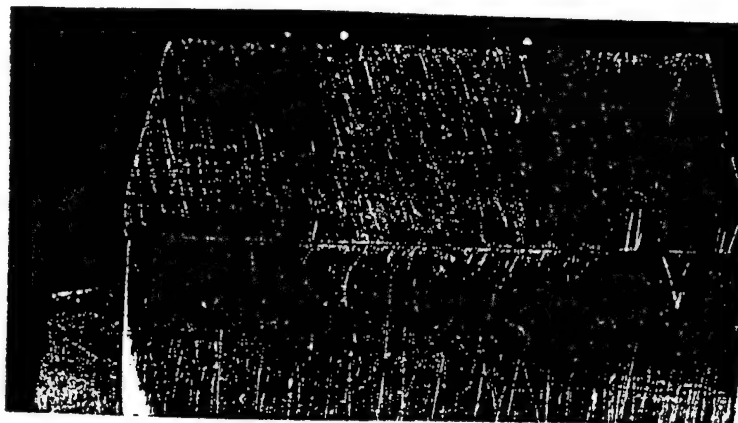


Figure 93 Flap Instrumentation Detail for Small-Scale Space Shuttle Model.

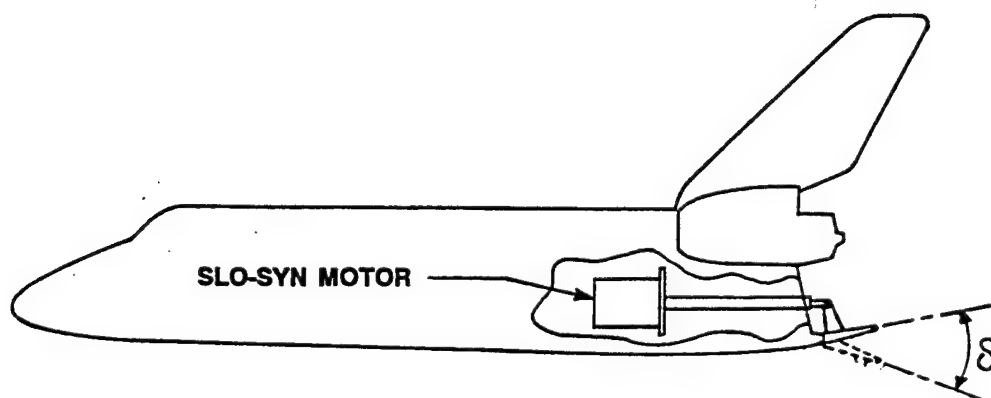


Figure 94 Larger, Dynamically-Tested Space Shuttle Model with On-board Motor-Driven Control Flap.

Uncertainty of Sweep vs No Sweep Data

Following the technical discussion presented by Wannenwetch, 1983, it has been shown that sweeping a model through a test profile rather than acquiring data statically results in a somewhat larger degree of uncertainty. To achieve adequate time resolution of the data, a higher rate of sampling is used. This rate, in the AEDC experiments was 0.01 seconds/loop (100 samples per second) rather than 0.0583 samples per loop (17+ samples per second). It has been shown that the uncertainty levels of sweep data are 135% higher than no sweep data and this is due simply to the faster data rate employed in acquiring data. Figure 95 shows the reduced heating rate data for the example run and Figure 96 shows the flap schedule producing

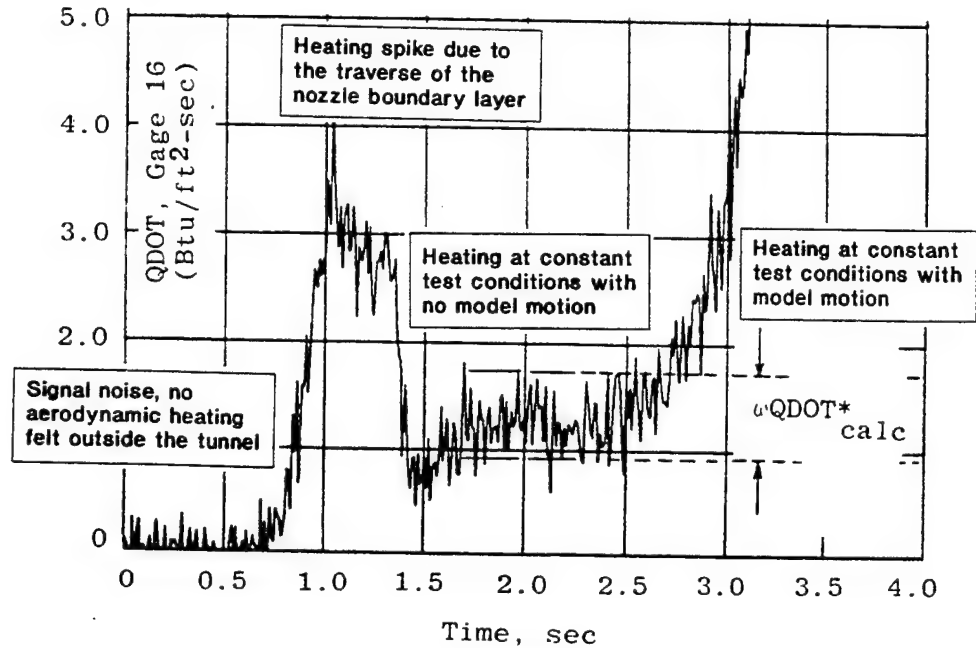


Figure 95 Reduced Heating Rate Data for the Space Shuttle Model Tested at AEDC Showing Model Dynamic Motion.

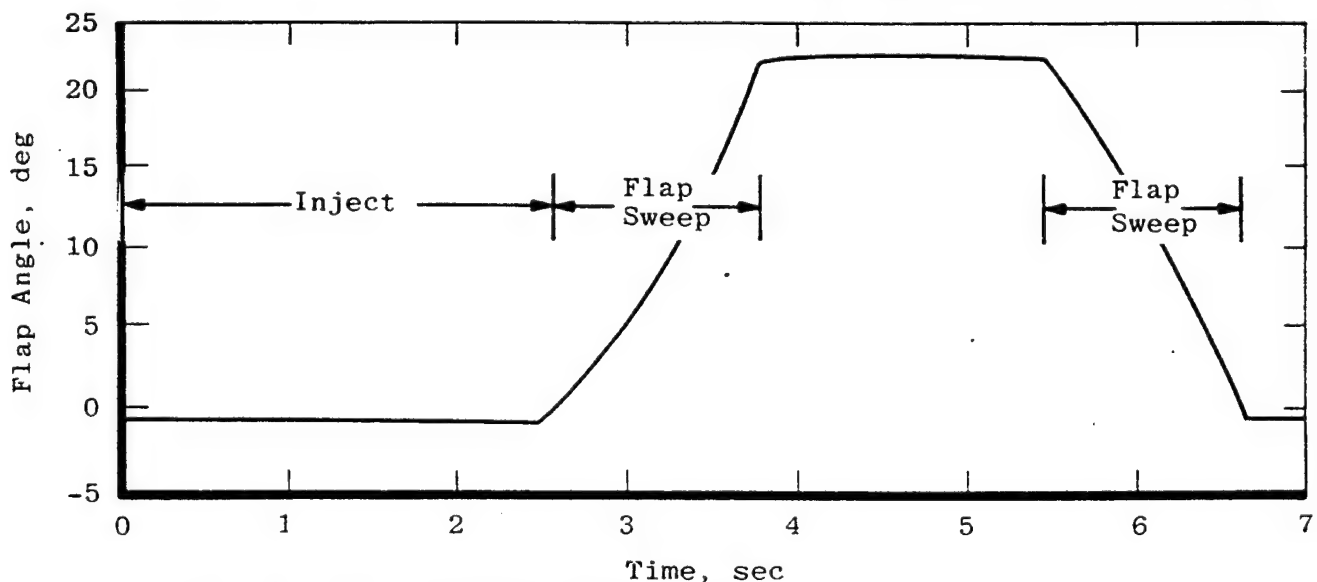


Figure 96 The Flap Deflection Schedule Producing the Heat Transfer Data Shown In Figure 95.

that data. The initial injection phase occurs with the model outside the tunnel and not affected by heat transfer. This is followed by an intense period of heating as the model traverses the tunnel-induced shear layer (boundary layer) where the heat transfer peaks. This, in turn is followed by a period of aerodynamic heating on the tunnel centerline when the heat transfer is constant. The uncertainty in output noise level for this example was experimentally determined during the initial phase of the model injection when the model was not subjected to aerodynamic heating (between 0 and 0.5 seconds in Figure 95). This level was estimated to be $\omega CENTS = 6 \text{ counts}$. This is read as the uncertainty in the data acquisition system counts at a constant wall temperature. Data accuracy can be improved either by an averaging technique or the application of a numerical filter technique. This improvement, using either technique, reduces the uncertainty by $1/\sqrt{m}$ where m is the number of points averaged or the number of points in the filter. It was shown by Wannenwetsch, 1983, that to acquire data of similar quality during pitch as in steady flow through filtering alone required a filter with an unreasonable number of points.

The uncertainty in heat transfer rate is given by the equation:

$$\omega \dot{q} = \left[\frac{10^4 (SENS)(CENTS)}{(GAIN)(SFC)} \right] \psi(t_{n,p}) f(properties)$$

where SENS is the basic sensitivity of the thermocouple in $^{\circ} R/mv$

GAIN is the gain of the amplifier

SFC is the number of counts to full scale

$$f(properties) \text{ is } \frac{2\sqrt{\rho c k}}{\sqrt{\pi}}$$

$\psi(t_{n,p})$ is a weak function of the time at which the heat transfer rate was calculated and a strong function of the speed with which the data is acquired. This sensitivity more than doubles as the acquisition speed increases from 17 to 100 samples per second.

For the specifics of the experiment discussed, the following numbers were quoted:

SENS = 29.41 $^{\circ} R/mv$ (typical of chromel/constantan thermocouples)

GAIN = 1000 a tunnel decision limited by saturation voltage

SFC = 16,384 counts (2^{14}) based on the data acquisition system characteristics of the facility

The thermal property data for the coax gages was given as $\sqrt{\rho c k} = 0.4 \text{ Btu/(ft}^2\text{-sec}^{1/2}\text{-}^{\circ} R)$.

From the numbers listed above, the term $\frac{10^4 (SENS)(\omega CENTS)}{(GAIN)(SFC)} = \frac{10^4 (29.41)(6)}{(1000)(16384)} = 0.04861$ is deduced.

Combining terms, the uncertainty of the heat flux rate, \dot{q} , is given by the expression: for amplifier noise indicative of the AEDC facility when this test was run.

$$\omega q = \pm 0.0861 [\psi(t_{n,r})]$$

It was shown through this uncertainty analysis that, given the tunnel acquisition system with its fundamental accuracy, (ω **CNTS**), and (SFC), data inaccuracies arising from the faster data acquisition time, $\psi(t_{n,r})$, must be balanced by improved data accuracy through increased amplifier gain, (GAIN). This, of course, is limited by the saturation voltage of the system. At any rate, amplifier gain should always be maximized for the coax gages to assure a resolved signal. Through cautious adjustment of the amplifier gains and through filtering and/or data averaging the quality of the sweep data can approach that of the steady state data.

The accuracy of heat transfer measurements can be experimentally determined by evaluating data during the interval immediately after the model has passed through the tunnel shear layer and before the flap sweep sequence was initiated (times between 1.5 and 2.5 seconds in Figure 95).

DYNAMIC TESTING: THE APPLICATION OF FAST FOURIER TRANSFORMS IN THE LIMIT OF RAPID MODEL MOVEMENT RELATIVE TO GAGE RESPONSE

There are two options with regard to measurement systems for data acquisition. Figure 97 indicates that these options are either a traditional measurement system in which the response is related to the measurement by a simple constant, k , or an alternative scheme in which the instrumentation cannot fully reproduce the measurement input but produces a distorted response which can be corrected off line through software.

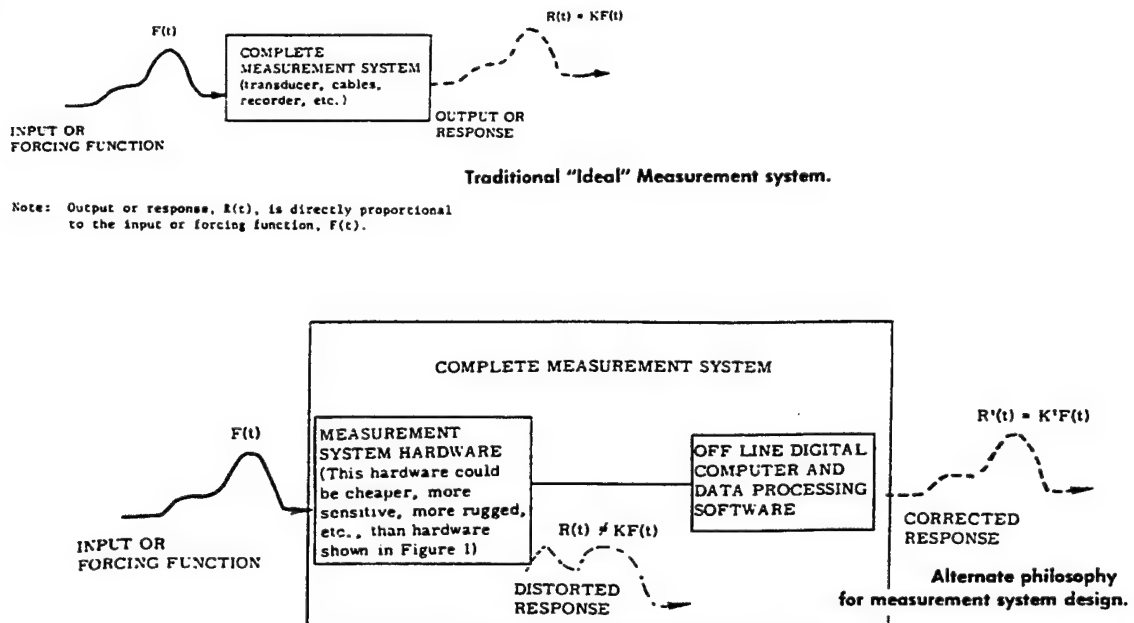


Figure 97 Alternative Techniques for Accurate Data Acquisition.

In the limit of dynamic testing in which the measurement signal is distorted by the rapid motion of the configuration and the characteristics of the instrumentation gage, the application of Fourier transforms through the facility of modern computational equipment has been successful.

Fourier transforms have been discussed by several authors including Harting, 1972. Essentially, Fourier established a unique transform between the time and frequency domains. Because of their LINEARITY, systems could change their distributions only in amplitude and phase between the input and output data. The basis of the technique is the Fourier integral (Fourier transform). Harting describes in detail the use of the Fourier transform to compensate for transient data distortion.

The technique involves generating a transformed calibration response to a known, manipulatable input signal, known as the "transform function" which; by design, contains sufficient energy within the bandwidth of interest. See Figure 98. Both calibration input and response are digitalized. These signals are transformed from the physical to the frequency domain and then ratioed, output/input, to produce the transfer function for the gage, H . The transfer function is a complex number having both a magnitude and phase angle associated with it. Favour details the mathematical method and its limitations.

Distorted data from a test program can then be corrected through the application of the calibration-defined transfer function which is defined in the frequency domain. Using this transfer function, distorted data transformed into the frequency domain can be divided by the transfer function to provide correction and then transformed back into the physical domain. This signal is corrected for distortion and provides an excellent simulation of the true signal that would be observed by an infinitely responsive gage.

In practice, this technique has been applied and reported by Jenke and Strike, 1978 and Strike, 1979. In their application to an oscillating sharp cone which is graphically described in Figures 99 through 101, a square pulse calibration signal to a Gardon gage is produced with the output of that signal, the gage response, shown as a distorted signal in time. Both the input and output signals are transformed into the frequency domain as shown on the right side of Figure 99. 60 Hz carrier noise is visible in the gage output signal. The components of the transfer function, formed from the transforms of the calibration input and output, are shown in

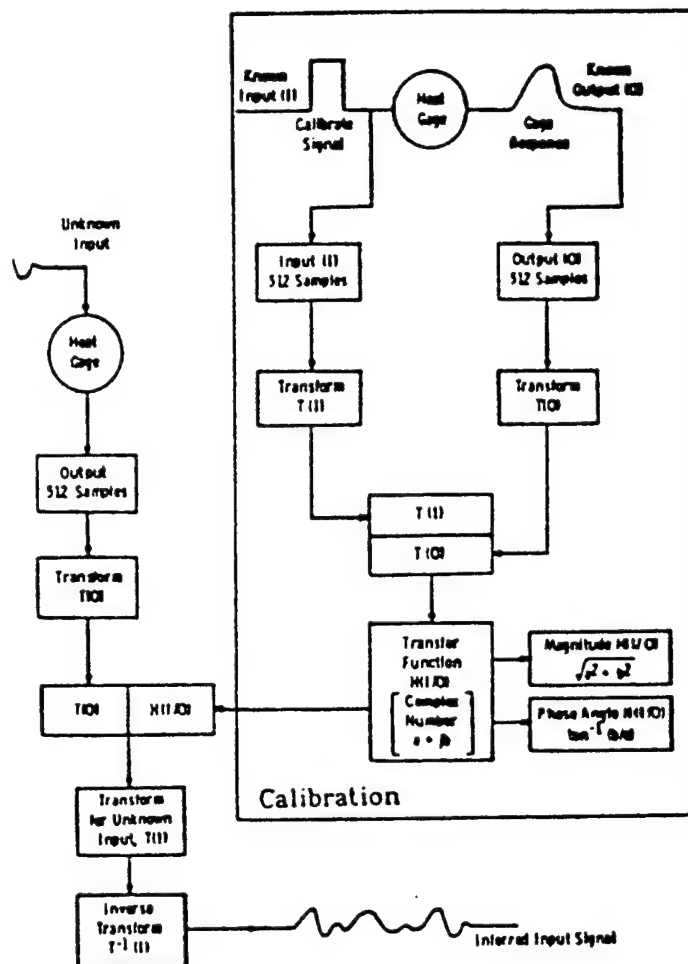


Figure 98 Schematic of a Calibration Technique for Data Evaluation by Fourier Transforms.

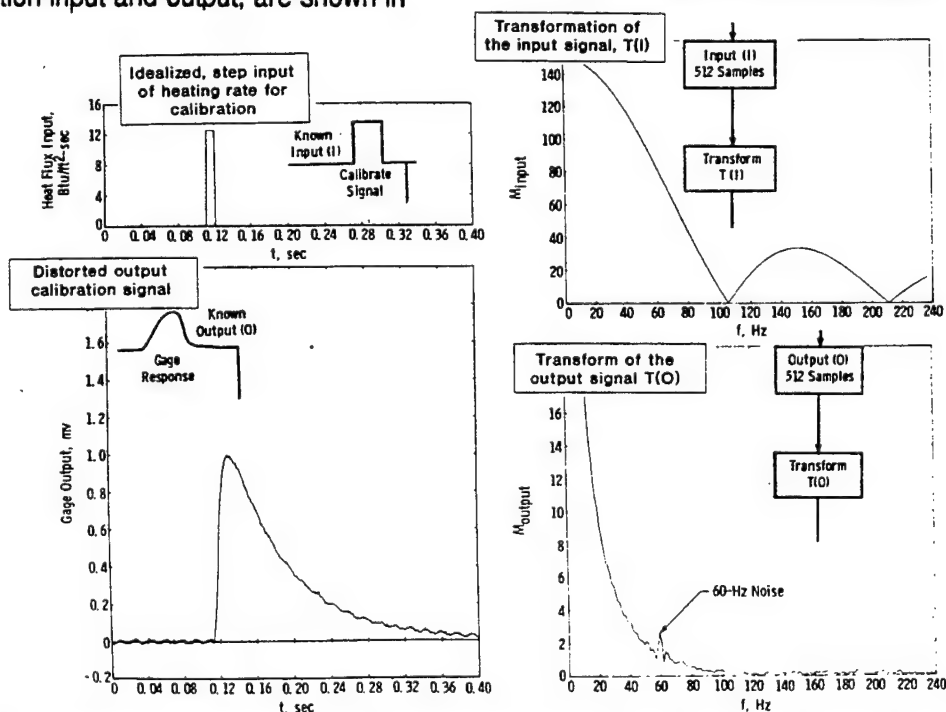


Figure 99 The Calibration Process to Form Transformed Input and Output Data From Which a Transfer Function Is Created.

Figure 100 produced by ratioing the input to output of the transformed signal. Figure 101 then indicates both the distorted test signal and its transform as well as the corrected test signal transformed back from the frequency to the time domain.

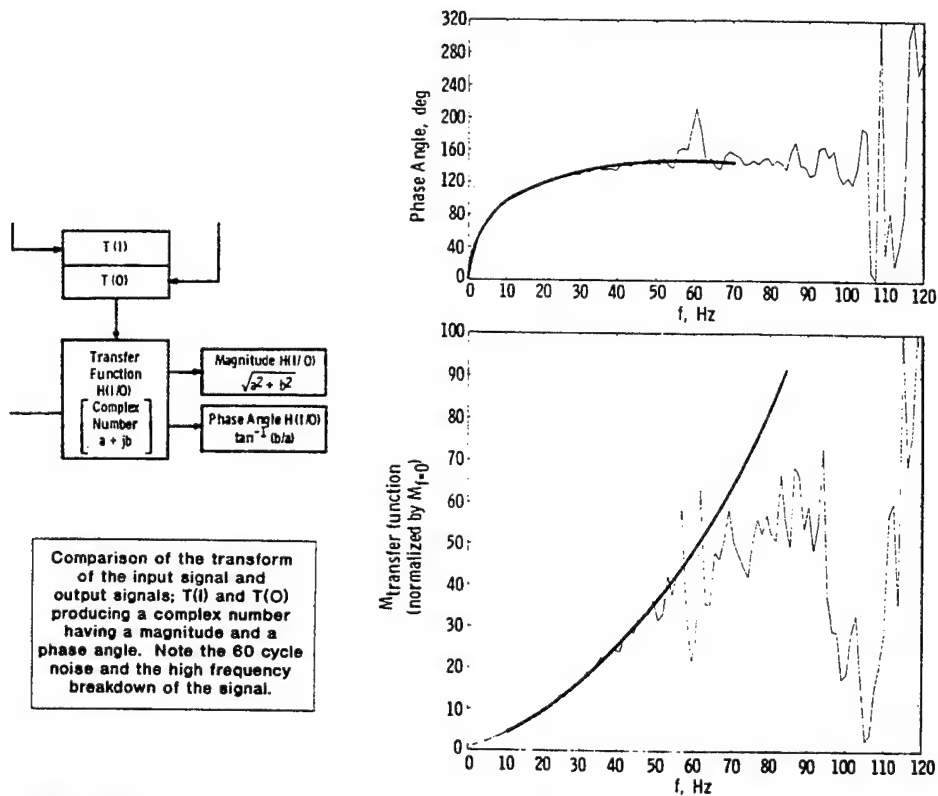


Figure 100 The Complex Transfer Function; Both Phase Angle and Magnitude.

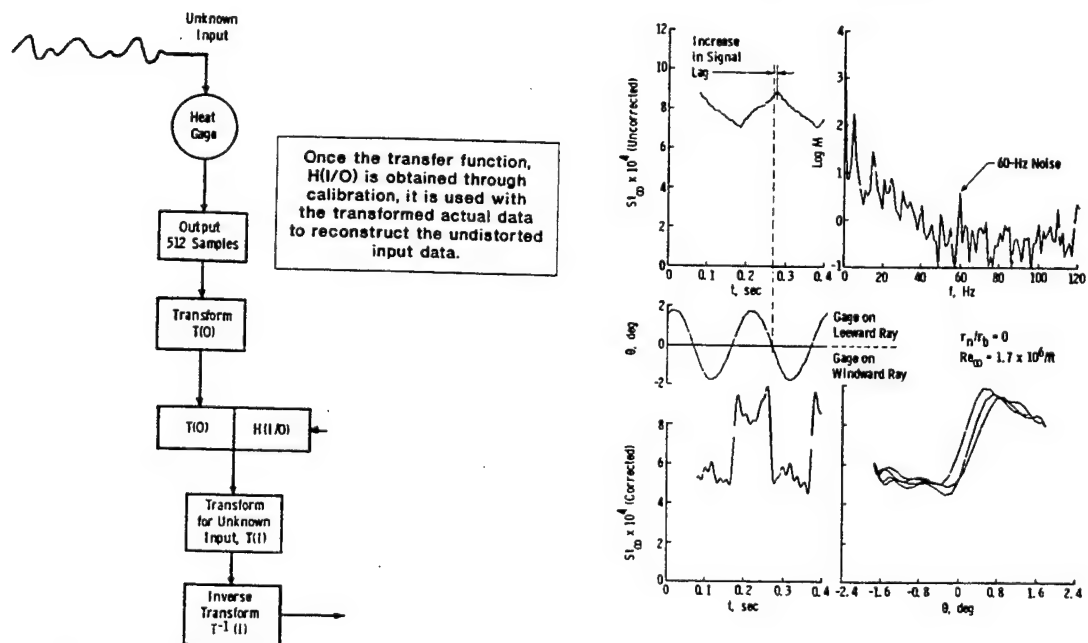


Figure 101 Reconstructed Test Data Using the Calibration-Developed Transfer Function, $H(I/O)$.

There are, of course, limitations to the technique. These were outlined by Favour, 1966. They are as follows:

1. The transformation only works with linear systems where the input and output are simply related by a linear relationship in the time domain.
2. The limits of integration of the transformation function with respect to time MUST contain the complete transient that the instrument is subjected to.
3. The limits of integration for the re-transformation process must contain the complete frequency spectrum of the transient
4. Since all time functions are defined by discrete samples, the sampling rate must satisfy the inequality $n > 2\omega$ to assure an accurate representation of the Fourier transform in the range of frequencies which define the complete frequency spectrum of the transient. In this inequality ω_m is the highest frequency component in radians per second of the time function.
5. Since each Fourier transform is defined at discrete frequencies over the range of interest in the transient, the resolution of the Fourier transform must satisfy the inequality

$$\Delta \omega < (\pi/T)$$

where T is the length of the transient in time. In other words, the minimum frequency of interest must be greater than the $\Delta \omega$ described by the inequality.

$$\omega_{\min} \geq \Delta \omega$$

6. In the calibration process, the input calibration transient selected must represent significantly all frequencies of interest in the test transient.

There are also requirements with respect to the character of the calibration pulse generator which must be considered. These are given in the reference by Favour, 1966.

SECTION VII

ADIABATIC WALL TEMPERATURES

Aerodynamic heating requires an understanding of the heating rates to the surface as well as the adiabatic level of temperature (T_R) available to the surface. Supersonically, both terms are important with the relative importance shifting from adiabatic wall temperature to heating rate as the Mach number increases. Hypersonically, although an accurate definition of the adiabatic wall temperature is significant, it has been difficult to measure in the past and is normally neglected in experimentation. Numerical approximations or an accepted convention are generally used in its place. These can be quite simple as in $T_R = rT_t$ or more elaborate as in $T_R = \frac{1 + r(\gamma - 1/2)}{1 + (\gamma - 1/2)M^2} T_t$ where the reader is left to ponder what constitutes the Mach number, M .

Classically, from the definition of an adiabatic surface, the adiabatic wall temperature can be experimentally found by holding a model in the tunnel until the rate of heat transfer to the surface goes to zero. The resultant surface temperatures are ideally the adiabatic wall temperatures (plural because a function of surface orientation among other factors). Early tests employed this technique both at supersonic and later hypersonic speeds. The major problem with this "classical" technique was that a special model was required which was perfectly insulated so that conduction effects were negligible. Additionally the surface temperature radiation to the tunnel walls becomes significant at hypersonic test conditions when the surface temperature approaches the adiabatic wall temperature, a factor that cannot be adequately accounted for in practical data reduction. Finally, inferred heating rates approaching zero at the adiabatic wall condition implies that the temperatures within the model material approach a constant value defined by a balance between the heating imposed by the flowfield on an insulating surface and that temperature gradients with time, dT/dt , within the model material at strategic points (those required to define a thermal model). Since most classical heat flux techniques rely on this gradient of temperature with time, the accuracy of the measurement becomes very poor as the adiabatic conditions are approached.

Supersonically, techniques exist to measure directly the adiabatic wall condition and these techniques appear accurate. These techniques will be discussed shortly. Hypersonically, several techniques have been attempted with varying degrees of success. Two hypersonic techniques attempted in the past at AEDC are:

1. Model exposure for an extended test period with heat gages wherein the surface temperature APPROACHES the adiabatic condition and the adiabatic temperature (at the gage) is defined by an extrapolation of the heating rate level as a function of the surface temperature as shown in Figure 2.
2. Successive test injections made at discrete model surface temperatures approaching the undetermined adiabatic wall condition. The testing is conventional in nature and the pre-injection model conditioning system is used to produce an isothermal model at the desired surface temperature.

The first technique is questionable in spite of being used. Success (in terms of accurate adiabatic temperatures) requires exceptional integration of the instrumentation into the model. Few thermal instruments can achieve the required level of thermal integration so that the adiabatic wall temperature will be in error. The instrumentation which was used in the experiments was not adequate. The second technique is reasonable and has been used to demonstrate detailed recovery temperature information. These are

extremely expensive data to generate because the model temperature must be stabilized and uniform at an elevated temperature outside of the tunnel. Instrument integration, while still a problem, is less demanding because testing begins from a uniform model temperature with heating data taken rapidly before non-isothermal wall effects are present.

The presence of non-isothermal model surface temperatures creates a severe problem in the conduct of these measurements and the interpretation of the data. A classic paper on the subject was written by Gates and Allen, 1974. Figure 102 from that paper indicates that the level of the recovery factor is directly proportional to the difference between the supply temperature, T_o , and the throat temperature of the facility for the specific case of a sidewall experiment. Further, Gates and Allen have demonstrated that non-isothermal wall effects at the leading edge of the model are both substantial and enduring even for substantial distances from the non-isothermal wall juncture. The paper is an excellent reference and should serve as a warning that these measurements of recovery factor are difficult to generate and prone to measurement errors.

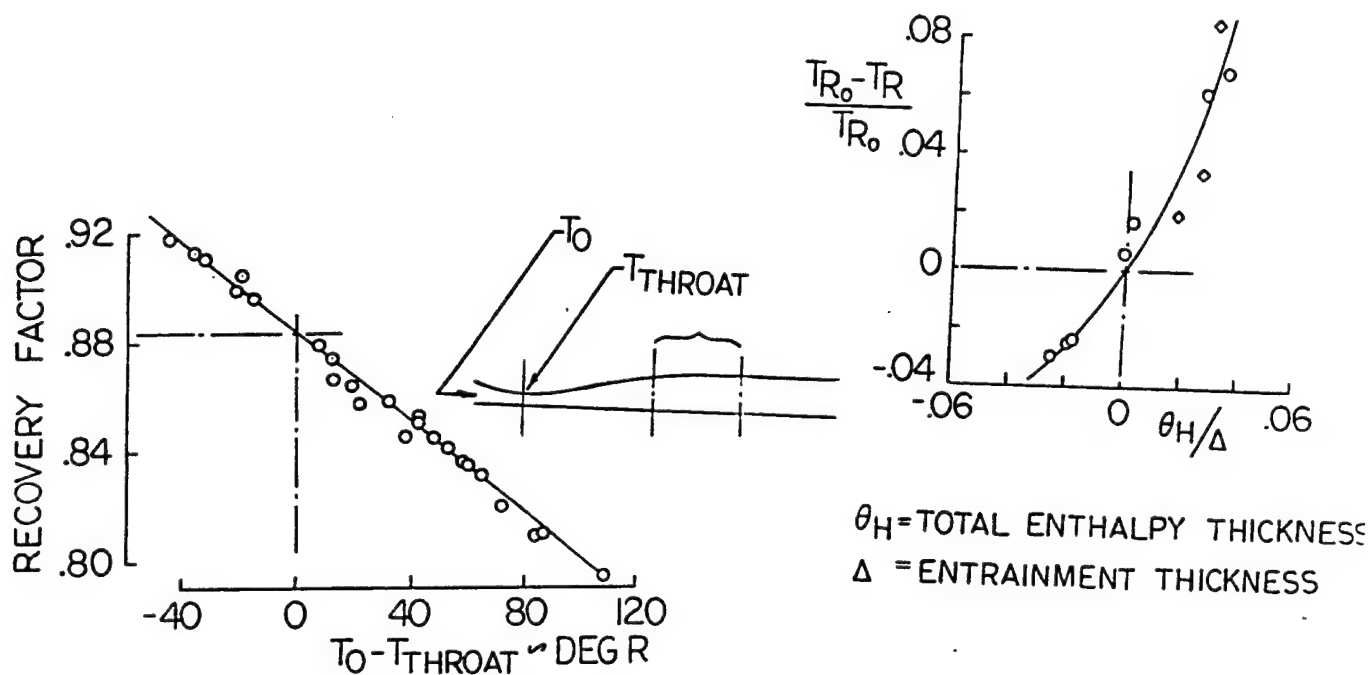


Figure 102 Results of the Paper of Gates and Allen, 1974, Demonstrating the Influence of Non-uniform Surface Temperature on the Level of Recovery Factor.

Recovery temperature experimental results were generated in the AEDC test facilities. Using a repeated injection technique (in which the wall is pre-heated to an elevated temperature before testing), heat transfer levels were measured at various ratios of the wall to total temperature. By fitting a straight line least squares curve through these data, the point of zero heat transfer could be inferred. This is, by definition, the adiabatic wall condition. The configuration chosen for this experiment was a complex, Three dimensional interaction process and the results are shown in Figure 103.

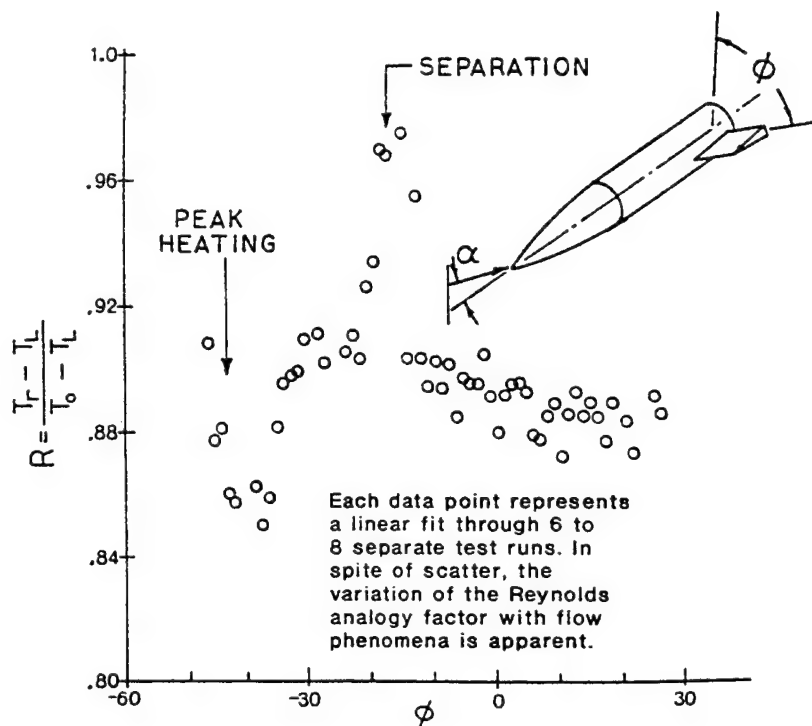


Figure 103 The Influence of Shock Interactions on the Distribution of the Recovery Factor.

measurement of recovery temperature easier. The work of Boscher et al, 1993, using IR scanning camera data has demonstrated an ability to measure recovery temperature distributions within a single data run through using repeated measurements of heating rates on an insulative surface. The quality of the resulting data is quite good and the results, once again, demonstrate the fact that recovery temperature is not constant but highly variable. Figure 104 shows the technique used to determine adiabatic wall temperature from IR measurements and Figure 105 shows the corresponding heat transfer coefficient and recovery temperature on a deflected flap in Mach 10 laminar flow at a given model station, $x=48\text{mm}$. Boscher has also evaluated the flows under small scale Gortler vortices.

From the results achieved, it appears that the adiabatic wall temperature agrees with classical results outside of the interaction but is sensitive to the details of the shock interaction process and, by inference, to many other local heating features that are present on any geometry probably including vortex interactions. To the extent that these details of the adiabatic wall flow are not known through such measurements or parallel numerical computations, there will always be uncertainties in the theory and data comparisons as well as the extrapolations of wind tunnel results to flight. It is possible that the Rockwell Space Shuttle fuselage scrubbing, observed in the wind tunnels, extrapolated poorly to flight application for this reason.

Very recently, new measurement techniques have made the

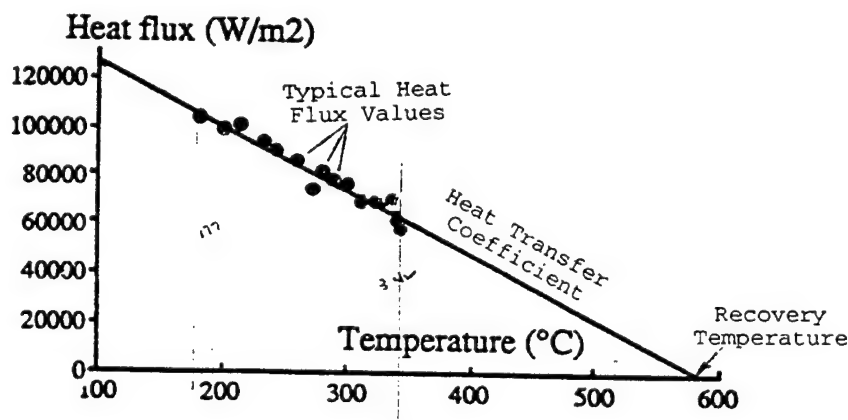


Figure 104 Evaluation of Recovery Temperature Using an Infrared Camera Technique from Boscher, 1992.

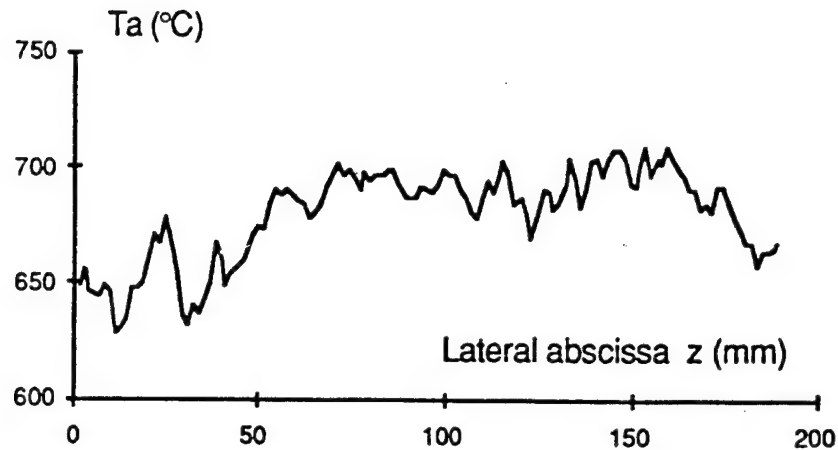


Figure 105 Lateral Distribution of Local Recovery Temperature in the Reattachment Zone at $x=48$ mm.

The technology with which recovery temperatures can be inferred is available today and has been demonstrated to be both accurate and spatially complete. Relatively large errors are possible in extrapolated wind tunnel data if classical assumptions are made regarding recovery temperature. Limited measurements to date indicate that these errors are largest in complex interacting flows where classical point measurements of heat flux are difficult to make.

It is also possible to generate adiabatic wall temperatures computationally by defining the wall boundary condition to be adiabatic (that is, that there is no heat transfer to the wall requiring that the derivative of the temperature with normal distance from the wall is zero). While computational heat flux data are very difficult to generate accurately in complex regions, it may be that in the future these "validated" computational procedures will be employed together with tests of heating rates to generate far more accurate representations of the non-dimensional heating parameters.

SECTION VIII INSTRUMENTATION IN SHOCK INTERACTION REGIONS

INTRODUCTION

Regions of shock interaction present a particularly complex problem in thermal instrumentation. These regions are characterized by high localized aerodynamic heating with large surface temperature gradients along the surface of the skin and away from the critical locations which develop with exposure time. Further, the location and extent of these critical peak heating locations are not precisely known (or vary with time) so that instrumentation is initially placed with some uncertainty. Finally, conventional model designs employ metallic surface materials which create conduction losses along the surface of the skin and away from the peak heating locations. Scale is also an important consideration. Small scale wind tunnel models with shock interactions may not, in any case, be instrumentable because the size of the interaction region is smaller than the dimensions of the measurement instrument and/or heating losses due to heat conduction away from the interaction may be more severe due to unfavorable model scaling issues.

It is common in configuration development to evaluate all phenomena using scaled model configurations. With shock interaction phenomena, this strategy is rarely acceptable: relative to the restrictive scale of the model, the interaction is insignificantly small. This results, all too often, in biased, low heating rates which are not representative of true peak values. As an example, the leading edge region of the Rockwell Space Shuttle was instrumented in a continuous flow facility to obtain shock interaction data. The instrumentation, thermocouples attached to a thin skin model, was improper to determine shock interactions on a model of this small scale in a continuous flow wind tunnel. The result was that the measured values were 1/3 the value of the heating rate impressed on the model by the test facility.

The Rockwell Space Shuttle, as well as several other development programs, have used survey test techniques (discussed in Chapter 3) to determine the location of such peak regions. Unfortunately, as has been discussed, these highly localized regions are never easy to clearly observe with such survey instrumentation. The result is that highly approximate locations of the interference peak are observed with the resultant level of the peak heating poorly defined.

Point measurements of interference heating peaks require either the use of a metallic based model system or the use of insulative models with either thin film gages or isothermal thermocouple staple gages. The metallic based model systems generate substantial conduction losses along the surface while the corresponding insulated material models can generate non-isothermal walls or break due to thermal shock caused by the severe thermal gradients in the small interaction region(s) (as in the case of Macor (R) models). Both the thin film and staple gages may span the entire shock interaction region (depending on its dimensions and the orientation of the gage in the flow along the gage sensing element). These effects require corrections for non-constant surface heating in the data reduction and analysis phase.

Conduction Across the Skin in an Interaction Region

Shock interactions create conduction across the surface of the model due to uneven surface heating that directly relates to uneven surface temperature. Conduction along the surface biases the data.

Dorignac and Vullierme, 1991, discussed the problems of surface conduction caused by shock interactions for the two cases of a semi-infinite slab (the model discussed in Section III of this report) and a thin-wall calorimeter (the model discussed in Section IV of this report). It was noted that the thin skin measurement technique was very sensitive to these lateral transfers of heat regardless of the test interval chosen. Figure 106 from their report shows the generalized correlation for this case. The semi-infinite slab technique was less sensitive to transverse fluxes. Figure 107 shows that correlation in similar terms.

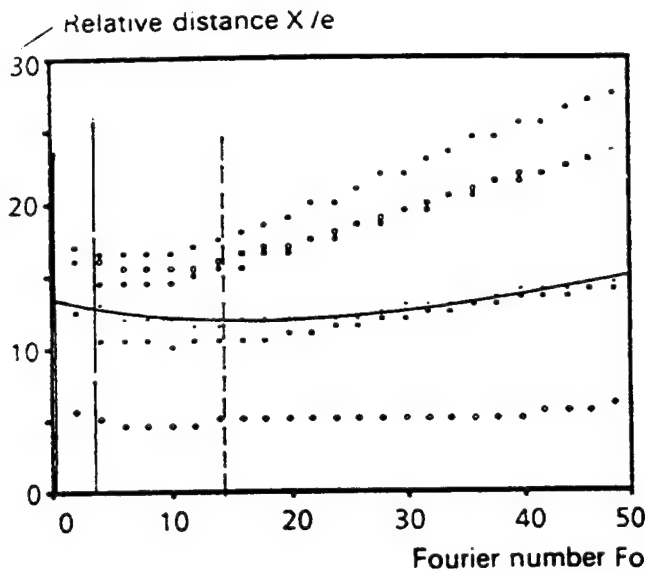


Figure 106 Non-dimensional Heating of a Thin Skin Surface after Dorignac et al, 1991.

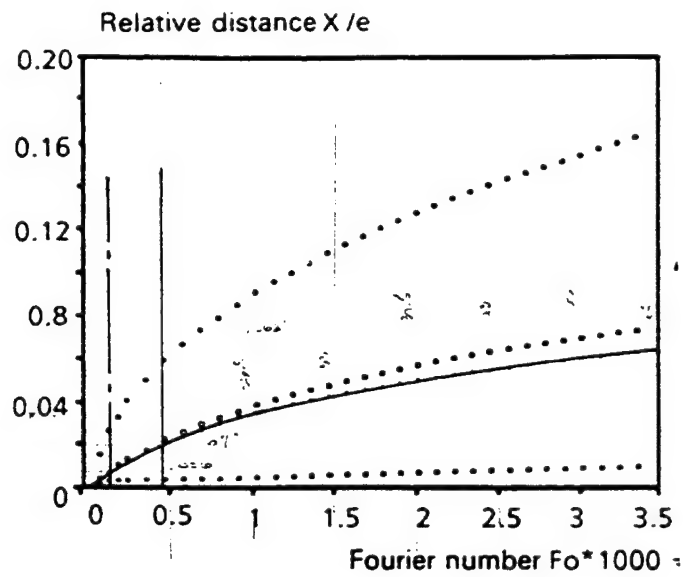


Figure 107 Non-dimensional Heating of a Semi-Infinite Slab Surface after Dorignac.

In both figures the non-dimensional distance, X/e , for which good accuracy is achieved is plotted as a function of the Fourier number, Fo , for various values of the Biot number, Bi . The Fourier number is defined as

$Fo = \frac{\alpha t}{e^2}$. This relationship has been previously used in this report to define the time required for heat

penetration into a material. It relates the thermal diffusivity of the material to the thickness of that material and the test duration. For example, cases of both insulators and conductors will be considered at shock tunnel, fast blowdown and continuous tunnel test durations.

The reduced Biot number, $B_i^* = \frac{B_1 - B_2}{B_1} = \frac{h_1 - h_2}{(\frac{h_1 + h_2}{2})}$ defines the relationship between the two levels of

heat transfer coefficient, h_2 and h_1 . In the example the reduced Biot number of 1.33 will be considered. That corresponds to $Bi_1 = 6 \times 10^{-3}$ and $Bi_2 = 31.1 \times 10^{-3}$. For stainless steel, the thermal diffusivity, α , is $4.5 \times 10^{-5} \text{ ft}^2/\text{sec}$. while for pyrex glass it is $6.8 \times 10^{-6} \text{ ft}^2/\text{sec}$.

TABLE 8.1
FOURIER NUMBER FOR SEMI-INFINITE SLAB ANALYSIS, $e = 0.375$ ins

	Stainless Steel	Pyrex
Shock Tunnel (10 ms)	0.46×10^{-3}	0.073×10^{-3}
Fast Blowdown (500ms)	23×10^{-3}	4×10^{-3}
Continuous (2 seconds)	92×10^{-3}	15×10^{-3}

TABLE 8.2
FOURIER NUMBER FOR THIN SKIN ANALYSIS, $e = 0.030$ ins

	Stainless Steel
Shock Tunnel (10ms)	72×10^{-3}
Fast Blowdown (500 ms)	3.6
Continuous (2 seconds)	14.4

For the example case, conduction-free data is achieved for the thin skin technique at distances greater than 0.375 ins for all test times. For the corresponding semi-infinite slab technique, conduction-free data is achieved at distances greater than 26 mils for pyrex and 70 mils for stainless steel operating at shock tunnel conditions and for distances greater than xxx for stainless steel at fast blowdown test conditions.

The fast blowdown test conditions were generated by Collier in the NSWC Tunnel 9 for the model shown in Figure 10 of Section I. Collier's data showed substantial conduction losses within 0.2 ins of the protuberance. The Fourier number for his experiment was 185×10^{-3} .

The features of concern are: (1) the use of thin skin techniques for protuberance measurements in any test medium, (2) the use of coax gages for steady state protuberance measurements at test times greater than those in a shock tunnel and (3) the need to test the 1D conduction-free assumption for models at all test conditions to tailor the size of the experiment and evaluate the quality of the data reduction assumptions.

Defining the Location of the Peak in the Shock Interaction Region

Properly instrumenting shock interaction regions requires some understanding of where the peaks exist, their distributions and expected values. Most of the errors observed within shock interaction regions were caused by poorly placed or badly scaled instrumentation. These problems do not cause additional scatter in the data, they seriously bias the data.

Table 3-x defined the relative sizes of these thermal instruments. This section of the report will discuss the scale and location of classical shock interaction regions. The comparison of the two; instrument scale against interaction scale, will determine whether shock interactions can be properly measured. Not all such interactions are measurable.

The Heating Peak Ahead of a Cylindrical Obstruction:

High levels of heat flux are present immediately ahead of a cylindrical obstruction. Neumann and Hayes, 1981, generated substantial data on this problem and noted, in some detail, the failings of previous experiments. Figure 21 from Gillerlain was a clear demonstration of how good the data can look and still be incomplete. For such interactions, the peak heating is located quite close to the causing obstruction. As a rule of thumb, peak heating occurs at or near 12% of the cylinder diameter. By observation it is clear that valid measurements of the peak heating will require cylinder diameters from 0.5 to 2.5 inches. These physical sizes are not found on scaled models of larger test configurations but require no-scale phenomena models to fully evaluate. Measurements made with smaller scale models will miss the peak heating and optimistically define unreasonable lower heating levels.

The Heating Peak Within a Two-Dimensional Interaction:

Two dimensional shock interaction regions produce heating rate distributions quite different from the classical model presented to students. Not only does the initiating shock interaction create a region of high surface pressures and heating rates on the receiving surface but also that region is seriously modified by the influence of the boundary layer on the receiver plate ahead of the interaction and by stray shock systems unrelated to the shock interaction phenomena; an artifact of the experiment.

Figure 108 shows earlier pressure data generated by Kussoy, 1975, on a centerbody as a result of shock interactions caused by a coaxial ring generator. Pressure rise data is shown for the cases of a 15 degree wedge angle on the shock generating surface. The data appears reasonable but observing the apparent levels of the peak, it is clear that while the generator angle doubled, the pressures were essentially the same. Comparing those measurements against simple, inviscid, oblique shock theory it is clear that while the data on the surface generated by the 7.5 degree ring was correctly predicted, similar data caused by the 15 degree ring was not. The expansion fan produced by the 15 degree ring generating surface interacted with the incident shock "sweeping away" the shock interaction. The apparent peak observed was not, in fact, related to peak heating at all but the location at which two competing processes meet; those processes are the pressure increase caused by the incident, wedge induced, shock and the pressure decrease caused by the expansion fan. This situation is not unlike that in the boundary layer, see Figure 1, where the static temperature rise and the influence of surface heat transfer interact.

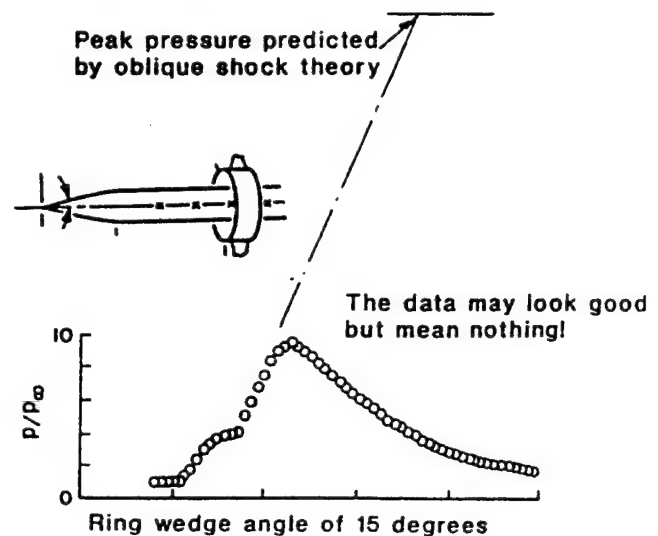


Figure 108 Pressure Rise Caused by an Experimental Interaction after Kussoy et al, 1975.

This can also be seen in latter heat transfer data from Kussoy, 1991. Figure 109 shows a heat transfer rise caused by a 5 degree wedge leading to a classically defined plateau. Figure 110 on the other hand

demonstrates a peaked distribution for an 11 degree wedge. The peak is an artifact of incidental test features caused by the competing processes of shock generation and expansion fan interaction. Changing the scale of the experiment and the span of the generating surface would effectively mitigate this interaction.

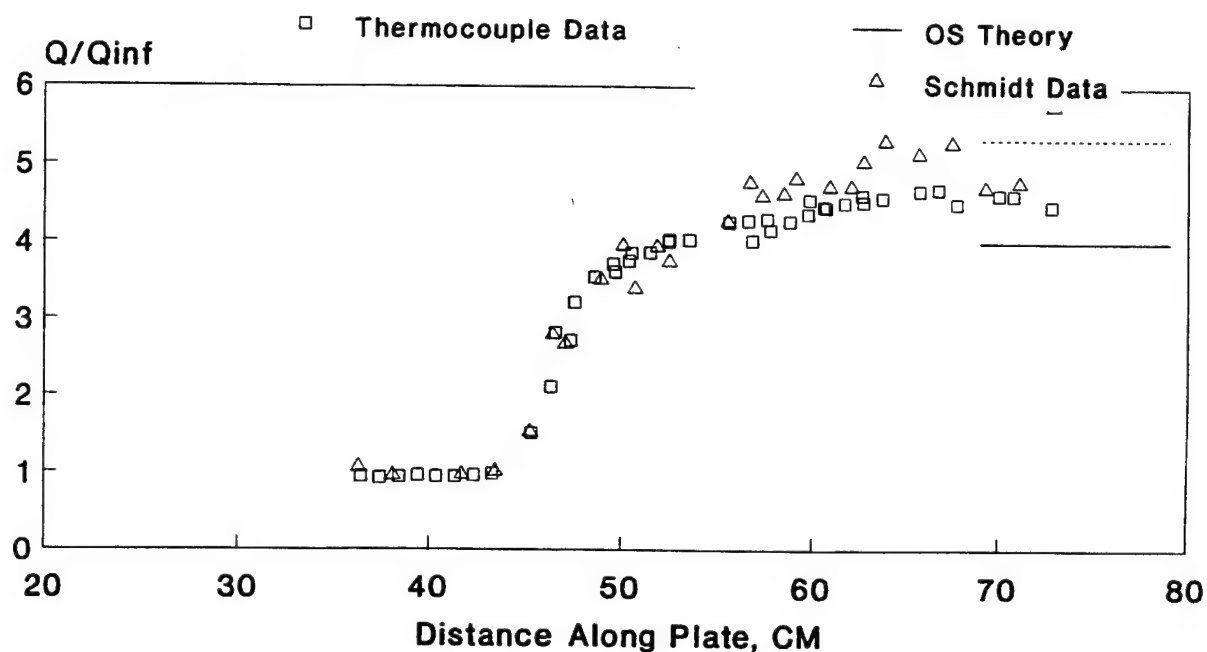


Figure 109 Heat Transfer Rise Caused by a 5 Degree Wedge Leading to a Classically Defined Plateau.

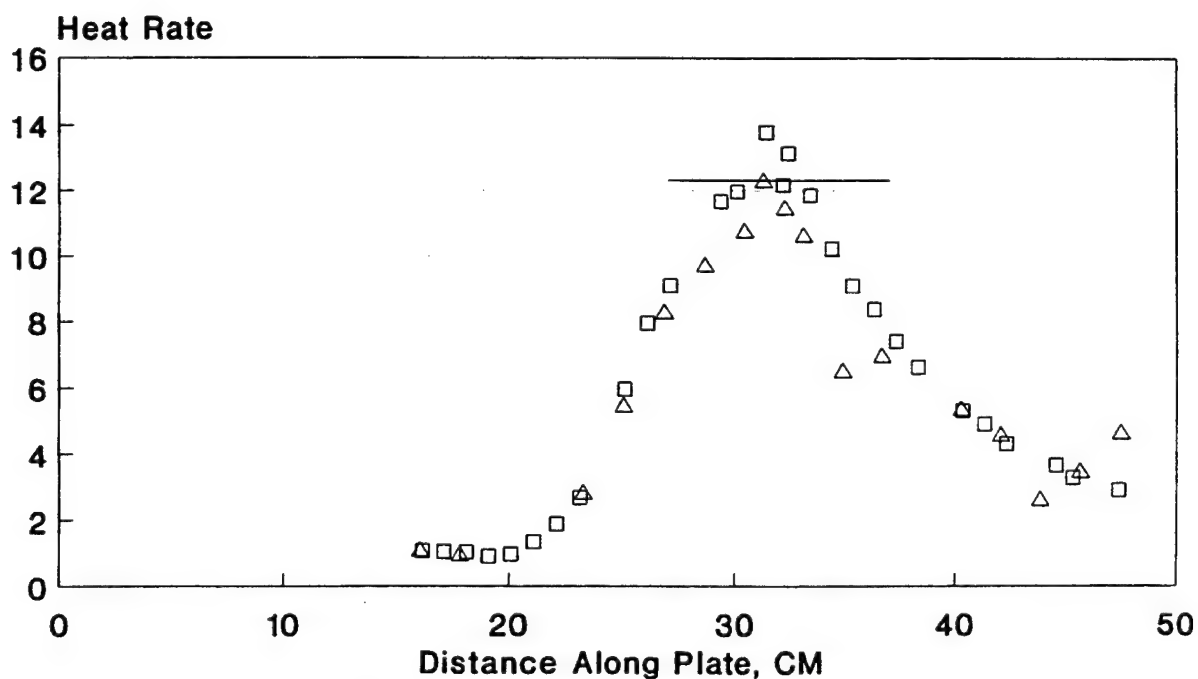


Figure 110 Demonstrating a Peaked Distribution for an 11 Degree Wedge.

The Heating Peak Caused By A Three Dimensional Fin Induced Interaction:

The location of the heating peak caused by a 3D fin interaction was defined by Token, 1974. That angular location can be defined in terms of the fin angle and Mach number as shown in Figure 111. From this figure, depending on the assumptions made regarding gage dimensions and spacing, a minimum fin length to define the peak heating can be determined. Fins from 5 to 10 inches long are required to capture the peak levels through measurements.

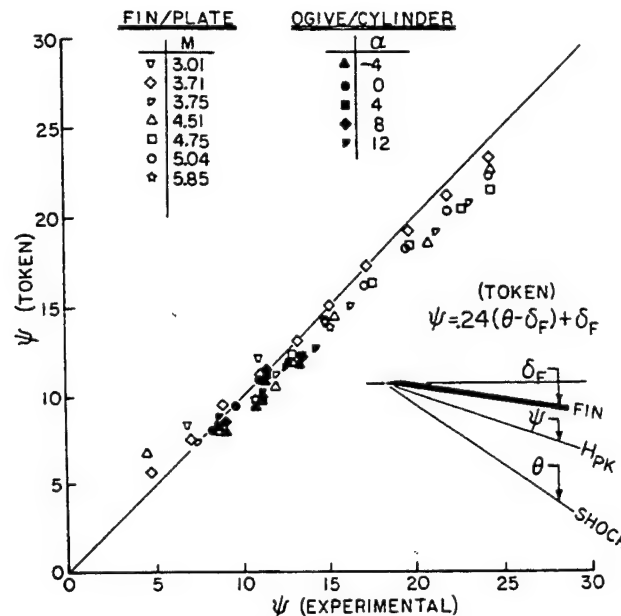


Figure 111 Angular Location Defined in Terms of the Fin Angle and Mach Number.

The Coax Gage in Interactions

(A) The Coax Gage With Uniform Heating

The thermal model was used to evaluate the response of a coax gage installed in a block of 17-4 PH stainless steel which was subjected to uniform external heating. The gage and the surrounding stainless steel were the same thickness such that the thermal differences between the two materials was minimized. Figure 112 indicates the response of the gage for (a) the gage in intimate thermal contact with the surrounding material but used in the classical mode wherein only the heated surface is measured and the backface is assumed to be isothermal; (b) the gage in intimate thermal contact with the surrounding material but with both the heated and backface temperature measured or inferred through computations and (c) the gage insulated from the surrounding stainless steel with a Teflon (R) insulating ring.

The classic operation of the coax gage assumes that the backface is isothermal such that when the thermal pulse from the test reaches the backface of the gage, the basis of the gage thermal management is changed. This is seen in the response of the gage as shown in the figure. Good data is generated for a period of a few seconds and then the gage drifts off and is not useful. This shortcoming of the coax gage can be overcome by either measuring the backface temperature or computing that temperature through the thermal

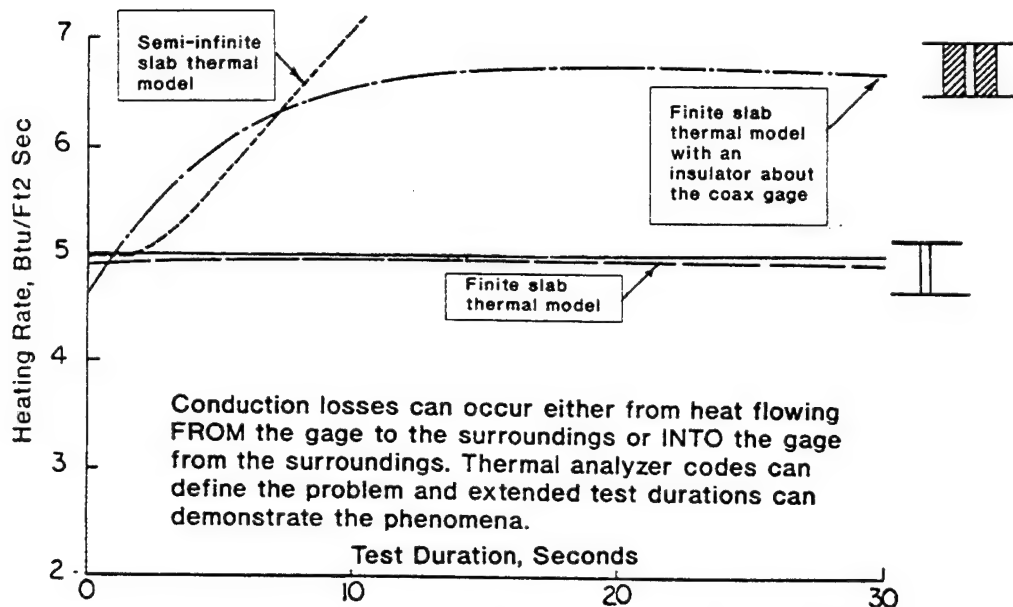


Figure 112 Responses of a Coax Gage in a Uniform Heating Environment.

model employed. With these improvements to the thermal model, the gage is useful for extended periods of test time. Here, the output to 30 seconds is shown. Installing the Teflon (R) cylinder about the gage was, in theory, to be used to enforce the one dimensionality of the gage. We were surprised at the response of the gage in this configuration. The increase in heating observed in this figure is due to the fact that the insulation material, for the same constant heating rate, creates a differential temperature history with respect to the coax gage and feeds heat into the sides of the gage. The result, as shown in the figure, invalidates the gage and is a dramatic example of how difficult measurements are in even a uniform heating environment.

(B) The Coax Gage With Non-Uniform Heating

Figure 113 indicates a further complication to the simple case of a uniform heating pulse. In this figure a heating pulse of magnitude equal to the uniform case was imposed over only a 1/4 inch interval. Five lines are shown on this figure representing the spectrum of responses caused by the coax gage being progressively wrapped in an insulation material made of Teflon (R). In this non-uniform heating case, the gage installed directly into the 17-4 PH stainless steel creates a non uniform response even though both the heated surface and backface surface is measured. The reason for this is that the thermal gradient produced across the heated plate draws heat from the gage. At the other extreme, the Teflon (R) insulated gage, as before, has the reverse effect but, with the non uniform heating across the plate, the Teflon (R) is thermally drained both into the coax gage and into the cold surrounding 17-4 PH stainless steel "model". The lines between these two extremes represent different configurations of the Teflon (R) insulator. The line closest to the actual 5 btu/ft² sec input is an optimized (and perhaps idealized) design.

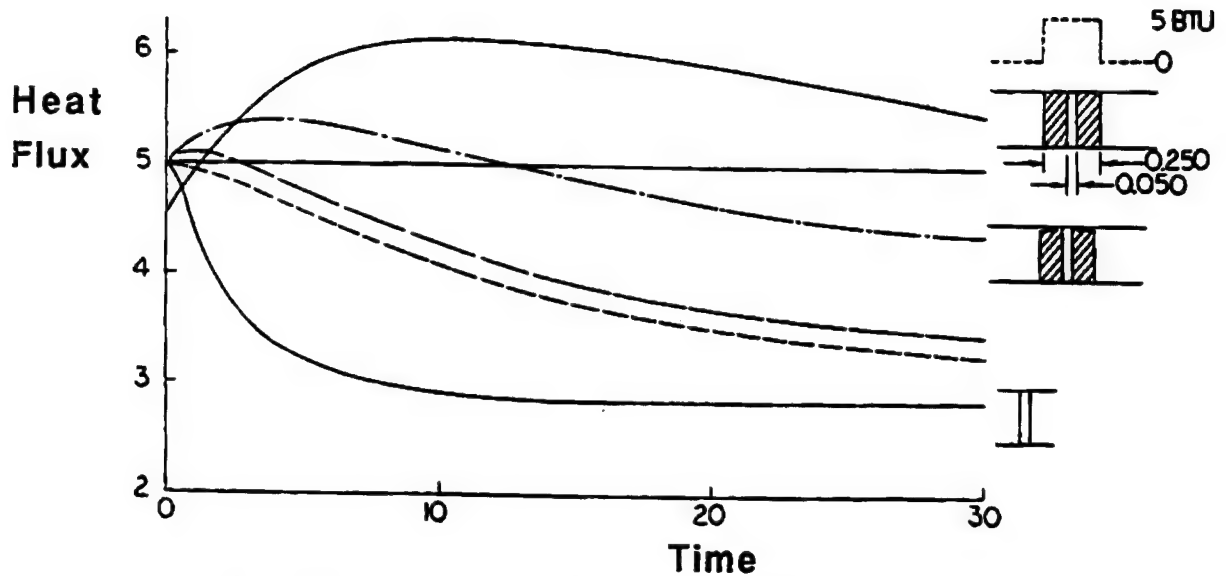


Figure 113 Responses of a Coax Gage to Non-Uniform Heating.

There are several consequences of the data presented in this figure. First, note that the trends presented in this figure are somewhat idealized although illustrative of the problem. The design of an experiment will require more detailed analyses using the thermal MODEL as well as validation of such a model. Secondly, the consequences of this figure which are apparent are the following:

1. It is necessary to use not only intuition but also numerical modeling techniques to correctly integrate instrumentation into a model for difficult situations such as shock interaction. The competing consequences of complex heat flows cannot be adequately deduced by ad-hoc rules of thumb. A corollary is that the details of this or any other installation will change with regard to the heating imposed and the incidental features of the model in which the gage is placed.

2. The figure demonstrates characteristic curves which are related to specific phenomena. These characteristic curves can be used to understand the results of the experiment with regard to the instrumentation and the corrections that must be applied after the experiment to correct the data of the incidental features of the model. Certainly it is best to design the experiment correctly but, in spite of best efforts, these features may still be present and require numerical correction.

3. The characteristic shape of the curve can, itself, be used to understand more about the experiment and extract more data from the experiment. This is technically termed "Parameter Estimation" and it is possible that an experiment, properly strategized, could generate not only the required data but secondary information on the quality of the instrumentation as well.

The fact is that this type of "thick wall" static instrumentation is not all that useful in the evaluation of interference heat pulses.

It is interesting to point out that this study was initiated because conflicting "expert opinion" existed on how to seat coax gages into a model. What we believed to be a simple afternoon exercise turned into a very interesting study of the interaction between such gages and their surroundings. It's all in knowing what questions to ask!

Coax data and the underlying semi-infinite slab thermal model are sensitive to transverse thermal gradients on the surface of the material. Recent analytic studies by Dorignac and Vullierme, 1991, demonstrate the problems in general terms but also demonstrate that more error-free measurements may be made at very short test times (which are consistent with the time constants of the coax gages). Practical measurements were reported by Collier et al, 1990, where, in addition to the IR measurements, coax data was taken ahead of a cylindrical protuberance attached in the nose-influence region of a blunt cone. Collier observed that "...the results from the two-dimensional analysis (of the coax data) differ as much as 25% from the one-dimensional (classic data reduction) results. This large difference occurs within a distance of 1/4 diameter from the protuberance leading edge. Outside of this distance, the temperature gradients along the surface apparently are not large enough to merit a two-dimensional analysis". What he observed within 1/4 protuberance diameter was a highly-spiked peak heating caused by the interaction. The gradients set up in the stainless steel material of the model caused the 25% difference in heating that was correctly interpreted by the more complex 2D analysis but totally missed by the simplicity of the 1D semi-infinite slab analysis. Using the simplified analysis equation presented in Section III of this report, the temperature rise within the interaction region could be predicted to the level of our knowledge concerning such heating patterns. Using that information, estimates of conduction losses could be made before tests are completed. Figure 114 from the data of Collier indicates that through perfect knowledge of surface heating, reasonable estimates of surface temperature can be achieved. The problems are that engineering estimates, themselves correlations, are less than perfect and these estimates tend to stress the levels of peak heating rather than the distribution of surface heating within interactions.

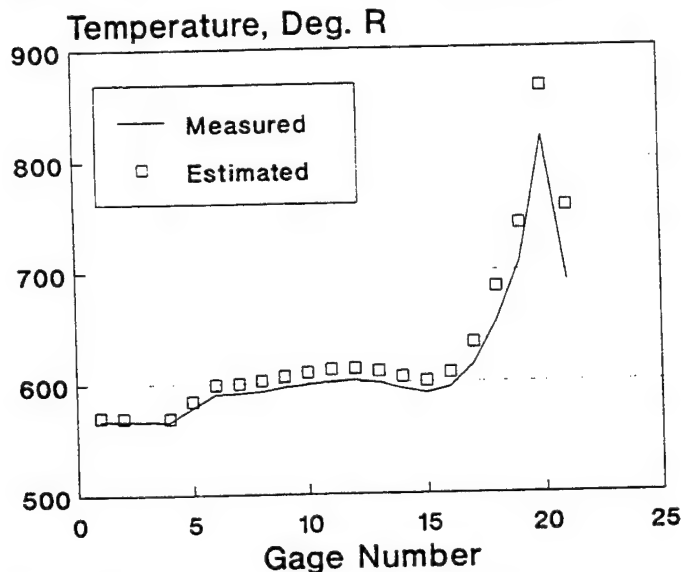


Figure 114 Measured and Estimated Heat Flux Through the Interaction for Data of Collier, 1990.

Coax Gages In a Shock Interaction Environment - Is There Any Hope?

Shock interaction phenomena are elusive. Many researchers do a poor job of even measuring such phenomena and the literature abounds with errors proven by data with regard to shock interactions. In fact, many times we simply do not know where the interaction is and much of our instrumentation is placed in the model in hopes that we will "somehow" capture the shock interaction process. Many times insufficient instrumentation is provided and so the true interference effects are never known. This is potentially dangerous because the results generated by insufficient cheap instrumentation are biased to give reassuringly low results. A stellar example of this was the mated configuration of the Rockwell Space Shuttle and the external tank booster. Instrumentation assignments in the mated configuration demonstrated not only inadequate instrumentation but also a lack of understanding of the underlying interference processes causing high heating.

Another example of this process was the shock interference tests run on the MX missile and reported by Carrol, 1982. These data, shown in Figure 115, indicate a very localized heating pattern "somewhat" ahead of the cylindrical protuberance with a level "somewhere in excess of" 2.3 times the undisturbed heating. These results were generated through the use of temperature sensitive paint.

The answer to this dilemma is either (1) the use of more instrumentation, (2) the ACCURATE use of survey techniques to observe and capture accurately the level of heating in these regions or (3) the use of new test techniques that will assure that the peak heating rates are seen by the limited gages. The first two techniques are available, brute force techniques that are labor and thus cost intensive. They get the job done but in the present

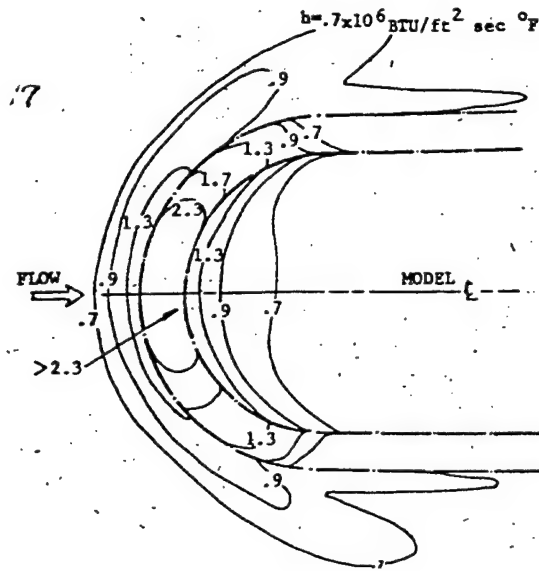


Figure 115 Measurements of Interference Heating with Poorly Selected Temperature Paint.

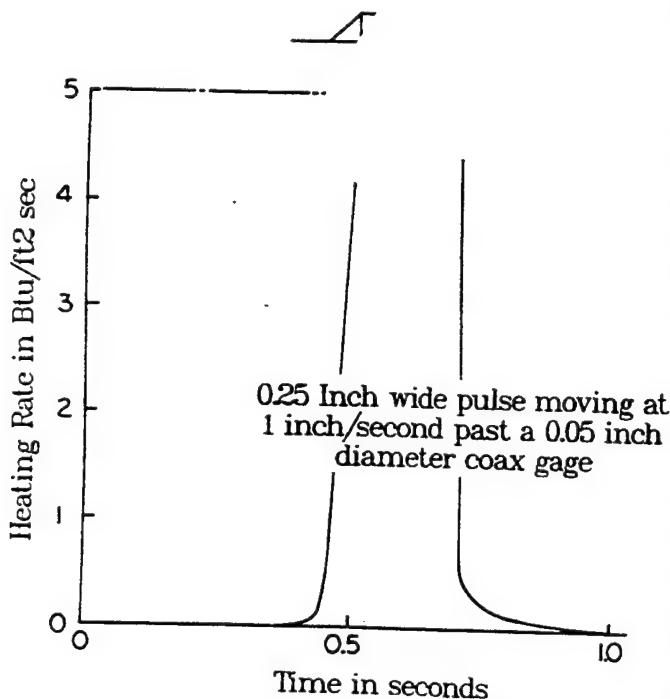


Figure 116 The Accuracy of Coax Gages Used In a Dynamic Sweep Mode for Shock Interaction Heating Studies.

and future environments of economically sound engineering, they are not competitive. The third technique allows cost effective testing of models using thick skinned gages, such as coax gages, by sweeping the model such that the interference patterns move across the available gages. This technique has been used to advantage several times in various demonstration programs. Each time it is used, orders of magnitude more data are generated during a given period of time than with competing state of the art techniques.

The installed coax gage was studied with the thermal analysis program for the case in which the localized heating rate was swept across the gage. Figure 116 shows the results of that study. It can be seen in the figure that sweeping the model such that the interference moves across the model allows the experimenter to generate accurate data for the gage since the dwell time is short and the response time of the coax gage is even shorter.

SECTION IX THE EFFECT OF TEST VARIABLES ON SHOCK TUNNEL SURFACE TEMPERATURES

The myth is that shock tunnels operate for such a short period of time that the temperature of the surface doesn't change and pre-test measurements of the model temperature may be used as surface temperatures during the test. That myth was correct in the early days of shock tunnel testing when the heating rates were low. It can no longer be taken for granted.

Surface heating rates are a function of the state of the boundary layer, the supply pressure and temperature of the facility as well as the duration of those effects and the presence of multiplying effects from shock interactions. Shock tube/tunnel technology has pushed each of these functions to satisfy user test requirements. As a result, current test capabilities create heating rates up to several thousands of Btu/Ft² Sec where surface temperatures do change appreciably, even in the test period of several milliseconds.

The operational supply pressures of shock tunnel-class facilities can easily reach 60,000 psia today. The Calspan 96 inch tunnel achieved 20,000 psia years ago and was upgraded to 30,000 psia. The Calspan LENS facility is designed to generate 40,000 psia and the VKI Longshot test facility, a piston driven shock tube/tunnel) has generated 60,000 psia.

The operational supply temperatures of these facilities can duplicate and exceed those of orbital velocities although not at the pressures just quoted. Shock Mach numbers, a measure of the tunnel total temperature, in excess of 10 are possible today.

The operational size of these test facilities has also increased dramatically. From a tunnel performance point of view, the diameter of the driven tube of the shock tube that powers the shock tunnel is the important dimension. Test duration is controlled both by the shock Mach number produced and by the diameter of the driven tube. Large driven tube facilities are designed both to generate a few milliseconds at extremes of the shock Mach number and to extend the test duration of the facility for other measurements; perhaps dynamic measurements. In recent years the Calspan test facilities have gone from a 4 inch driven tube to a 6 inch driven tube to an 8 inch driven tube for the LENS facility. The Ames shock tunnel facility has a 12 inch driven tube. At a given shock Mach number, increased diameter reflects in increased test duration. Test durations of up to 40ms are now possible for certain conditions. Figure 117 shows estimated test durations for two Calspan tunnels as well as the measured test durations for the Ames 16" shock tunnel.

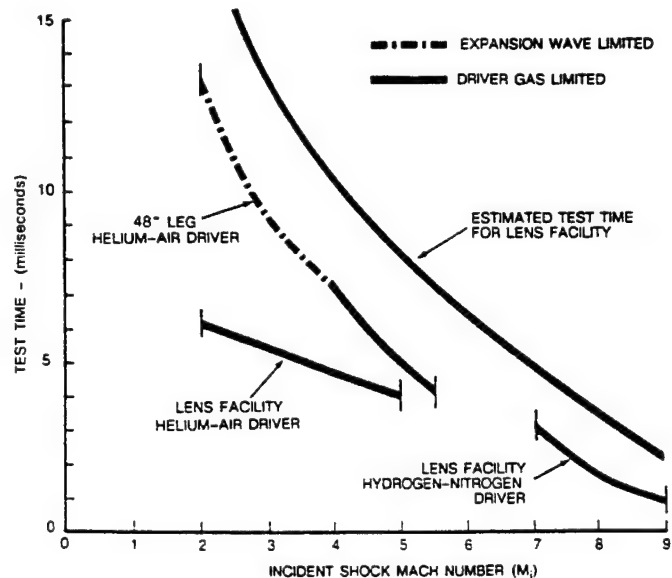


Figure 117. Test Duration of Calspan Shock Tunnels as a Function of Shock Mach Number, M₁, for Various Driven Tube Diameters.

The rise in surface temperature, as previously discussed in section III, is a function of the imposed heating rate, the thermal product, β , and the test acquisition time. Figures 118 and 119 present estimates of the temperature rise for pyrex and stainless steel respectively. Figure 120 combines the two and looks at the non-isothermality of the wall; the difference between the pyrex and steel temperatures.

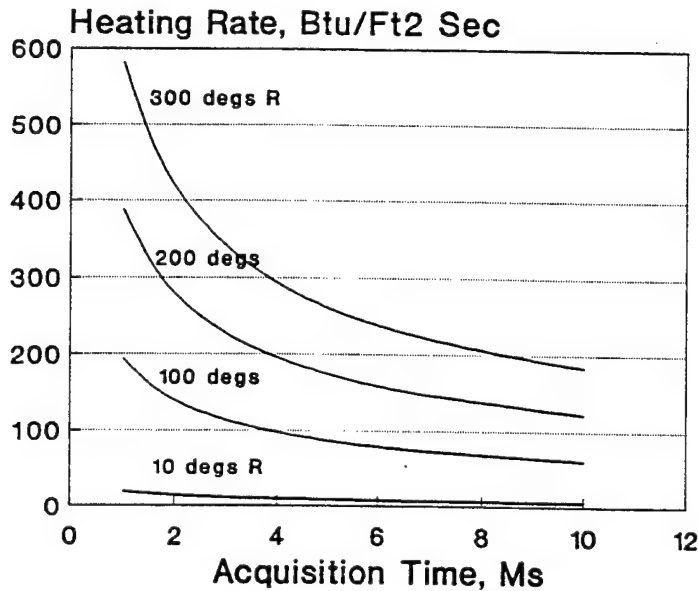


Figure 118 Temperature Rise for Pyrex Material Subjected to Various Levels of Heating for Various Test Durations.

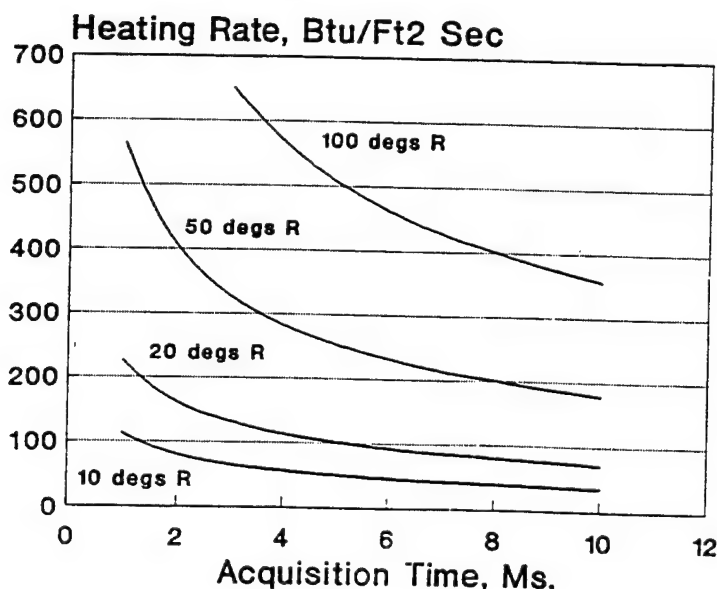


Figure 119 Temperature Rise for Stainless Steel Material Subjected to Various Heating Rates and Test Durations.

It is easy to have a temperature difference of 300 degrees or greater in these facilities. As an example, Holden conducted limited experiments on a very large cone/flare configuration at the Calspan shock tunnel. Figure 121a and b shows both the test configuration and the measured temperature data for run 6 from that study. The pertinent test conditions for that run were:

P0, 17,600 psia
T0,,3104 degs R
Ms, 3.6
Minf, 13.1
Rn/ft, 5x10+06/ft
Tw, 530 degs R

While the surface heating rate was tabulated, the only data on the wall

temperature was the pre-test measurement of 530 degrees R. Figure 122 demonstrate that incremental gage temperatures of 300 degrees were possible within 2 ms of the test start. Since this temperature scales as the root of the test acquisition time, wall temperature increases from 200 to 700 degrees could have been achieved on this model during test. In a later experiment Holden et al, 1991, evaluated the heating on a cylinder being impinged by a planar shock system. In this data set both the surface temperature as well as the surface heating rate were documented. Figure 123 shows the measured surface temperatures about the interaction as well as the corresponding temperature rise for the (assumed) stainless steel model at times less than 3 ms from the start of test. These test conditions were:

Total Pressure..... 4211 psia
 Total Temperature.. 3042 deg R
 Shock Mach Number.. 3.621
 Mach Number 8.14
 Reynolds Number ... $3.788 \times 10^{+06}/ft$
 Test Duration f(Mi)
 Test Section Diameter...24 or 48 inch

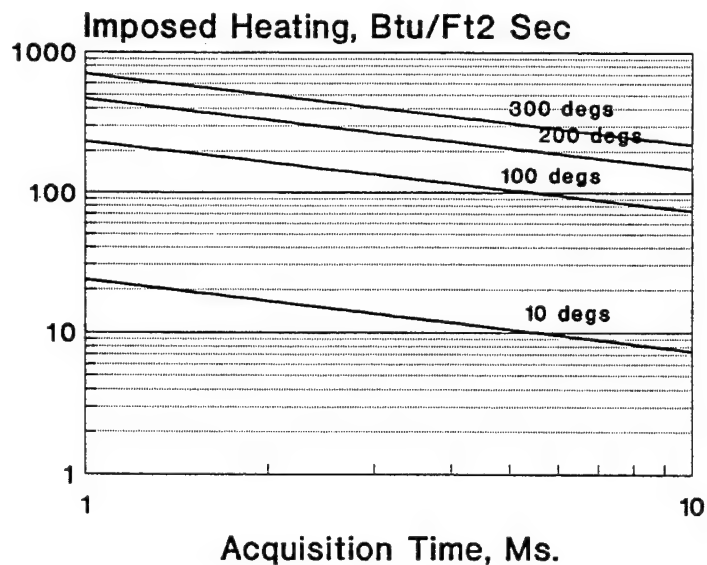


Figure 120 Temperature Difference Between Pyrex and Stainless Steel for Various Heating Rates and Imposed Test Durations.

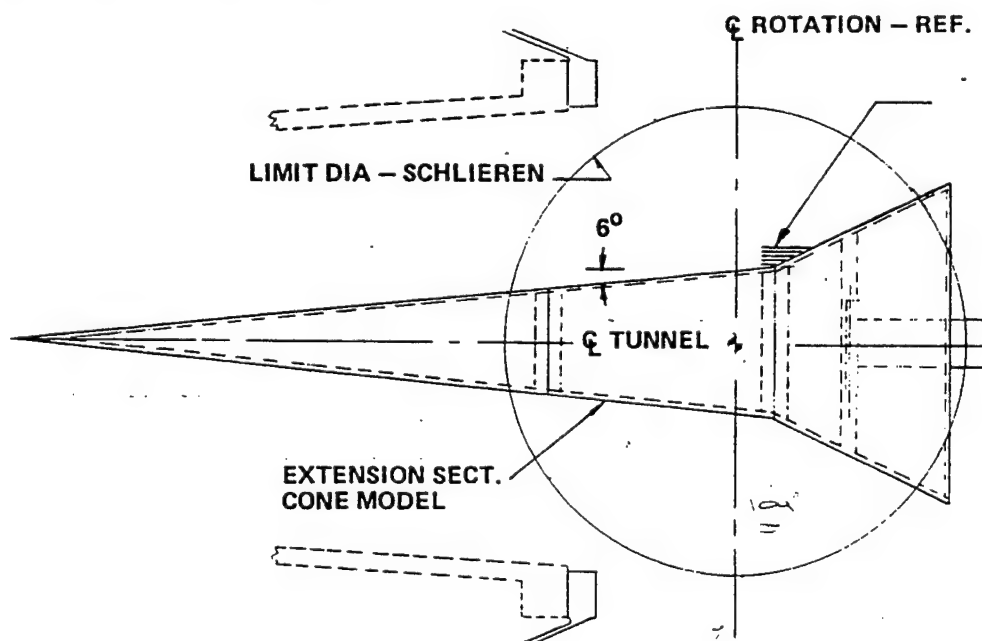


Figure 121a The Large CALSPAN Sharp Cone Model Located Within The CALSPAN Shock Tunnel after Holden, 1984.

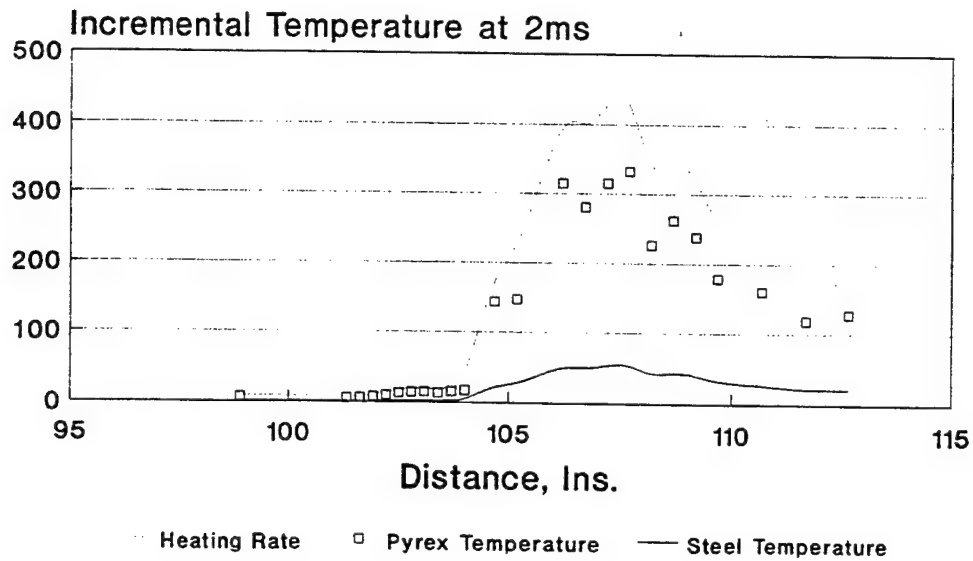
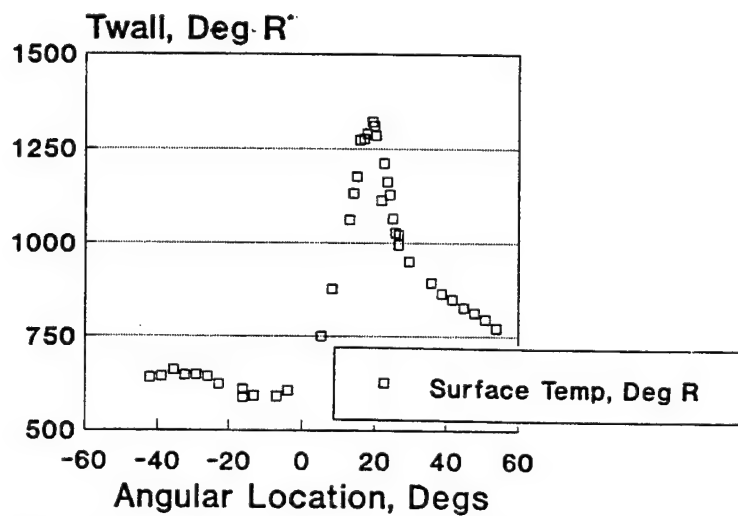


Figure 121b The Incremental Temperatures of Pyrex and Steel Materials for Test 6 of a Cone/Flare Heat Transfer Experiment after Holden 1984.



1. Assumes data taken at the same time
2. Cylinder diameter is 3.0 ins
3. Data from NASA CR 181893

Figure 122 Surface Temperatures Measured About a Cylinder Sustaining a Severe Shock Interaction in a Shock Tunnel Flow.

Interaction in a Shock Tunnel Flow.

There are several issues suggested by this example. (1) insufficient data is presented. Each gage MEASURES surface temperature and that measurement, together with the corresponding heating rate, should be presented. (2) For the case where wall temperature varies appreciably, the entire data stream of heating rates and temperatures vs acquisition time should be presented. The slope of the measured heating rate vs wall temperature should be used to extrapolate a heating rate at the initial wall temperature, 530 degrees, which was cited. (3) the effects of these nonuniform walls on boundary layer distortion need to be considered using numerical analysis techniques discussed in Section II; notably through the use of a code such as BLIMP. Analyses with the actual non-uniform surface boundary condition is beyond the scope of the available CFD codes. (4) Different gages should be selected that would have more uniform wall conditions. Two directions present themselves as off-the-shelf solutions: (a) the use of coax gages placed in stainless steel model material (a solution being adopted at Ames for their shock tunnel) or (b) the use of thin film gages placed in a solid Macor (R) model (a solution used at Langley research Center by Charles Miller). (5) Be aware of the problems and appropriateness of instrumentation solutions.

Tunnel 9 at NSWC has just developed a high Reynolds number, Mach 8 flow with the following test conditions:

Total Pressure 12,400 psia
Total Temperature .. 1500 deg R
Mach Number 8
Reynolds Number $52 \times 10^6/\text{ft}$
Test Duration 250 ms
Test Section Diameter ... 33 inches

This facility in relation to the Calspan shock tunnel will be discussed later in this section.

Example Case:

Recall that the Mach 8 test point in both the NSWC and Calspan test facilities was discussed. The question is ... which facility is the more stringent from the point of view of model temperatures? note the significant differences between the two:

Total Pressure: 12800 vs 4200 psia
Total Temperature: 1500 vs 3042 deg R
Test Duration: 250 vs 20 ms.

Since the stagnation point heating rate is defined by the functional equation: $\dot{q} = K \sqrt{P_t} H_o \sqrt{R_b}$, and since, for a constant Mach number, $P_{t_2} = K P_o$, It can be shown that the NSWC facility measures a lower heating rate to the stagnation point of a model if equal sized models are used and, depending on the nozzle selected in the Calspan facility, the heating rate ratio could be nearly equal (for the larger Calspan nozzle) or smaller for the smaller Calspan nozzle. Apart from heating rate levels, the temperature rise at the surface of the model is a function of instrumentation type, test duration and heating rate levels. Comparing the two facilities for temperature rise (realizing that thin film instrumentation will be used in the shock tunnel and coax instrumentation will be used at NSWC), the temperature rise, based on run durations, will be only 60% of the

Calspan facility increase in the NSWC test facility.

SECTION X OPTICAL FIBRE-BASED HEAT FLUX SENSORS

S.R. Kidd, 1993, has recently published documentation of a new point source heat transfer gage based on a fiber Fabry-Perot interferometer embedded in a model surface. While one may argue with the rationalization for the need of such a new gage, it must be understood that such a gage represents a new approach toward the measurement of surface temperature and the inference of surface heat flux. The flow in which these measurements were made is a benign, short duration Ludwig tube flow operating for 20 ms and generating 50 kW/m^2 of heat transfer. The sensor is placed in the surface of the material as shown in Figure 129.

The flow at the surface is addressed by a low power laser diode source. The phase shift of the optical signal is related to the surface temperature of the gage.

Heat transfer rates are inferred from the calorimetric equation:

$$4 \dot{q} = \rho C l \frac{dT}{dt} \quad \rho - \text{Sensor Density}$$

C - Sensor Specific heat

l - length of the sensing fibre

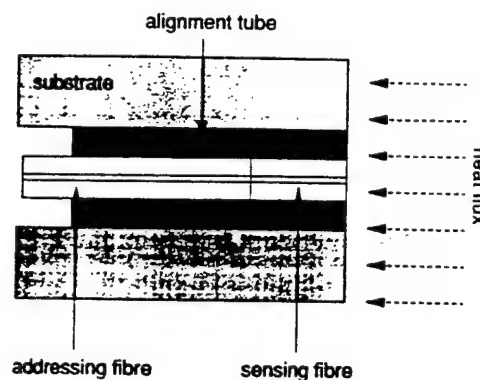


Figure 129 S.T. Kidd's Optical Fibre Heat Transfer Gage Embedded Within the Test Surface.

where the density and specific heat are those of the fused silica of the fiber.

Including the induced phase shift into the equation for heat transfer, the heating rate is inferred from:

$$\dot{q} = \frac{\rho C \lambda}{4\pi(n\alpha + \beta)} \frac{d\phi}{dt}$$

where n is the refractory index of the fibre, λ is the vacuum wavelength of the illuminating light, α is the coefficient of thermal expansion of the fibre and β is the thermo-optic coefficient of the fibre.

A somewhat different approach to the same sensor is taken by Fritsch and Flatco, 1993, working for the NASA Lewis Research Center. In their gage a Fabry-Perot etalon formed of a silicon film is sputtered directly onto the tip of the optical fibre of diameter $1.4 \mu\text{m} = 0.000055 \text{ ins.}$ as shown in Figure 129. The etalon is illuminated with a broadband light from a light emitting diode (LED). The intensity of the reflected light is then measured at two wavelengths by a miniature optical spectrometer. The ratio of the intensity at the selected frequencies is directly related to the sensed temperature of the gage as shown in Figure 130. Specifics of these two sensors, including areas as yet undocumented are shown in Table 11.1.

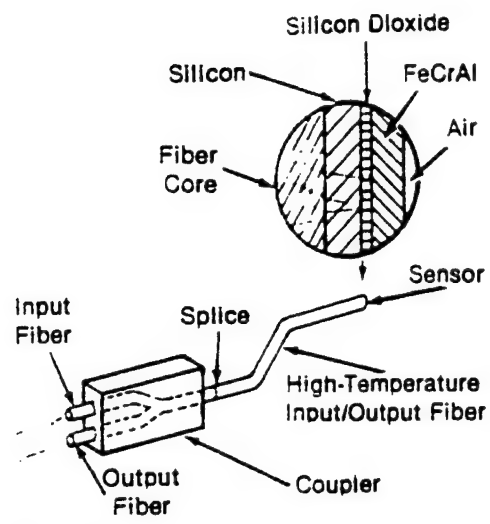


Figure 130 Silicon Film Sputtered Directly onto the Tip of the Optical Fiber.

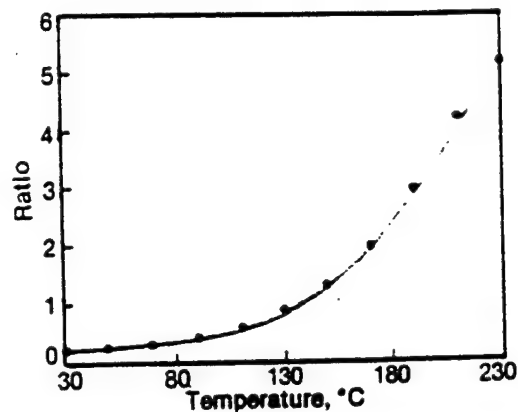


Figure 131 Ratio of the Intensity at the Selected Frequencies is Directly Related to the Sensed Temperature of the Gage.

TABLE 11.1
SPECIFICS OF TWO SENSORS, INCLUDING AREAS AS YET UNDOCUMENTED

Parameter	Paper of S.R. Kidd Calorimeter Gage	Paper of J.M. Flatico
Interrogating Light Source	10 milliwat laser diode light source operating at 780 nm	Broadband light from an LED
Optical Fibre	Single mode	Multimode, 1.4 μm
Temperature Sensed By:	Fabry-Perot Interferometer	Ratio of intensity of reflected light at 2 frequencies using a miniature optical spectrometer
Demonstrated Temperature Calibration		160-> 230 degs C
Demonstrated Heat Transfer Measurement	Yes on Turbine Blades	No
Discussed Problems:	Pressure sensitivity of fiber through strain in the installed	
Frequency of the Demonstrated Heat Transfer	20kHz at 50 kw/m2 for 20ms (8 μ sec response)	

APPENDIX A

REFERENCE HEAT-TRANSFER COEFFICIENTS

In presenting heat-transfer coefficient results it is convenient to use reference coefficients to normalize the data. Equilibrium stagnation point values derived from the work of Fay and Riddel (Ref. 12) were used to normalize the data obtained in this test. These reference coefficients are given by:

$$HREF = \frac{8.17173(PT2)^{1/2}(MUTT)^{0.4}[1 - P/PT2]^{0.25}[0.2235 + (1.35 \times 10^5)(TT + 560)]}{9rX)^{1/2}(TT)^{0.15}}$$

where

- PT2 = Stagnation pressure downstream of a normal shock wave, psia
- MUTT = Air viscosity based on TT, lbf-sec/ft²
- P = Free-stream pressure, psia
- TT = Tunnel stilling chamber temperature, °R
- rX = Where X = 1, 2, or 3 is the reference dimension used to calculate HREF for 2-D stagnation points. For Phase I, r1 = 0.0117, r2 = 0.0208, and r3 = 0.042, For Phase II, r1 = 0.0182
- RHO = Free-stream density, lbm/ft³
- V = Free-stream velocity, ft/sec

APPENDIX A

MATERIAL PROPERTIES

Material	$\sqrt{\rho c k} (kJ m^{-2} K^{-1} s^{-1/2})$
quartz (SiO ₂)	1.53
pyrex	1.53
macor	1.86
macor	2.00
macor	1.76
chromel	8.51
constantan	9.06
17-4PH stainless steel	8.35
chromel/const.thermoc. in 17-4PH insert	8.81
plexiglas GS	0.58

	$\frac{\sqrt{\rho c k(T)}}{\sqrt{\rho c k(T_i)}}$
pyrex	$1+0.0023(T-T_i)$
quartz	$1+0.0012(T-T_i)$
macor	$1+0.0006(T-T_i)$

where T is in Kelvin.

The relative values for the thermal properties of various backing materials are as follows:

Material	Density Lbm/Ft ³	Specific Heat Btu/Lbm R	Thermal Conductivity Btu/FtSec R	$B = \sqrt{\rho c_p k_w}$
Pyrex 7740	139	0.185	0.186x10-3	0.0692
Macor	157	0.180	0.270x10-3	0.0874
Stainless Steel	500	0.120	2.70x10-3	0.4025

Note that these values are representative only. Actual data manipulation will require higher precision information together with its actual variance with temperature.

Note also that the relation between Macor and stainless steel for this chart is the same as evaluated by Lyons and Gai, 1988 and that the Macor material is slightly more conductive than the pyrex backing material. The level of the parameter $\beta = \sqrt{\rho c k}$ is inversely related to the temperature rise of the substrate.

Material	Density lb/ins ³	Specific Heat Btu/lb-°F	Thermal Conductivity Btu(ins-sec-°F)	Thermal Diffusivity
Copper	0.322	0.092	5.16x10-03	0.174
Stainless Steel	0.291	0.120	0.217x10-03	6.21x10-03
Macor	0.0909	0.180	2.25x10-05	
Kapton	0.0512		2.074-6	
Aluminum Oxide				
Utem 1000	0.0459	0.27	3.241-6	
Silicon Dioxide	0.0793		1.739-5	

TABLE A.A-1
MATERIALS WITH MELTING POINTS ABOVE 900°K
[Data from ref.5]

Name or Symbol	ρ , g/cm ³ at:		k, watts/cm-°K at:		α , cm ² /sec at:	
	278°K	833°K	278°K	833°K	278°K	833°K
Ag	10.4	10.1	4.22	3.41	1.74	1.29
Au	19.3	18.7	3.46	2.99	1.42	0.955
Cu	8.93	8.68	4.08	3.51	1.18	0.903
Al	2.70	2.59	2.28	1.83	0.949	0.593
Molded graphite	1.73	1.73	1.28	0.779	0.885	0.283
Mg	1.74	1.66	1.38	1.33	0.789	0.616
Be	1.85	1.79	1.88	0.900	0.606	0.175
Mo	10.2	10.1	1.36	1.19	0.513	0.418
Cr	7.16	7.04	0.900	0.692	0.286	0.172
Ta	16.5	16.3	0.623	0.692	0.273	0.260
Pt	21.4	21.1	0.709	0.685	0.255	0.222
Fe	7.88	7.73	0.744	0.398	0.225	0.072
Nb	8.57	8.45	0.450	0.528	0.219	0.214
Ti	4.59	4.56	0.225	0.173	0.092	0.059
Inconel X	8.24	8.04	0.145	0.232	0.041	0.051
310 stainless steel	7.84	7.62	0.145	0.193	0.033	0.044

APPENDIX B
THERMAL PROPERTIES OF SELECTED MATERIALS

Material	$\sqrt{\rho ck/(kT)} m^{-2} K^{-1} s^{-1/2}$
quartz (SiO ₂)	1.53
pyrex	1.53
macor	1.86
macor	2.00
macor	1.76
chromel	8.51
constantan	9.06
17-4PH stainless steel	8.35
chromel/const.thermoc. in 17-4PH insert	8.81
plexiglas GS	0.58

	$\frac{\sqrt{\rho ck(T)}}{\sqrt{\rho ck(T_i)}}$
pyrex	$1+0.0023(T-T_i)$
quartz	$1+0.0012(T-T_i)$
macor	$1+0.0006(T-T_i)$

where T is in Kelvin.

The relative values for the thermal properties of various backing materials are as follows:

Material	Density Lbm/Ft ³	Specific Heat Btu/Lbm R	Thermal Conductivity Btu/FtSec R	$B = \sqrt{\rho c_p k_w}$
Pyrex 7740	139	0.185	0.186x10-3	0.0692
Macor	157	0.180	0.270x10-3	0.0874
Stainless Steel	500	0.120	2.70x10-3	0.4025

Note that these values are representative only. Actual data manipulation will require higher precision information together with its actual variance with temperature.

Note also that the relation between Macor and stainless steel for this chart is the same as evaluated by Lyons and Gai, 1988 and that the Macor material is slightly more conductive than the pyrex backing material. The level of the parameter $\beta = \sqrt{\rho c k}$ is inversely related to the temperature rise of the substrate.

Material	Density lb/ins ³	Specific Heat Btu/lb-°F	Thermal Conductivity Btu(ins-sec-°F)	Thermal Diffusivity
Copper	0.322	0.092	5.16x10-03	0.174
Stainless Steel	0.291	0.120	0.217x10-03	6.21x10-03
Macor	0.0909	0.180	2.25x10-05	
Kapton	0.0512		2.074-6	
Aluminum Oxide				
Utem 1000	0.0459	0.27	3.241-6	
Silicon Dioxide	0.0793		1.739-5	

MATERIALS WITH MELTING POINTS ABOVE 900°K

Name or Symbol	ρ , g/cm ³ at:		k, watts/cm-°K at:		α , cm ² /sec at:	
	278°K	833°K	278°K	833°K	278°K	833°K
Ag	10.4	10.1	4.22	3.41	1.74	1.29
Au	19.3	18.7	3.46	2.99	1.42	0.955
Cu	8.93	8.68	4.08	3.51	1.18	0.903
Al	2.70	2.59	2.28	1.83	0.949	0.593
Molded graphite	1.73	1.73	1.28	0.779	0.885	0.283
Mg	1.74	1.66	1.38	1.33	0.789	0.616
Be	1.85	1.79	1.88	0.900	0.606	0.175
Mo	10.2	10.1	1.36	1.19	0.513	0.418
Cr	7.16	7.04	0.900	0.692	0.286	0.172
Ta	16.5	16.3	0.623	0.692	0.273	0.260
Pt	21.4	21.1	0.709	0.685	0.255	0.222
Fe	7.88	7.73	0.744	0.398	0.225	0.072
Nb	8.57	8.45	0.450	0.528	0.219	0.214
Ti	4.59	4.56	0.225	0.173	0.092	0.059
Inconel X	8.24	8.04	0.145	0.232	0.041	0.051
310 stainless steel	7.84	7.62	0.145	0.193	0.033	0.044

TYPICAL MATERIAL PROPERTIES FOR THERMOCOUPLES

Material	ρ , lb/ft ³	C, Btu/lb °R	k Btu/ft-°R-sec	α , ft ² /sec	$\frac{BTU^2}{ft^4 sec^\circ R^2}$
Alumel	537	0.125	4.5×10^{-3}	6.7×10^{-5}	0.302
Aluminum	175	0.23	19.4×10^{-3}	48.2×10^{-5}	0.781
Chromel	545	0.107	2.9×10^{-3}	5.0×10^{-5}	0.169
Constantan	553	0.094	3.2×10^{-3}	6.2×10^{-5}	0.166
Copper	559	0.091	62.0×10^{-3}	122×10^{-5}	3.154
Iron	493	0.11	1.2×10^{-3}	2.2×10^{-5}	0.065
Nickel	556	0.11	12.6×10^{-3}	20.6×10^{-5}	0.77
Stainless Steel	500	0.12	2.7×10^{-3}	4.5×10^{-5}	0.162

All values are for material at 70°F

APPENDIX C
THERMAL SENSOR SENSITIVITY

TABLE C-1
REPRESENTATIVE SENSITIVITIES OF TYPICAL THERMOCOUPLE MATERIALS

Thermocouple material Combinations	Sensitivity $\mu V/^{\circ}K$
Copper-Constantan	40
Iron-Constantan	50
Chromel-Alumel	40
Chromel-Constantan	63
Platinum-Platinum/Rhodium (13% Rhodium)	6
Platinum-Platinum/Rhodium (10% Rhodium)	6

TABLE C-2
REPRESENTATIVE SENSITIVITIES OF TYPICAL RESISTANCE THERMOMETERS

Material	Temperature Coefficient of Resistance, (TCR)	Sensitivity $\mu V/^{\circ}K$, (SENS)
Aluminum	4.05	4050
Copper	3.90	3900
Gold	3.41	3410
Nickel	5.40	5400
Platinum	3.01	3010
Silver	3.79	3790
Rhodium	4.30	4300

Notes: 1. Data from Schultz, 1965, pg 9

2. SENS=1000*TCR

3. The temperature coefficient of resistance is defined by the equation $\alpha = \frac{1}{R} \frac{dR}{dT}$

4. Data shown is for a mean film voltage of 1.00 volts

REFERENCES

- Ainsworthy, R.W., et al, "Developments in Instrumentation and Processing for Transient Heat Transfer Measurements in a Full- Stage Model Turbine, Trans. ASME, Jour. of Turbomachinery, pp 20-27, Jan 1989
- Aliotta, J., "Effects of Impurities on the Thermoelectric Properties of Platinum", Instruments and Control Systems. March 1972. pp 106-107
- Anon, "Measurement Techniques in Heat Transfer", AGARDograph 130
- Aslam, M. and Masood, A., "Thin Film Diamond Temperature Sensor Array for Harsh Aerospace Environment", SPIE Vol 1694, paper 20, April 20-24, 1992.
- Aslam, M., "Piezoresistivity in Vapor-Deposited Diamond Films", Applied Physics Letters, Vol. 60, Nr. 23, 8 June 1992, pp 2923-2925 1992
- Avery, D.E., Ballard, G.K. and Wilson, M.L., "Electroless-Plating Technique For Fabricating Thin-Wall Convective Heat-Transfer Models", NASA TP 2349, 1984
- Balageas, D.L., Boscher, D.M., Deom, A.A., Fourier, J. and Gardette, G., "Measurement of Convective Heat-Transfer Coefficients in Wind Tunnels Using Passive and Stimulated Infrared Thermography", Rech. Aerosp. Nr. 1991-4, pp 51-71 also SPIE Volume 1341, IR Techniques XVI, 1990, pp 339-366
- Baughn, J.W., Takahashi, R.K., Hoffman, M.A. and McKillop, A.A., "Local Heat Transfer Measurements Using an Electrically Heated Thin Gold-Coated Plastic Sheet", Jour. of Heat Transfer, Volume 107, November 1985, pp 953-959
- Bendersky, "A Special Thermocouple for Measuring Transient Temperatures", Mech. Engr., Feb. 1953, pp 117-121
- Bickle, L. W. and Dove, R.C., "Numerical Correction of Triensient Measurements", ISA Transactions, Volume 12, Nr. 3, 1973, pp 286-295
- Baughn, J.W., Hoffman, M.A. and Makel, D.B., "Improvements in a New Technique for Measuring and Mapping Heat Transfer Coefficients". Rev. of Sci. Instrum., April 1986, pp 650-654
- Bogden, L., "Transient Heat Transfer Measurement with Thin-Film Resistance Thermometers -- Data Reduction Techniques", AFAPL TR 67-141, 1967
- Borell, G.J. and Diller, T.E., "A Convection Calibration Method for Local Heat Flux Gages", Jour. of Heat Transfer, February 1987, Volume 109, pp 83-89
- Borovoy, V. Ya, Osipov, V.V. et al, "Effect of Mach and Reynolds Numbers on the Heat Exchange on a Blunted Leading Wing Edge of Variable Sweepback in the Region of Incidence of the Bow Wave", TsAGI Uchenye Zapiski, (ISSN 0321-3429) volume 14, Nr. 2, 1983, pp 58-66

Borovoy, V. Ya, "Flow of Gas and Heat Exchange in Zones of Reaction of Shock Waves with Boundary Layers", *Tekhnicheskaya Gazy i Teploobmen v Zonakh Vzaimodeystviya Udarnykh Voin s Pogranichnym Sloym*", 1983

Borovoi, V. Ya, and Struminskaya, I.V., "Heat Transfer in the Shock Impingement Zone Around a Cylinder in a Hypersonic Flow" *Fluid Dynamics, Soviet Research*, 1991, pp 415-420

Boscher, "Measurement of Convective Heat Transfer Coefficients on a Wind Tunnel Model by Passive and Stimulated IR Thermography, *Society of Photo Optical Instrumentation*, pp 339-357, 1990

Boylan, D.E. et al, "Measurement and Mapping of Aerodynamic Heating Using a Remote Infrared Scanning Camera in Continuous Flow Wind Tunnels", *AIAA Paper 78-799*

Brazhko, V.N., Kovaleva, N.A. and Maykapar, G.I., "Errors of the Method of Measuring the Heat Flux to Wind-Tunnel Models by Means of Thermal-Indicator Coatings", *Fluid Dynamics, Soviet Research*, Vol. 19, Nr. 4, July-August 1990, pp 128-142

Boylan, D.E., Carver, D.B., Stallings, D.W. and Trimmer, L.L., "Measurement and Mapping of Aerodynamic Heating Using a Remote Infrared Scanning Camera in Continuous Flow Wind Tunnels", *AIAA 78-799*, 1978

Buck, G.M. "An Imaging System for Quantitative Surface Temperature Mapping Using Two-Color Thermographic Phosphors", *ISA Paper 88-0772*, 1988

Buck, G.M. "Surface Temperature/Heat Transfer Measurement Using a Quantitative Phosphor Thermography System", *AIAA Paper 91-0064*, 1991

Carlomagno, G.M., and de Luca, L., "Infrared Thermography in Heat Transfer", Chapter 32 of "Handbook of Flow Visualization" edited by Wen-Jei Yang, Hemisphere Publishing Company, 19xx

Carroll, H.R., "Technical Innovations in Testing and Analysis of Heat and Pressure Models in Hypersonic Wind Tunnels", *AIAA Paper 82-0578* (see also *AIAA Paper 80-1310*)

Carter, L.D., "Supersonic Boundary Layer Transition Detection Using Thermographic Phosphorescent Paint", M.S. Thesis, University of Tennessee, 1975

Cassady, 1991 **Reference is Embargoed**

Chapman, D.R., Mark, H., and Pirtle, M., "Computers vs Wind Tunnels For Aerodynamic Flow Simulation", *Aeronautics and Astronautics*, April 1975

Chproun, *AIAA Paper 89-1876*, pp 2758, A89-42101, 1989

Collier, A.S., Laggerty, J.F., Swinford, S.S. and Witte, D.W., "Aerodynamic Heat Transfer Testing in Hypersonic Wind Tunnels Using an Infrared Imaging System", 1990, *AIAA Paper 90-0189*

Collier, A.S., "Infrared Surface Temperature Measurements in NAVSWC's Hypervelocity Wind Tunnel No. 9", 1991, *ICIASF Paper pp 169-173*

Compton, D.L., "Use of an Infrared-Imaging Camera to Obtain Convective Heating Distributions", AIAA Journal, Vol. 10, No. 8, pp 1130-1132, 1972

Consigny, "Heat Transfer Measurement Techniques Used Or In Development At ONERA/ Chalais Meudon" "New Trends in Instrumentation for Hypersonic Research", A. Boutier ed., Series E: Applied Sciences - Vol. 224, Kluwer Academic Publishers, ISBN 0-7923-2024-7, 1993

Cook, W.J., and Felderman, E.J., "Reduction of Data from Thin Film Heat Transfer Gages: A Concise Numerical Technique", AIAA Journal, V4, #3, pp 560-563, 1966

Covert, G. and Gollnick, A.F., Jr. "Calibration of a Small Heat Transfer Gage and Its Applications", ISA Paper 68-535

Creel, T.R., Jr., "A Device For Rapid Determination of Thermophysical Properties of Phase Change Wind Tunnel Models", NASA TN D-3421, 1976

Cresci, R.J. and Libby, P.A., "Some Heat Conduction Solutions involved in Transient Heat Transfer Measurements", WADC TN 57-236, 1957

Cutting, J.C. and Fay, J.A., "High Heat Flux Effects in Wire Heat Gages", Jour. of Aerospace Sci., April 1961, pp 342-343

Czysz, P. and Dixon, W.P., "Quantitative Heat Transfer Measurement Using Thermographic Phosphors", S.P.I.E. Journal, March 1969, pp 77-79

Dabiri, D. and Gharib, M., "Digital Particle Image Thermometry; The Method and Implementation", Experiments in Fluids, Vol. 11, pp 77-86, 1991

Dean, W.G. and Connor, L.E., "A Study For Development of Aerothermodynamic Test Model Materials and Fabrication Techniques", NASA CR 2065, 1972

DeCoursin, D.G., Aerodynamic Heating and Heat Transfer Phenomena at Mach Number 2.7 Through 5.7", WADC TR 53-379, 1954

de Luca, L., "Computerized IR Thermography for Convective Heat Transfer Measurements", in Computational Methods and Experimental Measurement, V, eds Sousa, A et al, Elsevier, 1991

Dixon, W.P., "Precise Heat Transfer Measurements with Surface Thermocouples", Eighth Annual Conference on Thermal Conductivity. Purdue University, October 1968

Dixon, J., "Radiation Thermometry", J. Phys. E: Scientific Instrumentation, Volume 21, 1988, pp 425-436

Dorignac, E. and Vullierme, J.J., "Error Resulting from the Surface Conduction Effects when Determining Surface Transfers by "Thin Wall" or "Semi-Infinite Wall" Methods, La Recherche Aerospatiale, 1991-1, pp 67-73

Dunn, M.G. et al, "Heat-Flux Measurements for the Rotor of a Full-Stage Turbine: Part II- Description of Analysis Technique and Typical Time-Resolved Measurements", Trans. ASME, Journal of Turbomachinery, Vol. 108, July, 1986, pp 98-107

Dunn, M.G., George, W.K., Rae, W.J., Woodward, S.H., Moller, J.C. and Seymour, P.J., "Heat-Flux Measurements for the Rotor of a Full-Stage Turbine: Part II - Description of Analysis Technique and Typical Time-Resolved Measurements", Jour. of Turbomachinery, Trans. ASME, Vol. 108, 1986, pp 98-107

Durand, J.A., and Rhudy, J.P., "Procedure Used For X-15 Heat Transfer and Pressure Distribution Tests at Hypersonic Speeds", AEDC TN 59-04, 1959

Doorly, J.E. and Oldfield, M.L.G., "The Theory of Advanced Multi-Layer Thin Film Heat Transfer Gauges", Intl. Jour. of Heat and Mass Transfer, Volume 30, Nr 6, pp 1159-1168, 1987

Dorignac, E. and Vullierme, J.J., "Errors Resulting from the Surface Conduction Effects When Determining Surface Transfers by "Thin Wall" or "Semi-Infinite Wall" Methods", Rech Aerosp., 1991-1, pp 67-73

Eber, 1952

Edney, "Anomalous Heat Transfer and Pressure Distributions on Blunt Bodies at Hypersonic Speeds in the Presence of an Impinging Shock", FFA 115, 1968

Ehrich, F.F., "Differentiating of Experimental Data Using Least Squares Fitting", Jour.of Aeronaut. Sci., April 1961, pp 133-134

Epstein, A.H. et al, "The Design of the MIT Blowdown Turbine Facility", GTL Report No. 183, April 1985

Epstein, A.H., "The Theory of Advanced Multi-Layered Thin Film Heat Transfer Gages", Intl. Journal of Heat and Mass Transfer, Vol. 30, Nr. 6, pp 1159-1168, 1986 ?

Feldstein, N., "Selective Electroless Plating Techniques: A Survey", August 1978

Flannagan, M.J., "Pressure and Temperature Fluctuations in an Axisymmetric Flowfield Due to Shock-Boundary Layer Interactions at High Reynolds Numbers at Mach 6, AIAA Paper 91-3321, 1991

Flannagan, M.J., "Operation and Design Considerations for Unsteady Data Acquisition with PC-Based Systems in High Reynolds Number Hypersonic Flowfields", AIAA Paper 92-0204, 1992

Flannagan, M.J., "Time Dependent Heat Transfer Rates in High Reynolds Number Hypersonic Flowfields", in the 1992 NASA Langley Measurement Technology Conference, NASA CP 3161, 1992

Foster, T.F. and Wallace, G.A., "Photoetching Roughness Application and Transient Backwall Thermocouple Technique For Hypersonic Blowdown Wind Tunnel Models", ISA, 1980, ISBN 87664-473-6

Fritsch, K. et al, "Silicon-Etalon Fiber-Optic Temperature Sensor", NASA Tech Briefs, June 1993, pp 52-53

Gardon, R.G., "An Instrument for the Direct Measurement of Intense Thermal Radiation", The Review of Scientific Instruments, Vol. 24, pp 366-370, 1953

Gartenberg, Ehud and Roberts, A S., Jr., "Twenty-Five Years of Aerodynamic Research with Infrared Imaging", SPIE Volume 1467, Thermosense XIII, 1991,

Gates, D.F. and Allen, R.W., "Experimental Measurements of Upstream History Effects in Turbulent Supersonic Flow", 1974 Heat Transfer and Fluid Mechanics Institute, paper 21.

George, A.R. and Reinecke, W.G., "Conduction in Thin-Skinned Heat Transfer and Recovery Temperature Models", AIAA Journal, Vol. 1, Nr. 8, pp 1956-1958, 1963

George, W.K., Rea, W.J., and Woodward, S.H., "An Evaluation of Analog and Numerical Techniques for Unsteady Heat Transfer Measurement with Thin-Film Gages in Transient Facilities", Exp. Thermal and Fluid Sci., Vol 4, pp 333-342, 1991

Giedt, W.H., "The Determination of Transient Temperatures and Heat Transfer to a Gas-Metal Interface Applied to a 40 mm Gun Barrel", Jet Propulsion, April 1955, Volume 25, Number 4, pp 158-162

Gillerlain, 1979 **AIAA Paper** also NSWC/NOL/TR-75-63, 1975

Ginoux, J.J., "A Steady State Technique for Local Heat Transfer Measurements and its Application to the Flat Plate", J. Fluid Mech.

Gopel, W. et al, "Sensors", Volume 4, "thermal Sensors" edited by T. Ricolfi

Griffith, B.J. Maus, J.R. and Best, T., "Explanation of the Hypersonic Longitudinal Stability Problem - Lessons Learned", NASA CP 2283, 1983

Grossman, D.G., "Machining a Macinable Glass-Ceramic", Vacuum, Voiume 28, Number 2. pp 55-61

J.M. Hager et al., "Heat Flux Microsensors", 26th National Heat Transfer Conference, 1989,

Harting, D.R., "Digital Transient-test Techniques", Experimental Mechanics, Volume 12, Nr. 7, July 1972, pp 335-340

Harvey, W.D., "Continuous Skin Construction Technique For Fabricating Models For Aerodynamic Heat Transfer Studies Involving Very Small Transient Heating Rates", ISA Preprint 17.12-7-65, 20th Annual Conference, October, 1965

Hayashi, M., Sakurai, A. and Aso, S., "An Investigation of a Multi-Layered Thin Film Heat Transfer Gauge", Memoirs of the Faculty of Engineering, Kyushu University, Volume 44, Nr. 1, March 1984, pp 113-124

Hayashi, M., Sakurai, A. and Aso, S., "A Study of Multi-Layered Thin Film Heat Transfer Gauges and a New Method of Measuring Heat Transfer With It" Trans. of Japan Society of Aero. and Space Sciences, Volume 30, #88, pp 91-101, 1987

Hayes, J.R. and Rougeux, A., "The Application of Numerical Techniques to Model the Response and Integration of Thermal Sensors in Wind Tunnel Models", AIAA Paper 91-0063, 1991

Hedlund, E.R. et al, "New High Reynolds Number Mach 8 Capability", AIAA Journal, Vol. 30, Nr. 6, pp 1665-1667

Henckels, A., Herzog, P. and Maurer, F., "Experimental Study of Hypersonic Shock Wave Boundary Layer Interaction by Means of Infrared Technique", First European Symposium on Aerothermodynamics for Space Vehicles, 1991

Hodge, J.K. and Woo, Y.K. and Cappelano, P.Y., "Parameter Estimation for Imbedded Thermocouples in Space Shuttle Wind Tunnel Test Articles with Nonisothermal Wall", AIAA 83-1533, 1983

Holden, M.S., Weiting, A.R., Moselle, J.R. and Glass, C., "Studies of Aerothermal Loads Generated in Regions of Shock/Shock Interaction in Hypersonic Flow", 1988, AIAA Paper 88-0477

Holden, M.S., 1990 **Reference is Export Controlled although specific material is not**

Hornbaker, D.R. and Rall, D.L., "Heat Flux Measurements: A Practical Guide", Instrumentation Technology, February 1968, pp 51-56

Hung, Ching-Mao, "Computation of Navier-Stokes Equations for Three-Dimensional Flow Separation", AIAA Journal, Volume 29, No. 10, October 1991, pp 1659-1667...blunt and flat face fin on a plate.

Ireland, P.T. and Jones, T.V., "The Response Time of a Surface Thermometer Employing Encapsulated Thermochromic Liquid Crystals"
J. Phys. E: Sci. Instrum. Vol 20, 1987, pp 1195-1199

Jenke, L.M., "Application of Digital Fourier Analysis in Processing Dynamic Aerodynamic Heating Measurements", AIAA Journal, Volume 17, Nr. 6, pp 641-642, 1979 (see also AIAA 78-778)

Jenke, L.M. and Strike, W.T., "Application of Digital Fourier Analysis in Processing Heat Transfer Measurements on an Oscillating Cone in a Hypersonic Stream", AIAA 78-778

Jessen, C. and Gronig, H., "A New Method for Manufacturer of Thin Film Heat Flux Gauges", Shock Waves, v.1, pp 161-164, 1991

Jones, R.A. and Hunt, J.A., "An Improved Technique for Obtaining Quantitative Aerodynamic Heat-Transfer Data with Suitable Coating Materials", NASA TR R-230 and AIAA 65-131, 1965

Jones, T.V., "Heat Transfer, Skin Friction Total Temperature and Concentration Measurements", Chapter 4 to the book "Measurement of Unsteady Fluid Dynamic Phenomena", Edited by Dr. B.E. Richards, McGraw-Hill, 1977

Kayser, P, "Thin Gradient Heat Fluxmeters Developed at ONERA", New Trends in Instrumentation for Hypersonic Research, 1992

Kendall, D.N., Dixon, W.P. and Schulte, E.H., "Semi-Conductor Surface Thermocouples for Determining Heat Transfer rates", IEEE Transactions on Aerospace and Electronic Systems, Volume AES-3, Number 4, July 1967

Kidd, C.T., "A Durable, Intermediate Temperature, Direct Reading heat Flux Transducer For Measurements in Continuous Wind Tunnels", AEDC TR 81-19, 1981

Kidd, C.T., "Determination of the Uncertainty of Experimental Heat-Flux Calibrations", AEDC 83-13

Kidd, C.T., "Thin-Skin Technique Heat Transfer Measurement Errors Due to Heat Conduction into Thermocouple Wires", ISA Trans, Vol. 24, Nr. 2, 1985

Kidd, C.T., "Lateral Heat Conduction Effects on Heat-Transfer Measurements with the Thin-Skin Technique", ISA Trans. Vol. 26, Nr. 3, pp 7-18, 1987

Kidd, S.R. et al, "Wind Tunnel Evaluation of Novel Interferometric Optical Fibre Heat Transfer Gauges", Meas. Sci. Technol. Vol 4 (1993), pp 362-368

Kidd, S.R. et al, "Interferometric Fibre Sensors for Measurement of Surface Heat Transfer Rates on Turbine Blades", Optics and Lasers in Engineering, Vol. 16, 1992, pp 207-221

Kidd, C.T., "A Durable, Intermediate Temperature, Direct Reading Heat Flux Transducer For Measurements in Continuous Wind Tunnels", AEDC TR 81-19, 1981

Kidd, C.T., "High Heat Flux Measurements and Experimental Calibrations/Characterizations" in the 1992 NASA Langley Measurement Technology Conference, NASA CP 3161, 1992

Kidd, S.R., "Wind Tunnel Evaluation of Novel Interferometric Optical Fibre Heat Transfer Gages", Meas. Sci. Technol. v4, pp 362-368, 1993

Kussoy, M.I. and Horstman, C.C., "An Experimental Documentation of a Hypersonic Shock Wave Turbulent Boundary Layer Interaction Flow with and without Separation" NASA TMX 62,414, 1975

Kussoy, M.I., Kim, K.S. and Horstman, C.C., "An Experimental Study of Three-Dimensional Shock Wave Turbulent Boundary Layer Interaction at a Hypersonic Mach Number, AIAA Paper 91-1761, 1991

Kreider, K.G., "Transparent Thin Film Thermocouple", Thin Solid Films, Vol. 176, pp 73-78, 1989

Lewis and Turley, 19xx.....

Liebert, 1984.....

Lyons, P.R.A. and Gai, S.L., "A Method for the Accurate Determination of the Thermal Product $(\rho ck)^{1/2}$ for Thin Film Heat Transfer or Surface Thermocouple Gauges", J. Phys. E: Sci. Instrum, Vol 21 pp 445-448, 1988

Maegley, W.J. and Carroll, H.R., "MX Missile Thermal Mapping and Surface Flow Results", AIAA Jour. of Spacecraft and Rockets, Volume 19, Nr. 3, May-June 1982, pp 199-204 (see also AIAA 80-1310)

Maise, G and Rossi, M.J., "Lateral Conduction Effects on Heat Transfer Data Obtained with the Phase-Change Paint Technique", NASA CR 2435, 1974

Marrone, P.V. and Hartunian, R.A., "Thin-Film Thermometer Measurements in Partially Ionized Shock-Tube Flows", pp 719-721, Physics of Fluids, 1959

Matthews, R.K., "Wind Tunnel Testing in Hypersonic Facilities", Notes from a Short Course on Hypersonics, University of Texas, October 1987

Mentre, V. and Consigny, H., "An Improved Data Reduction Technique for Heat Transfer Measurements Using Surface Thermocouples or Thin-Films", ICIASF '87 Record, pp 369-377 also as ONERA TP 1987-74

Metzger, D.E., Bunker, R.S. and Bosch, G., "Transient Liquid Crystal Measurement of Local Heat Transfer on a Rotating Disk with Jet Impingement", Trans. ASME, Jour. of Turbomachinery, January 1991, pp 52-59

Miller, C.G., "Comparison of Thin-Film Resistance Heat Transfer Gages with Thin Skin Transient Calorimeter Gages in Conventional Hypersonic Wind Tunnels", NASA TM 83197, December 1981

Miller, C.G., "Refinement of an "Alternate" Method for Measuring Heating Rates in Hypersonic Wind Tunnels", AIAA Journal, Volume 23, Nr.5, pp 810-812

Moffat, R.J. "The Gradient Approach to Thermocouple Circuitry"

Moffat, R.J., 1988 **Experimental Methods in Heat Transfer QC 319.8**

Moffat, R.J., "Experimental Heat Transfer", paper KN-11, 9th International Heat Transfer Conference, 1990

Moffat, R.J., "Describing Uncertainties in Experimental Results", Experimental Thermal and Fluid Science, Vol. 1, pp 3-17

Neumann, R.D. and Hayes, J.R., "Protuberance Heating at High Mach Numbers - A Critical Review and Extension of the Data Base", AIAA Paper 81-0420, 1981

Neumann, R.D., "Aerothermodynamic Instrumentation", in AGARD R-761, "Special Course on Aerothermodynamics of Hypersonic Vehicles", pp 4-1 to 4-40, 1989

Noel, B.W., Borella, H.M., Franks, L.A., Marshall, B.R., Allison, S.W., Cates, M.R. and Stange, W.A., "Proposed Laser-Induced Fluorescence Method for Remote Thermometry in Turbine Engines", Jour. Propulsion and Power, AIAA, Vol. 2 Nr. 6, pp 565-568, 1986, also AIAA Paper 85-1468

Noel, B.W. and a cast of thousands, "Evaluating Thermographic Phosphors in an Operating Turbine Engine", Jour. of Engineering for Gas Turbines and Power, Vol. 113, pp 242-245, 1991

Noel, B.W., and a cast of thousands, "Evaluating and Testing Thermographic Phosphors for Turbine-Engine Temperature Measurements", AIAA Paper 87-1761, 1987

Noel, B.W. et al, "A 2-D Imaging Heat Flux Gage", Los Alamos National Laboratory, Report LA-12129-MS, 1991

Nutt, K.W., Matthews, R.K., and Best, J.T. Jr., "Analysis of Heat Transfer Measurements on the Shuttle External Tank Obtained in Two AEDC Wind Tunnels", AIAA 86-0774-CP

Oldfield, M.L.G., Jones, T.V. and Schultz, D.L., "On-Line Computer for Transient Turbine Cascade Instrumentation", IEEE Transactions on Aerospace and Electronic Systems, Volume AES 14, Number 5, September 1978, pp 738-749

Onishi, S. and Diller, T.E., "High Temperature Heat Flux Measurements", AIAA Paper 91-0165, 1991

Osgerby, I.T., "Operation of AEDC-VKF 100 Inch Hotshot Tunnel F with Air as a Test Gas and Application to Supersonic Combustion Testing", AEDC TR 67-242

Portat, M., "Measurements Possibilities on Turbomachines with Thin Film Transducers", 19xx.....

Puram, C.K. et al, "Measurement of Steady and Unsteady Temperatures Using Infrared Thermography", Fundamental Experimental Measurements in Heat Transfer, ASME 1991, HTD Vol 179, pp 23-29

Reddy, 1980 NASA TM 80207.....

Richards, B.E., "Measurement of Unsteady Fluid Dynamic Phenomena", Hemisphere Publishers, ISBN 0-07-05280-4, 1977

Rogers, C.E., Bogden, L., Kinzly, R.E. and Stratton, J.E., "A Thermal Mapping Technique for Shock Tunnels and a Practical Data Reduction Procedure", AIAA Paper 72-1031

Scaggs, N., Neumann, R.D., Laganelli, A., "Hypersonic Wind Tunnel Nozzle Study", AIAA Paper 92-4012, 1992

Schmitz, L.S., "Nonlinear Analog Network to Convert Surface Temperature to Heat Flux", CAL Report 130, 1963 (N64-18176)

Schultz, D.L. and Jones, T.V., "Heat Transfer Measurements in Short Duration Hypersonic Facilities", AGARD-AG-1G5, February 1965

Segletes, J.A., "Errors in Aerodynamic Heat Transfer Measurements when Using Phase Change Coating Techniques", AIAA Jour. Spacecraft, Vol. 12, Nr. 2, pp 124-126

Seymour, P.J., "Techniques for Numerical Evaluation of Unsteady Heat Flux from Thin Film Gages", M.S. Thesis, State University of New York at Buffalo, 1987

Simon, 1993, Personal Correspondance

Simonich, J.C., and Moffat, R.J., "New Technique for Mapping Heat Transfer Coefficient Contours", Rev. Sci. Instrum. May 1982, pp 678-683

Simeonides, G. et al, "Infrared Thermography in Blowdown and Intermittent Hypersonic Tunnels", J. Thermophysics, Volume 4, No. 2, April 1990, pp 143-148

Simeonides, G. et al, "Quantitative Heat Transfer Measurements in Hypersonic Wind Tunnels by Means of Infrared Thermography", ICIASF '91 Record, pp 178-195

Skinner, G.T., "Analog Network to Convert Surface Temperature to Heat Flux", Cornell Aeronautical Laboratory Report Nr. CAL-100, 1960

Smith, A.J.D. and Baxter, D.R.J., "Liquid Crystal Thermography for Aerodynamic Heating Measurements in Short Duration Hypersonic Facilities", ICIASF '89 Record, pp 104-112, 1989

Stalmach, C.J., Jr., "Developments in Convective Heat Transfer Models Featuring Seamless and Selected Detail Surfaces, Employing Electroless Plating", NASA CR 144364, (N75-29356)

Stallings, D.W. and Whetsel, R.G., "Use of Infrared Imagery in Continuous Flow Wind Tunnels", SPIE Vol. 371; Thermosense V, 1982

Stein, P.K., "Instrumentation and Data Analysis: The Response of Transducers to Their Environment", Shock and Vibration Bulletin, Volume 40, Nr. 7, pp 1-16, 1969

Stein, P., "A New Conceptual Model for Components in Measurement/Control Systems: Practical Applications to Thermocouples

Strike, 1979.....

Thomann, H. and Frisk, B., "Measurement of Heat Transfer with an Infrared Camera", Intl. Jour. of Heat and Mass Transfer, Volume 11, pp 819-826

Thompson, W.P., "Heat Transfer Gages", pp 663-685 of Methods of Experimental Physics: Fluid Dynamics, Part 7 of Volume 18b, Academic Press, 1981, ISBN 0-12-475956-4 (v.18B)

Throckmorton, D.A., "Model Wall and Recovery Temperature Effects on Experimental Heat Transfer Data Analysis", NASA TM X-71967, 1974

Udell, K.S. et al, "Microsensors for Heat Transfer and Fluid Flow Measurements", Experimental Heat Transfer, Fluid Mechanics and Thermodynamics, 1988, R.K. Shah et al editors, Elsevier Science Publishing Co., source of figure on comparison of microsensor dimensions with associated physical length scales.

Veatch, D.W. and Bogue, R.K., "Analogue Signal Conditioning for Flight Test Instrumentation", AGARD-AG-160-Vol 17, 19xx

Venkateswaran, S., Witte, D.W. and Hunt, L.R., "Aerothermal Study in an Axial Compression Corner with Shock Impingement at Mach 6", AIAA Paper 91-0527

Vermeulen, J.P. and Simeonides, G., "Parametric Studies of Shock Wave/ Boundary Layer Interactions Over 2D Compression Corners at Mach 6", VKI TN 181, 1992

Walenta, Z.A., "Analogue Networks for High Heat-Transfer Rate Measurements", UTIAS Technical Note No. 84, 1964

Wannenwetsch, G.D., Ticatch, L.A., Kidd, C.T. and Arterbury, R.L., "Measurements of Wing Leading Edge Heating Rates and Wind Tunnel Models Using the Thin Film Technique", AIAA 85-0972, 1985

Wendt, J.F., "Infrared Thermography", The Second Joint Europe/US Short Course in Hypersonics, 1989

Yakov Ben-Haim and Ezra, Elias, "Indirect Measurement of Surface Temperature and Heat Flux: Optimal Design Using Convexity Analysis", Int. Jour. of Heat and Mass Transfer, Volume 30, Nr. 8, pp 1673-1683, 1987

Zhang, Z.C., Roberts, G.T. and Pratt, N.H., "An Experimental Evaluation of Thermochromic Liquid Crystals for Surface Temperature and Heat Flux Measurements in Shock Tube Flows", pp 618-623 in Current Topics in Shock Waves, the 17th International Symposium on Shock Waves and Shock Tubes, 1989, AIP Conference Proceedings #208, 1989, ISBN 0-88318-776-0